אוסף עזרא אוריון
ארכיון אמנות במרחב הציבורי
Ezra Orion Collection
Public Art Archive

כותרת: בין גלאקטי - פיסול על מאדים, פיסול על מאדים
טקסטים

מיקום בארכיון
ארגז: 24
תיק: 5
תת תיק: --

Title: Intergalactic - Mars sculpture, Mars sculpture
Texts

Location in Archive
Box: 24
Folder: 5
Sub folder: --

המכון לנוכחות ציבורית
המרכז הישראלי לאמנות דיגיטלית, חולון
לחומרי המקור צרו קשר דרך archive@digitalartlab.org.il

The Institute for Public Presence
The Israeli Center for Digital Art, Holon
For original materials please contact us at archive@digitalartlab.org.il

מכון לנוכחות ציבורית
INSTITUTE FOR PUBLIC PRESENCE
معهد للحضور الجماهيري

SCIENTIFIC OBJECTIVES OF THE MARS 94 MISSION

Main scientific objectives of this mission are to investigate the evolution of Mars, that is of its atmosphere, surface, its interior. To reproduce the planet's evolution history it is necessary to make with various methods wide-scale comprehensive studies, of those physical and chemical processes which continue there now and which took place in the past. Along the Earth-Mars trajectory interplanetary space parameters will be measured and some astrophysical observations conducted.

Scientific experiments should help solve the following problems:

The Mars Surface:

- Topographic survey of the surface including high-resolution studies of terrain;
- Mineralogical mapping;
- Elemental composition of the soil;
- Studies of the cryolithozone and its deep structure.

The Atmosphere and the Climatic Monitoring of the Planet:

- Studies of the martian climate;
- Abundance of minor components in the atmosphere (H_2O, CO, O_3, etc.), their variation, vertical distribution, search for regions with higher humidity;
- Plotting of the 3D field of atmospheric temperatures;
- Pressure variations of different space and time scales;
- Typical features of the atmosphere near the volcanic mountains;
- Characteristics of atmospheric aerosol;
- Neutral and ion composition of the upper atmosphere.

The Inner Structure of the Planet:

- Crust thickness;
- Magnetic field;
- Heat flow;
- Search for active volcanos;
- Seismic activity.

Plasma:

- Parameters of the martian magnetic field; its momentum and orientation;
- The 3D distribution function; the ion and energy composition of plasma (near Mars and along the Earth-Mars trajectory);
- Plasma wave characteristics (electric and magnetic fields);
- The structure of the magnetosphere and its boundaries.

Astrophysical Studies:

- Localization of cosmic gamma-bursts;
- Oscillations of stars and the sun.

Reproduced from **MARS 94: A Brief Description**, published by the Space Research Institute, Russian Academy of Sciences; Vernadsky Institute of Geochemistry and Analytic Chemistry, Russian Academy of Sciences; and Babakin Center

MAPS OF THE SAMPLE FIELDS AND SUMMARY OF SURFACE SAMPLER ACTIVITIES OF VIKING LANDERS 1 AND 2

By

Henry J. Moore and Elizabeth M. Duwey, U.S. Geological Survey, 345 Middlefield Road, Menlo Park, CA 94025

As part of the activites of the Surface Samplers of the Viking Landers, an impressive number of tasks were accomplished for the scientific investigations on Mars. In general, these tasks resulted in the excavation of trenches during the acquisition of samples for the Biology, Molecular Analysis, and Inorganic Chemical Analysis experiments as well as special trenches for the Physical and Magnetic Properties investigations. During the course of investigations of the physical properties of the surface materials on Mars, maps of the sample fields that illustrate the results of the activities of the Surface Samplers have been prepared using stereoscopic and monoscopic techniques. In addition, tables that summarize the activites of the Surface Samplers (relevant to the Physical Properties Investigation) have been compiled. The maps and tables are attached with the hope that they might be useful to some scientific investigators and with the intent of illustrating the achievements of the Surface Samplers during the Primary and Extended Missions. The maps and tables are preliminary and have not been edited for conformity with the standards of the U.S. Geological Survey. They will eventually be part of a Professional Paper of the U.S. Geological Survey.

There are three generalized maps for each lander showing the sample fields: (1) prior to the excavation of the trenches, (2) at the end of the Primary Mission, and (3) at the end of the Extended Mission. The maps, which were originally prepared at 1/10 scale, are 1/25 scale. Each map shows, in the spacecraft coordinate system, locations of rocks and their informal names, areas and features and their informal names, and other features, such as the craters produced by engine exhaust gas erosion during landing (see map explanations). In the maps showing the sample fields at the ends of the Primary and Extended Missions, trenches are indicated by outlines and identified by letters and numbers that indicate the experiment for which the trench was excavated and the sequential number of the trench excavated for that experiment.

There are four tables for each lander. The first two summarize Surface Sampler activities for the Primary (Table C1A) and Extended (Table C1B) Missions of Lander 1. The second two summarize Surface Sampler activities for the Primary (Table C2A) and Extended (Table C2B) Missions of Lander 2. A few activities are not included such as temperature profiles for the Meteorology experiment, backhoe magnet cleaning sequences, engineering sequences, and activities during the interim period of Lander 2. Each entry in the tables has an item number, an activity identification or designation and number, the Local Lander Time when the activity occurred, achieved Surface Sampler positions, and remarks that describe the outcome of the activity.

Activity designations in the tables are correlated with abbreviated designations on the maps. The choice of designations is derived from the experiment or instrument for which the activity was performed and the associated number refers to the sequential number of the activity for that experiment. Trenches excavated during sample acquisitions for the Biology experiments are listed as Biology in the tables and BIO on the maps. Thus, Biology-1 (BIO-1 on the maps) is the first sample trench excavated by each lander for biological analysis. GCMS-2, a designation that refers to the Gas Chromatograph-Mass Spectrometer, is the second sample trench excavated by each lander for the Molecular Analysis experiment. GCMS is used both in the tables and on the maps. XRFS-12, a designation that refers to the X-ray Fluorescence Spectrometer, is the twelfth sample trench excavated by each lander for the Inorganic Chemical Analysis experiment. XRFS is used both in the tables and on the maps. Physical Properties-6 (PP-6 on the map) is the sixth trench excavated for the Physical Properties experiment. Designations for other activities, such as the construction of conical piles of surface materials, excavations of deep holes, and so forth, are indicated in the explanations on the maps and listed in a straightforward manner in the tables.

Detailed information on Surface Sampler activities and sequences can be obtained from Viking Flight Team documents: (1) Clark, L. V., Crouch, D. S., and Grossart, R. D., 1977, Viking '75 Project Summary of Primary Mission Surface Sampler Operations: VFT 019, one volume, and (2) Pike, D. D., Coulson, P. M., Crouch, D. S., and Yarbrough, J. P., 1978, Viking '75 Project Summary of Extended Mission Surface Sampler Operations: VFT 023, three volumes.

TABLE C2A. Surface Sampler Activities Related to the Physical Properties Investigation During the Primary Mission of Viking Lander 2

Item	Activity	Local Sol	Lander Time Hour	Min	Sec 1)	Surface Sampler Positions 2) Azimuth (degrees)	Extension (inches)	Elevation (degrees)	REMARKS
1.	Shroud Ejection	01	10	52	02	255.4	10.2	38.9	1. Shroud ejected at 3.2 m/sec, struck rock near footpad 3 at 3.7 m/sec, ricocheted from rock impacting surface 0.6 m beyond rock, and came to rest 1.1 m beyond rock. Rock near footpad 3 moved a small amount as a result of the impact.
2.	Biology-1, Sample (Beta)	08	16	10	20	124.7	85.2 91.7 79.6	29.1 -- --	2. Trenched by extending in crusty to cloddy material after surface contact and then retracting. Trench is about 3.5 cm deep, 7.0 cm wide, and 41 cm long from tip to rim crest of tailings. Sample delivered to Biology; coarse fraction purged to XRFS funnel but no sample was received. Small lumps in and around trench are probably clods. Collector head tip reached about 5 cm below surface.
3.	Backhoe Touch-down-1	21	10	08	58	216.3	93.6	30.0	3. Backhoe penetrated crusty to cloddy material 1.3 ± 0.2 cm. Collector head tip does not touch surface.
4.	GCMS-1, Sample (Bonneville)	21	10	10	19	216.3	93.6 88.8 97.3 91.2	30.0 -- --	4. Trenched by retracting after surface contact, extending in crusty to cloddy material, and then retracting. Trench is about 2-3 cm deep, 6.0 cm wide at far tip, and 28 cm long. Collector head tunneled beneath crust forming dome of crust near tip. Platy fragment of crust near 5 cm across and 1 cm thick was moved by backhoe.
5.	Purge (GCMS-1, coarse)	21	10	53	46	190.4	99.9	36.3	5. Purged material was greater than 2.0 mm; fragment 2.7 cm across and additional finer grains or clods 2 mm and larger were purged.
6.	Biology-2, Sample (Beta)	28	16	10	31	126.0	85.2 91.7 79.6	23.1	6. Trenched by extending in crusty to cloddy material after surface contact and then retracting. Trench is about 2.5 to 3.0 cm deep, 8-9 cm wide, and 45 cm long from tip to rim crest of tailings. Sample delivered to Biology.

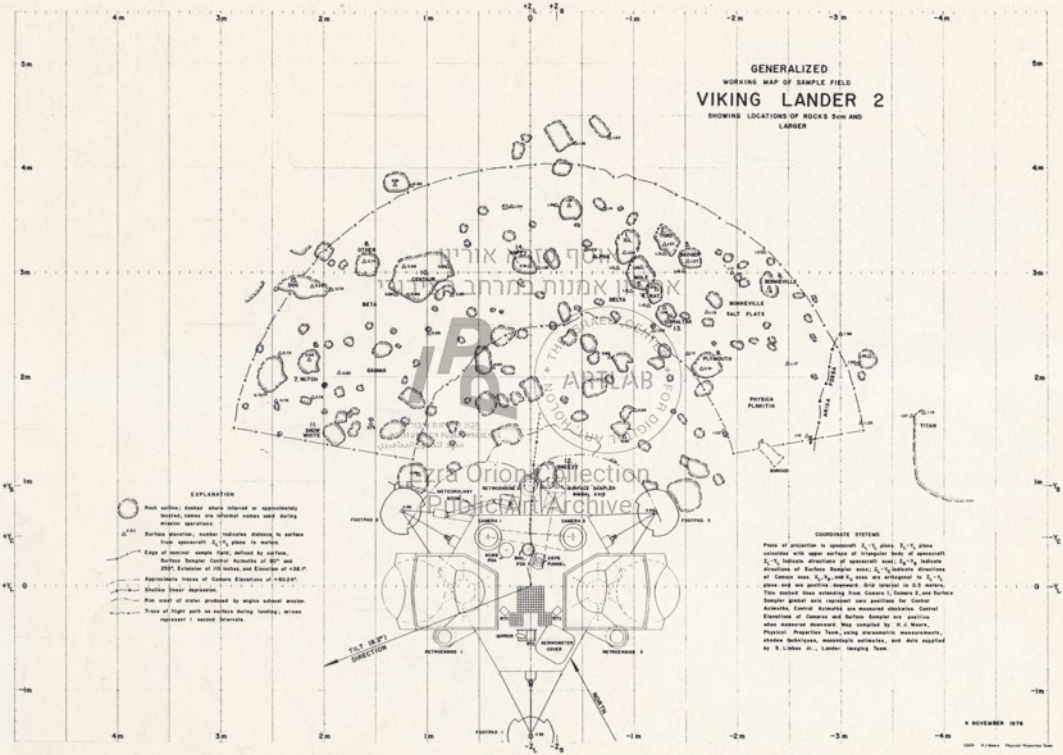
GENERALIZED
WORKING MAP OF SAMPLE FIELD
VIKING LANDER 2
SHOWING LOCATIONS OF ROCKS 5cm AND LARGER
EXPLANATION
COORDINATE SYSTEMS
4 NOVEMBER 1976

מוזיאון ישראל, ירושלים
the israel museum, jerusalem
متحف اسرائيل ، أورشليم - القدس

SCULPTURE ON MARS
Working Paper No. 2

1. Background

1.1 Following the positive decision of the Israel Museum to endorse the proposal of the sculptor Ezra Orion to establish an Israeli American team to plan and execute a Robotic Sculpture on the face of Mars, a robotic activity that is aimed to combine with the landing and the scientific activity of the NASA Mars Rover which is planned for the mid-90's - Yigal Zalmona (Curator of Israeli Art at the Israel Museum), Amnon Barzel (Director of the Luigi Pecci Contemporary Art Museum, Prato, Italy) and Ezra Orion met with Prime Minister Shimon Peres on 30.12.85 and presented him with this proposal.

1.2 Synchronically several personalities in the art scene were approached and asked to join a public supporting board for the project. So far we have received positive replies from: Mr. Mark Scheps, Director of the Tel Aviv Museum, Dr. Micha Levin, Chief Curator, The Tel Aviv Museum, Professor Hagai Netzer, Chairman of the Astrophysics and Astronomy Department, Tel Aviv University, Dr. W.W.L. Beeren, Director of the Stedelijk Museum, Amsterdam, John Perreault, Director of the Snug Harbor Cultural Center, Staten Island, New York; Philip Leider, Art Critic, Bezalel Academy of Art, Jerusalem; Professor Newton Harrison, Visual Arts Department, University of California at San Diego; Pierre Restany, Art Critic, Paris; Mr. Yona Fischer, Art Adviser, the Israel Museum, Jerusalem; Professor Akiva Flexer, Departament of Geophysics and Planetar Sciences, Tel Aviv University; Susan Goodman, Chief Curator, The Jewish Museum, New York;

1.3 Working Paper No. 1 was sent from the Prime Minister's Bureau to Dr. James C. Fletcher at NASA on 12.5.86.

1.4 NASA's answer to our message was sent back on 1.8.86.

91012 jerusalem, israel, pob 1299, cables: isramuseum, telephone (02) 698211 ירושלים 91012, ת"ד 1299, טלפון (02) 698211

2. Our Consideration of NASA's Reply

1.2 NASA's teams are presently beginning the process of defining the goals of the next mission to planet Mars, and their scientific and technological implications.

2.2 Up to this stage, the main objective of the Mission was defined: to analyze, in situ, samples in selected sites; to collect selected samples into a spacecraft returning to earth.

3.2 NASA does not presently see a possibility of including in this framework the suggested execution of stone sculpture on the face of Mars, which we proposed in our working paper No. 1.

4.2 The mission will be composed of two spacecrafts: a landing craft, which will return the samples to Earth; a mobile one for analyzing, in situ, collecting the samples, loadingthem into the waiting spacecraft, and returning to Earth.

3. Our Suggestions

1.3 We understand that the timetable of the Mobile Spacecraft (Mars Rover) will be overcrowded from the landing stage to completion of the loading of the samples into the spacecraft waiting to return to Earth. We assume that after the take-off the Mars Rover will commence a process of geographical survey of the planet. We assume that this stage will be more relaxed, and suggest considering the feasibility of executing the sculptural project within it.

2.3 We suggest that the sculptural work be a straight line on 100m. length, which will be made by positioning 20 local selected stones each 5m. apart We suggest that the site for the work be on the edge of the Vales Marineris cliff (see page 109 of the enclosed book "Sculpture in the Solar System"). However, we believe that it will be of pioneering human value even on a regular plateau.

3.3 We assess that the execution ofthe work, according to this plan, will not require any extra technological equipment for the Mars Rover, and could by fully accomplished by it.

4.3 We assess the time needed for the work to be done at 10-12 hours.

4.3 We assess that the photography of this process and of the finished sculpture could be received here on Earth. This will be the documentation for the art community and for the international public.

6.3 We suggest holding a meeting in the near future for the establishment of an American-Israeli team for clarifying the different aspects of the project, and the different possibilities of including it in the steps of conception, planning and realisation of the Mars Mission.

Yigal Zalmona

Amnon Barzel

Dr. Michael Levin

Ezra Orion

A rock is a universe, a slowndown, an aphemeral particles accretion. The particles are 20 billion years old, universe old --
Astronomy today identifies a cosmos which stretches across 20 billion light years ($2X10^9$) carries a suspence of uncountable galaxies of a billions "solar systems" and spiralic tempests of luminous gas. About 1/10% of the total mass of the cosmos is rocky deserts. In one arm of "our" galaxy, some hundred billion suns. We cruise, encircling its galactic center once in 250 million years so that we passed here last time in the Permian, and before then in the Cambrian -- and next -- in a quarter billion years time.
Light of receding galaxies, emitted billions of years ago, is reaching us now, so that we observe them as they were, a tele-flashback into an infinite astro-past -- The microscopic self infers the remoteness of its existence, meaninglessly, aimlessly cruising the intergalactic vastness, except for those who will be generated by its spiritual force. It shapes micromasses by its minute ability, thus joining, for a split second, the cosmic sculpturing processes --
Tectonic sculpture of the rocky crust of the earth, of Mars -- The erosion of the rocky, crumled, broken crusts — is an Erosional sculpture. Expanses of dunes are the shifting nations of quartz. On the face of the open stretches of the north pole of Mars, a sea of dunes is adrift. This is an Eolic sculpture. Rocky deserts are constantly bombarded by the salvos of meteors. The shaping of a crater-stoning is a Meteoritic sculpture. Etna, Vezuvius, saint Helen, Copernicus, Hellas, Olympus Mons, Tharsis; The basaltic Marias, the sea of rains, the sea of storms, Mare Serenitatis, Mare Nubium are Volcanic sculpture --
We encircl the sun at a rate of 30 kms. per second -- and the galactic axis at 220 kms. per second -- traversing the intergalactic infinity, with the Milky Way, at a speed of 300 kms. per second --
On November 28, 1964, the USA launched the "Mariner 4" toward the planet Mars. If flybyed that desert some 8000 miles from it and photographed for the first time from this range, its barren rockiness. "Viking 1" was launched from Cape Canaveral on August 20, 1975, arriving near Mars 10 month later, and its "Lander" touched down on July 20, 1976. The "Lander's" arm scratched the Martian dust for samples and removed some stones in a search for signs of life.

In summer 1982, I contacted the "Jet Propulsion Laboratories" in Pasadena, USA and met some scientists there. As a result of these talks, I proposed to perform, with the Lander's arm, a sculptural act: erecting a stone on another stone, vertically, and running a sequence of simulations of this act in a similar desert area in the west of USA.
A year later I proposed to the JPL to perform on Mars a sequence of robotic sculptural acts by means of the vehicle "Mars-Rover" now being developed for the nineties, and to run a series of simulations accordingly.
Valles Marineries is a canyon labyrinth splitting along 4000 kms. East-West of the equatorial of Mars, as a result of powerful extensional tectonic efforts in its geological past, somewhere in its middle, along its northern edge, stretches a huge cliff, rising 4 kms. to 9 kms. above its bottom, overlooking the Coprates chasm or abyss, 800 kms. in length. I proposed directing the "Mars-Rover" to the edge of this cliff, performing a geo-sculptural survey and laying a few rows of stones along this cliffs edge, by sequences of radio instructions from Earth. The desert works which I carried out on the rims of the Tzin cliffs here might serve as a model.
As the erosional processes on the Martian surface are as slow as astonomical time, these geometrical works will disappear only after billions of years -- This is an advancement of the sculptural launching pads by hundreds of millions of kms., outward, into the astro-abysses --

אוסף עזרא אוריון

Mars Terrain Design Environment

Ben Clark

MARTIN MARIETTA

— — סֶלַע הוא יקום — —
מְסלע הוא הָאטוֹת, הצטופפוּיוֹת חולפות בשטף אבק החלקיקים —
גיל החלקיקים הוא כ־20 מיליארד — — גיל יקום — —
האסטרונומיה מזהה כיום חלל המשתרע לקוטר של 20 מיליארדי
שנות אור (2×10^{9}); נושא תְּרחִיף אֵינספוֹר גאלאכּסיות ספיראליות
בנות מיליארדי "מערכות שמש" וסופוֹת גאז זוהר — —
כ־1/10% מכלל מסת היקום היא מְסלע — — מדבריות — —
— — באחת מזרועותיה של הגאלאכּסיה "שלנו", כמאה מיליארד
שמשות, אנו דוֹאים; מקיפים את הציר הגאלאכּתי כאחת למאתיים
וחמישים מיליון שנה — — כך שעברנו "כאן" לאחרונה בעידן פֶּרם;
ולפני כן בעידן קֶמבּריום; ונעבור כאן שוב בעוד רבע מיליארד — —
אור גאלאכּסיות מתרחקות, אשר שאגר לפני מיליארדי שנים, מגיע
אלינו עכשיו, כך שאנו צופים בו לתוך עבר אינסופי — —
— — האני המיקרוסקופי מסיק את נִידְחוּת קיומו. אין לו משמעות או
שחר על פני הטווחים האלה מלבד אלה שיטענו בו כוחות רוחו — —
מעצב מיקרו־מסות בכוחותיו המְזעריים; מצטרף עשירית שנייה
לתהליכי הפיסול הקוסְמיים — —

— — פיסול טֶקטוני של הקרום הסלעי של כוכב ארץ, של מאדים,
של מדבריות דוֹאים יקוּמים מכאן — — בליית פני קרומים סלעיים,
מקוּמטים, שבורים היא פיסול אירוזיבי — — מרחבי דיונות הם מִישורי
נדידת עמֵי קווארץ אינסופיים — — על פני מרחבי הקוטב הצפוני של
מאדים נע ים־דיונות — — זהו פיסול אֶאוֹלי — —
מדבריות סלע מורעשים ללא הרף במטחי מטאוריטים — — עיצוב
סקילה מכתשי — — זהו פיסול מטאוֹריטי — — בקיעי הלבּה
ששפעו כאן בקְרֵטיקון התחתון, ובמיליונים האחרונים, אֶתנה, וֶזוב,
סנט הלן — — קופרניקוס, הֶלַס, אולימפּוּס מוֹנס, טָרסיס — —
מְריות הבזלת, ים הגשמים, ים הסופות, מָרֶה סֶרֶניטטיס, מרה נוּבּיוּם,
הם פיסול וולקאני — —

ב־28 לנובמבר 1964 שיגרה ארצות־הברית את החללית "מרינר 4"
לעבר מאדים וזו חלפה על פניו (flyby) ב־14 ביולי 1965 במרחק של
מעט מעל 8000 מיל וצילמה, לראשונה מטווח זה, את המדבר ההוא.
"ויקינג I" שוגר מכף קרנבל ב־20 באוגוסט 1975, הגיע והחל מקיף
אותו ב־19 ביוני 1976 והנחית "לֶנדֶר" על פניו ב־20 ביולי. זרוע ה"לנדר"
גירדה את פני האבק והזיזה אבנים מספר בחיפוש אחר סימני
חיים — —

בקיץ 1982 יצרתי קשר עם "המעבדות להנעה סילונית" פסדינה,
ארצות־הברית, ונפגשתי שם עם כמה מדענים. בסופן של שיחות אלו
הצעתי לבצע בזרוע ה"לֶנדר" אַקט פיסולי: הצבת אבן על אבן, אנכית.
וכהכנה לאקט זה לבצע סִדרה של סימולציות בשטח מדברי דומה.
כשנה לאחר מכן הצעתי ל־J.P.L. לפסל על מאדים פיסול רובוטי על־
ידי רכב "מַארס רוֹבֶר" שנמצא עתה בפיתוח לקראת שנות ה־90,
ולבצע סדרת סימולציות באותו כיוון.
— — וָלֶס מרינֶרִיס (Valles Marineris) הוא מבוך קניונים המבקע
לאורך כ־4000 ק"מ את אזור קו המשווה, כתוצאה של מאמצי
התרוממות ומתיחה טקטוניים. בחלקה המרכזי של מערכת קניונים זו
משתרע קו מצוק שאורכו כ־800 ק"מ, חומת סלע אנכית, שגובהה
כ־9000 מ' המהווה את שפתה הצפונית של תהום קוֹפּרֵטֶס
(Coprates Chasma). אל שפת מצוק זו הצעתי להסיע "מארס
רובר" כדי לערוך לאורכו סקר גיאו־פיסולי, לאתר אתרים לפיסול ולבצע
בסדרות של פקודות רדיו מתוּוֹת של אבנים מקומיות אל שפתו כשקוי
האבן שעיצבתי על שפת מצוקי הצין, כאן, מהווים להם דגם — —
— — מאחר שתהליכי הבליה על המאדים איטיים כזמן האסטרונומי,
ייִמחו מתווי אבן גיאומטריים אלה רק לאחר מיליארדי שנה — — זהו
קידום כְּנֵי שיגור של ההכרה מאות מיליוני ק"מ מכאן אל תוך
האסטרו־תהומות — —

JERUSALEM ISRAEL
1994

IAF-94-P.3.319

VISIONS OF MARS: A CULTURAL AND SCIENTIFIC EXPERIMENT ON MARS 96

Louis D. Friedman, Walker E. Giberson, Jon Lomberg

The Planetary Society
Pasadena, CA 91106 USA

Terry Cole

Jet Propulsion Laboratory,
California Institute of Technology
Pasadena, CA 91109 USA

45th CONGRESS OF THE INTERNATIONAL ASTRONAUTICAL FEDERATION

October 9-14, 1994 / Jerusalem, Israel

VISIONS OF MARS: A CULTURAL AND SCIENTIFIC EXPERIMENT ON *MARS 96*

L.D. Friedman, W.E. Giberson, J. Lomberg
The Planetary Society
Pasadena, California
T. Cole
Jet Propulsion Laboratory
Pasadena, California

Abstract

The Mars 96 mission scheduled to be launched by Russia in November 1996, will deploy two small stations as fixed landers on the martian surface. The Planetary Society conceived the idea of placing an artifact on these landers, which would serve as a gift to the future human explorers of Mars. The artifact is a CD-ROM, primarily containing works of science fiction literature about Mars, which were instrumental in inspiring the current generation of space scientists and engineers to explore this planet. Because of the nature of the small station design, the CD had to be physically placed inside the spacecraft at a location that could not be visible from the outside where it was hoped the human explorers might someday visit. Thus, an additional requirement was developed: to place a label on the outside of the spacecraft with information for finding and playing the CD. The requirement led to the development of a scientific experiment known as MAPEX: the microelectronics and photonics exposure experiment. It provided an opportunity for innovative development of miniaturized technology to be employed on a planetary spacecraft, on an extremely short time scale and at very low cost. Six scientific instruments plus a "nanolith microdot" comprised the MAPEX experiment. The scientific experiments basically measure incoming radiation falling on the lander in such a way that it is recorded in the experiments for eventual recovery and analysis (there is no telemetry or data storage and the eventual human or conceivably robotic explorers would have to pick up these experiments and analyze them in a laboratory). The scientific experiments were conceived and developed at the Jet Propulsion Laboratory Micro Devices Laboratory. The Planetary Society selected the text, audio and pictorial contents of the disc and produced it as an interactive CD ROM with the assistance of Time Warner Interactive. The discs were manufactured by Digipress Corporation in France. The Digipress CD is made of silica, in order to ensure its lifetime of at least 100 years. The MAPEX will be mounted on a label which is to be placed on an exterior surface of the lander in a way that will be obvious to future explorers of Mars.

Background

Before our technology caught up with our dreams, the way to Mars was pointed out by the great writers of science fiction. Those who built and operated the robot explorers, **Mariner** and **Viking**, and those who are now designing new missions for robots -- and for humans -- often recall how they were motivated by reading about space travel in works of fiction. Truly, the first adventures in space exploration were cooperative ones of fiction and reality, interacting in the minds of the explorers.

Visions of Mars is a collection of science fiction text, audio and images on a compact disc that chronicles humanity's fascination with Mars and its imagined martians. A copy

of the disc will be placed inside each of the two small stations that **Mars 96** (formerly **Mars 94**) will land on the surface of the Red Planet in October 1997 (References 1 and 2; Figure 1). This collection is a gift from our era to the future generations of humans who will one day explore, and perhaps settle, Mars.

The **Visions of Mars** project consists of three major elements: the CD- ROM, which will be placed inside the **Mars 96** spacecraft; a label on the outside of the spacecraft, designed to direct any future finder to the CD-ROM; and a scientific experiment, known as MAPEX (microelectronics and photonics exposure experiment), which will record the radiation that falls on the outside of the spacecraft. This paper gives a summary description of each of the components.

The CD-ROM

The contents of the **Visions of Mars** CD-ROM were selected to show how human beings in different cultures and different times have imagined that planet. Selections represent 26 nations and four centuries. Astrological and mythological references were deliberately excluded, as the intent was to show humanity's evolving appreciation of Mars as a neighboring world rather than as a god or mystical force.

During the selection process, the editors consulted recognized experts from several countries in the fields of science fiction literature, planetary astronomy, astronomical and science fiction art, and radio broadcasting. The contents fall into four major categories: text, images, radio broadcasts, and greetings from Earth to Mars. The first three categories were limited to existing work (plus explanatory and introductory material supplied by the editors). The messages in the last category were specially created for the disc.

The disc opens with photographs of and short quotations by Konstantin Tsiolkovskii and Robert Goddard, the two humans most responsible for initiating the efforts that allowed us to send spacecraft to Mars. The title, **Visions of Mars**, appears on screen in English and in Russian, and various names for the planet appear in the scripts of 10 languages: Sumerian (cuneiform), Chinese/ Japanese, Greek, Thai, Hebrew, Arabic, Inuktitut (Eskimo), Sanskrit, Korean, and Armenian.

The text falls into three groupings: (1) works of science fiction, (2) writings by scientists about Mars, and (3) introductory and appended material included to help contextualize the writings to an audience of humans living on Mars in the future. The works of science fiction include 73 short stories, full novels, and novel excerpts by writers from 13 countries: the United States, Russia, Canada, England, Northern Ireland, France, Germany, Italy, Japan, Finland, Argentina, Syria, and Kirghizia. All works are recorded on the disc in the language in which they first appeared.

The earliest works include a fragment of a verse by 10th-century poet, Abul Ala' al Murray, inspired by the red color of the planet, and passages from Jonathan Swift (1726) and Voltaire (1752) describing the two martian moonlets well over a century before their actual discovery. Modern Mars fiction starts with Percy Greg's Across the Zodiac (1880), and the roster of authors includes many of the great names of the genre. The fiction selection effort was coordinated through the Merril Collection of Science Fiction, Fantasy, and Speculation in Toronto, with assistance from the distinguished editor and anthologist Judith Merril, librarian Lorna Toolis, writers John Robert Colombo and Mark Washburn and many other people and institutions around the world.

Fifty-four images of Mars from many countries were selected from the genres of science fiction illustration, astronomical art, and popular culture (films, comic books, cartoons). Works include realistic paintings of Mars and spacecraft, science fiction book

and magazine covers, movie posters from Aelita and Flash Gordon, a poster of the Russian Phobos spacecraft from the Space Research Institute of the Russian Academy of Sciences, and a famous Warner Brothers' cartoon character named Marvin Martian. For those of you who may have forgotten, Bugs Bunny prevented Marvin from blowing up the Earth "because it blocked his view of Venus." Besides these images, 12 drawings of Mars and martians by contemporary children from different countries are included.

The audio portion of the disc includes selections from three radio programs about Mars, including a rare tape that was supplied to the editors by Arthur C. Clarke. A documentary prepared in 1976 by the Canadian Broadcasting Corporation about the Viking 1 landing on Mars, with commentary by science-fiction luminaries Robert Heinlein, Ray Bradbury, and Gene Roddenberry, is included. The tape was made the night the first lander touched gently down. The "Radio Mars" selections are linked by narration read by the distinguished actor Patrick Stewart, who plays the role of Captain Jean-Luc Picard in the Paramount Television series Star Trek: The Next Generation.

Short videotaped greetings from 20th-century Earth to the future inhabitants of Mars were recorded by people of four nations who have played key roles in science fiction, astronautics, and planetary astronomy. The speakers are Carl Sagan (U.S.), Arthur C. Clarke (Sri Lanka), Judith Merril (Canada), and Vyacheslav Linkin (Russia). Each sends a message of hope and good wishes to those humans on Mars who may someday recover the disc and hear their words.

The CD-ROM was produced by Time Warner Interactive. The manufacturer of the CD was the Digipress Corporation of France, selected because of its expertise in the manufacture of archival discs made of silica. The silica discs were chosen over conventional polycarbonate CDs after an extensive analysis and review of environmental test data. Our requirement was that the disc last at least 100 years on the hostile martian surface (with very cold temperatures and direct ultraviolet and cosmic ray radiation). No conclusive data showed that polycarbonate discs would not last in that environment, but environmental tests did show outgassing and thereby raised some concerns about the viability of the discs over the long term. Archival discs made of silica are expected to last indefinitely.

The location of the CD-ROM on one of the petals of the small station was chosen by the Russian scientists responsible for the vehicle. The CD-ROM will be mounted on an electronics box built by the Jet Propulsion Laboratory for the Mars Oxidant Experiment that will also be included in the mission.

The Exterior Label

The 120 mm X 30 mm label was designed to fit on the inside of the small station petal (which, when it opens up, becomes the outside). It contains just enough information for the eventual finders to locate the CD-ROM. A picture of it is shown in Figure 2. The label contains a brief message in the five principal languages involved in the Mars 96 lander: Russian, French, Finnish, German, and English. The text is as follows:

This spacecraft was launched from Earth in 1996. Inside is an 8 cm disc (CD-ROM) with recorded text, sounds and images. This disc is a gift for the future explorers of Mars.

The diagram on this plaque shows where the disc is. An aluminum-gallium-arsenide laser reads the surface and a computer decodes and shows the contents. The silicon chip on this plaque contains instructions for playing the disc and an explanation of the devices on this chip. These appear in letters 1 micron high in the center of the chip.

The label is gold anodized aluminum and has a place (as shown) for attachment of the microchip described in the next section. The picture shows the location of the CD-ROM on the spacecraft (cf. Figure 2).

MAPEX

MAPEX is a passive material science technology experiment developed by the Jet Propulsion Laboratory's Micro-Devices Laboratory (MDL). The purpose is to provide a lightweight, passive way to measure the effect of long-term martian environmental exposure (50-100 years) on key microelectronics and optoelectronic components of the late 20th century. Material studies and active operational tests would be conducted before and after the mission to determine whether there is damage and/or degradation in performance. This concept is envisioned as a precursor to more advanced active monitors that might one day be placed on all spacecraft to record their environmental history.

Salient features of this experiment include small size (less than 5 square centimeters), light weight (20 grams), and simplicity -- thereby incurring low cost and accelerated development and fabrication time. A unique aspect of the experiment is that complete documentation on the experiment design will be recorded on an embedded nano-lithograph and CD-ROM, providing future explorers with suitable directions on how to retrieve and interpret the results (Reference 3).

MAPEX includes silicon microchips, assorted optoelectronics components --laser diode, Positive-Intrinsic-Negative (PIN) doped photodiode, optical fibers -- and passive sensors to monitor temperature excursions extremes, total dose radiation, cosmic ray radiation, sunlight intensity, and surface dust accumulation. The entire experiment is passive (there is no power requirement).

The Planetary Society Visions of Mars label provides a target of opportunity for the MDL experiment -- a chance to put in place a miniature martian environmental station for the benefit of future explorers. The Space Research Institute of the Russian Academy of Sciences agreed to carry the MAPEX as part of the Visions of Mars project.

Acknowledgments

The Planetary Society would first like to acknowledge the cooperation of the Space Research Institute of the Russian Academy of Sciences, particularly V.M. Linkin, Principal Scientist of the Mars 96 Small Station, for agreeing to carry Visions of Mars and assisting in its development. The Jet Propulsion Laboratory Mars Oxidant Experiment team, particularity Frank Schutz, Barbara Brown and Arthur Lane, also assisted.

Time-Warner Interactive, particularly Blake Lewin and James Bumgardner, cooperated with an agreement to program and manufacture the flight CD-ROMs and to produce replicas for Earth sales and promotion. A generous agreement with The Planetary Society enabled technical work to be performed at little cost to the Society, and royalties from CD-ROM sales will go both to The Planetary Society's research and development projects and to the Space Research Institute.

Digipress agreed to manufacture the silica CD-ROM at no cost to The Planetary Society, as a donation for future Mars explorers.

The Jet Propulsion Laboratory Micro-Devices Laboratory, particularly Martin Buehler and Paul Maker, conceived MAPEX and suggested its incorporation onto the Visions of Mars label. The innovative ideas of the MDL made Visions into an interesting scientific technology project, as well as a cultural one. The MDL also agreed to produce, at cost, an electro-beam lithography "dot" of the names of all Planetary Society members to be included on MAPEX together

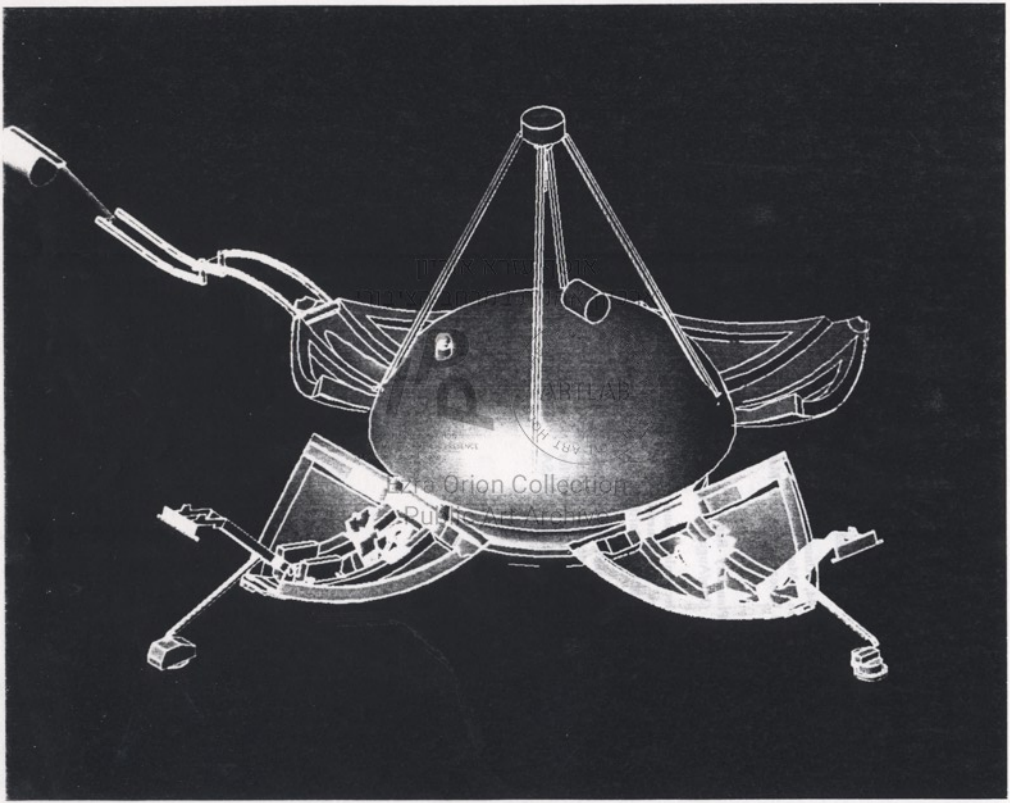

FIGURE 1

with the documentation already on the chip. Thus, we are able to also thank the approximately 100,000 members of The Planetary Society whose interest in Mars exploration makes all our work possible.

References

1. **Mars 94, Unmanned Spacecraft Mission to Mars, Brief Description**, Space Research Institute, Moscow, 1992.

2. **The Planetary Report**, Vol. XIV, No. 4. (July/August 1994), pg. 25.

3. **Microelectronics and Photonics Exposure Experiment: MAPEX**, May 6, 1994, by Martin G. Buehler of the Center for Space Microelectronics Technology, Office of Space Science and Instruments, Jet Propulsion Laboratory for the Office of Space Science, NASA.

FIGURE 2

VIKING

PROJECT REPORTS

(1)

from the barriers the plateaus form islands with teardrop shapes (Fig. 2). Many plateau remnants are regularly terraced, possibly as a result of differential erosion of strata in the plateau material, or they could represent terraces from progressively lower fluvial levels. Toward the northwest the outliers of plateau material are less affected by the channeling process and appear to have undergone erosion by mass wasting along the margin, producing hummocky terrain.

In the southwest part of the A1 area, the lightly cratered plains have been etched, or stripped away in angular patches, to reveal a light toned, topographically lower, and presumably stratigraphically older unit (Fig. 3). Two possible agents of removal are wind and water. The exact stripping process is not known but the removal of material has been influenced by local structure. The general trend of the etched zone is parallel to Tiu Vallis and suggests a genetic relation to the formation of the channel. The northern end of the etched zone grades into incipient chaotic terrain, indicating that the etching may have been initiated or enhanced by ground-sapping processes.

At about 37.5°W and 22.5°N, 250 km northwest of the original A1 site, a channel segment possibly related to Tiu Vallis cuts through plateau material. The floor of the channel in this area is characterized by a network of fractures that are several hundred meters wide and several kilometers long. The general trend of the fracture system is parallel with the channel: a less pronounced set of fractures is transverse to the channel axis.

Knobs occur throughout the plains unit and range in size from several hundred meters to several kilometers across. They appear to be of diverse origin—some have distinct summit craters and are interpreted as volcanic in origin (perhaps cinder cones), others appear to be erosional remnants of plateau material, and still others are undoubtedly remnants of degraded and nearly buried crater rims. Small pancake-shaped features superimposed on both plains and etched terrain are interpreted to be constructional features possibly of volcanic origin (Fig. 3). Central craters and knobs, and possible dikes, support this interpretation.

On rev 10, 80 frames were taken of an area centered at 23°N, 43°W, close to the center of the Chryse basin (Fig. 1). It was anticipated that the region would be free of the fluvial features, etched terrain, and upland remnants that characterized the original A1 area. This prediction was largely fulfilled. Most of the area consists of lightly cratered plains, which in the western part are typified by north-south trending marelike ridges. Two islandlike, streamlined remnants of plateau material occur within the plains. Each remnant is topped with a 5-km-diameter, partly filled crater. Knobs as much as 1 km across occur throughout the area, but the density is greatest in the southeast. Overlying the smooth plains are craters up to 18 km in diameter.

In the search for a landing site on the west side of the Chryse basin, two areas were photographed. The first, centered on 49°S, 22°N, was photographed on rev 20; the second region, centered at 55°W, 22°N, was photographed on rev 22 (Fig. 1). Both regions, being to the west of the center of the Chryse basin, are at a higher elevation than the area photographed on rev 10.

As anticipated, both these areas show evidence of channeling related to Kasei Vallis and other channels farther south. The rev 20 coverage (which includes the final landing site) can be divided into two halves according to the degree of channeling. In the western half, channel-sculptured terrain is common (Fig. 4); in the east are mainly plains that resemble the lunar maria, and which are a continuation of those described above. They are crossed by ridges which, like those on the lunar mare, usually consist of two parts—a low broad linear rise on top of which is a narrower, more steeply sloping ridge. The ridges are mostly north-south trending and are spaced approximately 40 km apart. The plains surface is less cratered than the lunar maria and several ghost craters suggestive of filling are present. In common with other areas observed, the ejecta around large craters are sharply delineated and appear to consist of several flow lobes. The gradual transition from chaotic ejecta outward into secondary crater fields, characteristic of lunar craters, is rarely seen.

The western half of the area photographed on rev 20 has been extensively modified, apparently by fluvial action. Channels appear to have originated to the west and flowed eastward through the area toward the center of the Chryse basin. The whole region is sculptured by linear channels that wind through the

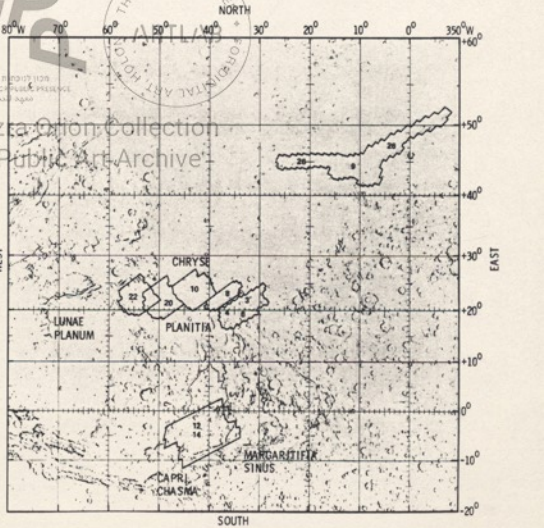

Fig. 1. Index map to show Viking orbital photographic coverage prior to the Viking 1 landing. Orbit numbers for the coverage are indicated. The Viking landing site is in rev 20 coverage.

of the atmosphere increases more rapidly with depth less than 15 km than does the atmospheric density. Infrared thermal mapper temperature measurements, which have a very broad weighting function but which center near 20 km, show that the highest tropical haze layers cannot be CO_2 ice.

Discrete clouds, as distinct from diffuse regional haze, seem to have several morphological forms. The classical white clouds of Tharsis, known for decades to observers on Earth, are seen in Fig. 11b, which was obtained through a violet filter at a range of 300,000 km as Viking 1 initially approached Mars. Images taken when this region was clear to the morning terminator do not show these clouds, and we hope that orbital images will provide additional information about their growth phase. They were observed by Mariner 9 only when fully formed (*12*).

Several diffuse bright clouds of similar size have been seen within the morning haze in the north. Figure 11c shows one covering about 40 square degrees that appeared near the final A1 landing site on rev 28. It contrasted more with its surroundings in this violet image than in a corresponding red one. Images 6 minutes apart revealed no motion with respect to surface features; an upper limit on its motion is estimated to be 10 m/sec.

Equatorial clouds seen thus far are much less diffuse and are made up of many patches with dimensions of a few kilometers. Figure 12a shows one seen on rev 4 at 23°W, 1°S. It is typical of condensate clouds and showed much higher contrast in violet light than in red. Its motion was 46 ± 3 m/sec westward. Since no shadows were identified, the height of the cloud above the surface is unknown. However, such clouds appear to have a convective structure and are inferred to be within a few kilometers of the surface. Westward cloud motions at speeds ranging from 15 to 45 m/sec are expected theoretically in this region and at this season (*13*). This east-west flow is part of an expected anticyclonic circulation around the Chryse basin.

Similar clouds were also detected in low-altitude vertical imaging of candidate landing sites, as illustrated in Fig. 12b, which shows a portion of two C1 site mosaics centered at about 40°W, 4°S. Frames in the second mosaic were taken two martian days after those in the first mosaic under similar viewing conditions. Both sets of frames were acquired through a clear filter and have been processed in such a way as to enhance high spatial frequencies. Sequences designed to provide stereoscopic coverage of the landing sites yield repeated coverage of those regions over time intervals of about 2 minutes. Changes in position and appearance of these cloudlike features over such short time intervals confirms them to be atmospheric phenomena.

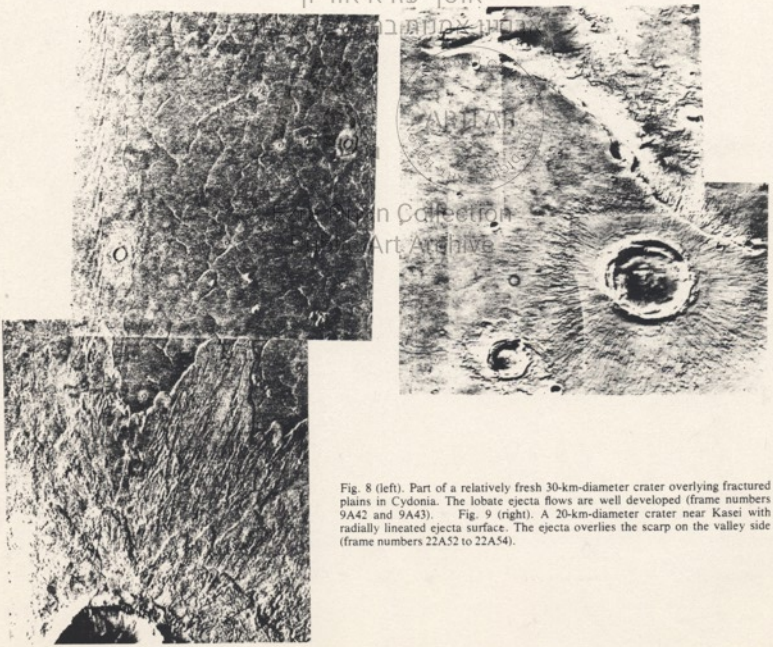

Fig. 8 (left). Part of a relatively fresh 30-km-diameter crater overlying fractured plains in Cydonia. The lobate ejecta flows are well developed (frame numbers 9A42 and 9A43). Fig. 9 (right). A 20-km-diameter crater near Kasei with radially lineated ejecta surface. The ejecta overlies the scarp on the valley side (frame numbers 22A52 to 22A54).

area and cut across one another. Lenticular bars are common, as are convergent and divergent flow lines. Immediately upstream from the mare ridges sculpturing is often absent as though the fluid pooled there and had little erosive capability. Where gaps occur in the mare ridges the flow lines converge, indicating funneling of the flow through the gap (Fig. 4). Deeply incised channels occur downstream of the gaps. At the southern end of the channeled area the flow appears to have been contained and diverted by a large ridge. The sculptured area over which flow has presumably occurred is approximately 150 km wide. The length of the channels will not be known until more photographs are taken to the southwest. The general impression is of a flood, fairly evenly spread over a large area with very shallow slopes. The northern end of the rev 20 coverage includes part of Kasei Vallis. Again, as in the south Chryse region, long, lenticular, plateau remnants occur and linear striae attest to east-west flow. A low escarpment with a rectilinear outline, which seems to be unsculptured by flow, marks the edge of Kasei Vallis. The scarp consists mostly of intersecting alcoves that give it a serrated outline, although there are some linear sections. In general, it lacks streamline forms. Isolated areas of plains, surrounded by an escarpment, occur within the Kasei Vallis. Large craters superposed on these escarpments suggest a very old age (Fig. 5).

South of Kasei the region photographed on rev 22 can be divided east-west into two broad areas. In the east is a continuation of the lightly cratered plains. They resemble lunar maria and in the south are extensively sculptured by channel processes. The western half of the region is distinctively different from any region yet photographed. From the Mariner 9 data, it appears that a narrow strip of ancient cratered terrain separates Lunae Planum from Chryse Planitia. Numerous large craters within the strip typically have subdued rims and indistinct ejecta patterns, somewhat similar to those of the craters in the C site area described below. The plains between craters are, however, extremely hummocky and are crossed by several channels that are distinctly different from those at the C site. A section of one channel, which runs approximately east-west at 21°N, resembles some of the larger lunar rilles such as Schröters Valley. Other channels farther south have rounded cross sections and numerous tributaries. All appear to empty onto the plains to the east. These channels are quite old with numerous superposed impact craters. The hummocky deposits in the west on the lunarlike mare plains also appear to be relatively old, since ejecta from several large craters covers both upland and plains.

Fig. 2. Photomosaic to show teardrop "islands" on the southern side of the Chryse basin. The islands consist of remnants of the plateau material that forms a more continuous outcrop farther south. Here the plateau material has been largely eroded, apparently by fluvial action; craters on the upstream ends of the islands have protected the plateau material downstream of them from erosion. Each island is about 40 km long (frame numbers 4A50 to 4A54).

Cydonia region (B1 site). The Cydonia site (revs 9 and 26; 44°N, 12°W), as mapped from Mariner 9 (*4*), lies near the boundary between the mottled cratered plains and the smooth plains and includes the transitional boundary between mantled and unmantled terrain (*5*). The area shows a complex history of erosion and deposition. To the west and north, the surface is cut by a complex of curvilinear fractures typically 1 km wide and 10 km long that in plan view forms of a set of roughly polygonal-to-circular forms, most of which are 5 to 20 km across (Fig. 5). Southeast, the fractures seem to be buried by a younger unit that has undergone subsequent erosional stripping. This younger plains unit has a relatively featureless surface apart from superposed degraded craters.

Isolated angular-to-rounded mesas in the south are either (i) the remains of a once-continuous unit which overlay the fractured plains or (ii) the remnants of an ancient eroded surface projecting through the fractured plains from below. The mesas and fractured plains clearly underlie a younger plains unit to the southeast, which indicates that at least one phase of erosion occurred to produce the mesa landforms before deposition and erosion of the plains. Craters on surfaces below the plains are flat floored and have smooth rims surrounded by low, outward-facing scarps.

The youngest unit is a mantle of relatively bright material, probably of aeolian origin, that buried preexisting small craters. Other subsequently formed craters deposited ejecta from lower units on top

of the mantle. During a later phase of erosion most of the mantle in the southern and western part of the area was stripped away, presumably by aeolian activity, leaving material trapped inside small bowl-shaped craters, and under and within ejecta deposits. These remnants of bright materials throughout most of the region give the mottled appearance observed in Mariner 9 and Viking pictures.

The origin of the fractured plains is not immediately apparent. Although the fractures could be the result of cooling contraction of extensive, thick lava, the scale of the pattern is larger by an order of magnitude than is normally found in such rocks. Another possibility is that they are of tectonic origin, but the lack of a marked regional trend to the pattern does not support such an origin. The possibility that they are related to a deep permafrost layer is an attractive alternative. However, this layer of permafrost would have to be abnormally thick. The region shows an extremely complex history of volcanic, tectonic, aeolian, and, possibly, periglacial processes, which yield a complex variety of landforms and materials.

Capri Chasma region (C1 site). On revs 12 and 14, frames were taken of the C site at 6°S, 43°W, one of the alternative sites for the second lander. The site is adjacent to Capri Chasma, a branch of the equatorial canyon system. The area outside the canyon is characterized by numerous large, flat-floored, subdued craters, between which are areas of relatively smooth intercrater plains. North of the site are several areas of chaotic terrain in which several large channels appear to originate. The channels drain northward, converge with other channels, and ultimately debouch into the Chryse basin.

The views of the canyon are some of the most spectacular pictures yet acquired. Landslides (Fig. 6) are clearly visible on both walls. The walls are as much as 2 km high and display several stratigraphic units that erode differentially. The uppermost layer breaks into large blocks while the lower layers seem to have poor cohesion and exhibit more fluid flow. There are a few low hills or knobs on the canyon floor, some of which may be remnants of coherent materials that have slumped into the canyon. Much of the canyon floor is featureless, devoid even of craters at the limiting resolution of the cameras. This suggests that the canyon floor is relatively young, certainly younger than any other surface yet observed on Viking pictures. The presence of bright streaks and dune fields (Fig. 6) indicates an active aeolian regime. These observations imply that the canyon is enlarged by collapse of the canyon walls to produce debris flows and removal of the material by wind. Although the causes of slope failure are uncertain, groundwater sapping or undercutting by aeolian action (or both) may be contributing processes (6).

Most of the large (> 50-km-diameter) craters in the region are flat-floored and have low rims; their ejecta appears to be covered by intervening plains material, indicating that the craters are older than the plains. However, some large craters are younger than the plains and have well-developed albeit subdued ejecta. Strings of secondary craters are abundant in some areas. Since Mariner 9, the origin of the intercrater plains has been a subject of some controversy. It has been variously ascribed to ballistic and base surge phenomena associated with impacts (7), atmospherically redistributed impact debris and weathering products (8), and volcanic activity (9). The layers in the canyon wall provide a cross-sectional view of the plains, and the morphology of the landslides provides an impression of the mechanical properties of the near-surface materials. It is possible that coherent layers resistant to erosion form the surface and that they are underlain by more easily erodible, less coherent materials. An inter-

Fig. 3. Photomosaic to show the light-toned, "etched" terrain on the southern side of the Chryse basin. Also shown are light, domical features (*v*) thought to be volcanic shields. The mosaic covers an area about 60 km from top to bottom (frame numbers 4A78 to 4A81).

Wave clouds have been observed in midmorning images of the equatorial region. A wave pattern can be seen in the lower left corner of Fig. 12b, but some better examples are found in Fig. 12c. A comparison with frames of the same area taken on another day indicates that many discrete albedo features in Fig. 12c, such as bright splotches and crater tails, are

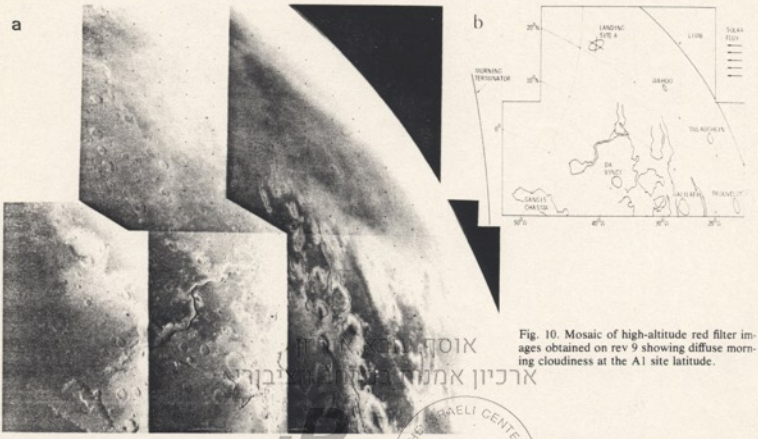

Fig. 10. Mosaic of high-altitude red filter images obtained on rev 9 showing diffuse morning cloudiness at the A1 site latitude.

Fig. 11. (a) Southern hemisphere winter limb in the Noachis region imaged in red light from medium altitude on rev 22. (b) Large white clouds on the western flanks of Olympus Mons (upper) and Ascraeus Mons (lower), imaged through a violet filter during approach. (c) White cloud near the A1 landing site imaged through a violet filter on rev 28.

on the surface, but that the whole area is overcast with a nonuniform haze. The presence of wave clouds, presumably composed of water ice, provides an indication of the wind direction and of the static stability of the atmosphere (*14*). Observed wavelengths are on the order of 10 km.

At the lower right of the images in Fig. 12d is a bright patch seen in Capri Chasma from high altitude on rev 4. It does not obscure or diffuse surface detail, therefore it evidently lies closer to the surface than the resolution limit (about 2 km). It may be either a fog of water ice or possibly a thin frost patch. The former seems rather more likely in view of the smaller amount of water required to produce the observed brightness.

No direct evidence for dust clouds has been seen in early Viking 1 orbiter images, although the presence of micron-size dust particles could well be postulated in some of the haze without contradicting the observed characteristics.

On the basis of preliminary examination of about 1000 frames obtained from Viking 1 orbiter, the following conclusions are reached.

1) Most of the surfaces examined are old. Crater frequencies on the various plains range from one-tenth that of the lunar maria to approximately the same as the lunar maria. Only the floor of Vallis Marineris is significantly younger, on the basis of crater frequencies.

2) Despite the seemingly old age, of almost all the surfaces so far photographed, small craters are preserved, thereby suggesting that aeolian erosion is extremely slow.

3) Abundant new evidence of catastrophic floods has been revealed in the southern and western margins of the Chryse basin; however, no evidence for a thick accumulation of sediments was found in the middle of the Chryse basin.

4) One mechanism for growth of the equatorial canyon system is slumping of the canyon walls into the canyon and subsequent removal of the slumped debris by wind.

5) In most of the areas examined, crater ejecta morphology is distinctively different from either the moon or Mercury; the principal mechanism of ejecta emplacement appears to be surface flow rather than ballistic deposition.

6) At 44°N numerous intersecting cracks on the surface of the plains form polygonal patterns reminiscent of patterned ground in the Arctic regions of Earth.

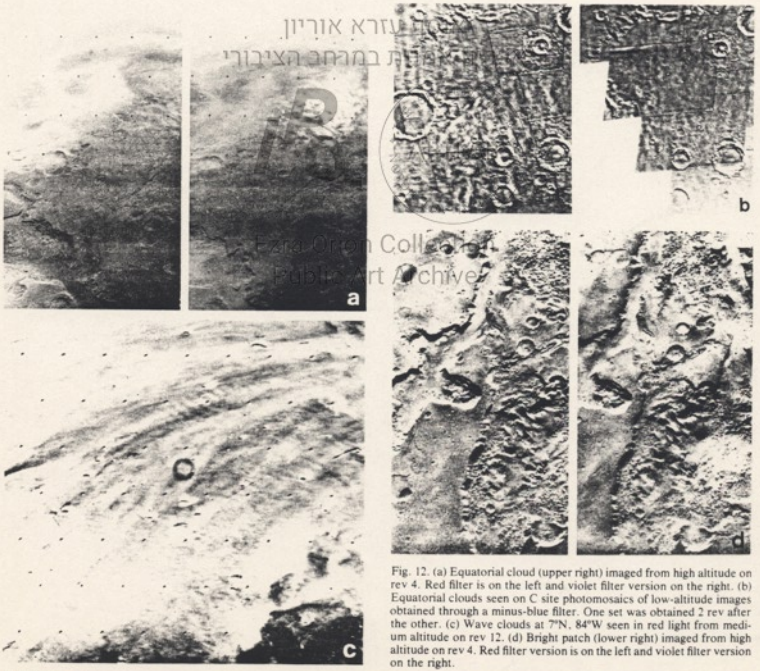

Fig. 12. (a) Equatorial cloud (upper right) imaged from high altitude on rev 4. Red filter is on the left and violet filter version on the right. (b) Equatorial clouds seen on C site photomosaics of low-altitude images obtained through a minus-blue filter. One set was obtained 2 rev after the other. (c) Wave clouds at 7°N, 84°W seen in red light from medium altitude on rev 12. (d) Bright patch (lower right) imaged from high altitude on rev 4. Red filter version is on the left and violet filter version on the right.

pretation of the general terrain of the C1 area is that it is composed of highly brecciated rocks of the ancient cratered terrain overlain by plains-forming deposits. The origin of the plains is not clear but the volcanic hypothesis is supported by the presence on the surface of numerous ridges and scarps similar to those on the lunar maria.

The close relation between fluvial features and chaotic terrain, noted on the basis of Mariner 9 observations, is clearly seen in the northern part of the site (Fig. 7). An area of chaotic terrain 50 km across is at the head of a series of fluvial-like features. The surface at the head of the channel appears to have collapsed into a jumbled, chaotic mass of debris, as though the underlying material had been removed. The area to the west has been sculptured and shaped into streamlined forms, suggesting flow to the west. The channel-like feature can be traced about 400 km to the west, where it passes off the edge of the photographic coverage into the region of the Hydrocates Chaos from which the channels of the Simud Vallis originate. These latter channels lead to Chryse Planitia, where the first Viking has landed. It thus appears that some of the materials that were carried out of the chaotic terrain in the C site ultimately may have been deposited far to the north, close to the present Viking landing site. The origin of the chaos and the channels is still unclear, but massive removal of subsurface materials, including a transporting fluid, is amply demonstrated.

Fig. 4. Photomosaic of the landing site region in Chryse. Channeling is seen to the west (left). To the middle and right the plains have ridges similar in appearance to lunar mare ridges, implying that the plains were formed by extensive lava flows. The distance across the mosaic is about 240 km.

Fig. 5. Photomosaic of the fractured plains (*pf*) and overlying plains (*p*) in Cydonia. Eroded mesas of plateau material (*pl*) appear to have been exhumed by scarp retreat of the plains material. The area shown is about 120 km across (frame numbers 9A62 to 9A64).

Craters. Craters with fresh ejecta blankets and associated secondary craters were rarely seen in Mariner 9 pictures. It was predicted that, because the surface gravity on Mars is about the same as it is on Mercury, martian craters would have a similar morphology to those on Mercury (*10*) with the secondary crater field much closer to the crater rim than on the moon, where the surface gravity is less. Viking pictures, however, show that fresh craters do exist on Mars and that at least in the areas photographed, the morphology (Figs. 8 and 9) is dissimilar to that on Mercury or on the moon. Fresh craters are surrounded by lobate flow scarps and ridges, outside of which, in some cases, are bright rays and secondary crater clusters. The ejecta were apparently emplaced largely by flow. On arrival at the surface from ballistic throwout, the ejecta may have transformed to a fluidized sheet, possibly as a result of melted and vaporized ice or entrapped atmospheric gas. The lack of this distinctive ejecta pattern on the moon and Mercury may be explained by their lack of atmospheres and subsurface ice.

Not all martian craters have the same form. Many are degraded to smooth forms with flat floors and are encircled by an erosional scarp that faces outward. However, other apparently fresh craters, such as those near Kasei (Fig. 9), have closely spaced radial lineations on the continuous ejecta and few or no lobate forms. Whether such differences between fresh craters result from different states of target material or from other parameters remains to be determined.

Another striking characteristic of the areas photographed thus far is the presence of fresh crater clusters and irregularly shaped craters similar in form to lunar secondary craters. Some of the smaller clusters can be related to nearby

fresh craters but there are other, often extensive clusters, particularly at the C site, which are not obviously related to large fresh craters. It is possible that some craters resembling secondary craters result from the impact of meteoroid showers produced by breakup of a large meteoroid on entry into the martian atmosphere.

Variable features. Four types of variable features (*11*) are prominent in the Viking orbiter pictures: (i) bright streaks associated with craters, (ii) bright streaks associated with small hills, (iii) dark streaks associated with craters, and (iv) sand dune fields. These were compared with the available Mariner 9 coverage to determine the changes that have occurred since 1972. As a result of the increased resolution of the Viking photography, many more small craters and streaks are visible in the Viking images. Comparison with the Mariner 9 data shows that the bright streaks are generally unchanged in direction and outline since 1972, although in a few places they have increased in size or new bright streaks have appeared.

In the Chryse region dark streaks are less prominent than bright streaks and trend southwest to northeast, opposite to the bright streak direction. The dark streak direction coincides with the regional wind flow expected at the present season (northern summer). The bright streak pattern defines wind flow from northeast to southwest, the direction of strong winds that are expected during southern summer dust storms. The directions and outlines of bright crater streaks are unchanged since the Mariner 9 coverage in 1972, thereby confirming the speculations that bright streaks, unlike some dark streaks, are stable over many martian seasons and are unaffected by the weaker winds that occur during the present season. Evidently, the winds responsible for the formation of the dark streaks did not significantly modify the bright ones.

Westward across the Chryse basin the bright streak direction shifts from an azimuth of 220° to 230° near 34°W to 255° near 58°W, a pattern consistent with that observed by Mariner 9. Wind streaks appear to be concentrated in regions that look generally smooth at orbital picture resolution. This correlation of streak density with terrain type may be valid down to roughness scales of tens of centimeters since, for example, in the rev 20 coverage the only large area that appears to be smooth but which is devoid of streaks appear rough to radar. There is supporting evidence, based on Mariner 9 data, that wind streaks are best developed in regions where the areas between craters are relatively smooth.

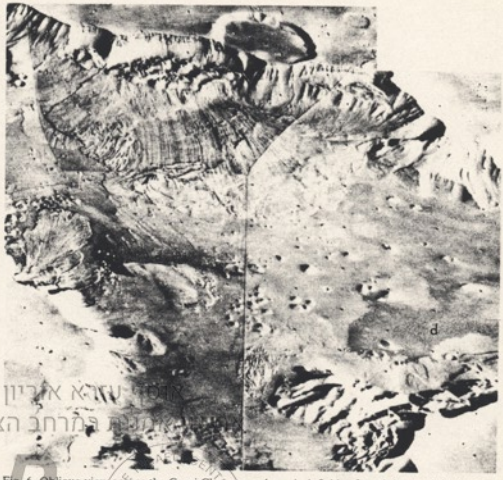

Fig. 6. Oblique view across the Capri Chasma to show dark fields of sand dunes (*d*) in the floor of the canyon, and landslides on the walls. Distance from foreground to background is about 150 km; the canyon is about 2 km deep (frame numbers 14A29 to 14A32).

No wind directions in the Cydonia region can be mapped because the area lacks streaks that are associated with craters and other evident wind markers. At least during this season (northern summer), wind transportable material appears not to move; either the texture of the surface is too coarse, or the fine particles are effectively bound together. The annual dust storm fallout that probably blankets the area after perihelic dust storms could be swept up effectively into the numerous troughs which occur in this region. Significantly perhaps, some of the troughs show definite signs of infilling by high albedo material.

In the Capri region, bright streaks trend northeast to southwest and are unchanged in orientation and outline since 1972 (Mariner 9 data). Low albedo dune fields occur on the floor of neighboring Gangis Chasma (Fig. 6). Bright, streaklike markings behind hills on the canyon floor are common in the vicinity of dune deposits and may represent protected areas where no sand has accumulated. The directions of these bright streaks associated with hills show that the dominant regional northeast to southwest wind flow is channeled by the canyon walls into a general east-west direction.

High-altitude pictures of the Oxia Palus region show that the general albedo boundaries and bright streak patterns are unchanged since 1972. Nevertheless, conspicuous albedo changes have occurred in some localized areas, such as within and around the crater Galilaei. A new bright streak, trending south from a 4-km crater, has appeared since 1972, and a streaklike bright area emanating from a channel has grown significantly during the past 4 years. These areas will be studied at high resolution later in the mission.

Atmospheric phenomena. Numerous atmospheric phenomena have been observed in the orbiter camera images, both on approach and from high altitude in orbit. Approach images indicated that the atmosphere of Mars was then relatively clear in the southern hemisphere but obscuring hazes were present at all longitudes in the north. After Mars orbit insertion, most of the high-altitude images were acquired in order to monitor a broad area around the planned landing site for dust activity. In this coverage, taken from a range on the order of 30,000

7) Variable features, when compared to Mariner 9 pictures taken 4 years ago, show relatively little change.

8) Several types of clouds were observed, including diffuse morning hazes in the northern hemisphere, discrete equatorial white clouds, and extensive wave clouds.

9) A direct measurement of wind velocity from cloud motion was achieved for the first time.

MICHAEL H. CARR
U.S. Geological Survey, Menlo Park, California 94025
HAROLD MASURSKY
U.S. Geological Survey, Flagstaff, Arizona 86001
WILLIAM A. BAUM
Lowell Observatory, Flagstaff, Arizona 86001
KARL R. BLASIUS
Science Applications, Inc., Pasadena, California 91101
GEOFFREY A. BRIGGS
Jet Propulsion Laboratory, Pasadena, California 91103
JAMES A. CUTTS
Science Applications, Inc., Pasadena
THOMAS DUXBURY
Jet Propulsion Laboratory, Pasadena
RONALD GREELEY
University of Santa Clara, Santa Clara, California 95053
JOHN E. GUEST
University of London Observatory, London, NW72QS, England
BRADFORD A. SMITH
University of Arizona, Tucson 85721
LAURENCE A. SODERBLOM
U.S. Geological Survey, Flagstaff
JOSEPH VEVERKA
Cornell University, Ithaca, New York 14853
JOHN B. WELLMAN
Jet Propulsion Laboratory, Pasadena

References and Notes

1. J. B. Wellman, F. P. Landauer, D. D. Norris, T. E. Thorpe, *J. Spacecraft Rockets*, in press; T. E. Thorpe, *Icarus* **27**, 229 (1976).
2. L. Tyler, personal communication.
3. D. H. Wilhelms, *U.S. Geol. Surv.* (1976), p. 1-895; H. Masursky, N. J. Trask, M. E. Strobell, A. L. Dial, G. W. Colton, *U.S. Geol. Surv. Map*, in press; D. Milton, *U. S. Geol. Surv.* (1974), p. 1-894.
4. M. H. Carr, H. Masursky, R. S. Saunders, *J. Geophys. Res.* **78**, 4031 (1973); D. Scott, *U.S. Geol. Surv.*, in press.
5. L. A. Soderblom, T. J. Kreidler, H. Masursky, *J. Geophys. Res.* **78**, 4117 (1973).
6. R. P. Sharp, *ibid.*, p. 4073.
7. M. Malin, thesis, California Institute of Technology (1976).
8. B. C. Murray, L. A. Soderblom, R. P. Sharp, J. A. Cutts, *J. Geophys. Res.* **76**, 313 (1971).
9. D. E. Wilhelms, *ibid.* **79**, 3933 (1974).
10. D. E. Gault, J. E. Guest, J. B. Murray, D. Dzurisin, M. Malin, *ibid.* **80**, 2444 (1975).
11. Variable features were first defined during the Mariner 9 mission to mean surface albedo patterns which changed with time; the term has since been used to include all surface forms that are commonly attributed to aeolian or wind processes [C. Sagan *et al.*, *J. Geophys. Res.* **78**, 4163 (1973)].
12. C. B. Leovy *et al.*, *ibid.*, p. 4252.
13. J. B. Pollack, C. B. Leovy, Y. Mintz, W. Van Camp, *Geophys. Res. Lett.*, in press; P. W. Webster, in preparation.
14. J. A. Pirraglia, *Icarus* **27**, 517 (1976).
15. We thank the following people for their untiring help during the early hectic stages of this mission: J. Boyce, P. S. Butterworth, K. W. Farrell, E. A. Flinn, H. Ferguson, A. Jankevics, K. P. Kaasen, C. Leavy, B. Lucchitta, J. MacQueen, T. E. Poe, Jr., G. Schaber, A. Spra[illegible], E. E. Theiling, D. T. Thompson, and T. [illegible] Thorpe. Financial support for the work of [illegible] members was provided by NASA Viking Proj[illegible] Office, NASA Office of Planetary Geology (R.G.), and U.K. Natural Environment Research Council (J.E.G.).

26 July 1976

Viking: Mars Atmospheric Water Vapor Mapping Experiment—Preliminary Report of Results

Abstract. *Observations made from the Viking 1 orbiter show very little water vapor in the Mars atmosphere in the southern hemisphere (0 to 3 precipitable micrometers) with a gradual increase across the equator to northern latitudes. Maximum amounts between 20 and 30 micrometers have been observed in the short period covered by the observations to date. The season, northern midsummer, corresponds to the beginning of the water vapor cycle in that hemisphere. A strong repetitive diurnal cycling between the solid and vapor phases is observed at a site to the east of the Tharsis Ridge at 10° north latitude; the vapor lies close to the martian surface and is most probably in saturation equilibrium with a surface haze or fog throughout much of the day.*

The water vapor mapping experiment is designed to determine the variability of the martian atmospheric vapor over a wide range of spatial and temporal scales. In order to separate the effects of spatial (global and vertical) and time dependent (diurnal, seasonal, and perhaps longer-term) characteristics, the study must take advantage of the maximum flexibility available from the orbital coverage of the planet, particularly in securing nonsynchronous observation periods (*1*) and continuing through the seasonal progression obtainable from the Viking extended mission. Many of the characteristics of the martian water vapor, and especially those related to its variability, have been indicated by the behavior observed from Earth-based measurements (*2*, *3*), and the strategy for the present Viking orbital study is based in large part on a model for the interaction between the planet's atmosphere and surface or subsurface material which the past observations have suggested. Thus, one of the principal objectives of the Viking measurements is to refine or revise this model; in this context, the present report must be of a very preliminary nature, since only a very restricted set of measurements made over a relatively short time span from synchronous orbit has been possible so far. The period covered is from approach [Mars orbit insertion (MOI) − 2 days] through Viking 1 lander separation (rev 30), during which emphasis has of necessity been placed on observations related to the characterization of the landing sites. Therefore, many of the water vapor mapping observation sequences necessary for the investigation as a whole have not yet been initiated.

It is pertinent at the outset to comment on the timing of the measurements reported here with respect to the seasonal variation of martian water vapor. Orbit insertion occurred (19 June 1976) when the planetocentric longitude (L_s) of Mars was 84° (L_s = 90° corresponds to the northern summer solstice). The accumulation of data from Earth-based observations has revealed a seasonal variation in the appearance of the vapor coincident approximately with midsummer in each respective hemisphere and the maximum being reached some 2 months later. (The period of high vapor content and the time interval between the solstice and the maximum atmospheric vapor abundances are longer in the south than in the north.) Maximum values of about 50 precipitable micrometers (pr μm) averaged over a horizontal scale of ~ 10^3 km have been observed for both hemispheres, with the maximum apparently occurring at temperate latitudes. Against this framework the present observations have been made at the onset of the northern "wet" season, and have so far covered the southern (dry) hemisphere and northern latitudes to about 20°, with a few isolated afternoon measurements in the latitude band 40° to 50°.

Instrument and observations. The instrument, the Mars atmospheric water detector (MAWD), is a grating spectrometer operating in the 7200 cm^{-1} (1.4 μm) water vapor bands. Absorption by the atmospheric vapor of solar radiation diffusely reflected from the surface of the planet is measured by five radiatively cooled PbS detectors located in the exit focal plane of the instrument. The detectors are arranged so that, when the grat-

km, the site is seen in morning hours and each pixel spans about 800 m.

Figure 10 shows a mosaic of a typical high-altitude, five-frame sequence taken through a red filter by the Viking 1 orbiter cameras and processed without spatial frequency discrimination. Although some differences are seen from day to day, the general haziness of the morning sky in the northern hemisphere has looked much like Fig. 10 since Viking 1 arrived. The midday and afternoon skies are not visible for comparison, but the finding of diffuse morning cloudiness is consistent with long-term photography of Mars from Earth. On some days, high-altitude pentads have been obtained through violet and green filters as well as through red, and the overall differences in haziness are not very great.

In regions of Fig. 10 where surface features such as crater rims can be detected, the atmospheric extinction coefficient γ can be estimated from contrast measurements. Where craters are near the threshold of detection, the local values of γ for blue light turn out to be comparable with Earth's atmosphere on a relatively clear day, but values for red light are somewhat greater than on Earth. When expressed in terms of equal air paths, however, this morning scattering above threshold craters is fully two orders of magnitude greater than in clear Earth air. In regions of similar emission angles where craters exist but cannot be detected, the martian atmosphere is optically still thicker.

The morning haziness in the north that is shown in Fig. 10 would not, on the basis of photography from Earth, be expected to typify other latitudes and times of day. Indeed, Fig. 11a, which was obtained on 11 July 1976, shows a much clearer atmosphere around 50° to 60°S in midafternoon, where the extinction coefficient of red light was found to be $\gamma \sim 0.1$ per air mass. It was approximately winter solstice ($L_s = 93°$) in the southern hemisphere, thus the terminator lies only a few degrees below the bottom of Fig. 11a. In Viking approach images, there were bright patches in this region that did not obscure underlying topography and that contrasted more strongly with their surroundings in violet images than in red, but their nature is not yet clear, and further observations are planned for distinguishing between fog and frost.

Figure 11a, taken at a range of about 18,000 km, also illustrates well the layered structure of the atmosphere. From the foreshortening of craters, we infer the true surface limb to lie about 3 km under the bright low-altitude haze, while upper layers extend to nearly 40 km above the surface. At the limb, the low-altitude haze is optically thick, but the uppermost layer has an edge-on extinction of only about 0.3. This implies that the uppermost layer has a vertical extinction coefficient less than 0.01 per air mass, thus it plays very little role in the total atmospheric obscuration.

The height of the limb haze in the tropics has been estimated in an image from rev 4. Landmarks in the scene were used to locate the surface limb, which was more heavily obscured than in Fig. 11a. In the rev 4 image, the highest visible haze layer occurs at 25 km, and the height of unit optical depth on the limb (normal optical depth ~ 0.02) occurs at 15 km. Since the surface optical depth in the same region as judged from crater contrasts is ~ 0.5, the scattering power

Fig. 7. Photomosaic of a 120-km-long channeled area near Capri Chasma. The apparent source of the fluid that cut the channels is a depression enclosing chaotic terrain (right) which appears to have been formed by collapse (frame numbers 14A67 to 14A69)

Reports

The First Viking Mission to Mars

The Viking 1 lander has landed on Mars in the Chryse Planitia basin at approximately 22.5°N, 48.0°W and has begun to transmit data back to Earth.

Two unmanned 3500-kg Viking spacecraft were launched from the Kennedy Space Center on 20 August and 9 September 1975, by Titan-Centaur launch vehicles. Each spacecraft consists of an orbiter-lander combination. During the Earth-to-Mars cruise the spacecraft were relatively inactive, with some of the scientific instruments being exercised only for check-out and calibration. Viking 1 went into orbit about Mars on 19 June and Viking 2 will follow it on 7 August.

Viking 1 was placed into a Mars-synchronous orbit (period 24.6 hours) with its periapsis near the preselected landing site of 19.5°N, 34.0°W. Pictures of this region taken by the orbiter cameras indicated it to have features that may represent hazards, and nearly 4 weeks were spent in searching for a nearby landing site which appeared safe on the basis of the evidence of orbiter photography and Earth-based radar data.

On the 30th orbital revolution, the lander separated from the orbiter in response to a command from Earth, and 3 hours 22 minutes later it touched down on the surface at 11:53 G.M.T. on 20 July. Measurements were made of the properties of the interplanetary plasma, the ionosphere, and the atmosphere. Immediately after landing two pictures of its surroundings were taken by one of the lander cameras, and these were received on Earth and displayed within 1 hour.

At landing the local Mars time was about 4 p.m., the season was seven Mars days past the summer solstice in the northern hemisphere, the Earth-Mars distance was 341.5 million km or 19.0 light-minutes, and the orbital relation of the two planets was 128 days before solar conjunction.

The orbiter is currently in a synchronous orbit with a period of 24.61 hours, inclined 37.74° to the equator; the distance from the planet center is about 4900 km at periapsis and 36,000 km at apoapsis. On each orbit, it passes over the lander about 3 minutes before periapsis at an altitude of approximately 1500 km, at which time it receives a radio transmission of data from the lander for up to 40 minutes. This information is stored and transmitted to Earth shortly thereafter. A two-way direct radio link between the lander and Earth is established daily for about 1 hour, during which the program of stored commands in the lander's computer controller is updated and additional data are transmitted. The transmission of data collected by the scientific instruments on the orbiter is nearly continuous.

Orbiter and lander have begun to carry out their planned scientific investigations, which will continue for at least 40 days before the commencement of a similar mission by Viking 2. Preliminary results of the investigations are presented in the reports that follow (Table 1).

The Viking spacecraft. The Viking spacecraft (Fig. 1) consists of the orbiter, the lander capsule, and the lander support structure that is jettisoned by the orbiter after the landing. The orbiter is similar in construction and operation to the series of Mariner planetary spacecraft, particularly Mariner 9, which is in Mars orbit; but it is considerably larger and has expanded capabilities for the storage and execution of commands and for the storage and transmission of data. Like its Mariner ancestors, it is three-axis stabilized, solar-powered, and carries two antennas (high-gain parabolic and low-gain omnidirectional) for two-way communication with the NASA (National Aeronautics and Space Administration) Deep Space Network stations. To accommodate its passenger, the lander, it has a relay antenna for receiving the data transmissions from the Mars surface and facilities for supplying power and command information to the encapsulated lander and for accepting information from it so that the lander subsystems can be thoroughly checked out before separation. Some characteristics of the spacecraft are summarized in Table 2.

The Viking lander. The Viking lander is a three-legged 450-kg aluminum hexagonal structure. Within the body are the computer, power, data, thermal control, and science instrument systems. Mounted on top are the cameras, seismometer, antennas, and radioisotope thermoelectric generators to supply power. When attached to the orbiter, the lander is within a double capsule. It is nested in an aeroshell used during the descent. The other half of the capsule connects to a base-cover and parachute system. The second and outer capsule consists of a bioshield and base and cap. All systems in the lander were sterilized at 111°C for 40 hours just prior to launch. The bioshield cap was deployed after launch. The bioshield base was retained on the orbiter until after landing. The aeroshell was released in the Mars atmosphere as was the parachute and the base cover.

Viking 1 mission chronology. The spacecraft was launched from the Kennedy Space Center in Florida on 20 August 1975 into an orbit that would bring it

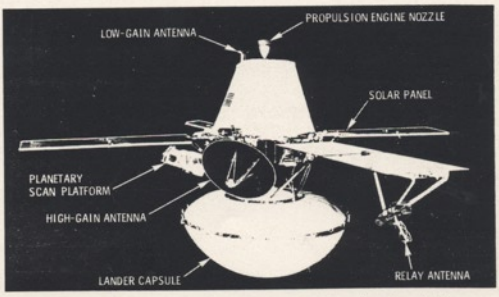

Fig. 1. The Viking spacecraft (the flag is upright in the launch configuration).

ing is in its nominal "locked" position, their locations correspond to the wavelengths of three relatively strong absorption features close to the band center, and two "window" regions which can be used to define the local continuum. The spectral resolution of the instrument, 1.2 cm^{-1}, allows a detection capability of < 1 μm, under average to good conditions of the observation geometry. A brief description of the instrument and a discussion of the choice of spectral region and channel frequencies has been given by Farmer and LaPorte (*4*).

Because the three line channels (at 7223.13, 7232.20, and 7242.74 cm^{-1}) span a range of transition intensities of more than an order of magnitude, the three independent values of absorption measured at each position of the instrument field of view on the planet's surface can be used to determine the total atmospheric pressure and temperature at the level at which the bulk of the vapor resides. These values, in turn, provide an indication of the height of the vapor above the surface. It should be pointed out, however, that under martian conditions all three lines are in the saturated region of their curves of growth and therefore such simultaneous solutions for column abundance (W), pressure (P), and temperature (T) can only be satisfactorily obtained under the most favorable conditions (that is, line of sight abundance > 30 pr μm and incidence and emission angles $< 60°$).

Most of the planetary data are taken with the instrument operating in the "locked-up" mode, that is, with the grating position servo fixed at the nominal line and continuum center frequencies. A second mode of operation is available in which the grating is scanned over a small angular range (corresponding to a frequency range of $\pm$ 8 cm^{-1} about each channel center frequency) to provide continuous spectral coverage of the region between 7215 and 7251 cm^{-1}. Instrument operation in the wavelength scanning mode is included occasionally in the observation sequences in order to monitor the spectral resolution of the five channels together with a number of other instrument functional parameters, and (initially) to verify the spectral details assumed for martian atmospheric conditions in the design of the instrument and the data reduction software.

The angular size of the instantaneous field of view (IFOV) of MAWD is 2 × 16 mrad, which corresponds to a spatial resolution of 3 × 24 km on the surface at a periapsis altitude of 1500 km. This field is stepped sideways by increments equal to the short dimension to provide a raster consisting of 15 contiguous elements covering a total area of ~ 20 × 45 km (at periapsis). The signal integration time for each IFOV is 0.28 second, so that the raster scan time, including flyback, is 4.48 seconds. The raster pattern is used in conjunction with the scan platform motion in the design of the individual observation sequences to provide the variety of low-resolution (high-altitude) and high-resolution coverages needed to carry out the vapor mapping investigation.

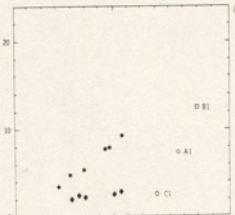

Fig. 1. Diurnal behavior of martian water vapor at three sites: (●) 10°,83° and (◆) − 15°,69° and − 17°,77°.

The data reduction and analysis programs are designed to enable the three parameters W, P, and T to be determined from the five measured channel radiances at the IFOV spatial scale, or from radiance averages taken over larger areas corresponding to one or more complete rasters. The extraction of water vapor data at degraded spatial resolution is important in that measurements can be made under conditions of greatly reduced illumination (for example, close to the morning and evening terminators) and which would otherwise be unreliable at the IFOV scale. This aspect has been of significance in the data taken so far because of the emphasis which has been placed on characterization of the landing sites: from the present synchronous orbit the accessible sites at all three candidate site latitudes (− 5°, 20°, and 44°) can only be viewed at local times within 1 or 2 hours of sunrise or sunset—indeed the solar elevation angle at the 44° prime site for the Viking 2 lander at the time of overflight of the Viking 1 orbiter is $< 10°$, and the corresponding signal radiance more than an order of magnitude lower than that required for reliable vapor abundance measurements at the highest (IFOV) spatial resolution. Thus, averaging over the area of some tens of rasters was necessary for the reduction of the B site data.

Approach observations. Several observations of Mars were obtained before orbit insertion. While intended primarily to be instrument performance checks, these approach observations allowed us to see, albeit at poor resolution, regions of the planet that are inaccessible from the Viking 1 synchronous orbit. Viking 1 approached Mars from the morning side, so the amounts of water measured on approach refer to midmorning abundances. In general, where comparison with later orbital observations was possible, the results were consistent.

Approach observations of areas not observed during orbital operations showed abundances similar to those obtained at about 90° west longitude from orbit, with a couple of notable exceptions. The approach observations of the Hellas–Sinus Sabaeus area, about 310° west, show three to four times as much water vapor as at points at corresponding latitudes on the planet. The other exception is the Elysium-Amazonis region, where we measure 30 μm, the largest abundance we have observed to date anywhere on the planet. We hope to be able to confirm the latter measurements later in the mission when we are able to observe the planet from an asynchronous orbit.

Diurnal behavior. One of the most powerful observational clues to the water cycle on Mars is the behavior of the abundance of water vapor at a particular location from sunrise to sunset. Very little water vapor can be retained in the vapor phase at low altitudes during the cold martian night; how rapidly it returns from the solid to the vapor phase when the ground and atmosphere start to warm up in the morning is controlled by whether the ice is on the surface, diffused into the soil, or suspended in the low atmosphere. When, and how rapidly, it returns to the solid phase as the atmosphere cools off in the afternoon and evening is controlled by how far up in the atmosphere the vapor manages to mix during the day.

In order to view a particular site at several local times in both the morning and evening, it is necessary to be in an asynchronous orbit. During the site certification time period the orbit was synchronized over the nominal A1 landing site, and we were therefore only able to get partial diurnal behavior at any particular location on the planet. We monitored three sites at coordinates (latitude, longitude) of 10°,83°; − 15°,69°; and − 17°,77° from dawn to local noon. The 10°,83° site was chosen because it was the site closest in latitude and elevation

to the A1 site which could be observed for an extended period of time; the second two were chosen because of their similiarity to the C1 site. None of the actual sites A1, B1, or C1 could be observed for an extended period of time from the Viking 1 synchronous orbit.

Figure 1 shows the diurnal behavior of the water vapor in the three areas, with the A1, B1, and C1 periapsis observations included for reference. The two C-site analogs had identical diurnal behavior; this, together with their topographical similarity to C1, leads us to believe that these southern areas are very

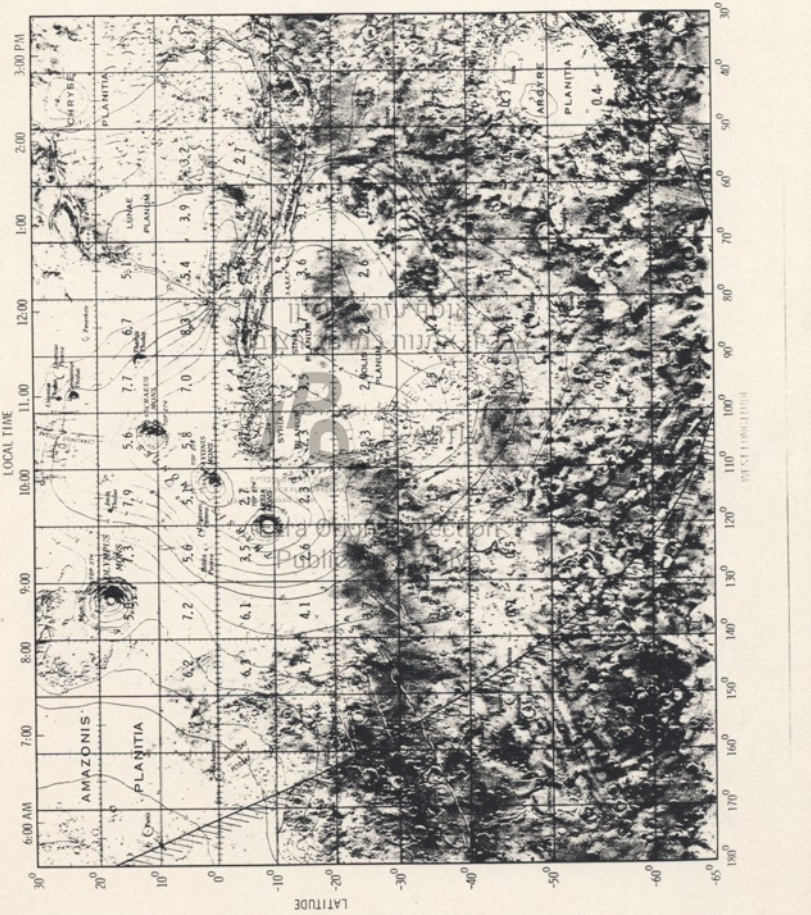

Fig. 2. Low-resolution map of total atmospheric vapor content (precipitable micrometers) from observations made approximately 1.5 hours before periapsis on revs 6 to 9, 12, and 13. The crosshatched line represents the position of the terminator.

similar in behavior, and that the composite diurnal behavior displayed by them is typical of the region just south of the equator in the vicinity of Valles Marineris at this season.

We do not expect 10°,83° to be a very good analog of the A1 site. The two areas are in different geologic regions, and the 10°,83° area is about 5 km higher. Therefore, it is not safe to assume that 10°,83° and A1 display the same diurnal behavior. Further comments on the inferences to be drawn from the diurnal behavior are given in the discussion below.

Low-resolution mapping. During the first 13 orbits, box scans were made of the planet at various times from periapsis. In general, the Viking 1 orbit allows extended observation sequences of the morning areas of the planet only; the afternoon and evening regions are overflown very quickly right at periapsis. The most extensive series of observations were made about 90 minutes before periapsis, while the spacecraft was viewing the region south of and including Tharsis and Valles Marineris. Figure 2 is a map of water abundance obtained by combining the results obtained from the high-altitude scans made on revs 6 to 9, 12, and 13. Also included for reference are the terminator (morning terminator on the left side) and the local time.

The most striking feature of the map is the strong latitude dependence of the water vapor abundance. Near the south polar cap we find < 0.5 pr μm; this value increases almost linearly with decreasing latitude across the equator to 20°, the northern limit of the observations. In Fig. 3 we have displayed the latitude dependence of the average vapor content between longitudes corresponding to 0930 and 1330 hours local time.

In the equatorial and northern latitudes shown in Fig. 2, the early morning longitudes show as much water vapor as the longitudes observed at local noon. If all sites displayed the same diurnal behavior as the 10°,83° site, we would expect to see an increase in vapor abundance from the morning terminator to noon; since this is clearly not the case, we must conclude that there are significant differences in the behavior of water vapor at different areas of the planet. In particular, compared to 10°,83°, the region to the west of Tharsis either reaches its maximum much earlier in the day or, if it has the same gradual buildup of vapor, must reach a value of some 15 to 20 μm by noon. In the latter case it is interesting to note (as mentioned in the section on approach observations) that the region about 70° west of Tharsis showed the largest amounts of water vapor we have so far observed. Selection between the two hypotheses will have to await observations from asynchronous orbit.

Table 1. Comparison of landing sites.

Site	Latitude	Longitude	Local time (hours)	Water vapor abundance (pr μm)
A1	20°	30°	1620	7.3 ± 1.2
B1	45°	10°	1800	12.4 ± 3.8
C1	−5°	45°	1530	2.7 ± 0.8

There is an indication from the map of an anticorrelation between elevation and water abundance in the area of the Tharsis Ridge. Measurements taken over Tharsis tend to be 20 to 50 percent lower than those over adjacent areas to the east and west. Part of this effect is due to the method of calculation used in these preliminary data. The calculated water abundance depends on the effective pressure assumed for the vapor. For the data presented in this report we have assumed a pressure of 6 mbar independent of location. If a lower pressure had been used, the calculated amount of water would have been higher—a 5-km change in elevation would produce a 25 percent change in water abundance, fairly close to the observed decrease over the Tharsis area.

Landing site comparison. As part of the site certification process for Viking 1, measurements of the water vapor over the original A1 site were obtained on revs 3 to 7. In order to help determine the latitude for the Viking 2 lander, observations were also made of two potential sites for Viking 2. Table 1 gives the relevant data for the three sites A1, B1, and C1. Errors quoted are 1 standard deviation. The A and C site data show the same trend of increasing water abundance to the north as the global map; the B site data indicate that the trend continues at least as far north as 45°. Since the B site is observed much closer to the evening terminator than the C site, and since it is hard to imagine a situation where the abundance would be increasing with time near dusk, lack of knowledge of the diurnal behavior in the late afternoon does not affect the conclusion that the B site has far more atmospheric water vapor during the day than does the C site.

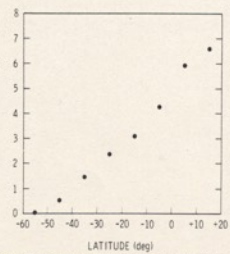

Fig. 3. Mean latitude dependence of water vapor between 0930 and 1330 hours local time.

Discussion. The linear character and repeatability of the growth of vapor at the diurnal site suggest that, at this location and season at least, the vapor is contained within the atmospheric layer closest to the surface. Although the local time at which the maximum of this daily cycle is reached is not observed in the data, it is clear that at least 80 percent of the vapor returns to the solid phase at some time between noon and the following dawn. The low altitude of the vapor on a planetwide scale at the time of maximum vapor abundance had been suspected from the results of Earth-based spectroscopy (5), which gave a rotational temperature for the water vapor (225°K) higher than that of the bulk atmosphere (204°K). In the present instance, the low altitude of the vapor is inferred from the fact that the only region of the atmosphere which undergoes sufficient diurnal temperature excursions (6) to cause the condensation and reevaporation of the measured quantities of vapor is the boundary layer—that is, the layer whose temperature is closely coupled to the temperature of the surface.

The sublimation of a layer of *exposed* ice deposited on the surface must be discarded as the direct source of the vapor observed at the diurnal site, because its lifetime in the solid phase at dawn would be too short to give the observed slow increase in vapor. For example, the insolation on a horizontal surface 1 hour after sunrise (4×10^{-3} cal cm^{-2} sec^{-1}) is equivalent to the latent heat of vaporization of 2×10^{17} mol cm^{-2} sec^{-1} of ice (assuming an albedo of 0.9), so that the lifetime of 10 μm of frost under these conditions would be about 5 minutes. The rapid evaporation of the surface frost at sunrise could, however, be the initial source of a ground fog, whose subsequent evaporation would produce the observed increase of vapor. The diurnal variation of vapor from exposed surface ice which does *not* pass through a second condensation phase to form an atmospheric haze layer would characteristically reach a maximum very early in the day, and this behavior may explain the trend observed in Fig. 2 for the region to the west of Tharsis mentioned earlier.

The presence of a ground fog is not unexpected, and has been discussed in recent papers by Flasar and Goody (*7*), Hess (*8*), and Farmer (*3*). While this is a possible explanation for the observed diurnal behavior (at 10°.83°), we cannot at present entirely rule out the release of vapor from ice entrained in the topmost layer of the regolith material, or the gradual reduction of opacity of a higher-elevation cloud layer above the vapor, as possible alternate explanations. Unfortunately, we have not yet obtained any high-altitude images of this area to aid in the interpretation of the data.

A further inference can be drawn from the fact that, since the vapor is still increasing at the time of the last diurnal observation, ~1300 hours, it is reasonable to assume that there is still some condensate in the atmosphere or near-surface layer at that time. This result suggests that some fraction of the water remains in the solid phase throughout the day; one interpretation of the latitude–time of day trend shown in Fig. 2 is that this fraction increases toward the northern midlatitudes. Hence we might expect that, as the northern summer progresses, the lower-latitude limit of the atmospheric condensate layers will recede, with a corresponding increase in the fractional amount of ice vaporized during the day, and a decrease in the amplitude of the diurnal vapor cycle as the vapor becomes mixed into the bulk atmosphere above the boundary layer trap. At this stage the meridional circulation will carry the vapor to the cooler latitudes (principally the winter hemisphere).

The Viking 1 orbital observations conveniently cover the period of the northern water vapor growth and decay, and the second spacecraft (Viking 2 orbiter) will give good polar coverage of the latter stages of this phase. The extended mission, with both spacecraft, will enable the progression of the seasonal cycle into the southern hemisphere to be followed. The mission plans for the orbiters thus present an excellent opportunity during the forthcoming months to study the variability of the vapor and its interaction with the surface of the planet over a wide range of spatial and temporal scales, and to test the validity of some of the theories which have been proposed to explain its cyclic behavior.

CROFTON B. FARMER
DONALD W. DAVIES
Jet Propulsion Laboratory, California Institute of Technology, Pasadena 91103

DANIEL D. LAPORTE
Santa Barbara Research Center, Goleta, California 93017

References and Notes

1. For a discussion of the orbit geometry and the corresponding opportunities for observational coverage, see G. A. Soffen and C. W. Snyder, *Science* **193**, 759 (1976).
2. See E. S. Barker, *Icarus* **28**, 247 (1976), and references contained therein.
3. C. B. Farmer, *ibid.*, p. 279.
4. ——— and D. D. LaPorte, *ibid.* **16**, 34 (1972).
5. R. A. Schorn *et al.*, *ibid.* **11**, 283 (1969); R. G. Tull, *ibid.* **13**, 43 (1970).
6. Day and night vertical profiles of temperature for this region of the planet at this season were obtained from Mariner 9 (IRIS); see B. Conrath *et al.*, *J. Geophys. Res.* **78**, 4267 (1973). The expected small variation in the diurnal temperature extremes for the bulk atmosphere above the boundary layer was first discussed by P. Gierasch and R. Goody, *Planet. Space Sci.* **16**, 615 (1968).
7. F. M. Flasar and R. M. Goody, *Planet. Space Sci.* **24**, 161 (1976).
8. S. L. Hess, *Icarus* **28**, 269 (1976).
9. A large number of people have contributed to the design and construction of the flight instruments, which have operated flawlessly, and to the development of the special-purpose computer and its software system used for the data analysis. We are grateful to all of these, whose enthusiastic involvement has ensured the success of the experiment. We thank especially W. Carls, H. Clark, J. Geiselman, E. Goldyn, S. Hanson, A. Holland, R. Kares, R. Killian, D. Langford, F. Murphy, J. Riccio, and D. Rupnik for their considerable efforts over the past months; this is submitted on their behalf. This report presents the results of one phase of research carried out at the Jet Propulsion Laboratory under NASA contract NAS 7-100.

26 July 1976

Infrared Thermal Mapping of the Martian Surface and Atmosphere: First Results

Abstract. *The Viking infrared thermal mapper measures the thermal emission of the martian surface and atmosphere and the total reflected sunlight. With the high resolution and dense coverage being achieved, planetwide thermal structure is apparent at large and small scales. The thermal behavior of the best-observed areas, the landing sites, cannot be explained by simple homogeneous models. The data contain clear indications for the relevance of additional factors such as detailed surface texture and the occurrence of clouds. Areas in the polar night have temperatures distinctly lower than the CO_2 condensation point at the surface pressure. This observation implies that the annual atmospheric condensation is less than previously assumed and that either thick CO_2 clouds exist at the 20-kilometer level or that the polar atmosphere is locally enriched by noncondensable gases.*

Experiment description. The Viking infrared thermal mapper (IRTM) contains four telescopes, each with seven detectors. Thermal emission from the planet's surface is measured in four bands, 6.1 to 8.3, 8.3 to 9.8, 9.8 to 12.5, and 17.0 to 24 μm; there are three detectors in each of the first two bands and seven in each of the last two. One detector at 14.56 to 15.41 μm, centered on the CO_2 vibration band, measures the stratospheric temperature. Brightness temperatures in these bands are identified as T_7, T_9, T_{11}, T_{20}, and T_{15}. Seven detectors at 0.3 to 3.0 μm respond to reflected sunlight.

An objective of this investigation was to achieve good spatial resolution. The field of view is defined by focal plane stops 5.2 mrad in diameter. The spatial response has been measured in the laboratory and verified in flight to be nearly diffraction-limited. In the longest wavelength band, the signal at the planetary limb drops to 10 and 1 percent of maximum when the limb is at distances of 6 and 17 mrad from the center of the field of view. The radiation level is integrated in all channels simultaneously; this arrangement allows measurements of the brightness temperatures and the reflected radiance at seven locations on the planet each 1.12 seconds.

The response of all channels is nearly linear with flux, and is digitized into 1000 data numbers (DN). The maximum response of the solar band corresponds to 75 percent of a perfect white diffuser at normal incidence at the mean Mars distance from the sun. The thermal bands have maximum temperatures between 300 and 330 K. The one-sample noise is less than 1 DN for all channels except T_{15}, where it is about 2.5 DN. The equivalent temperature uncertainty varies with band and temperature; the 7- and 9-μm bands are well on the short wavelength side of the Planck function at 200 K, and only the 20-μm band has good temperature resolution below 170 K.

The angular resolution, detector configuration, sample rate, and scan-platform slew rate were designed to allow approximately uniformly spaced, nonredundant, continuous coverage so that the IRTM experiment can produce two-dimensional images in the solar and thermal bands (*1*). The in-flight performance of the IRTM has been entirely as expected, including some sensitivity to thermal radiation from the Viking lander prior to separation. The results reported here were obtained on revolutions (revs) 3 through 22, occurring over 22 June to 11 July 1976.

Global surface temperatures. From apoapsis to approximately 2 hours before periapsis the entire disk of Mars can be scanned in a single observation se-

quence. In observations taken near apoapsis, when the disk is largely dark, the major features are the latitude variation expected for the insolation distribution at this season and the rapid rise in temperature after dawn. There is considerable thermal structure in the equatorial region, and a regional low extending northward toward the Chryse Planitia area can be seen.

An example of the view obtained 4½ hours before periapsis as shown in Fig. 1. The disk is half-illuminated, and temperatures rise to above 240 K at noon at the equator. The most conspicuous thermal feature is the minimum of 142 K at dawn, unexpectedly low for the equatorial region, followed by a rapid rise into morning to the east. The minimum is near the summit of the large shield volcano Arsia Mons. The low temperatures near the west limb are in the area of Memnonia Fossae, where clouds or frost were seen after dawn with the approach imaging. Some thermal structure is apparent in the south polar region, where temperatures drop below 140 K.

The thermal behavior of different areas can be more readily seen after the diurnal, latitudinal, and seasonal temperature variations expected for the average martian surface are removed. For this report, we use the temperatures (T_m) from the homogeneous thermal model determined by the Mariner 9 late observations: the model uses bolometric albedo $A = 0.25$ and a thermal inertia $I = 0.0065$ cal cm^{-2} sec$^{-1/2}$ K^{-1} (2). The temperature just before dawn is most readily related to the surface physical properties. In the equatorial region, a predawn temperature 10 K above the martian average, if attributed to thermal inertia alone, can be interpreted as about a twofold increase in the average particle size (from 0.3 to 0.6 mm) or as a 25 percent increase in the area of large blocks or exposed bedrock.

The differences ($T_{20} - T_m$) for predawn portions of the data in Fig. 1 and in an apoapsis sequence 8 hours earlier are shown on a Mercator projection in Fig. 2. The two observation sequences show comparable behavior south of −20°, and there is little structure between −40° and −65° latitude, with the exception of a cold region over the Argyre basin. The area on the Tharsis ridge west of Arsia Mons is as much as 18 K colder than expected for average martian surface material. The major canyon areas are generally warm, from Coprates Chasma eastward and northward to Chryse Planitia and Acidalia Planitia. These two regional extremes of residual temperature correspond to topographic

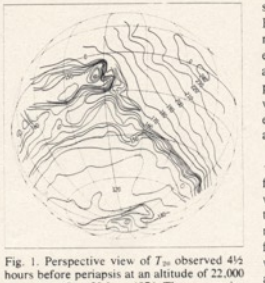

Fig. 1. Perspective view of T_{20} observed 4½ hours before periapsis at an altitude of 22,000 km on rev 10 on 29 June 1976. The contour interval is 2 K over the night area and 10 K over most of the illuminated disk. Latitude and longitude lines are shown every 20°. The nighttime minimum and rapid dawn heating near −10°, 120° are in the region of Arsia Mons volcano. Closed contours in all figures are positive unless identified as depressions.

high and low areas, respectively. The variation of thermal conductivity with gas pressure expected for the average martian surface material can account for about one-third of the residual temperature for these two large areas.

There is considerable thermal structure at the resolution limits of these observations in the canyon areas, suggesting geologic heterogeneity. The morphology in the canyon areas indicates that a variety of processes have been active (3). There is some correlation of other warm regions with the areas depicted as dark features in the Mariner 9 maps.

Solar reflectance. Measurements of the surface brightness in absolute units are being obtained in the solar band. A contour map, with about 130 km resolution, of brightness normalized to the solar irradiance is shown in Fig. 3. These data were obtained simultaneously with the thermal data shown in Fig. 1. The phase of Mars was very nearly 90° during the observations, so the terminator bisects the disk, and, if the planet were of uniform Lambert albedo (A_L) (4), all brightness contours would parallel the terminator. Were the surface locally flat and Lambertian, the contour intervals would be uniformly spaced from terminator to bright limb.

In Fig. 3 several features can be noted:

1) There is a tendency for A_L to increase toward the limb, particularly near the northern terminator. This effect is possibly a consequence of scattering by haze in the martian atmosphere.

2) The mean A_L is near 0.25, and its variations are correlated with many classical light and dark areas identified from Earth-based observations in the much narrower visual wavelength band. For example, Juventae Chasma (−6°, 62°) and Eos Chasma (−17°, 55°) regions appear darker than their surroundings, whereas Syria Planum (−12°, 83°) and eastern Sinai Planum (−18°, 67°) regions appear brighter than their surroundings.

3) The visible surface area north of −10° and west of 90° is about twice as reflective as the area south of −20° and west of 50° ($A_L \approx 0.35$ and 0.17, respectively). This northern hemisphere brightness may be due to early morning ground fog or surface ices. This explanation would be consistent with the larger amounts of water vapor detected for this area of the planet during approach observations (5). The relative uniformity suggests that the higher reflectivity may be due in part to an intrinsically higher regional surface albedo. The four major volcanoes are included in this area.

4) Argyre Planitia (−50°, 40°) is anomalously bright ($A_L \geq 0.35$) as compared to the area immediately to its northwest ($A_L \leq 0.20$). The brightness of Argyre and the surface areas south of Argyre is consistent with the temperature measurements, which show that a major portion of the Argyre basin is at the sublimation temperature of CO_2 ice.

5) The brightness gradients are steeper near the four major volcanoes, particularly near Ascraeus Mons (11°, 106°), most likely as a result of slope effects.

6) The brightness increases rapidly north of the central portion of Coprates Chasma. This may be a result of the unusual geology of this region. Low-altitude observations show the major canyons to have low A_L values. Visual imaging on the plateau north of Coprates suggests an extensive aeolian covering of the underlying geology; this wind-transported material may be brighter than the average material in its source region.

Atmospheric temperatures. The 15-μm channel measures the thermal emission of atmospheric CO_2, weighted by a function with maximum amplitude at 0.63 mbar and half-maximum points at 0.17 and 1.56 mbar for normal viewing (6). A typical contour map of T_{15} over the period from dawn to noon is shown in Fig. 4, which does not refer to an isobaric surface on account of varying air mass.

In Fig. 4 and other global maps obtained in the predawn period, the general behavior of stratospheric temperature is characterized by a strong latitudinal dependence in the winter hemisphere and weak diurnal variation. The latter behavior is expected from the prediction of

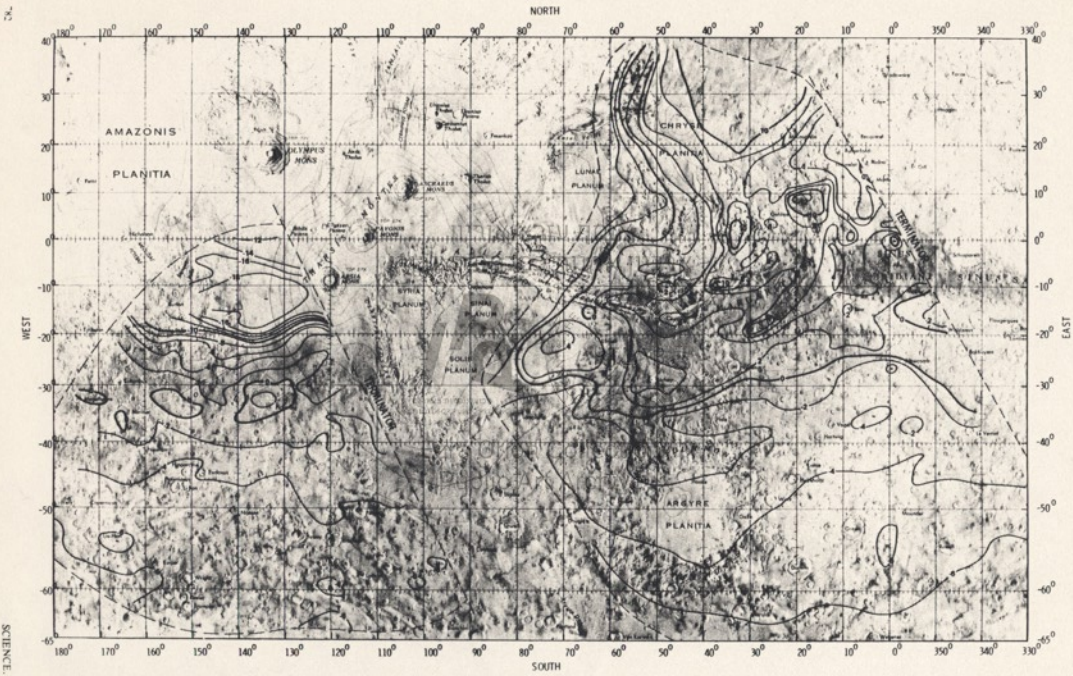

Fig. 2. Mercator map of the residual $T_{2a} - T_{2m}$ from observations 14 and 4½ hours before the rev 10 periapsis on 29 June 1976. The contour interval is 1 K. The data at the left correspond to the observations shown in Fig. 1. Most of the thermal behavior shown here is attributed to variations in thermal inertia.

general atmospheric temperature models (7). The temperatures measured by the Mariner 9 infrared interferometer spectrometer (IRIS) experiment for the 0.65-mbar level at the same season (areocentric longitude of the sun $L_s = 97°$) and latitude +20° are very similar to the T_{15} values near dawn shown in Fig. 5, which displays surface and atmospheric temperatures specific to the region of the Chryse landing site. In the afternoon, however, T_{15} is about 10 K higher than the IRIS temperatures. The origin of this discrepancy has not been clarified, but it could arise from the grossly different field of view of the two experiments or as a result of a manifestation of temporal changes in the martian atmosphere.

The southernmost latitudes, only partly shown in Fig. 4, reveal surprisingly low stratospheric temperatures, well below those found in the IRIS experiment for polar regions (8). The temperature uncertainty of a single measurement for T_{15} (140 K) is ≈ 5 K, but averaged data show clearly that temperatures below 136 K, near the CO_2 condensation point at stratospheric pressures, do occur south of −70° latitude. The T_{15} measurements do not represent a constraint on the formation of CO_2 clouds in these latitudes.

Local areas. Orbiter observations thus far have emphasized potential landing areas, this being especially true for high-resolution observations. The determination of diurnal thermal behavior from the Viking 1 synchronous orbit is compromised by the low resolution accessible for predawn observations; the predawn spatial resolution decreases rapidly north of the equator, and no predawn observations are possible north of 35°. Three areas considered as Viking landing sites are discussed below.

Chryse. The measurements of T_{11} for the Chryse Planitia are shown in Fig. 5. The morning data have been collected within the +20° to +24° latitude and 46° to 49° longitude area over several revolutions. Variations in thermal inertia within this area can account for the scatter in the morning data. At 0600 hours, areas with thermal inertia differing by 0.001 in the vicinity of $I = 0.008$ would show a temperature difference of 2 K. The data near 1500 to 1600 hours in Fig. 5 refer to the smaller area between +22.0° and +23.2° latitude and 47° to 48° longitude (9). The homogeneous thermal model which best fits the morning T_{11}, based on the use of A equal to the value $A_L = 0.26$ measured in the solar band, is obtained with $I = 0.009$ (10). However, there is clear disagreement between this model and T_{11} measured in the afternoon. These departures of T_{11} from the predictions can be explained by several effects not considered in the simple model:

1) An admixture of materials with low and high thermal inertia is suggested by the existence of rocks at the Viking 1 landing site (11). Two-component flat models which account for the predawn temperatures fail, however, to predict afternoon temperatures as low as those observed. The observation geometry at the landing sites has been optimized for visual imagery, the resolution of which improves toward angles of solar incidence near 70°. In addition, the westward search for the eventual Viking 1 landing site resulted in oblique viewing such that the IRTM afternoon observations preferentially include the shaded faces of rocks and their shadows. The A_L values derived from observations at a time of day when shadows are present will underestimate A. Inclusion of these effects into simplified models leads to predicted temperatures more nearly in agreement with the observations. Local variations in these effects within the afternoon areas could explain the scatter found in the measurements.

2) The existence of a regional atmospheric haze, revealed by orbital imagery over the landing areas, may also help to explain the discrepancy between the measured afternoon surface temperatures and those predicted by the thermal models which disregard the presence of clouds. If clouds are sufficiently opaque; they impede solar heating of the surface, thereby reducing temperature.

3) Increased thermal coupling between the ground and atmosphere in the afternoon would tend to decrease surface temperatures. This last effect was suggested to explain the departures of the Mariner 9 observations from the homogeneous model predictions in the region of +10° to +40° latitude (2). However, implausibly high winds are required if the discrepancy is to be explained by this effect alone.

Capri. This region is bounded on the

Fig. 3. Perspective view of solar band brightness obtained at the same time as the data in Fig. 1. The units are brightness relative to that of a white Lambert surface with normal incident sunlight. Brightness contours for such an ideal surface would parallel the terminator and be uniformly spaced. Latitude and longitude lines are shown every 20°.

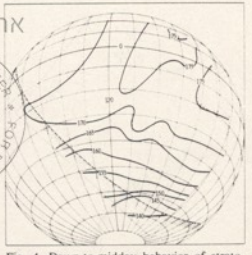

Fig. 4. Dawn-to-midday behavior of stratospheric atmospheric temperatures. Observations were made on rev 9 at a range of 12,000 km. The nominal sampled pressure level is 0.63 mbar at air mass 1.0. No correction has been made to account for the sampling of greater altitudes toward the limb. Latitude and longitude lines are shown every 20°.

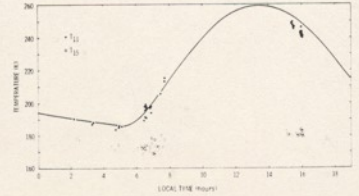

Fig. 5. Diurnal surface and atmospheric temperature variation in the Chryse region. Closed circles represent T_{11} measurements within the area bounded by latitudes +22°, +23.2°, and longitudes 47°, 48°. The curve depicts the surface temperature prediction for $A = 0.26$, $I = 0.009$. Open circles represent atmospheric temperatures within the area bounded by latitudes +21°, +24°, and longitudes 40°, 56°; measurements are reduced to the 0.63 mbar level (air mass, 1.0).

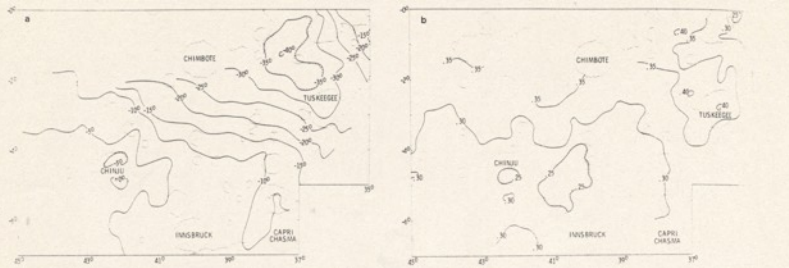

Fig. 6. (a) Thermal relief map of the Capri region at 1530 hours. The contours shown are 5 K apart and represent the difference between T_{15} and T_{20}. The model uses an A value of 0.25 and an I value of 0.0065 cal cm^{-2} sec$^{-1/2}$ K^{-1}. The dark irregular line near the bottom is the north rim of the Gangis and Capri Chasma. The substantial thermal depression, with deviations in $T_{15} - T_{20}$ to −40 K, must be due to clouds. (b) Map of A_L values of the Capri region. The contours shown on this map [which is the same scale and projection as (a)] were derived from radiances measured in the 0.3- to 3-μm band. A comparison with (a) indicates general agreement in the sense that temperatures are lower where the albedo is higher, but the highest albedo, 0.40, is by itself insufficient to explain the magnitude of the thermal depression.

south by the Gangis and Capri Chasma and extends in the north to the equator. A sketch of some of the prominent features in this region is shown in Fig. 6a. This region was mapped once at low altitude on rev 11. The local Mars time at the center of the region was 1530 hours, the viewing angle varied between 35° and 70°, and the observation range varied between 2000 and 2500 km.

This region exhibits the largest thermal relief seen in any of the high-resolution mapping data yet collected, as shown in Fig. 6a. The thermal structure in this region is dominated by the large depression in the northeast, where the temperature deviates 40 K from the thermal model. A comparison of the thermal differences (Fig. 6a) with the A_L values observed at the same time (Fig. 6b) indicates general agreement, in the sense that the temperature depression corresponds to a region of high A_L. But this A_L increase by itself is insufficient to explain the temperature depression since the expected change in temperature with A at this time of day is ≈ −8 K per 0.1 change in A. Clouds are common in images of this region taken on rev 14 at this time of day but they appear not to be substantial enough to account for the observed thermal results. Although the four thermal channels exhibit parallel behavior over this feature, the depth of the thermal depression in T_7 is only half that observed for the other bands. Mariner 9 spectra indicate that the 9-μm band should be the least affected by H_2O ice clouds (*12*). Although an H_2O cloud is the least unlikely cause of this feature, the relative spectral behavior remains to be explained.

Cydonia. In contradistinction to Capri, the Cydonia region (4° to 13° longitude, 42° to 46° latitude) appears as predicted thermally. The $T_{15} - T_{20}$ contrast across the region is less than 10 K, and the thermal relief agrees with geologic boundaries mapped in photographs taken on rev 9. The ejecta blankets of the two largest craters in the region [DK and DKb in MC-4 (*13*)] stand above the mantled terrain to the east and the polygonally patterned terrain to the west. Although variations in thermal inertia cannot be inferred directly from observations at this time of day (1800 hours), it seems apparent that a mappable thermal behavior is being caused by variation of some surface physical property, such as surface texture, associated with the identified geologic units.

South polar region. The Viking 1 orbit allows viewing of the southern hemisphere, to the south pole, when the spacecraft is about 3 hours before periapsis. Observation scans of the planet covering the south polar region have yielded brightness temperatures well below those reported by the infrared radiometers and spectrometers on Mariner 7 and Mariner 9 (*14*). Earlier measurements of the brightness temperatures of the southern and northern polar caps made during the spring and summer seasons were near 148 K, as expected for solid CO_2 subliming at a pressure of about 6 mbar. There are no earlier observations of any kind of the midwinter polar regions.

The T_{20} values measured by the IRTM over the south polar region on rev 22 are shown in Fig. 7. Observations were made during two scan patterns, each of which went off the dark limb of the planet, allowing the zero flux point to be accurately determined. There is a strong temperature gradient southward to −50°, where T_{20} reaches approximately 148 K. The temperatures decrease less rapidly to 145 K, and there follows a broad thermal plateau between 145 and 143 K, which constitutes most of the polar region. Poleward from −70°, T_{20} shows considerable structure. In addition to a sharp minimum of approximately 134 K, there are several arcuate lows which extend outward from the geographic pole. These cool regions have a temperature contrast of 2 to 3 K and a breadth of approximately 200 km, with a form resembling that of terrestrial polar troughs.

Where T_{20} is greater than 150 K, north of −50°, the stratospheric temperature T_{15} shows small variation from 167 K. Across the plateau in T_{20} at 143 to 145 K, T_{15} decreases steadily poleward, from 165 K to less than 145 K. South of this plateau, where T_{20} is less than 141 K, T_{15} varies from 145 K down to about 130 K. At 140 K, the noise equivalent temperatures in T_{15} and T_{20} are approximately 4.5 and 0.5 K, respectively. Although simultaneous measurements are made in these two channels, since the T_{20} thermal contrast near the geographic pole is only marginally greater than the noise in T_{15}, it is unlikely that a correlation can be obtained without further observations that would allow averaging of the 15-μm temperatures.

Although not shown in Fig. 7, T_{15} exhibits sharp limb brightening, rising up to 150 K in the last sample on the planet. This temperature is approximately that expected for the atmosphere on the ge-

metric limb, based on T_{15} measurements at the corresponding latitudes nearer the subspacecraft point.

Simultaneous measurements of T_{11} and T_{20} show a strong correlation over the polar region. Where T_{20} is less than 150 K, the mean variance in $T_{11} - T_{20}$ is less than the T_{11} digitization limit (2 K at 140 K). This finding suggests that the two wavelengths are sampling the same region, whether on the surface or in the atmosphere.

There are several mechanisms which individually or collectively could be invoked to explain such low values of T_{20}. These are low emissivity, the presence of clouds, high surface elevations, cyclonic low pressures, or dilution of CO_2 by noncondensable gases. Although more than one of these effects is likely to be contributing, it is simplest to evaluate them independently, under the assumption of a mean surface pressure of 6.1 mbar of CO_2 at mean Mars elevation, with a corresponding saturation temperature of 147.7 K.

If the surface kinetic temperature were 148 K, the minimum brightness temperature observed, 132 K, would require an emissivity of 0.58. Although the emissivity of a pure CO_2 frost is not known, this value seems implausibly low for a natural rough surface. The broad thermal plateau beginning at 145 K suggests that this region is completely covered with CO_2 and has a uniform kinetic temperature near 148 K. This temperature corresponds to a frost emissivity of 0.92. Such an emissivity partly accounts for the lower temperatures measured near the geographic pole.

The other four explanations are all equivalent to lowering the partial pressure of CO_2 over the region sensed at 20 μm: the minimum required partial pressure is 0.46 mbar. This could be accomplished if clouds were present at an elevation of 19 km above the mean martian surface. Imagery obtained simultaneously with these observations shows a remarkably clear atmosphere north of the polar night. The clear atmosphere at $-50°$ seen in limb imaging is in concert with thermal results, which show the temperature at 0.63 mbar to be about 163 K, well above the CO_2 condensation temperature. Poleward of $-65°$, T_{15} is below T_{20}, and extensive CO_2 clouds are possible (visual imaging is not).

Surface elevations of 19 km could also be invoked to explain the observed temperatures. However, elevation determinations in the south polar region by radio occultation, IRIS, and ultraviolet spectrometry, while generally of lower quality than for more temperate regions, do not indicate unusually high values (greater than 5 km). Also, imaging observations do not indicate large topographic variations.

Fig. 7. Brightness temperatures at 20 μm in the south polar region. The contour intervals are 1 K below 145 K and 10 K above 150 K. Longitude lines are spaced by 20° and latitude lines by 10°. The minimum temperature of 134 K is well below that expected for surface CO_2 condensation. The arcuate low-temperature regions extending from the pole are similar to terrestrial winter circulation patterns. It is not certain whether the observed temperatures represent the surface or high clouds.

The CO_2 partial pressure will be lowered through dilution by an accumulation of noncondensable minor constituents. As the net radiation loss causes CO_2 condensation and the atmosphere moves to maintain constant total pressure, the concentration of noncondensable gases increases locally. The magnitude of CO_2 dilution—noncondensable gas enrichment—depends on the relative time scales of CO_2 condensation and mixing of CO_2-depleted "old" polar atmosphere with "fresh" atmosphere from the nonpolar regions. The time scale required for the atmosphere to be enriched by a noncondensable gas is 44 days, the period over which a blackbody at 144 K radiates the latent heat of condensation of the CO_2 contained in an atmospheric column.

If condensation is occurring at the surface, near-surface enrichment of a noncondensable gas could occur with a very short time scale. For example, the lowest 100 m could acquire a 16-fold enrichment in about 10 days. The first results from the Viking entry mass spectrometer (*15*) indicate that about 5 percent of the martian atmosphere is composed of argon, nitrogen, and oxygen, which would not condense under martian polar conditions. A 16-fold increase to 80 percent would lower the CO_2 condensation temperature to 137 K. The resulting low-temperature, near-surface layer might be stable, notwithstanding an adverse stratification of the molecular weight.

Finally, dynamic meteorological processes are unlikely to lower the atmospheric pressure at an equipotential surface by more than 1 mbar (*16*).

On the basis of the available data, it is not possible to discriminate between the high-cloud and the low-level dilution hypothesis. Further observations of possible time changes or motion of the polar thermal structure may allow such a distinction to be made.

Whichever explanation is correct, the net flux emitted by the polar region south of $-55°$ is 85 percent of that emitted by a uniform 147.7 K surface over this region. To the extent that this behavior holds throughout the polar winter, the amount of atmospheric condensation and the concomitant annual variation in surface pressure, considering the southern hemisphere only, are correspondingly less than in existing theories.

HUGH H. KIEFFER
University of California, Los Angeles 90024

STILLMAN C. CHASE, JR.
Santa Barbara Research Center, Goleta, California 93017

ELLIS D. MINER
FRANK DON PALLUCONI
Jet Propulsion Laboratory, California Institute of Technology, Pasadena 91103

GUIDO MÜNCH, GERRY NEUGEBAUER
California Institute of Technology

TERRY Z. MARTIN
University of California, Los Angeles

References and Notes

1. A description of the IRTM instrument and investigation at the conceptual design stage has been given by H. H. Kieffer *et al.*, *Icarus* **16**, 47 (1972). The major differences are the actual use of four small (9-cm aperture) telescopes, a "V" pattern detector configuration, and the inclusion of the 15-μm channel.
2. H. H. Kieffer, S. C. Chase, Jr., E. Miner, G. Münch, G. Neugebauer, *J. Geophys. Res.* **78**, 4291 (1973).
3. H. Masursky, *ibid.*, p. 4009.
4. Lambert albedo is herein defined as the ratio between the measured radiance R in the solar band and the incident flux

$$A_L = \frac{\pi U^2 R}{F \cos i}$$

where F is the solar constant, U is the distance from the sun in astronomical units, and i is the incidence angle.
5. C. B. Farmer, D. W. Davies, D. D. LaPorte, *Science* **193**, 776 (1976).
6. The pressure sampled at normal viewing was derived under the assumption that the atmo-

close to Mars in June 1976 but not so close as to entail a significant risk of impacting and contaminating the planet. On day 7 after launch (L + 7) an orbit correction maneuver was executed, which was so precise that the spacecraft could have gone into Mars orbit with only the single propulsive maneuver at the planet without any earlier adjustments to the orbit.

A preliminary check-out of the subsystems in the encapsulated lander was made soon after launch, and during the next few months several tests were run on the gas chromatograph–mass spectrometer (GCMS) and on the temperature sensors of the meteorology experiment. Certain engineering subsystems on the lander, including the gyroscopes and the tape recorder, were checked out periodically. The computers were programmed and batteries were conditioned by telemetered command, but the scientific instruments of the lander were otherwise dormant until the next to last day of the 304-day interplanetary cruise.

SPACECRAFT ORBIT DESCRIPTION

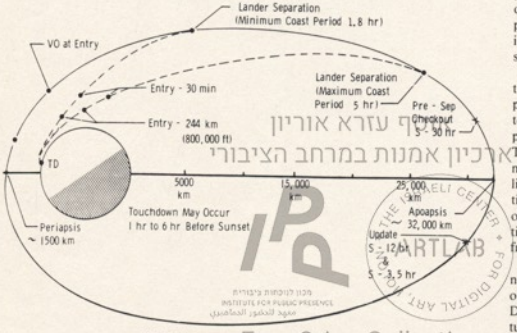

Fig. 2. Viking orbit and descent trajectory.

Table 1. The Viking science projects.

Investigations	Instruments
	Orbiter
Imaging (VIS)	Two vidicon cameras
Water vapor mapping (MAWD)	Infrared spectrometer
Thermal mapping (IRTM)	Infrared radiometers
	Entry
Interplanetary plasma and ionospheric properties	Retarding potential analyzer
Atmospheric composition	
Atmospheric structure	Mass spectrometer Pressure, temperature, and density sensors
	Lander
Imaging	Two facsimile cameras
Biology	Three analyses for metabolism, growth, or photosyntheses
Molecular analysis	Gas chromatograph–mass spectrometer (GCMS)
Inorganic analysis	X-ray fluorescence spectrometer
Meteorology	Pressure, temperature, wind velocity
Seismology	Three-axis seismometer
Magnetic properties	Magnet on sampler observed by cameras
Physical properties	Various engineering sensors
	Radio
Orbiter/lander location atmospheric and planetary data, interplanetary medium	Orbiter or lander radio and radar systems

On day L + 61 a picture of Earth was taken with one orbiter camera, for purposes of calibration. Over the next 8 months several large sets of pictures of star fields were taken to provide geometric and photometric calibrations of the cameras and to determine accurately the pointing of the scan platform on which the orbiter science instruments are mounted.

Fifty-seven days before Mars orbit insertion (MOI − 57) preparations for orbital operations began with the first of several lander battery conditioning sequences involving discharge and recharge of the batteries, with power supplied by the orbiter. Subsequently both orbiter cameras recorded pictures of the planet Jupiter to provide photometric calibration, and the other orbiter science instruments were also calibrated.

Between days MOI − 33 and MOI − 6, three optical navigation sequences were performed in which one orbiter camera took pictures of Mars and the other took pictures of the star field close to Mars. These pictures were analyzed to determine the position of the Viking-Mars line, and this technique of optical navigation considerably increased the precision of our knowledge of the spacecraft position which had previously been obtained from radio tracking data.

During the last 3 days before MOI a final set of optical navigation pictures was obtained, this time showing the satellite Deimos against the star background. Pictures of the whole lighted disk of Mars were also taken at 2-hour intervals down to MOI − 20 hours, some being taken in two or three colors.

It had been planned to have a single final orbit correction maneuver on day MOI − 10, but when the propulsion system was made ready for that event, a small leak was detected in a pressure regulator. To prevent excessive pressure buildup from that leak, three maneuvers were made. Each reduced the spacecraft velocity slightly so that the arrival at Mars was 6.2 hours later than planned. This delay was compensated by inserting the spacecraft into an orbit with a period of 42.6 hours so that it reached its first periapsis at precisely the time that had been planned for the second periapsis. A maneuver at that time settled the spacecraft into the desired 24.61-hour orbit, and thereafter the mission proceeded on the preplanned schedule until the rejection of the original landing site.

The Mars orbit insertion maneuver began on 19 June at 10:38 G.M.T., and the propulsion engine burned for 38 minutes, reducing the spacecraft velocity by 1.1 km/sec.

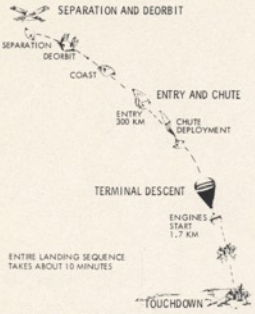

Fig. 3. The lander descent sequence.

With the spacecraft safely in orbit, the site certification phase of the mission began (*1*). An extensive program of observations by the orbiter cameras and the other orbiter science instruments was planned, leading, as we hoped, to the choice of a specific landing target in the preselected area and a 4 July landing.

The site certification observations began on rev 3 (this was actually the second revolution after orbit insertion because of the double length of the first revolution, but the original numbering was retained to prevent confusion) with a set of widely dispersed pictures surrounding the preselected site at 19.5°N, 34.0°W. Swaths of contiguous pictures to cover in stereo the dispersion ellipse around the nominal landing site were laid down on revs 4 and 6. These pictures show unexpected detail and clearly indicated the presence of fluvial features and some mottled terrain, which looked too hazardous to attempt a landing. (The resolution of the orbiter cameras is about two orders of magnitude from seeing the rock hazards that could be fatal to the lander.) Consequently the picture sequences for revs 8 and 10 were retargeted to the northwest of the original site in the direction of the Chryse Planitia basin. These pictures did not look reassuring; therefore after a few days for replanning and redesigning the command sequences (during which observations of possible mission 2 landing areas were made), an orbit trim was made on rev 19 to lengthen the orbital period slightly so that the subperiapsis point on the surface moved westward by about 2° of longitude per day. Pictures were taken on revs 20 and 22 of areas westward of the rev 10 coverage. Study of these pictures together with the results of radar data in the area from Arecibo observations in early July resulted in selecting an acceptable landing site at 22.4°N, 47.5°W. Landing was planned for rev 30 on 20 July.

The checking out of the lander began 30 hours before separation from the orbiter. The separation command was sent from Earth and received within 28 minutes of actual separation. The descent capsule with the Viking lander was separated at a preprogrammed time for the completely automated 3-hour descent to the Mars surface (Fig. 2). The round-trip light time (38 minutes) precluded any real-time control from Earth.

After separation, the lander aligned itself for the deorbit maneuver with the use of small attitude control jets (Fig. 3). At this time it was traveling at 4.6 km/sec. After deorbit and a 3-hour coast period, the braking was performed by three systems: an ablative aeroshell, a supersonic parachute, and terminal descent rocket engines.

The lander entered the Mars atmosphere with its attitude still controlled by the jets. Instead of a ballistic entry, the angle of attack was set to obtain a small amount of lift, which contributed to the deceleration needed for the soft landing. The first lander investigations to measure the ions, electron, and neutral species of the Mars upper atmosphere were performed during this phase (*2*). During entry, the ablation of the aeroshell heat shield protected the capsule from atmospheric heating.

Sequential operation of the systems was accomplished by the use of the landing radar system, operating with the onboard computers, gyros, and accelerometers, to determine the direction and distance to the surface. Peak deceleration occurred at 25 km above the surface.

Table 2. Viking spacecraft characteristics.

Weights (kilograms)	
Spacecraft at launch	
Total spacecraft	3530
Orbiter	2330
Orbiter propellants	1430
Lander capsule and adapter	1200
Orbiter without propellants	900
Lander capsule at separation	1185
Lander on Mars	605
Dimensions (meters)	
Spacecraft overall length	5.08
Solar panel tip-to-tip wingspread	9.88
Lander capsule diameter	3.66
Lander capsule thickness	2.03
Lander overall height (to top of high-gain antenna)	3.1
Lander camera height	1.3
Lander body ground clearance (minimum)	0.22
Diameter of circle through center of landing legs	2.79
Soil sample collector extension	2.9
Electrical power (watts)	
Orbiter solar panel output	800
Lander radioisotope thermal generator output	70

At an altitude of 6 km (descending at 250 m/sec) the parachute was deployed by a mortar, and 7 seconds later the aeroshell was jettisoned. Eight seconds later the lander's legs were extended. The aeroshell was carried away from the landing site by aerodynamic lift. The parachute operated for 45 seconds until the lander was 1.5 km above the surface (descending at 60 m/sec). The terminal descent engine fired for 40 seconds to reduce the final velocity to 2 m/sec, and touchdown on the Mars surface was successful.

During the final descent (30 m) the lander was in a vertical flight path at a

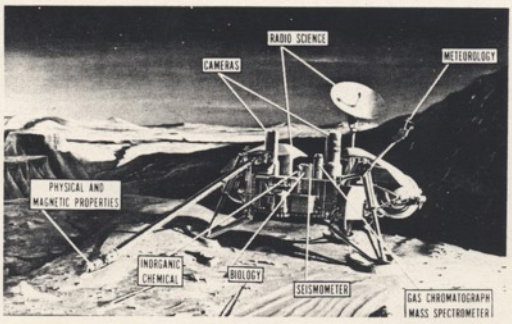

Fig. 4. The lander and its investigations.

constant velocity. A switch on the lander footpad automatically shut off the descent engine when the first leg touched the surface. Honeycomb aluminum shock absorbers in the legs helped to cushion the impact.

The computers and the landing radar systems were critical to all events, including deployment of the parachute and ignition of the descent engines. Every system worked flawlessly. The Viking 1 lander was landed in a flat valley within 3° of vertical, the cameras facing to the southeast. Figure 4 is an illustration of the lander on an imaginary Mars surface.

After 25 seconds one camera was initiated and began to take a high-resolution picture of one of the lander's footpads. The slow scanning camera performed in this mode for 4 minutes and the first picture from Mars was obtained (*3*). During this time the lander activated itself. A high-gain antenna was erected and pointed for the direct communication to Earth. The meteorology boom with its sensors was deployed (*3*, *4*). The second picture of the 300° panoramic scene was taken in the next 7 minutes. (At the time the President of the United States telephoned his congratulations to the Viking team scientists.) On the day after landing the first color picture of the surface was taken.

The two means of returning data to Earth from the lander are (i) by a relay link up to the orbiter and back, and (ii) by the direct link to Earth. The relay link will carry about ten times the data of the direct link. The capacity of the relay link is 10 to 20 million bits per day, of the direct link, of the order of 1 million per day.

Planned mission timeline. The basic plan of the lander mission is to continue to take different pictures of the terrain throughout the mission. Within the first week, GCMS was used to perform several atmospheric analyses (*5*). During the second week the samples will be ob-

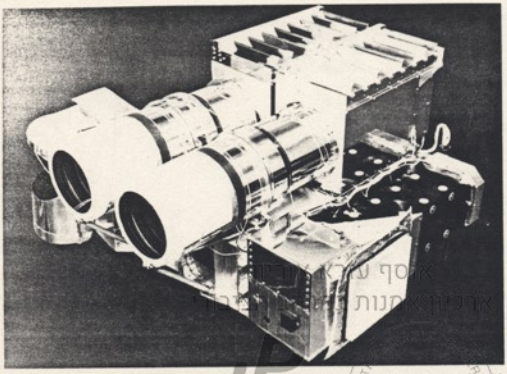

Fig. 5. The planetary scan platform. The MAWD is on the right and the IRTM on the left, with the two VIS cameras between. In flight it is covered by a thermal control blanket.

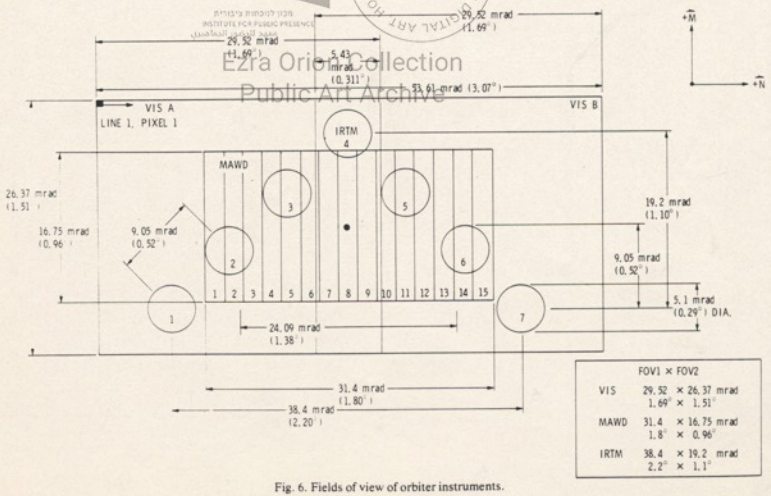

Fig. 6. Fields of view of orbiter instruments.

tained from the surface for analysis by the biology, molecular analysis, and inorganic chemical investigations. Meteorological and seismic data are gathered every day. The mission plan provides the flexibility to respond to the data that are returned. The plan is to continue to gather and analyze surface and atmospheric samples until the Viking 2 is landed, now scheduled to occur on 4 September. The two spacecraft have identical payloads but will land at different sites.

During the first few weeks after landing, the orbiter will remain in the synchronous orbit with periapsis near the lander, and the orbiter observations will be constrained to the areas that are accessible from this orbit. The visual imaging subsystem will be searching for evidences of changing weather near the lander and will be covering with contiguous mapping frames an ever enlarging region near the lander and to the southwest along the orbital ground track. Specific targets that are of interest geologically or because of frequent cloudiness will be photographed. Some areas will be photographed in color or stereoscopically.

The infrared thermal mapper (IRTM) and the Mars atmospheric water detector (MAWD) will make daily observations of both extended and restricted regions (including, for IRTM, those in the dark) to search for changes in water vapor, temperature, and albedo.

At the end of the first primary mission, and when the second orbiter becomes available to handle the data relay from lander 1, and, if needed, it is planned to have the first orbiter "walk around the planet" in a slightly nonsynchronous orbit. This will make other regions of the surface accessible, substantially increasing the capability to observe diurnal variations.

The timeline for the second mission, with MOI on 7 August and landing currently scheduled for 4 September, will be generally similar, and the activity of both orbiter 1 and lander 1 will be greatly restricted during the second mission. Both missions will terminate when the radio communication links become degraded because of the proximity of the sun about 2 weeks before superior solar conjunction on 25 November. In mid-December it is planned to reactivate all four spacecraft to commence an extended mission which is planned to extend for a full martian year, until July 1978.

The orbiter science instruments. Since Viking was to be predominantly a lander mission, a very small complement of scientific instrumentation was included on the orbiters. The instruments were chosen primarily for their potentialities for contributing to the choice and certification of landing sites and for supplementing and complementing the observations made by the landers. Each has the capability also to make observations pertinent to solving some of the major scientific problems about the planet Mars.

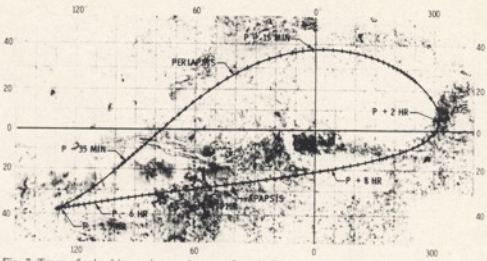

Fig. 7. Trace of suborbiter point on planet surface during one orbit. Points marked are discussed in the text.

The visual imaging subsystem (VIS), comprising two slow-scan vidicon cameras, each with a telescope of 475-mm focal length and a six-position color filter wheel, has been used to provide very precise navigation information by photographing Mars or Deimos against the star background. Its pictures from orbit enabled us to reject several prospective landing sites and finally to settle on the one where the landing was successfully made. They have also revealed many new features of the martian landscape such as had not been seen clearly in the Mariner 9 pictures (6). The VIS will continue to make frequent observations of the site to monitor its weather and look for changes in the surface. It will also map a large area in the vicinity of the lander at higher resolution than was previously obtained and will observe in detail the various geologically interesting features—such as volcanoes, canyons, faults, and "river" channels—that are accessible.

The MAWD is a grating spectrometer operating in the 1.4-μm region of the infrared (7). In its principal operating mode it measures, every 280 msec, the intensity of reflected sunlight in five narrow spectral bands, from which the quantity of water vapor along the line of sight can be inferred. Thus, it can measure the abundance of atmospheric water vapor with a spatial resolution considerably surpassing that of any earlier measurements. Its observational program is designed to measure the variations in water vapor abundance diurnally, seasonally, and spatially so as to understand the details of water transport on the planet. Its contributions to the certification of the mission 1 landing site were minimal because safety of the landing was the overriding consideration, but it is expected that the water measurements will be an important input into the landing decision for the second craft.

The IRTM has four small telescopes, each focusing incident light on an array of seven small thermopile detectors to measure the thermal emission of the martian surface and atmosphere and the total reflected sunlight (8). Various filters divide the 28 detectors among six wavelength bands. Making a full set of measurements every 1.12 seconds, and utilizing the motion of the spacecraft or the scan platform to move the line of sight over the surface, the IRTM can map the variations of radiation intensity at each wavelength. By measuring the diurnal variation of radiation at a given location, the thermal inertia of the surface can be computed, and inferences can be drawn regarding the mean grain size of the surface. These data were helpful in understanding the landing site. The IRTM maps may also indicate variations in mineral content of the surface. A major scientific objective of the investigation is the study of the polar region.

The details of the observations by these three instruments are discussed in the reports that follow.

A fourth orbiter science experiment is provided by the radio subsystems, including the X-band and S-band on the orbiter. Doppler and ranging measurements on the two-way radio link between the spacecraft and the Deep Space Network tracking station determine the spacecraft velocity and range with great accuracy. These data can be analyzed to

yield a variety of information about the gravitational field, the atmosphere, and the ephemeris of the planet, as has been done on all planetary missions since Mariner 4. The first result of this investigation has been to determine the location of the lander on the surface (9).

The lander science instruments. The retarding potential analyzer and the mass spectrometer were attached to the aeroshell (*1*). The other lander science instruments are mounted in or on the lander body. Meteorological sensors are mounted on an extendable boom to avoid interference with the lander body. A three-axis seismometer is mounted on the lander surface. A retractable sampler boom, protected and cleaned of organics, is used to pick up samples from the Mars surface. This boom with its scoop can be extended to 3 m and swing through 110° of azimuth. The two slow-scan facsimile cameras can take pictures in black and white or color, stereoscopically, and have channels sensitive to the infrared. Each of the surface analytical experiments has a separate hopper into which the samples are introduced. Biology and molecular analysis hoppers were capped to prevent contamination, and were opened after landing by firing pyrotechnic devices. Inside the lander are batteries, a tape recorder for recording data, a power conditioning system, a system for processing the data, the computer, and the telecommunications electronics. The terminal descent rockets have been designed to avoid displacement or heating of the surface in the last few meters. Hydrazine is the sole propellant: its products are H_2 and N_2, and small amounts of NH_3 and H_2O. A special design of the rocket engines enable touchdown with no more than 1°C increase of local temperature and no more than 1 mm of surface stripping beneath the engine. The engines were

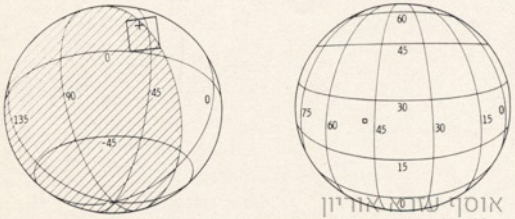

Fig. 8. Perspective plots of Mars as viewed by the orbiter: (left) at lander sunrise, 10 hours before orbiter periapsis (the cross marks the landing site), and (right) at periapsis.

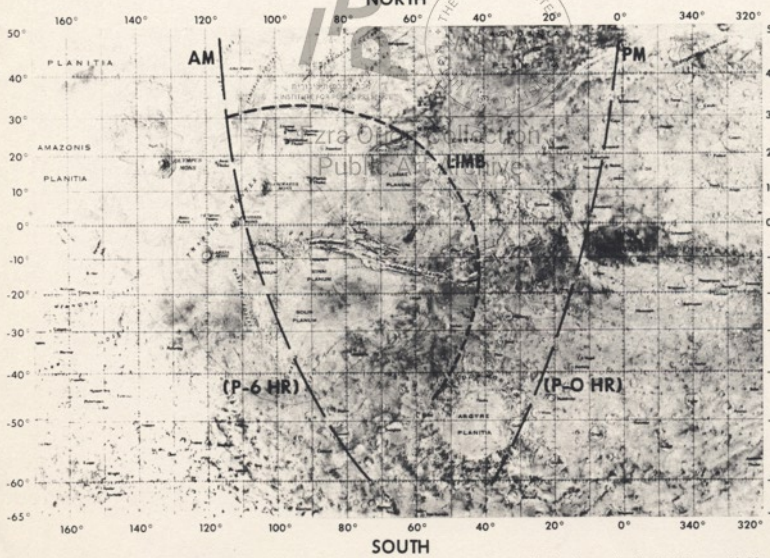

Fig. 9. Map showing the region in which observations at a wide range of local times can be made. The background is the 1976 Topographic Map of Mars (M25M3RMC) prepared by the U.S. Geological Survey.

throttled during descent before touchdown.

Other experiments associated with the lander are the magnetic and physical properties experiments. Small magnets are mounted strategically and will be photographed. Engineering aspects of the lander will be used by the physical properties team (*1*).

The planetary scan platform and instrument fields of view. The Viking orbiter is a three-axis stabilized spacecraft; its orientation is normally maintained fixed by special optical sensors that provide the signals for locking onto the sun and the star Canopus. When it is required for changing the orbit or for observing a particular spot, some other orientation can be chosen and maintained gyroscopically. All three orbiter science instruments are mounted on the planetary scan platform (see Fig. 5) which can move with two degrees of freedom—azimuthally in "clock angle" about the orbiter's axis of symmetry (normally the spacecraft-sun line) and in "cone angle" which is measured from the symmetry axis. The platform can be moved in steps of one-fourth of a degree, and its control system can be programmed to move it as desired about either or both rotation axes at rates of one or four steps per second. These motions, combined with the orbital motion of the spacecraft, provide a reasonable flexibility in covering the planet surface.

The fields of view of the three instruments overlap so that simultaneous observations are obtained whenever the VIS is operating. The pattern of observation in the absence of spacecraft or platform motion is as shown in Fig. 6. The optic axes of the two cameras diverge by 1.38°, and since the cameras are shuttered alternately, there is normally a considerable overlap between successive pictures. The seven circles represent the "chevron" pattern of each of the four sets of IRTM sensors. For pure cone-angle motion, these give seven parallel equally spaced tracks of observation; for other motions, the width of coverage is smaller and the overlap greater. The 15 small rectangles represent the individual fields of view (IFOV) of the MAWD which result from the rotational stepping motion of a small mirror inside the instrument aperture. For pure cone-angle motion the resulting surface coverage is 1.8° wide and everywhere dense; less optimum coverage is obtained for other directions of motion.

Surface coverage and observation conditions. The Mars synchronous orbit passing over the lander imposes viewing constraints on the orbiter instruments and restricts the scientific measurements that can be made, since the viewing conditions are essentially identical day after day. The effect on the IRTM and MAWD investigations is particularly severe, as it is the diurnal variations of temperature and water vapor that are of primary interest, and it is essential to observe the same area at as many different times of the day as possible. For this reason, it is planned on both Viking missions that the orbiter will be released from its lander for a few days. The orbital period will be changed by 2 or 3 hours so that the periapsis point will move around the planet. Synchronism will then be reestablished.

Since all observations up to now have been made from near-synchronous orbit, it will suffice for an understanding of the observational conditions to describe the orbit on rev 30, the landing orbit. The subspacecraft track during this orbit is shown in Fig. 7. The crosses are spaced 2 minutes apart on the northern portion and 20 minutes on the southern. Passing over the landing site and through the periapsis point, the track moves approximately toward the northeast. The sun elevation at lander overfly is 31°, the local time corresponding to just after 4 p.m. During this passage, the landing site is in view for only about 50 minutes. The track crosses the terminator into the dark 15 minutes after periapsis, and the lighted planet is a rather thin crescent between about 1 and 8 hours after periapsis, the minimum being 2.3 hours. Between 2 and 3.5 hours before periapsis, the spacecraft is almost stationary over the vicinity of 37.5°S, 128°W, and the track crosses the terminator into the light at 3.3 hours before periapsis, when the orbiter is at an altitude of about 18,000 km.

Consider now the observability of the landing site, starting with the spacecraft at the extreme right of the track in Fig. 7, at 5°N, 297°W, 2 hours after periapsis. As the orbiter moves south, gains altitude, and slows down and the planet rotates beneath it, about 8 hours after periapsis the site appears over the dark northwest limb, becoming "visible" to the IRTM, and it remains in view near the northern limb for more than 10 hours as the orbiter goes through apoapsis far to the south. Ten hours before periapsis the site crosses the terminator into the light (sunrise), and 4 hours later it disappears over the northeast limb. On the low-altitude pass over the site, it reappears over the northeast limb 35 minutes before periapsis and disappears over the southeast limb 15 minutes after periapsis, and soon thereafter the sun sets on the site out of view of the orbiter.

This orbit chronology is summarized by the numbers on the ground track in Fig. 7. The landing site is visible to the VIS and the MAWD for only 50 minutes at low altitude at a local time around 4 p.m. and at high altitude for only 4 hours after sunrise when the site is so near the limb that good observations are difficult. Figure 8 illustrates the views of the planet from the orbiter at lander sunrise and at periapsis, the rectangle in each picture being the coverage of one VIS picture.

The geometrical considerations above explain why many of the infrared observations in the synchronous orbit are made on areas away from the landing site. A particularly favorable area is near the equator between 60°W and 100°W. Figure 9 shows the situation 6 hours before periapsis; the sunlit and visible portion of the planet lies between the morning terminator (marked *AM*) and the arc delineating the limb. Portions of this area remain visible from this time until periapsis, permitting observations from sunrise until late afternoon. For the IRTM the important predawn observations are also available in this general region. The evening terminator (*PM*) is in the position shown at the time of periapsis passage.

At the time of this writing the Viking lander 1 has collected a surface sample for the biology instrument and the inorganic chemical instrument (*11*). Analysis has begun. The seismometer instrument is still caged. The Viking 2 orbiter is approaching Mars and has made its final approach maneuver.

G. A. SOFFEN
NASA Langley Research Center, Hampton, Virginia 23665
C. W. SNYDER
Jet Propulsion Laboratory, Pasadena, California 91103

References and Notes

1. H. Masursky and N. L. Crabill, *Science* **193**, 809 (1976); G. L. Tyler, D. B. Campbell, G. S. Downs, R. R. Green, H. J. Moore, *ibid.*, p. 812.
2. A. O. Nier, W. B. Hanson, A. Seiff, M. B. McElroy, N. W. Spencer, R. J. Duckett, T. C. D. Knight, W. S. Cook, *ibid.*, p. 786.
3. T. A. Mutch, A. B. Binder, F. O. Huck, E. C. Levinthal, S. Liebes, E. C. Morris, W. R. Patterson, J. B. Pollack, C. Sagan, G. R. Taylor, *ibid.*, p. 791.
4. S. L. Hess, R. M. Henry, C. B. Leovy, J. A. Ryan, J. E. Tillman, T. E. Chamberlain, H. L. Cole, R. G. Dutton, G. C. Greene, W. E. Simon, J. L. Mitchell, *ibid.*, p. 788.
5. T. Owen and K. Biemann, *ibid.*, p. 801.
6. M. H. Carr, H. Masursky, W. A. Baum, K. R. Blasius, G. Briggs, J. A. Cutts, T. C. Duxbury, R. Greeley, J. E. Guest, B. A. Smith, L. A. Soderblom, J. B. Wellman, J. Veverka, *ibid.*, p. 766.
7. C. B. Farmer, D. W. Davies, D. D. LaPorte, *ibid.*, p. 776.
8. H. H. Kieffer, S. C. Chase, Jr., E. D. Miner, F. D. Palluconi, G. Munch, G. Neugebauer, T. Z. Martin, *ibid.*, p. 780.

9. W. H. Michael, R. H. Tolson, A. P. Mayo, W. T. Blackshear, M. B. Kelly, D. L. Cain, J. P. Brenkle, I. I. Shapiro, R. D. Reasenberg, *ibid.*, p. 803.
10. R. W. Shorthill, R. E. Hutton, H. J. Moore, II, R. F. Scott, C. R. Spitzer, *ibid.*, p. 805.
11. B. C. Clark, P. Toulmin, III, A. K. Baird, K. Keil, H. J. Rose, Jr., *ibid.*, p. 804.
12. The Viking mission is a part of NASA's Office of Space Science Planetary Exploration Program and is managed by the Langley Research Center. The orbiter was built by the Jet Propulsion Laboratory and its subcontractors; the lander by Martin Marietta Corporation and its subcontractors. The launch vehicle was provided by Lewis Research Center. The mission's operations are conducted by a 750-man Viking flight team, managed by the Langley Research Center. The flight team is a totally integrated organization, staffed by personnel from NASA, JPL, Martin Marietta, their subcontractors, and all of the Viking scientists. The effort is the result of thousands of dedicated men and women who provided the ingenuity, the loyalty, the perseverance, and the faith in our future to make the Viking mission possible. A special note of thanks goes to the student interns for their technical assistance. The interns were supported by grants from the Alfred P. Sloan Foundation and NASA. Finally, it should be recognized that the project was organized and led by James S. Martin, A. T. Young, B. T. Lee, P. Lyman, and J. Goodlett.

26 July 1976

Preliminary Results from the Viking Orbiter Imaging Experiment

Abstract. *During its first 30 orbits around Mars, the Viking orbiter took approximately 1000 photographic frames of the surface of Mars with resolutions that ranged from 100 meters to a little more than 1 kilometer. Most were of potential landing sites in Chryse Planitia and Cydonia and near Capri Chasma. Contiguous high-resolution coverage in these areas has led to an increased understanding of surface processes, particularly cratering, fluvial, and mass-wasting phenomena. Most of the surfaces examined appear relatively old, channel features abound, and a variety of features suggestive of permafrost have been identified. The ejecta patterns around large craters imply that fluid flow of ejecta occurred after ballistic deposition. Variable features in the photographed area appear to have changed little since observed 5 years ago from Mariner 9. A variety of atmospheric phenomena were observed, including diffuse morning hazes, both stationary and moving discrete white clouds, and wave clouds covering extensive areas.*

This report is a preliminary assessment of pictures acquired from the Viking 1 orbiter during its first 30 orbits (designated as revs). During this period, attention was focused on the selection of landing sites. However, the pictures acquired have broad scientific interest, both for geology and for studies of the martian atmosphere.

The Viking visual imaging system (VIS) (*1*) consists of two high-resolution, slow-scan television framing cameras. Conceptually similar to the Mariner camera systems used in previous Mars, Mercury, and Venus missions, the VIS incorporates improvements designed to increase both spatial resolution and coverage. Each camera employs a 475-mm diffraction limited telescope and a 37-mm-diameter vidicon, the central region of which is scanned with a raster format of 1056 lines by 1182 samples and produces a 1.54° by 1.69° field of view. The optical axes of the cameras are offset by 1.38°. Cameras are shuttered alternately, resulting in contiguous swaths of images 80 km wide, with resolution better than 100 m near periapsis. Six color filters are available to restrict the image spectral bandpass to limited portions of the cameras' near-visual response characteristics.

The orbiter imaging experiment started acquiring calibration data 50 days before Mars orbit insertion (MOI); acquisition of scientific Mars data did not, however, begin until 120 hours before MOI when red and violet picture pairs were acquired every 4 hours. Beginning at MOI−56 hours, three-color pictures were taken every 2 hours through MOI−25 hours. A series of pictures taken with the red, the minus blue, and the violet filters completed the approach imaging. These early frames allayed any fears that the planet's atmosphere would interfere with photographing the surface. In several regions, particularly Hellas, Argyre, and Memnonia, they also revealed local brightenings interpreted as surface frost or ice clouds low in the atmosphere. One surprise was the visibility of the surface in the regions of the south pole, where a hood of clouds had been anticipated. After MOI, the orbiter cameras were devoted to finding suitable sites for the Viking landers.

Prior to insertion, detailed plans had been formulated to evaluate potential hazards at the landing site (A1) at 19°N, 34°W (Fig. 1), near the mouth of the large Chryse channels at the southern edge of the Chryse basin. The plan involved a calibration sequence on rev 1, extended coverage of the A1 site area on rev 3, and stereo coverage of the specific landing area on revs 4, 6, and 8. Because of a delayed arrival at the planet, the rev 1 observations were not made; the first high-resolution frames were acquired on rev 3. These revealed surprising detail in the A1 area (discussed below), sufficient to cause apprehension about its suitability as a landing site. Consequently, it was decided to look elsewhere for a safer site. The region to the northwest of the original site appeared most likely to yield a smooth area because it is farther from the mouths of the large channels, close to the deepest part of the Chryse basin, and might therefore be a site of fluvial deposition. This area (A1NW) did appear smooth in the pictures. Radar data (*2*) acquired later, however, indicated adverse conditions and resulted in searches on revs 20 and 22 for additional sites to the west, where a suitable site was eventually found. During this period two sites for the second lander were also examined (Fig. 1). These are the B site at 10°W, 44°N (revs 9 and 26) and the C site at 44°W, 6°S (revs 12 and 14). While the low-altitude coverage was being acquired, high-altitude observations continued to monitor atmospheric activity.

The Chryse Planitia region. Regional and local geological analyses (*3*) on the basis of pre-Viking data show that the area consists of relatively smooth plains of Chryse Planitia near the terminus of three large channel systems (Ares Vallis, Tiu Vallis, and Simud Vallis) that originate in chaotic terrain of Margaritifer Sinus and drain northward into the Chryse basin (Fig. 1). These channels and their associated distributary networks are considered to be primarily fluvial in origin and to have been modified by aeolian processes; however, the degree of modification by wind has not been established.

The predominant feature in the A1 area is lightly cratered plains typified by ridges similar to those on the lunar maria, and which increase in frequency and prominence to the northwest. By analogy to lunar geology, presence of the ridges suggests that the plains are lava flows with low viscosity in the melting range and are probably of basaltic composition. The second most extensive unit in the area forms plateaus which stand topographically above the plains. These are probably remnants of a surface that is older than the lava plains. Almost everywhere in this region streamlined plateau forms indicate sculpturing by fluid flow. In the transition zone between the Chryse basin and the cratered uplands, individual impact craters formed effective barriers to flow; downstream

VIKING

PROJECT REPORTS

2

to the right, where an accumulation of large boulders and possible outcrops can be seen (see Fig. 7).

Blocks and their size distribution. The images display an impressive abundance of blocks of many sizes and shapes. The blocks near the spacecraft are coarsely granular, possibly breccias formed by impact processes. Other blocks are pitted, possibly reflecting a vesicular texture. One block has an indication of rough striations, suggestive of layered basalt. On the horizon, which is about 3 km away for a spherical surface, at least three topographically high regions reminiscent of crater profiles can be seen (Figs. 2 and 5). The change is brightness of the surface from dark near the sun to bright at 180° away in azimuth is primarily due to illumination: features are backlit close to the sun and frontlit 180° away.

Any azimuth alignment of long axis directions of blocks remains to be determined. If such alignment does not exist, the implication is that streamlining by fluid (water or wind) has not occurred, or has since been altered. That interpretation is consonant with the angularity of most of the blocks. Several rocks in the field of view do, however, exhibit unusual shapes. South of southeast (Figs. 2 and 5) are two peculiarly shaped rocks, one of which has a tapering cylindrical cross section, while the other has an elongated concave indentation in its upper surface. Although the angularity of the blocks may be due to wind-faceting, the lack of clustering of facets in particular azimuths argues against this hypothesis.

Rocks of unusual forms can be produced by various physical weathering processes such as frost shattering, spalling, and aeolian sandblasting. Some of these unusual forms resemble technological artifacts or biological forms (*6*). Care must be exercised in interpreting the rocks seen in the Viking pictures. Some rocks in these pictures appear to have unusual shapes and surface markings, which are, however, due to highlights and shadows cast by irregularities on the rock surface. The true shapes of rocks can be determined only by viewing them at a variety of illumination angles.

Very few craters can be discerned on the panoramas (Figs. 1 and 5). Our first estimate is that crater area densities on the martian surface are several orders of magnitude below impact saturation for crater sizes less than about 50 m. However, there may be a number of shallow secondary craters that would be difficult to detect from our perspective. In addition, some of the smooth patches on the survey images may be craters filled with sand or dust.

Interblock regions are covered by or composed of smooth to granular surfaces (Fig. 8). The smooth surfaces are probably fine-grained sediments. Analysis of the high-resolution imagery indicates that the fines are < several hundred micrometers in size.

Block size distributions were tabulated using the sol 0 survey image for a region from southeast to southwest and from − 15° to − 40° in elevation (see Fig. 3). Those coordinates translate to a 15.48-m² area on Mars with a poorest resolution of 1 cm and a best resolution of 0.4 cm. Counts were truncated below three times the poorest resolution. The resulting size distribution, normalized to 100 m², is shown in Fig. 9, along with counts from Surveyor 3 and Surveyor 7 locations on the moon (*7*). The block size distribution is similar to that obtained with Surveyor 7, which landed within one crater radius of Tycho, a crater 85 km in diameter. The Surveyor 7 location is unique in lunar landings, exhibiting a surface with a thin regolith and

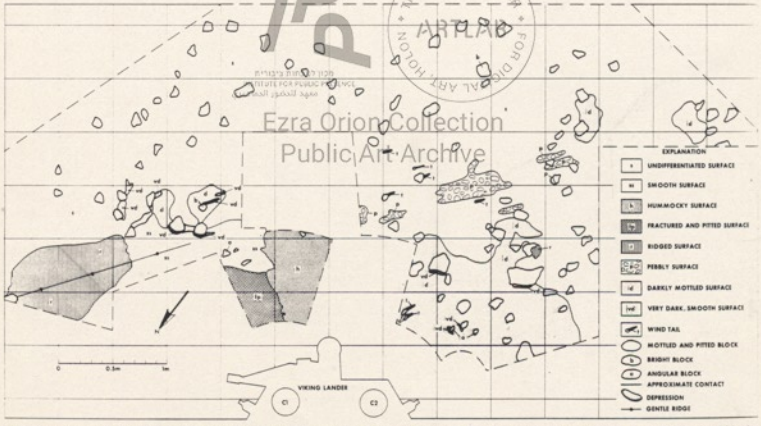

Fig. 3. Orthographic sketch map of terrain immediately surrounding the Viking 1 lander. The following units are found: mottled and pitted blocks (heavy lines); (*a*) angular blocks with smooth, flat sides; (*b*) bright, smooth, rounded blocks; (*d*) mottled surface having smooth, dark patches of fine-grained material; (*h*) hummocky surface composed of small clods emplaced during landing; (*fp*) fractured, pitted, and grooved surface resulting from disturbances during landing; (*p*) pebbly surface having a less reddish hue than the undifferentiated surface, and interpreted to be an aeolian lag gravel; (*r*) fine sinuous ridges on smooth surface; (*s*) undifferentiated surface having small blocks interspersed with fine-grained material of generally reddish hue; (*ss*) smooth surface with few blocks; (*t*) tapering reddish deposits on the lee side of boulders, interpreted to be wind tails; (*vd*) very dark surface composed of fine-grained smooth material that is deposited mostly in depressions, and against and on top of some boulders; and horseshoe-shaped depressions interpreted to be scour marks on the windward side of blunt blocks (shown in Fig. 10).

abundant blocks. Tycho is only 100 million years old (*8*) and, within a crater radius, postcratering events have served only to excavate blocky ejecta, with minimum generation of fine-grained regolith. With more data on larger block sizes, the size distribution curve would allow (*9*) estimates to be made on the landing hazard due to blocks.

At least three possible impact craters can be seen in the sol 0 survey image, providing positive evidence for one process capable of producing a regolith. The angularity of the block also argues for production by fracturing, most likely by mechanical crushing. The possible bedrock outcrops on the sol 0 survey images between −4° and −7° elevation south of southwest together with the fact that boulders seem to become larger close to the rim of the possible crater south of southeast argues for production of regolith by impact into coherent strata. But a range of other processes may also be operating, as already mentioned.

Evidence for aeolian activity. To the south of the spacecraft, several features commonly found on desert floors can be seen. Small, flat patches of pebbly ground lie at a lower level than adjacent fine-grained materials (Fig. 8). This pebbly surface has the appearance of a lag gravel, indicating scouring by wind and removal of fine-grained material. Crescentic depressions occur adjacent to some boulders. Opposite the scour marks, some boulders exhibit fine-grained deposits with thin ridge crests. The consistent direction of these deposits and the presence of scour marks suggest that both are caused by the wind action, scours being on the windward, tails on the leeward sides of the boulders. Such features resemble wind tails commonly observed in terrestrial deserts, where sand accumulates in the aerodynamically quiescent zone immediately downwind of obstacles. Very prominent scour marks on boulders can be seen to the east of the spacecraft (Fig. 10).

The indicated wind direction derived from measurements of the directions of 43 tails of fine-grained material in these images is 197° ± 14° clockwise from the north. A similar wind direction can be inferred from the accumulation of fine-grained material adjacent to the large boulder visible just below the high-gain antenna, if the material has accumulated downwind (Fig. 4). In a larger scale of kilometers to tens of kilometers, Mariner 9 (*10*) and Viking orbiter (*4*) imagery reveal both bright and dark streaks in the lees of craters and other obstacles. The flow direction indicated by Mariner 9 bright streaks is about 225° clockwise from north, suggesting that dominant sediment transport occurs during major dust storms. Mariner 9 bright streaks are most likely produced by high winds acting on deposits of fine-grained material recently settled out of the atmosphere during the last stages of the 1971–1972 global dust storm (*10*).

Fig. 4. This is a part of the sol 0 panorama, directly adjacent to (and to the right of) the region shown in Fig. 2. The boulder seen just above the reference test chart has a patch of dune material piled on its left side. One of three reference test targets used to calibrate the cameras is in the center of the image. Just to right of the test target is a plaque with the microdot signatures of the 10,000 participants in the Viking program.

An extended field of apparently fine-grained material is also visible to the east of Viking 1. Brightness variations within this field suggest transverse dune crests. The lower left-hand corner of the survey image contains curvilinear dark lines that may be ripple crests.

The areas containing abundant wind tails and fine-grained deposits are bright and relatively redder on the color images. The pebbly areas of lag are slightly less red. A third material is considerably grayer in color and lower in albedo. It is very fine-grained and smooth in appearance, and occurs both banked against the bases of some boulders and astride the tops of others (Fig. 3). It also thinly covers the ground in this area, and causes the surface to look slightly mottled. This dark material may be superposed on red sand although the contrary possibility is not ruled out. It could be material moved by winds at the saltation threshold, or deposited from a cloud of dust raised during landing. It may be significant that this dark material does not have the red color that is present on the other fine-grained material associated with the wind tails.

Surface coloration. The striking reddish coloration of the martian surface, revealed by Viking lander photography (cover), has of course been anticipated by telescopic and naked-eye observations extending to prehistoric times. But we now see that the coloration applies to boulders, rocks, and fine grains; indeed it is a rare patch of the accessible surface which is not vividly reddened. The observed color hues and saturations are, we believe, accurately rendered (*11*); from terrestrial experience they are strongly reminiscent of limonite.

Limonite is a poorly defined mixture of minerals, comprised chiefly of goethite and hematite and often written as $FeO \cdot OH \cdot nH_2O$. It has been proposed before for Mars on a variety of photometric and polarimetric grounds (*12*). However, it seems clear from analysis of the Mariner 9 infrared spectrometric observations of dust suspended in the martian atmosphere that this dust, at least, cannot be composed primarily of limonite (*13*). It is a natural suggestion that the limonite is present as a relatively thin coating of "desert varnish," as first proposed by Binder and Cruikshank and Van Tassel and Salisbury (*12*). The uniformity of this coating on the martian surface suggests that the coloring mechanism is efficient and is operating in geologically recent epochs.

The limonite stain observed on the fines and rocks of terrestrial deserts is produced by the oxidation and hydration of the mafic minerals of the rocks themselves, and in most cases these rocks are

igneous. If the limonite observed on the martian rocks and fines were produced in the same way, then the stain must be a fossil from an earlier period in martian history when the atmosphere was richer in H_2O and O_2 than it is today; limonite cannot be formed by the usual weathering processes under the current martian atmospheric conditions. However, there is considerable evidence to suggest that at least liquid water was abundant on the surface in the past and so the possibility that the limonite surface stain is a fossil is not without support. Alternatively (*14*), the limonite could have been produced by photooxidation of the mafic minerals in the rocks in the presence of the small amounts of water currently available in the martian surface environment. This process occurs on Mars and not on Earth because of the high martian surface flux of solar ultraviolet radiation. At the present, neither of these two modes of origin for limonite can be excluded and it seems possible that both have played a role in producing the rusty color of the martian surface on images by Viking 1.

Atmospheric properties. Images obtained by the Viking lander cameras offer a unique opportunity to study separately the surface and sky of Mars. Except for studies of the planetary limb, Mars light observed from above its atmosphere typically contains contributions from both the sky and the surface.

All quantitative estimates of sky surface brightness are based on ground-based calibration of the cameras before launch (*2*). Little change in camera response has been observed since launch on the basis of periodic use of the in-

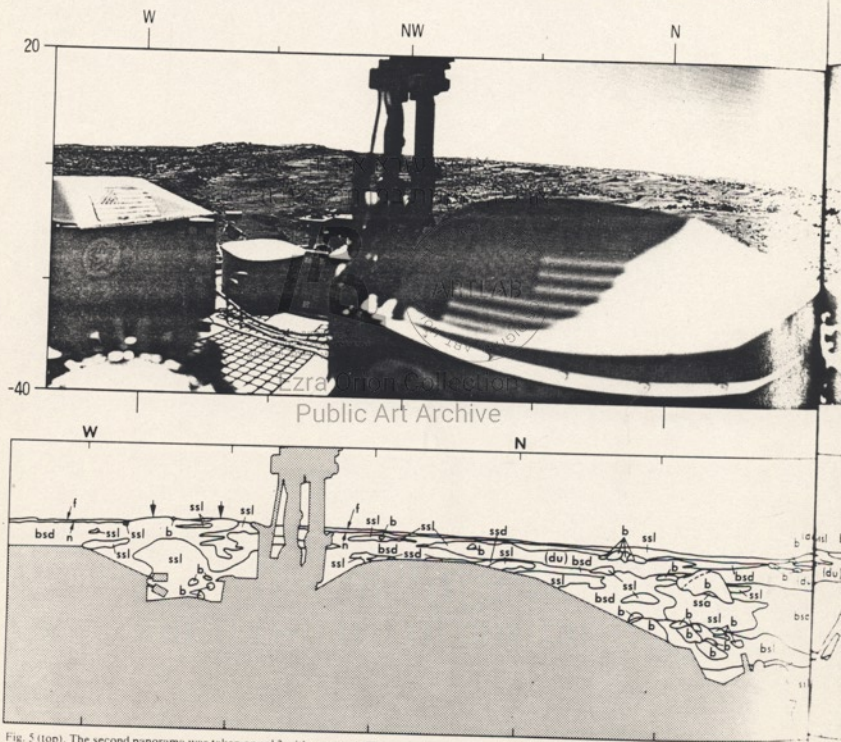

Fig. 5 (top). The second panorama was taken on sol 3 with camera 1. The central region reveals the landscape not previously imaged in Fig. 2. The large boulder northeast of the lander is about 8 m away and about 3 m high. Behind the surface sampler arm is a small dune field. Refer to Fig. 6 for sketch map of this landscape. This panorama, combined with Fig. 2, provides stereo coverage of about 240° in azimuth. Fig. 6 (bottom). Viking lander 1, sol 3, camera 1 survey panorama terrain sketch map, compiled from enlargements of returned Viking 1 lander images. The sketch map covers an azimuth range of about 300°. Several terrain units were mapped. The scene is dominated by light and dark blocky surface material (*bsl* and *bsd*) with block sizes ranging from centimeters in the near field to tens of meters near the horizon. The blocks are frequently angular and show no obvious preferential orientation. Block surface density is relatively uniform on the scale of tens of meters, although the

nal calibration lamps—at least for the photodiode channels used in the measurements discussed in this report. More reliable data reduction must also include the use of at least one of three reference test charts on the lander (see Fig. 4). These charts consist of calibrated color and gray reflectance patches. However, their use for absolute radiometric camera calibration is made difficult because the exact amount of light falling onto the reference test chart is difficult to assess. Total lighting includes contributions from direct sunlight as well as skylight, some of which may be reflected off the lander structure onto the charts.

As illustrated in Figs. 1 and 5 and on the cover, the brightness of the martian sky is comparable to that of the surface. This skylight is produced by air molecules and suspended particles, which scatter the sunlight incident on the atmosphere from above and reflected by the surface from below. Preliminary quantitative studies of imagery from the first week of Viking 1 lander operations, as discussed below, provide estimates of the relative contributions from particles and molecules, the abundance of suspended particles, their composition, time variation, and mean size.

The relative importance of the contributions of air molecules and particles to the observed skylight can be assessed by examining its observed absolute brightness. We express this brightness in terms of r, the ratio of the observed brightness to that expected from a perfectly reflecting Lambert scattering surface at Mars' distance from the sun which is illuminated by sunlight falling normal to its surface. For the sol 0 panorama, $r = 0.2$ at

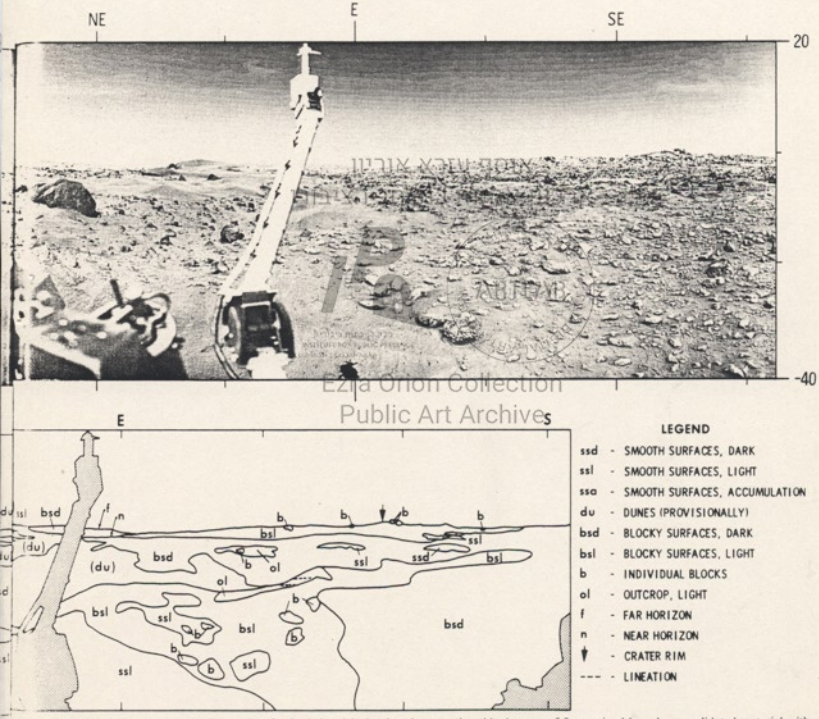

distribution is patchy at smaller scales. In the *bsl* and *bsd* units, there are interblock areas of fine-grained loosely consolidated material with variable albedo: light (*ssl*) and dark (*ssd*) surface materials are mapped. An *ssa* unit is used to denote an accumulation of smooth material, probably emplaced by aeolian processes. The (*d*) material is assumed to be a dune field. Three small lineaments have also been mapped, including two lineaments in one of the light outcrop (*ol*) units and what appears to be a fracture or ledge in the largest block in the scene. Possible crater rims on the horizon are delineated by vertical arrows where considered fairly definite. Blocks are outlined where prominent due to size or where intersecting a terrain contact. The near horizon is denoted by *n* and the far horizon is denoted by *f*. The nominal horizon is calculated to be about 3 km distant. Compass headings are indicated across the top of the scene.

the planet for much of a martian year. The martian season of our observations is antipodal to the times when global dust storms arise. The optical depth of this background aerosol may vary on time scales of months, but the important point is that τ may be appreciable much of the time.

The presence of large quantities of partially absorbing dust particles in the atmosphere implies that the dust particles are an important source of atmospheric heating. As a result, the lapse rate in the upper portion of the troposphere may be more subadiabatic and the height of the convection zone during the day may be shallower than values pertinent to dust-free conditions. Also, a considerable depth of the lower atmosphere may undergo significant diurnal temperature fluctuations, which may in turn generate diurnal variations in atmospheric pressure and winds; in contrast, when there is no suspended dust the atmosphere is warmed chiefly from the surface, and only a shallow lower region of the atmosphere would experience significant diurnal temperature fluctuations. It is interesting to note that rather large diurnal fluctuations in surface pressure and winds have been detected by the Viking lander meteorology experiment (*17*).

Surface photometric properties. The presence of a bright sky may imply that skylight has made an important contribution to light from Mars observed by past flyby and orbiter missions, and by ground-based observations, and could have biased previous estimates of the surface albedo. This is substantiated by very preliminary analysis of Viking orbiter and lander image data. While analysis of Viking orbiter imagery (*4*) suggests that the mean albedo in the landing ellipse is higher than the mean albedo of Mars averaged over bright and dark areas, analysis of initial Viking lander imagery suggests that the local albedo is lower than this average value. Alternatively, the Viking lander may have touched down in an area which has a lower albedo than the regional average, such as near a dark-haloed crater or on a dark streak.

Lander imagery data—both the sol 0 survey and the sol 1 color picture—were reduced as follows. Images were divided into small (20° by 20°) sections covering the unobstructed portion of the martian surface between the meteorology boom and the RTG windscreen. The brightness in each section was then calculated for a flat surface using three theoretical photometric functions: a near-Lambertian surface, an empirical function (*15*) based on Mariner 9 data, and a lunarlike (backscattering surface. These predictions (*3*) were then compared with measured values of surface brightness averaged over the same image sections. The best agreement was found for an albedo lower than the average Earth-based value for Mars and for a lunarlike backscattering surface. This result implies that, on the scale of at least a few micrometers, the surface may have a complex microrelief, porosity, and fine-grain size distribution not very dissimilar from those of lunar regolith. Preliminary quantitative reduction of the six three-color images indicates a surface reflectivity spectrum in the visual wavelength range which is consistent with Earth-based observations.

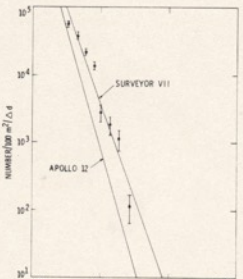

Fig. 9. Block size distributions for Viking lander 1 site, taken from the sol 0 survey image (Fig. 2). Counts are plotted as incremental frequencies per area. Error bars are binomial sampling standard errors about most probable values. Apollo 12 and Surveyor 7 plots are shown for comparison.

Motion detection and variable features. The imaging investigation includes a search for variations in the scene caused by windblown dust, albedo changes in the surface material, or, possibly, motion of macroscopic organisms (macrobes).

In the variable features experiment, a half-dozen regions on the surface and a grid target atop the lander are monitored at 1- to 10-day intervals at similar sun elevations. Preliminary studies have shown no changes on the surface besides those produced by ejection of the sampler arm shroud and locking pin. The shroud eject exposed a surface darker than the overlying material, and the area is being examined for albedo change due to dust deposition and chemical weathering. The grid target appears to be particle-free and it therefore seems that material was not raised to the level of the lander body (~ 1 m) after landing.

The motion of objects that are larger than several picture elements appears primarily as geometric distortion, rather than blurring of detail as in film cameras. It is difficult to classify the extent of geometric distortion in a general sense, as, for example, by recognition limits as a function of object size and velocity, because the extent of geometric distortion depends not only on these factors but also on the direction of object motion (*18*). No obvious examples of this type of distortion have been observed. An example of unusual features parallel to the scan direction is seen in the leftmost portion of the sol 0 picture (Fig. 1) of the footpad (*5*).

There is a repeated scanning mode in which the camera azimuth advance is inhibited and a scene which is one resolution element in angular width is repeatedly imaged with a period of either 0.22 or 14.13 seconds (Fig. 10). During the first week of imaging this mode was exercised for a total of about 35 minutes (primarily at the longer period) during both middle morning and late afternoon. The only variations observed thus far can be explained by brightness changes caused by sun movement during the imaging, and elongation of shadows projected by large rocks or the lander itself.

The dearth of observable changes to date is consistent with the low seasonal winds as measured by the meteorology instrument. The theoretical wind velocity in the boundary layer required to induce particle saltation (*13*) is several times greater than the highest gust velocities recorded (*16*). However, the repeated scan technique is extremely sensitive to changes as subtle as the vibration of a single specularly reflecting particle well below the resolution of the camera optics, and it is possible that meteorology results combined with such observations will yield the threshold velocity for particle movement, during anticipated periods of higher winds later in the mission.

Biology. With the discovery by the Viking entry mass spectrometer (*19*) and by the lander gas chromatograph–mass spectrometer (*20*) of molecular nitrogen in the martian atmosphere, all essential prerequisites for a martian biology based on terrestrial biochemistry have been satisfied: CO_2, H_2O, N_2, and sunlight. But necessary conditions are, of course, not the same as sufficient ones, and the question must be settled experimentally. The Viking 1 lander camera has a resolution

Fig. 7. This blocky surface extends from a few meters from the lander out to the highest point on the local horizon (150 ± 75 m). There are several smooth mounds in the background that appear to be dunes of windblown sediment. At the right in the middle of the frame is a patch of fractured and jointed rock that may be an outcropping.

an elevation angle of 15° and an angular distance β of 90° from the sun. Somewhat smaller values pertain at larger β, and somewhat larger values at smaller β. The effective wavelength of the survey diode used for this picture, weighted by the transmittance characteristics of the camera and the solar spectrum, is ≈ 0.73 μm. For an optically thin Rayleigh scattering atmosphere, the measured surface pressure of the landing site, and the above geometry, we find (*16*) that the value of r expected solely from molecular scattering is ~ 0.0003 times the observed value of r. Thus almost all the sky brightness is due to scattering by particles present in the atmosphere.

For an elevation angle of 10° and a scattering angle of 50° on the sol 0 panorama, $r = 0.3$. To estimate the extinction optical depth τ we assume that $\tau < 1$ and thus that the observed sky light is principally due to singly scattered sunlight. We find (*16*) that $\tau \approx 0.2$, where $\tilde{\omega}_0$ and p are, respectively, the single scattering albedo and the scattering phase function at 50°. For many different phase functions $p \sim 1$ at 50°. Also, at a wavelength of 0.73 μm, $\tilde{\omega}_0 \sim 1$ because of the high brightness of Mars in the red. Thus $\tau \sim 0.2$, and the amount of suspended particles in the martian atmosphere over the Viking 1 lander is comparable to values typical of continental areas on the earth. This value for τ is intended merely as an order of magnitude estimate.

The cover picture indicates that the sky is an orange cream to pink. We employ the color composite obtained on sol 1 to obtain $C \equiv r(\text{red})/r(\text{blue})$, where $r(\text{red})$ and $r(\text{blue})$ are, respectively, r values for the sky in the red and blue pictures. A value $C = 1$ implies a gray sky, while $C > 1$ means preferential scattering of red light. Note that C is independent of the spectrum of the incident sunlight, while the color pictures shown on the cover exhibit the product of C and the solar spectrum. From observed values of r and ground-based calibration of the camera, we find that $C = 2.5$. However, comparison of r for the test charts with values predicted from the ground-based calibration indicates that the latter give values of C that are about 25 percent too large. With this correction we find that $C = 1.9$. Part of the discrepancy could be caused by a contribution to the light incident on the test chart from a red-colored sky. In any event, $1.9 < C < 2.5$.

These values of C provide information on particle composition. The two leading candidates are soil particles blown into the atmosphere by strong winds and water ice particles formed by atmospheric condensation. Very small ice particles—that is, ones much smaller than the wavelength of visible light—will have a much larger cross section for scattering blue than red light, and thus $C \ll 1$. Larger ice particles will have extinction cross sections more nearly comparable in the two colors. Because ice is very transparent at visible wavelengths, the extinction cross section will be identical with the scattering cross section. Hence, at most angles of scatter, $C \approx 1$ for ice. Allowance for light reflected from the surface and subsequently reflected again by the atmospheric particles slightly increases C to about 1.1. Thus the observed value of C is inconsistent with values expected from ice particles. However C significantly > 1 is consistent with the presence of red surface particles suspended in the atmosphere. Surface particles large enough to have comparable extinction cross sections in blue and red light would preferentially absorb blue light while preferentially scattering red light. A conservative *lower* bound on the mean particle radius needed to meet this condition is 0.1 μm. Several lines of evidence suggest that the particles suspended in the great 1971 martian dust storm were ~ 1 μm in radius (*13*).

The sky brightness values obtained on different days for similar lighting geometries are very similar, suggesting that we are not witnessing a transitory or isolated dust storm passing over the landing site (none was detected by Viking orbital photography), but rather a background aerosol that is present over large areas of

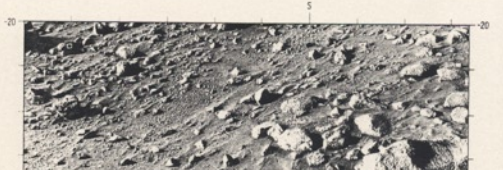

Fig. 8. This picture illustrates the variety of rock textures from smooth to extremely pitted or vesicular. Near the center is a pebbly patch that is probably analogous to a terrestrial lag gravel. Most of the rocks in this scene have depressions on the presumed windward side and elongated piles of sediment to the lee. There are numerous small pits, particularly in the lower center, that probably formed during landing, as material thrown out by the retrorocket exhaust impacted near the lander.

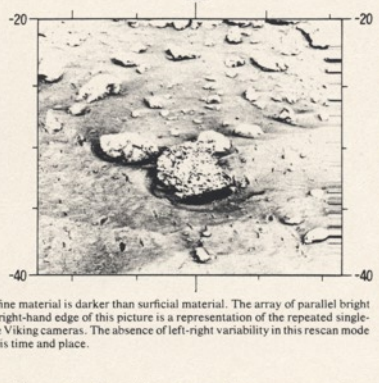

Fig. 10. The semicircular depressions around the two rocks at the center of this picture are clear evidence of wind scouring. Indirectly they also demonstrate that much of the surficial material is in the size range that can be eroded and transported by high winds, probably between 50 and 300 μm. The larger rock has a very rough texture and appears to be crudely banded. Numerous small depressions in the surface around the rocks probably formed at landing. The darker interiors of the pits suggest that subsurface fine material is darker than surficial material. The array of parallel bright and dark lines along the right-hand edge of this picture is a representation of the repeated single-line scan capability of the Viking cameras. The absence of left-right variability in this rescan mode indicates no motion at this time and place.

ranging from a few millimeters in the near field to 2 m at the nominal horizon 3 km away, when run in the high-resolution (0.04°) mode. Similar panoramic photographs obtained in most places on the land area of Earth would show unambiguous signs of life—largely grasses, bushes, and trees. No apparent signs of life would be obtained by such photographs taken on the surface of the terrestrial oceans, which comprise some 60 percent of the surface area of the earth, or in some desert and polar regions, comprising at least a few percent of the land area of the earth. While the Viking biology experiments tend principally toward microbiology, it has been thought possible that large organisms also exist on the planet (*21*), and one of the objectives of the imaging experiment has always been (*1*) the search for such macrobes.

In the 2×10^{-5} percent of the surface area of Mars accessible in varying resolutions to the Viking 1 lander camera, and in the first week of imagery, no apparent signs of life have been detected—for example, arrays of complex morphological forms exhibiting elaborate bilateral symmetry, or top-heavy forms in strong mechanical disequilibrium. In the polychromatic imagery there are no patches of anomalous color to suggest photosynthetic pigments. Comparison of both repeated single line scans and full pictures reveals no relevant changes in the configuration of surface features. There are no pits, hollows, or furrows which are uniquely attributable to mobile organisms, nor were any other features discerned which might plausibly be considered spoor. There are no objects which are obvious artifacts of intelligent life. Possible models of martian biology exist in which organisms are, because of the high ultraviolet flux, largely subsurface or largely coated with rocklike ultraviolet shields; or in which the photosynthetic pigments are red or black; or in which, in order to obtain access to brief periods of available liquid water, organisms live in shadows; or in which the macrobes do not reside in this time or place. The search for martian macrobes or their fossil equivalents by the Viking spacecraft will continue.

Lander orientation and geometry. The position of the sun in the martian sky at a specified place and time on Mars is known from astronomical observations of the relative location of Mars and the sun. We therefore know something about the expected shadows cast by the lander onto the martian surface at the time and place of landing, and how these shadows are likely to appear in the first few pictures sent back by the lander cameras. Since the lander is a very irregular object, its shadow profile changes radically depending on how the lander is oriented relative to the sun. From this information we are able to ascertain to within about 1° of accuracy the azimuth of the lander relative to the sun by comparing the shadow profile observed in the sol 0 panorama with the shadows cast by a 1/6 scale model of the lander. By more careful comparison of shadows, we can obtain an estimate of the lander tilt to an accuracy of about 5°. We achieve this comparison both by illuminating the model with a collimated light source to simulate the shadow profile produced by the sun, and by mathematically connecting particular shadow points with the positions of objects on the lander which cast them. Our result for lander orientation is 321.4° ± 1° east of north for leg 1, and < 5° for lander tilt.

We have also fit a plane to a series of lines from the camera to points on the horizon for the survey picture, using the method of least squares. From this we determine the relationship between the lander horizontal plane and the plane that contains the seven vectors and the coordinate system origin. We find an azimuth of 321° and a slope of 3.6°.

For comparison, planned orientations were, respectively, about 324° and 1°. The accelerometer readout gave, respectively, 321.91° and 2.99°. The azimuth direction of downward tilt is 285.17° clockwise from north. Thus, all data are consistent with an orientation azimuth of 321° to 322°, and a slope of the lander away from horizontal of 3° to 4°. These values were employed in a computer transformation of the apparent horizon sinusoid (Figs. 2 and 5) to a horizontal line (local relief excepted).

THOMAS A. MUTCH
Department of Geological Sciences, Brown University, Providence, Rhode Island 02912
ALAN B. BINDER
Institut für Geophysik, University of Kiel, Federal Republic of Germany, and Science Applications, Inc., Pasadena, California 91101
FRIEDRICH O. HUCK
Flight Instrumentation Division, NASA Langley Research Center, Hampton, Virginia 23665
ELLIOTT C. LEVINTHAL
Department of Genetics, School of Medicine, Stanford University, Stanford, California 94305
SIDNEY LIEBES, JR.
Department of Genetics, School of Medicine, Stanford University
ELLIOT C. MORRIS
Branch of Astrogeologic Studies, U.S. Geological Survey, Flagstaff, Arizona 86001
WILLIAM R. PATTERSON
Division of Engineering, Brown University
JAMES B. POLLACK
Space Science Division, Ames Research Center, Moffett Field, California 94305
CARL SAGAN
Laboratory for Planetary Studies, Cornell University, Ithaca, New York
GLENN R. TAYLOR
Viking Project Office, NASA Langley Research Center

The relative importance of the various processes for disposing of the missing volatiles, as well as an improved estimate of their total bulk, must await further analysis. It is reassuring to realize that the Viking landers have the capability for performing some of the most critical experiments needed to answer these questions.

TOBIAS OWEN
Department of Earth and Space Sciences, State University of New York, Stony Brook 11794

K. BIEMANN
Department of Chemistry, Massachusetts Institute of Technology, Cambridge 02139

References and Notes

1. D. M. Anderson *et al.*, *Icarus* **16**, 111 (1972).
2. K. Biemann, *Origins Life* **5**, 417 (1974).
3. C. A. Barth, W. G. Fastie, C. W. Hord, J. B. Pearce, K. K. Kelley, A. I. Stewart, G. E. Thomas, G. P. Anderson, O. F. Raper, *Science* **65**, 1004 (1969); A. Dalgarno and M. B. McElroy, *ibid.* **170**, 167 (1970).
4. M. B. McElroy, *ibid.* **175**, 443 (1972).
5. A. O. Nier, W. B. Hanson, A. Seiff, M. B. McElroy, N. W. Spencer, R. J. Duckett, T. C. D. Knight, W. S. Cook, *ibid.* **193**, 786 (1976).
6. V. G. Istomin and K. V. Grechnev, *Icarus* **28**, 155 (1976).
7. T. Owen, *Comments Astrophys. Space Phys.* **5**, 175 (1974); *Science* **183**, 763 (1974).
8. J. S. Levine, *Icarus* **28**, 165 (1976); T. Owen, *ibid.*, p. 171; F. P. Fanale, *ibid.*, p. 179; R. L. Hugenin, *ibid.*, p. 203.
9. Many investigators suggested this possibility in the wake of the Mariner 9 discovery of the channels. For a review of fluvial processes, see H. Masursky, *J. Geophys. Res.* **78**, 4009 (1973); D. J. Milton, *ibid.*, p. 4037. For a cyclical model of climate history, see C. Sagan, O. B. Toon, P. J. Gierasch, *Science* **181**, 1045 (1973).
10. We thank our fellow team members, D. Anderson, L. Orgel, J. Oro, and P. Toulmin, III, and especially A. O. Nier, for helpful discussions and support. We thank J. E. Billie, A. V. Diaz, D. W. Howarth, A. L. LaFleur, E. M. Ruiz, D. R. Rushneck, and R. Williams for their innovative assistance in the development of this experiment. There are others, too numerous to mention, who have made essential contributions; we thank them all. Supported by NASA research contracts NAS 1-10493 and NAS 1-9684.

30 July 1976

Viking Lander Location and Spin Axis of Mars: Determination from Radio Tracking Data

Abstract. *Radio tracking data from the Viking lander have been used to determine the lander position and the orientation of the spin axis of Mars. The areocentric coordinates of the lander are 22.27°N, 48.00°W, and 3389.5 kilometers from the center of mass; the spin axis orientation, referred to Earth's mean equator and equinox of 1950.0, is 317.35° right ascension and 52.71° declination.*

Analysis of the first few days of radio tracking data from the Viking 1 lander has provided preliminary determinations of the location of the lander on the surface of Mars, the radius of Mars at the landing side, and the orientation of the spin axis of Mars. Determination of these parameters constitutes part of the overall experimental objectives of the Viking radio science team (*1*). These results illustrate the strength of the precise Viking radio tracking data in the determination of astrodynamic constants; they are also important for the interpretation of data from other Viking experiments and for providing accurate reference points for measurements involving topographic parameters.

The Viking lander data used in this analysis consist of approximately 1 hour of Doppler (range rate) measurements at 1-minute count rate on each of the first 3 days after landing, and approximately 10 minutes of ranging data (three range points) on each of the first 2 days after landing. The estimated precision of the Doppler data is better than 1 mm/sec, and that of the ranging data is better than 15 m.

The spin axis orientation and the two components of the lander position in cylindrical coordinates, the longitude and the distance from the spin axis, are best determined from the Doppler tracking data. The third position component, the distance from the equator along the spin axis, is best determined from the ranging data but is subject to large uncertainties if there are even small relative errors in the ephemerides of Earth and Mars. A previously developed special technique (*2*) that uses nearly simultaneous orbiter and lander tracking data has been used to correct the ephemeris errors.

The present analysis consists of a simultaneous solution for five parameters, three lander coordinates and two spin axis orientation components, with all other parameters fixed at their nominal or best-known values. The results obtained for the lander position components, expressed in areocentric coordinates are: latitude, 22.27° ± 0.02°N; longitude, 48.00° ± 0.07°W; radius from the center of Mars, 3389.5 ± 0.3 km. The corresponding value for the latitude in areographic coordinates, frequently used as the reference latitude on maps, is 22.48°N. These results were obtained with a nominal (*3*) and unadjusted spin rate for Mars; any adjustment in spin rate will affect the longitude.

The results indicate that Viking 1 landed about 28 km from its targeted landing site, well within the expected landing dispersions. The radius to the center of Mars is in good agreement (within 1 km) with earlier estimates of the radius at the indicated surface location (*4*), which included consideration of regional topographic variations.

The values determined for the right ascension α_0 and declination δ_0 of the spin axis, referred to Earth's mean equator and equinox of 1950.0 are:

$$\alpha_0(1950.0) = 317.35° \pm 0.06°$$
$$\delta_0(1950.0) = 52.71° \pm 0.01°$$

When compared with the values of Lorell *et al.* (*5*) and of de Vaucouleurs, Davies, and Sturms (*3*), these values and the corresponding uncertainties represent a statistically significant improvement. The larger uncertainty for the right ascension is due to its high correlation with the lander longitude. Since long arcs of lander tracking data provide an excellent data source for these determinations, additional data will improve these estimates and could provide information on pole motion.

W. H. MICHAEL, JR.
R. H. TOLSON
A. P. MAYO, W. T. BLACKSHEAR
NASA Langley Research Center, Hampton, Virginia 23665

G. M. KELLY
Analytical Mechanics Associates, Inc., Hampton, Virginia 23665

D. L. CAIN, J. P. BRENKLE
Jet Propulsion Laboratory, California Institute of Technology, Pasadena 91103

I. I. SHAPIRO, R. D. REASENBERG
Massachusetts Institute of Technology, Cambridge 02139

References and Notes

1. W. H. Michael, Jr., D. L. Cain, G. Fjeldbo, G. S. Levy, J. G. Davies, M. D. Grossi, I. I. Shapiro, G. L. Tyler, *Icarus* **16**, 57 (1972).
2. W. T. Blackshear, R. H. Tolson, G. M. Day, *J. Spacecr. Rockets* **10**, 284 (1973).
3. G. de Vaucouleurs, M. E. Davies, F. M. Sturms, Jr., *J. Geophys. Res.* **78**, 4395 (1973).
4. Topographic map of Mars, M-25M-3-RMC (1 : 25,000,000) (U.S. Geological Survey, Denver, Colo.).
5. J. Lorell, G. H. Born, E. J. Christensen, P. B. Esposito, J. F. Jordan, P. A. Laing, W. L. Sjogren, S. K. Wong, R. D. Reasenberg, I. I. Shapiro, G. L. Slater, *Icarus* **18**, 304 (1973).
6. We thank T. A. Komarek, J. T. Findlay, and G. L. Sievers for assistance and support; E. J. Christensen, C. E. Hildebrand, and H. Hokikian of the Viking navigation team for comparison of independent results, which essentially agree with ours; and the members of the Viking project and Viking flight team, who provided hardware, software, data, and support. Financially supported by the National Aeronautics and Space Administration.

30 July 1976

References and Notes

1. T. A. Mutch, A. B. Binder, F. O. Huck, E. C. Levinthal, E. C. Morris, C. Sagan, A. T. Young, *Icarus* **16**, 92 (1972).
2. F. O. Huck, H. F. McCall, W. R. Patterson, G. R. Taylor, *Space Sci. Instrum.* **1**, 189 (1975).
3. F. O. Huck and S. D. Wall, *Appl. Opt.* **15**, 1748 (1976).
4. M. Carr *et al.*, *Science* **193**, 766 (1976).
5. The left side of the footpad picture contains two particularly interesting features. Neither is a real surface feature, since they do not appear in later images of the same area. The first picture was taken about 25 seconds after touchdown. In the first 75 lines of the picture, which took 15 seconds to acquire, there are a large number of fine, bright striations in the image. The effect is similar to what one would expect if the scene illumination were varying markedly from line to line; that is, on a time scale of 0.2 second. The cameras show no electrical anomalies and there were no activities scheduled on the lander which might have caused electrical interference. These lines might be the result of a turbulent cloud of fine dust raised by the lander's retrorockets. Since the lines are brighter than the scene, the dust must, in this explanation, be between the camera and the surface region viewed. The scene detail is not degraded. The turbulence would have to vary very rapidly, and, to the extent that the effect influences entire scan lines, the turbulence would have been correlated over distances of 75 cm. Dust seems to be a plausible explanation, although we have not yet completed our analysis of the time and space variations of these early digital data. The second feature is a distinct vertical dark band crossing the picture. Several explanations might be proposed. First, the dark band could be the shadow of the lander's parachute passing the lander. However, the duration of the shadow is inconsistent with the diameter of the parachute and the wind velocity. Second, it is possible that the band could be the shadow of a martian cloud, in which case other similar bands should be seen as the mission progresses. Through sol 7 no other such bands have been detected. Third, the band could be produced by clods of regolith ejected during descent maneuvers, rapidly deposited on the camera window and slowly sliding off. However the time delay between landing and the appearance of the dark band seems to rule out this explanation. Finally, the dark band could be the shadow of a cloud of dust raised by the landing. This model has been investigated and is consistent with the parameters of the landing if the cloud is roughly 100 m across and 200 m above the surface. Applying the Stokes-Cunningham equation to the particles in the cloud yields an upper limit on particle diameter of roughly 200 μm, a plausible value.
6. E. C. Morris, T. A. Mutch, H. E. Holt, *Atlas of Geologic Features in the Dry Valleys of South Victoria Land, Antarctica; Possible Analogs of Martian Surface Features* (U.S. Geological Survey Interagency Rept.; Astrogeology 52, 1972).
7. E. Morris and E. Shoemaker, *Icarus* **12**, 188 (1970).
8. R. Arvidson, R. Drozd, E. Guinness, C. Hohenberg, C. Morgan, *Proceedings of the 7th Lunar Science Symposium*, in press.
9. H. Moore, R. Pike, G. Ulrich, "Lunar terrain and traverse data: Lunar roving vehicle design study" (U.S. Geological Survey, informal report, 1969).
10. C. Sagan *et al.*, *J. Geophys. Res.* **78**, 4163 (1973); *Icarus* **17**, 346 (1972); J. Veverka *et al.*, *ibid.* **21**, 317 (1974).
11. The Viking cameras record picture information on one or more of 12 silicon photodiodes positioned in the focal plane. The photodiodes are sensitive to light from approximately 0.4 to 1.1 μm in wavelength. Six of the diodes are covered with interference filters which transmit light only in selected wavelength ranges. In acquiring a color picture, data are recorded with three photodiodes which have blue, green, and red filters. Three filtered photodiodes in the near infrared are used to acquire infrared imagery. Color data returned to the earth are used in the laboratory to modulate the intensities of red, green, and blue light ray bundles which are simultaneously scanned over a sheet of color film. Because the voltages recorded by the diodes are a complex function of the diode sensitivities, the filter characteristics, and the atmospheric transmission, it is necessary to scale the relative contributions of each of the three channels to compensate for these effects. The necessary compensation has been calculated in two substantially independent ways which yield similar results. One method depends on prelaunch measurements of the relative spectral responsivities and of the absolute response to a broadband light source to compute the compensation required for equal output for a neutral gray reflecting scene. This assumes that the cameras are stable and that the atmospheric attenuation is negligible. The second method depends on the measured camera response to viewing a reference target (Fig. 4) on the lander top. This target has red, green, and blue color reference patches and also 11 gray patches with integrated reflectances between 0.1 and 0.9. The color compensation is adjusted to optimize the target reproduction; then that compensation is applied to the scene. The disadvantage of this technique is the uncertainty in the human judgment of the "best" reproduction of the target. Both techniques are complicated by the fact that some of the interference filters have small "leaks." For example, the blue filter transmits a small amount of light in the infrared. An object in the scene which reflects large amounts of light in the infrared will appear deceptively bright when imaged with the blue diode. In order to determine such spurious contributions from the scene it is necessary to obtain both a color and an infrared picture of the same scene under approximately the same illumination conditions, and then to balance the colors in a manner which is empirically consistent with the data. Among other reasons for accepting the reality of the colors portrayed, however, is the correct rendering of the gray spacecraft surface and the orange cables.
12. A. Dollfus, *Ann. Astrophys. Suppl. 4* (1957) (NASA Tech. Transl. TT-F-188); A. Binder and D. Cruikshank, *Commun. Lunar Plan. Lab. 193* (1964); R. A. van Tassel and J. W. Salisbury, *Icarus* **3**, 264 (1964); C. Sagan, J. P. Phaneuf, M. Ihnat, *ibid.* **4**, 43 (1965); J. B. Pollack and C. Sagan, *Space Sci. Rev.* **9**, 243 (1969).
13. O. B. Toon, J. B. Pollack, C. Sagan, *Cornell Univ. Rep. CRSR 639* (1976); *Icarus*, in press.
14. R. L. Huguenin, *Icarus* **28**, 203 (1976).
15. T. Thorpe, *ibid.* **20**, 482 (1973); personal communication.
16. J. Pollack, *Icarus* **6**, 42 (1976).
17. S. Hess *et al.*, *Science* **193**, 788 (1976).
18. F. O. Huck, S. D. Wall, E. E. Bucher, *NASA TND-7668* (1974).
19. A. Nier *et al.*, *Science* **193**, 786 (1976).
20. T. Owen and K. Biemann, *ibid.*, p. 801.
21. C. Sagan and J. Lederberg, *Icarus* **28**, 291 (1976).

22. A large number of people have made substantial contributions to this report, in areas of mission design and science analysis. In a very real sense, these persons should be considered coauthors. They include R. E. Arvidson, P. Avrin, C. E. Carlston, R. D. Collie, N. Coradini, R. E. D'Alli, E. W. Dunham, P. L. Fox, S. U. Grenander, E. A. Guinness, B. W. Hapke, J. W. Head, K. L. Jones, R. A. Kahn, B. K. Lucchitta, D. Nummedal, D. C. Pieri, C. W. Rowland, R. S. Saunders, R. H. Stockman, R. B. Tucker, S. D. Wall, and M. R. Wolf. Andrew T. Young played an important role in the early design studies of the lander imaging system. A number of college undergraduates assisted in the operational phase of the investigation. They include A. L. Chaikin, R. G. Cooper, W. E. Dieterle, C. Eberspacher, F. D. Eckelmann, Jr., E. A. Hildum, H. W. Printz, D. W. Thompson, and J. C. Thompson. Their participation was made possible by support from the Alfred P. Sloan Foundation and by the NASA Planetology Office. Because the success of each science investigation is crucially dependent on the efforts of the 750 members of the flight team headed by J. S. Martin, Jr., Viking project manager, and A. Thomas Young, Viking mission director, as well as the 10,000 contractor employees who designed and built the spacecraft, its components, and support equipment, our acknowledgement should also include the 10,000 signatures in the microdot carried to Mars on the spacecraft (Fig. 4). Design and manufacture of the Viking lander cameras was performed by the ITEK Corporation, with active cooperation by Langley Research Center and Martin Marietta Corporation. The Image Processing Laboratory, Jet Propulsion Laboratory, is responsible for special processing of imaging data returned from Mars to the earth and processed the images in Figs. 2, 5, 7, 8, and 10. The images in Figs. 1 and 4 were processed with the real-time software developed by the Data Systems Division of JPL. Financial support for the work of team members was provided by the NASA Viking Project Office.

30 July 1976

Composition of the Atmosphere at the Surface of Mars: Detection of Argon-36 and Preliminary Analysis

Abstract. *The composition of the martian atmosphere was determined by the mass spectrometer in the molecular analysis experiment. The presence of argon and nitrogen was confirmed and a value of 1 to 2750 ± 500 for the ratio of argon-36 to argon-40 was established. A preliminary interpretation of these results suggests that Mars had a slightly more massive atmosphere in the past, but that much less total outgassing has occurred on Mars than on Earth.*

The objective of the Viking molecular analysis experiment is twofold: to detect and identify the organic compounds, if any, present in the surface of Mars, and to determine periodically the composition of the lower atmosphere (*1*). The central part of the instrumentation for this experiment is a mass spectrometer, coupled to a gas chromatograph for the organic analysis and, by way of a molecular leak, to a gas sample reservoir. Although the instrument was designed primarily for the detection of organic compounds in the gas chromatographic mode (*2*), the mass spectrometer's high sensitivity (dynamic range, six to seven orders of magnitude), high mass range (m/e 12 to 200), and resolution (1 : 200 at m/e 200; better at lower mass) were used to advantage in determining the composition of the atmosphere, particularly its minor constituents. The penalty one pays for resolution and sensitivity is a certain loss of accuracy, mainly because the residual background in the instrument becomes more significant and the long-term reproducibility of the fragmentation pattern is lowered.

Since the more important questions concerning the composition of the martian atmosphere centered around the minor components and certain isotopic ratios, an attempt was made to optimize the experiment toward that goal. In particular, the detection of even traces of N_2 was deemed to be extremely important because previous data (*3*) suggested that it must be a minor component or could be almost completely absent (*4*). One of the major problems in a mass spectromet-

Table 1. Preliminary data on the abundances of gases detected in the martian atmosphere.

Component*	Abundance (%)
Carbon dioxide	95
Oxygen	0.1 to 0.4
Nitrogen	2 to 3
Argon	1 to 2
$^{36}Ar/^{40}Ar$ ratio	1 : 2750 ± 500

*Variable amounts of water, 0.16 percent carbon monoxide, and 0.03 ppm of ozone have been found in the martian atmosphere by ground-based or spacecraft observations [see (7) for references]. Because of surface absorption the mass spectrometric data on H_2O are rather meaningless. The reasons for the CO remaining undetermined are mentioned in the text, and ozone is far below our detection limit.

ric determination of N_2 in the martian environment is the interference of CO^+ (from CO or CO_2) with the ion current of N_2^+ at *m/e* 28. For this reason the gas reservoir of the instrument is coupled via separate valves to two cavities, one containing Ag_2O and LiOH, for the oxidation of CO to CO_2 and absorption of all CO_2, and the other containing $Mg(ClO_4)_2$ for the removal of the resulting water. During the fourth and fifth day after the landing of Viking 1 (20 July 1976) a total of six atmospheric analyses were performed at approximately 6-hour intervals. In the first four of these analyses, CO and CO_2 were removed; in the last two analyses, samples of unaltered atmosphere were used. During the third analysis the spectrometer shut down temporarily, leaving us with a total of five sets of mass spectral scans. Analysis of these spectra gave the averaged results shown in Table 1.

It is clear from these results that the N_2 content is consistent with earlier limits (*3*) and corroborates the results of the upper atmosphere analysis (*5*) performed during the descent of the Viking 1 lander. The argon content is much lower than most recently suggested (*6*) and again supports the value found for the upper atmosphere (*5*).

Of most importance is that the high sensitivity of our mass spectrometer permitted the determination of the abundance of ^{36}Ar which was found to be about ten times lower than the value corresponding to the terrestrial ratio of ^{36}Ar to ^{40}Ar. Neon, krypton, and xenon could not be detected at the limits shown in Table 2. It should be pointed out that for this preliminary analysis the quoted detection limit of neon is higher than the amount of ^{36}Ar actually determined. This is because of the low instrument background and little interference at *m/e* 36 (the absence of a corresponding signal at *m/e* 35 excludes any contribution from HCl) and because of the finite contributions of $^{40}Ar^{2+}$ to *m/e* 20 even at 45 ev.

Low concentrations (less than a few percent) of CO cannot be detected with our system, because of the interference by the large amount of CO_2 in the two analyses of the unmodified atmospheric sample and the concomitant removal of CO when removing the CO_2 in the analyses where it was exposed to Ag_2O. Also, the determination of O_2 is reliable only in the unaltered atmosphere, because of the possibility that some of the Ag_2O produces O_2. For this reason the value for O_2 in Table 1 is from only two measurements.

The determination of other minor constituents, including the isotope ratios for N_2, must await further refinement of the data and additional analyses, which are planned. The abundances of ^{13}C and ^{18}O as determined from the *m/e* 44, 45, and 46 signals appear to be equal to the terrestrial values within the accuracy of our preliminary measurements.

At this stage of the analysis and acquisition of data, it would be premature to draw any firm conclusions regarding the outgassing history of the planet. We can, however, relate some of our results to a theoretical consideration of this problem using ideas developed in anticipation of the experiment (*7*).

The noble gases provide a particularly useful measure of the degree of planetary outgassing. The report by Istomin and Grechnev (*6*) that the martian atmosphere might contain as much as 35 percent ^{40}Ar was widely interpreted to indicate that Mars had outgassed as thoroughly as Earth, and led to the prediction that massive amounts of concurrently produced volatiles had either escaped from the planet or were presently buried in the regolith (*8*). The discovery that the ^{40}Ar abundance is only 1 to 2 percent of the present atmosphere indicates that the other volatiles should be proportionately reduced in such models. But the fact that the $^{36}Ar/^{40}Ar$ ratio is less on Mars than it is on Earth by a factor of 10 suggests that the interpretation of martian outgassing may not be quite so straightforward. The ^{40}Ar may be anomalously abundant on Mars. It should be safer to scale the abundances of other volatiles relative to ^{36}Ar, the nonradiogenic isotope.

If we compare the absolute abundances of ^{36}Ar on Mars and Earth, taking ratios of the mass of gas to the mass of the respective planet, we find that the amount in the martian atmosphere is approximately 100 times smaller than the terrestrial value. This implies

Table 2. Upper limits on the gases not detected in the atmosphere.

Gas	Initial upper limit (ppm)*
Neon	10
Krypton	20
Xenon	50

*We expect to decrease these limits for the analysis of the atmosphere under conditions of enrichment of the minor constituents.

that the total degassing of Mars is less complete than that of Earth by about the same factor, if we ignore the possibility of ^{36}Ar escape. The ratios $CO_2/^{36}Ar$ and $N_2/^{36}Ar$ are both roughly ten times smaller in the martian atmosphere than in Earth's inventory of volatiles. It is especially interesting that the relative abundances of N_2 and CO_2 now in the martian *atmosphere* are very similar to the values found in Earth's *inventory*.

One interpretation of these results is that Earth and Mars have a similar bulk composition, so gases are produced in similar proportions but degassing and subsequent weathering on Mars have been much less complete. The present martian atmosphere would then represent about one-tenth the mass of the total outgassed volatiles exclusive of water. The corresponding amount of water is equivalent to a layer a few tens of meters deep.

The missing volatiles may be trapped in subsurface permafrost (H_2O) and at the polar caps (H_2O, CO_2), chemically bound in the soil (nitrates, oxides, carbonates), and some portion must have escaped from the planet (*4*). In this view, the ^{40}Ar abundance represents an anomaly, being roughly ten times more abundant than predicted. This discrepancy could result from several causes, for example, an enrichment of potassium in the martian crust relative to Earth, or a different degassing history for ^{40}Ar compared with the other volatiles, an interpretation that would be consistent with its radiogenesis from ^{40}K.

This Earth-analog model implies that the martian atmosphere was never much more than ten times as massive as it is now, producing a maximum surface pressure of ~100 mbar. But with the possibility that CO_2 can be trapped at the poles and that large amounts of water could be present in the form of permafrost, we leave open the opportunity for cyclical or at least episodic variations of the mean climatic conditions on the planet, which would permit the formation of the sinuous channels by water erosion during temperate periods (*9*).

spheric temperature profile has a shape given by the mean Viking engineering model (NASA Langley Research Center M75-125-2).
7. P. Gierasch and R. Goody, *Planet. Space Sci.* **16**, 615 (1968).
8. B. Conrath, R. Curran, R. Hanel, V. Kunde, W. Maguire, J. Pearl, J. Pirraglia, J. Welker, T. Burke, *J. Geophys. Res.* **78**, 4267 (1973).
9. An oversight in currently used ground software produces geometry errors that can have a maximum value of 3.8′ in the direction of scan platform motion. That uncertainty has been removed by hand from maps used in this report but remains in the morning data of Fig. 5, contributing to the scatter there to an unknown degree.
10. Predawn air temperatures measured 167 cm above the surface during the first day after landing as part of the lander meteorology experiment show excellent agreement with the predawn T_{11} values.
11. T. A. Mutch, A. B. Binder, F. O. Huck, E. C. Levinthal, S. Liebes, E. C. Morris, W. R. Patterson, J. B. Pollack, C. Sagan, G. R. Taylor, *Science* **193**, 791 (1976).
12. R. J. Curran, B. J. Conrath, R. A. Hanel, V. G. Kunde, J. C. Pearl, *ibid.* **182**, 381 (1973).
13. The MC charts are a set of 30 topographic shaded relief maps (scale, $1:5 \times 10^6$) produced by the Department of the Interior, U. S. Geological Survey, Reston, Va. 22092.
14. K. C. Herr and G. C. Pimentel, *Science* **166**, 496 (1969); G. Neugebauer, G. Munch, H. H. Kieffer, S. C. Chase, Jr., E. Miner, *Astron. J.* **76**, 719 (1971); R. Hanel, B. Conrath, W. Hovis, V. Kunde, P. Lowman, W. Maguire, J. Pearl, J. Pirraglia, C. Prabhakara, B. Schlachman, G. Levin, P. Straat, T. Burke, *Icarus* **17**, 423 (1972).
15. A. O. Nier, W. B. Hanson, A. Seiff, M. B. McElroy, N. W. Spencer, R. J. Duckett, T. C. D. Knight, W. S. Cook, *Science* **193**, 786 (1976).
16. S. Hess and C. Leovy, personal communication.
17. The two Viking IRTM experiments represent a fourfold increase in the total number of thermal detectors flown to other planets. Their success is the result of the individual efforts of a large number of people during design, fabrication, and the complex flight operations of this instrument. The prolonged efforts of Mike Agabra, Jack Engel, Howard Eyerly, Claude Michaux, Richard Ruiz, and Don Schofield are representative of this group. The massive data reduction system is a tribute to and from Bob Mehlman, John Gieselman, and Elliot Goldyn. We hope all involved take satisfaction from this evidence of their effort. Supported by Jet Propulsion Laboratory contract 952988 to the University of California.

26 July 1976

Composition and Structure of the Martian Atmosphere: Preliminary Results from Viking 1

Abstract. *Results from the aeroshell-mounted neutral mass spectrometer on Viking 1 indicate that the upper atmosphere of Mars is composed mainly of CO_2 with trace quantities of N_2, Ar, O, O_2, and CO. The mixing ratios by volume relative to CO_2 for N_2, Ar, and O_2 are about 0.06, 0.015, and 0.003, respectively, at an altitude near 135 kilometers. Molecular oxygen (O_2^+) is a major component of the ionosphere according to results from the retarding potential analyzer. The atmosphere between 140 and 200 kilometers has an average temperature of about 180° ± 20°K. Atmospheric pressure at the landing site for Viking 1 was 7.3 millibars at an air temperature of 241°K. The descent data are consistent with the view that CO_2 should be the major constituent of the lower martian atmosphere.*

The Viking spacecraft which landed on Mars on 20 July 1976, about 4 hours after local noon, included a set of instruments which measured the physical and chemical properties of the martian atmosphere during entry. The upper atmosphere, above about 100 km, was sampled with a mass spectrometer sensitive to neutral gases in the mass range 1 to 50. Properties of the martian ionosphere were determined with a planar retarding potential analyzer (RPA) designed to provide information on the temperature, composition, and concentration of atmospheric ions. The RPA, which also measured electron energy spectra, was expected in addition to clarify the nature of the interaction between Mars and the external solar wind. The RPA and the upper atmospheric mass spectrometer (UAMS) were mounted on the spacecraft aeroshell. Pressure, temperature, and acceleration sensors gave data on the structure of the atmosphere below 100 km. These results, combined with information from the spacecraft's gyroscopes and radar altimeter, allow one to determine the variation of atmospheric density, pressure, temperature, and winds over an extensive height range for the lower atmosphere.

In this report we present a preliminary account of the results obtained from the various entry science experiments. More detailed accounts of the instruments are given elsewhere (*1*). The UAMS employed an open ion source mounted in such a manner as to allow ambient atmosphere to enter the instrument directly, an important design feature which permits a qualitative measurement for reactive gases such as O. The concentration of chemically inert species may be determined with some confidence from laboratory calibrations obtained prior to flight. The instrument was also exposed to a high-speed molecular beam designed to simulate motion of the spacecraft through the martian atmosphere. These data allow one to establish a quantitative relation between measured quantities and ambient atmospheric densities (*2*).

A spare instrument, identical to the flight instrument, was set up in the laboratory to facilitate a number of studies not possible in preflight tests. Figure 1 reproduces a variety of spectra obtained with pure CO_2, CO_2 with 2 percent Ar, and CO_2 with 5 percent N_2. The mass peaks at 44, 28, 22, 16, and 12 in Fig. 1a correspond to CO_2^+, CO^+, CO_2^{2+}, O^+, and C^+, respectively. The incident electrons in Fig. 1, and for the martian spectra shown in the other figures, have energies equal to 75 ev. Figure 1a also indicates mass peaks at 46, 45, 30, 29, 23, 22.5, and 13, due to $(^{12}C^{18}O^{16}O)^+$, $(^{13}C^{16}O^{16}O)^+$, $(^{12}C^{16}O)^+$, $(^{12}C^{18}O^{16}O)^{2+}$, $(^{13}C^{16}O^{16}O)^{2+}$, and $(^{13}C)^+$. Mass peaks at 32 and 14 are associated with a small quantity of O_2^+ and CO^+ formed during the ionization of CO_2. Peaks at 17 and 18 are due to residual concentrations of H_2O present as an impurity in the instrument. Addition of Ar (Fig. 1b) gives rise to peaks at 40 and 20. The peak at 28 is approximately doubled by addition of 5 percent N_2 (Fig. 1c), and the presence of N_2 is further confirmed by the peak at mass 14 due to N^+ and $(N_2)^{2+}$.

Figure 2 gives a sample spectrum for Mars obtained at an altitude of approximately 135 km above the martian surface. Prominent peaks at masses 40 and 20 show clear evidence for Ar. The mixing ratio for the gas at this altitude, relative to CO_2, is approximately 0.015 by volume, in major disagreement with an indirect measurement of Ar inferred from data obtained by the Soviet probe Mars 6. Istomin and Grechnev (*3*) reported a mixing ratio of 0.54 ± 0.2 for an inert constituent of the martian atmosphere which they attributed to Ar. The mixing ratio of ^{40}Ar in the lower martian atmosphere cannot be this high and must lie somewhere in the range 0.01 to 0.02.

The peak at mass 28 in Fig. 2 contains contributions from CO^+ formed by the ionization of CO_2 and CO, in addition to N_2^+ formed by the ionization of N_2. The peak at mass 14 is composed primarily of N^+ and $(N_2)^{2+}$ from N_2, although it includes also a small contribution from $(CO)^{2+}$ formed by the ionization of CO and CO. The data in Fig. 2 indicate a mixing ratio of N_2 relative to CO_2 of about 0.06. Much higher mixing ratios were detected at higher altitude, as would be expected as a result of the diffusive separation of the lighter gas, N_2. A preliminary attempt to extrapolate the present data to lower altitude suggests a mixing ratio N_2 to CO_2, of between 0.02 and 0.03 for the bulk atmosphere, consistent with an upper limit for this parameter imposed earlier (*4*) based on analysis of the ultraviolet day glow spectra measured by Mariner 6 and Mariner 7 (*5*).

The peak at mass 32 is due primarily to O_2 and suggests a mixing ratio, O_2 to

Argon Content of the Martian Atmosphere at the Viking 1 Landing Site: Analysis by X-ray Fluorescence Spectroscopy

Abstract. *The argon content of the martian atmosphere at the Viking 1 landing site is ≤ 0.15 millibar or ≤ 2 percent by volume (95 percent confidence level).*

The Viking x-ray fluorescence spectrometer (*1*), although designed for elemental analysis of martian surface soil, also detects the gaseous elements within its sensitivity range. Operation in the calibration mode, that is, without a soil sample in the analysis chamber, thus provides data on the abundance of elements with $Z > 12$ in the martian atmosphere.

The analysis chamber is a hollow square prism 2.5 cm on a side, with thin windows on two adjacent sides which permit x-rays from radioactive ^{55}Fe and ^{109}Cd sources to irradiate its interior. Backscattered and fluorescent x-rays from the chamber are detected by sealed, gas-filled proportional counters flanking the radioactive sources. The chamber walls opposite the windows have calibration plaques that produce reference spectra when the instrument is operated without a sample.

The question of pressure and concentration of Ar in the martian atmosphere has aroused much interest recently (*2*), largely because of an interpretation of the engineering data from the mass spectrometer on the Soviet probe Mars 6 (*3*). The anomalously high ion-pump current reported was consistent with a large content of inert gas in the atmosphere. From what is known of the geochemistry of Mars, this gas is probably Ar, and contents up to 30 mole percent were implied (*2*, *3*). Reevaluation of previous observations and models of the planet and its atmosphere did not preclude such Ar contents (*2*).

In addition to being of scientific interest, the determination of the Ar content of the martian atmosphere at the Viking landing site is of considerable operational importance. The ion pump of the gas chromatograph–mass spectrometer on the lander has a limited tolerance for inert gases; important operational decisions with respect to the use of this instrument for atmospheric analysis depend on knowledge of the partial pressure of Ar and other inert gases. Accordingly, a strategy was developed that would permit the measurement of Ar as early as possible in the Viking mission, first in the upper atmosphere by the Viking entry mass spectrometer (*4*, *5*), and then by taking optimum advantage of the independently planned calibration sequence for the x-ray fluorescence spectrometer (*1*). After it was established that the Ar content does not exceed 0.5 mbar, a complete sequence of atmospheric measurements was executed by the lander mass spectrometer (*6*, *7*).

Counter 2 of the x-ray fluorescence spectrometer is the most useful for Ar determination because of the absence of calibration target peaks at the Ar emission energy (2.96 kev). The calibration spectrum of counter 2 in vacuo has an Al K_α peak (1.49 kev), mainly from the calibration plaque, and one caused by backscattered Mn K_α x-rays (5.9 kev) emitted by the ^{55}Fe radioisotope source (Fig. 1a).

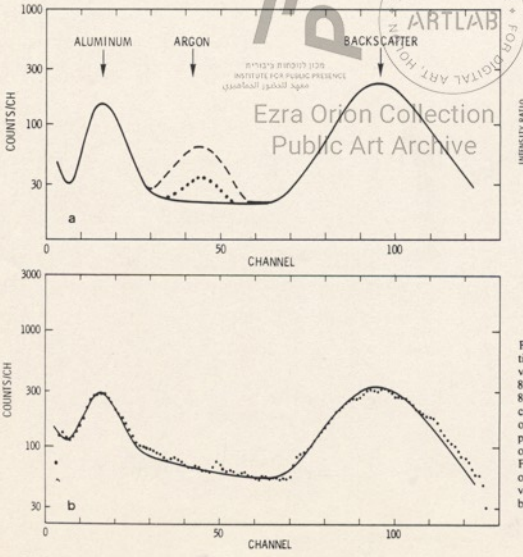

Fig. 1 (left). Spectra used in Ar determinations. (a) Calibration spectra: Solid line, in vacuo; dashed line, 20 percent Ar with CO_2 at 8 mbar; dotted line, 5 percent Ar with CO_2 at 8 mbar. (b) Experimental spectra: Solid line, calibration in Mars orbit prior to separation of the lander; dotted line, data points (three-point sliding average) for spectrum obtained on sol 0 at the Viking 1 landing site on Mars. Fig. 2 (above). Ratio of integrated intensities of Ar peak to backscattered ^{55}Fe radiation versus partial pressure of Ar in laboratory calibration experiments (mixtures of Ar and CO_2).

Spectra taken in the terrestrial atmosphere and in laboratory mixtures of varying proportions of CO_2 and Ar show a strong peak at 2.96 kev that is caused by Ar K_α x-rays (Fig. 1a). Calibration of the instrument for Ar determinations (Fig. 2) was made by introducing mixtures of CO_2 and Ar in various proportions and at different pressures into a vacuum chamber in which a flight-type x-ray fluorescence spectrometer was installed. Spectra were obtained at three combinations of total pressure and seven different ratios of Ar to CO_2. Appropriate integration limits for the Ar K_α and ^{55}Fe backscatter peak were chosen by inspection. In addition, the instrument on Viking 1 lander was calibrated in an atmosphere (6.9 ± 0.13 mbar) of pure Ar prior to being installed on the spacecraft. After correction for source decay (2.60-year half-life of ^{55}Fe), the instrument sensitivity was 471 count/mbar (69.1 seconds, channels 35 to 50) at the time of landing. The spectral characteristics for 5 percent and 20 percent Ar in CO_2 (8 mbar total pressure) are shown in Fig. 1a. Two days prior to landing a baseline spectrum was taken of the instrument on Viking 1 lander to verify instrument settings. This spectrum, which because of mission constraints was taken at a lower gain than the bulk of the landed spectra, was mathematically expanded and normalized to the backscatter peak. It is presented as a solid line in Fig. 1b for comparison with a smooth curve of the pooled data from three separate scans after landing. No Ar peak is apparent in the spectrum taken after the instrument was landed on Mars. Also not detected are gases containing chlorine (channel 36) or sulfur (channel 30). Over the total measurement period of 6 hours, the temperature at the sample cavity slowly dropped from 25° to 19°C (calibration was at 28°C). Integrated over the Ar peak, the total count measured in situ was virtually identical to that prior to landing. When the above Ar sensitivity is combined with the background count, the Ar concentration determined at the landing site of the Viking 1 lander is less than 0.15 mbar at the 95 percent confidence level. The reported 7.7 mbar total pressure (8) at the landing site would place the Ar concentration at not more than 2 percent by volume. This result is in good agreement with the data reported by the entry mass spectrometer (5) and the mass spectrometer on the lander (7), which reported 1.5 percent and 1 to 2 percent by volume, respectively.

The abundance of Ar in the martian atmosphere reflects (i) the original abundance and (ii) the balance of processes supplying and removing the element from the atmosphere. Because of the high $^{40}Ar/^{36}Ar$ ratio (5, 7), most of the atmospheric Ar is radiogenic in origin, having been formed by decay of ^{40}K. Clearly, considerable importance will be attached to the K contents of the martian surface materials analyzed by the x-ray fluorescence spectrometer on the lander, and it is hoped that clues can be provided by the x-ray fluorescence data not only regarding the internal and surficial differentiation of Mars but also regarding the evolution of its atmosphere.

BENTON C. CLARK
Planetary Sciences Laboratory, Martin Marietta Aerospace, Denver, Colorado 80201
PRIESTLEY TOULMIN III
U.S. Geological Survey, Reston, Virginia 22092
A. K. BAIRD
Department of Geology, Pomona College, Claremont, California 91711
KLAUS KEIL
Department of Geology and Institute of Meteoritics, University of New Mexico, Albuquerque 87123
HARRY J. ROSE, JR.
U.S. Geological Survey Reston, Virginia 22092

29 July 1976

References and Notes

1. P. Toulmin, III, A. K. Baird, B. C. Clark, K. Keil, H. J. Rose, Jr., *Icarus* **20**, 153 (1973).
2. J. S. Levine and G. R. Riegler, *Geophys. Res. Lett.* **1**, 285 (1974); L. D. Kaplan, P. Connes, J. Connes, M. H. Smith, *Trans. Am. Geophys. Union* **56**, 405 (1975); J. S. Levine, *ibid.*, p. 405; *Icarus* **28**, 165 (1976); T. Owen, *ibid.*, p. 171; F. P. Fanale, *ibid.*, p. 179.
3. V. I. Moroz, *Izvestiya*, 28 March 1974; *Icarus* **28**, 159 (1976); V. G. Istomin, K. V. Grechnev, L. N. Ozerov, M. Ye. Slutskiy, V. A. Paulenko, V. N. Tsvetkov, *Kosm. Issled.* **13**, 16 (1975); V. A. Krasnopolsky, *Icarus* **24**, 28 (1975); V. S. Avduevsky, E. L. Akim, V. I. Aleshin, N. F. Borodin, V. V. Kerzhanovich, Ya. V. Malkov, M. Ya. Marov, S. F. Morozov, V. G. Perminov, M. K. Rozhdestvensky, O. L. Riabov, M. I. Subbotin, U. M. Susiov, Z. P. Cheremuchina, V. I. Shkirina, *Kosm. Issled.* **13**, 21 (1975); V. G. Istomin and K. V. Grechnev, *Icarus* **28**, 155 (1976).
4. A. O. Nier, W. B. Hanson, M. B. McElroy, A. Seiff, N. W. Spencer, *Icarus* **16**, 74 (1972).
5. A. O. Nier, W. B. Hanson, A. Seiff, M. B. McElroy, N. W. Spencer, R. J. Duckett, T. C. D. Knight, W. S. Cook *Science* **193**, 786 (1976).
6. D. M. Anderson, K. Biemann, L. E. Orgel, J. Oro, T. Owen, G. P. Shulman, P. Toulmin, III, H. C. Urey, *Icarus* **16**, 111 (1972).
7. T. Owen and K. Biemann, *Science* **193**, 801 (1976).
8. S. L. Hess, R. M. Henry, C. B. Leovy, J. A. Ryan, J. E. Tillman, T. E. Chamberlain, H. L. Cole, R. G. Dutton, G. C. Greene, W. E. Simon, J. L. Mitchell, *ibid.*, p. 788.
9. Essential contributions to the design, construction, and operation of the Viking x-ray fluorescence spectrometer were made by A. Castro and W. Kellner. R. R. Moore ran laboratory argon calibrations. C. D. Rowe and R. P. Christian performed data reduction. J. L. Gooding and P. H. Evans assisted in analyzing the calibration data. This work was supported in part by NASA (Viking Program), grants NAS 1-11855, NAS 1-11858, L-9717, and NAS 1-9000. We thank S. Dwornik for his continuing help and assistance.

Physical Properties of the Martian Surface from the Viking 1 Lander: Preliminary Results

Abstract. *The purpose of the physical properties experiment is to determine the characteristics of the martian soil based on the use of the Viking lander imaging system, the surface sampler, and engineering sensors. Viking 1 lander made physical contact with the surface of Mars at 11:53:07.1 hours on 20 July 1976 G. M. T. Twenty-five seconds later a high-resolution image sequence of the area around a footpad was started which contained the first information about surface conditions on Mars. The next image is a survey of the martian landscape in front of the lander, including a view of the top support of two of the landing legs. Each leg has a stroke gauge which extends from the top of the leg support an amount equal to the crushing experienced by the shock absorbers during touchdown. Subsequent images provided views of all three stroke gauges which, together with the knowledge of the impact velocity, allow determination of "soil" properties. In the images there is evidence of surface erosion from the engines. Several laboratory tests were carried out prior to the mission with a descent engine to determine what surface alterations might occur during a Mars landing. On sol 2 the shroud, which protected the surface sampler collector head from biological contamination, was ejected onto the surface. Later a cylindrical pin which dropped from the boom housing of the surface sampler during the modified unlatching sequence produced a crater (the second Mars penetrometer experiment). These two experiments provided further insight into the physical properties of the martian surface.*

General description of the landing area. The specific physical properties of the martian surface at the landing site relevant to the physical properties of the martian surface must be considered in the broader context based on the use of Viking orbiter images and the general scene viewed by the lander cameras in order to achieve balanced interpretations (*1*). Orbital images of the entire Chryse

area viewed by Viking 1 orbiter clearly revealed that the uppermost martian surface has been modified by wind. In the immediate vicinity of the initial site (19.5°N, 34°W), images revealed what appeared to be volcanic cones, necks, dikes, dark flows, and both ridges and depressions controlled by conjugate joint sets in a dark layer of probable volcanic origin—the stark relief of these features attested to erosional processes. In the northern part of Chryse (20°N, 35°W) small dark halo craters (approximately 600 m in diameter) surrounded by a lighter background indicated that dark material was excavated by impact cratering and deposited on a lighter surface material which presumably had been deposited or modified by the wind. Some craters had bright wind tails on their southwestern sides, confirming aeolian modification of the surface materials.

Likewise, farther to the northwest at the actual landing site, the surface displayed evidence of deflation and erosion as well as deposition by the wind. Here too, small craters, hundreds of meters in diameter, had excavated material from a dark layer, and were subsequently modified by the wind, producing bright wind tails on the southwestern sides of the craters and stripping the northwestern flanks.

Of equal importance to the physical properties of the surface are the ubiquitous impact craters ranging in size from 200 m to several tens of kilometers in diameter. These craters evidently ejected to great distances large blocks, fragments, crushed rock, and frothy chunks of shocked rocks. Thus, the general setting for the description of physical properties of the martian landing site is a surface material of crater ejecta modified by aeolian processes.

Lander camera images confirm the interpretation of the Viking orbiter images (2). The Viking lander camera images reveal a panorama similar to that seen in the southwestern parts of the United States: the large number of blocks and fragments were reminiscent of some lunar surfaces such as areas on the flank of the crater Tycho where Surveyor 7 landed (3). Thus, an initial impression of the martian surface is that it is intermediate between a lunar mare and a terrestrial aeolian environment. As in the orbiter images, there is evidence for a northeasterly wind which has produced deflation hollows on the northeastern sides of the rocks and left aerodynamically shaped ridges pointing downward toward the southwest. The detailed character of the physical properties of the martian surface materials are discussed below.

Fig. 1. Lander camera image of the surface near footpad 3, showing the general character of surface and the crater produced by the impact of the shroud (event L..L..T. 002 102950; Fr 12 A 013/002; sun elevation angle is 65.5°, sun is to the right). The width of the footpad shown is 20 cm.

Surface erosion by descent engines. In the site alteration studies simulated in 1971 (4), an 18-nozzle descent engine similar to those on the Viking lander was fired while it was lowered at a rate of about 1.52 m/sec (5 feet/sec) from a height of about 12.2 m (40 feet) above a soil bed. The thrust employed was 667 newtons (150 pounds), and the chamber pressure was that of the Mars surface in a carbon dioxide atmosphere.

Viking 1 descended on Mars at about 2.44 m/sec at a thrust of about 743 newtons per engine so that, although the descent velocity and thrust employed in the 1971 site alteration studies are both slightly low, they are not dissimilar to those involved in the Viking 1 landing. At the present, the best estimate of the mechanical properties of the Viking 1 landing site is that they are consistent with a material somewhat stronger or denser, or both, than the "lunar nominal" soil (5) used, among others, for preflight site alteration tests.

During the tests, observations were made of the depth and extent of the crater formed in the soil below the descent engine, and the amount and distribution of the soil removed from the crater. In addition, before each test firing, rocks of varying sizes and other features such as model craters, troughs, and ridges were placed or located at different distances from the engine descent axis.

In the lunar nominal soil the area below the descent engine was scrubbed and some soil removed to a depth of a few millimeters, but no distinct crater was formed. Finer grains were removed until coarse particles were exposed at the soil surface, giving the appearance of a fine-grained lag gravel. No sign of separate craters caused by the individual engine nozzles was apparent. By contrast, in the dune sand (6) individual craters were visible in a general broad erosion crater up to a centimeter deep. Furthermore, regions of the lunar nominal soil which had been prepared (7) at lower density than the bulk of the test bed showed no difference in erosion. This finding indicates that the soil's grain size is more important in the erosion process than its density.

During the surface alteration tests blowing dust was observed as soon as the descent engine was ignited at 12.2 m above the soil surface. The test area was totally obscured by blowing dust after engine shutdown and several minutes were required for the chamber to clear. It seems likely, on the basis of the presence of fine-sized grains on Mars, that the dust cloud caused by the landing would also last several minutes in view of the lower Mars gravity. Subsequent meteorological observations (8) indicate that, for the most part, the prevailing winds at the landing site of the Viking 1 lander blow from the northeast at a few meters per second. At the time of landing, the sun was in the southwest. Thus the dust cloud generated by the landing would drift to the southwest and could have passed between the lander and the sun. Depending on the dispersion of the cloud, a shadow would therefore be cast on the lander within a few seconds to a minute or so after touchdown. The first picture of the footpad commenced 25 seconds after landing, and shows a shaded vertical band at a time approximately 40 seconds later. It seems quite possible, therefore, that the streaks in the first martian picture frame (12 A 001/000) are due to the landing dust clouds passing between the sun and the scene in view at the time the camera was scanning this portion of the frame. In addition, the noise in the first few seconds of the first picture may have been caused by the imaging of coarse particles falling out of the dust cloud.

Soil fillets or tails, generally ascribable to aerodynamic processes, are visible adjacent to a number of Mars rock fragments. The direction of these tails is parallel either to wind direction or to the pattern of exhaust gases from the nearer descent engine (engine 2) and may depend on both sources. In this area [near footpad 3 (see Figs. 1 and 2)] the tails are generally parallel to the currently prevailing northeast winds and are also ap-

proximately radial to descent engine 2. Discrimination is therefore difficult, although it appears more likely that they have developed in the prevailing wind.

In the course of the site alteration tests in 1971, rocks located at a distance of 0.6 m from the descent engine axis were moved by the exhaust gas; the largest of these had a (terrestrial) weight of 74 g and was roughly equidimensional with a size of about 3.0 cm. The pressure required to move this rock was approximately 0.7×10^3 newton/m^2 (0.10 pound per square inch). The rock traveled 1.65 m from the engine axis; an initial pressure of about 0.35×10^3 newton/m^2 was required to keep it moving at this distance. On Mars, a rock of the same dimensions and density would weigh 0.38 times as much as the rock on Earth. With the same engine pressure conditions, therefore, larger rocks will be moved on Mars if they are not embedded. At a radial distance of 0.61 m from a descent engine axis on Mars, equidimensional loose rocks with dimensions up to about 7.0 cm would be moved under the nominal descent engine thrust conditions. At distances of 1.65 m on Mars, rock fragments on the surface up to dimensions of about 3.5 cm would be moved.

In the first image made after landing, several rocks which appear to be resting on the surface may have in fact been moved to their present positions by the engine exhaust gases. One such fragment appears at location 1 in Fig. 2. It is about 1.6 m from engine 2 and is estimated to weigh about 80 g on Mars. It could have been moved by the engine to its present position if it had been initially about 0.60 m or closer to the engine axis, for example at location 2, where a remnant fillet of soil appears to indicate the former presence of a rock. Other rocks that may have been moved are shown at location 3. Smaller loose rocks at the martian surface close to the engine axis could have been lifted off the surface, traveled through the martian atmosphere, and landed nearby. The soil seen in the footpad is additional evidence of soil moved during the landing either by footpad impact or engine-induced erosion. This finding is dramatic indication that some of the particles are less than 1 mm in diameter.

A view of the area below engine 2 was obtained by means of the mirror mounted on the side of the surface sampler. In this picture (Fig. 1), two small depressions are apparent. They occur at a spacing and in locations consistent with their formation by the jets out of two of the nozzles of engine 2. This appears to indicate that the grain size and cohesion of the surface material are different from those of the lunar nominal soil used in the site alteration tests. Since the grain size is below the resolution of the high-resolution frames, it is finer and has a broader range of sizes than the dune sand of the tests. This result may demonstrate that the finer grains are not as small as those of the lunar nominal material.

Interaction of the footpads with the martian surface. Although there is no distinct visual evidence of disturbance of the surface (by the footpad) in the area adjacent to footpad 3 (some of the apparently unsettled rock fragments may have been moved by the pad), analysis of the

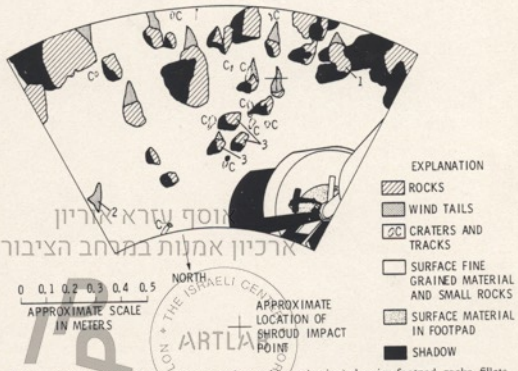

Fig. 2. Map of the area in Fig. 3 (on an orthographic projection) showing footpad, rocks, fillets (wind tails), debris in footpad, small craters and tracks, and the location of shroud impact crater. Rocks appear longer than they actually are because of the type of projection. This map was prepared from an image obtained prior to shroud impact. Numbers correspond to selected objects referred to in the text.

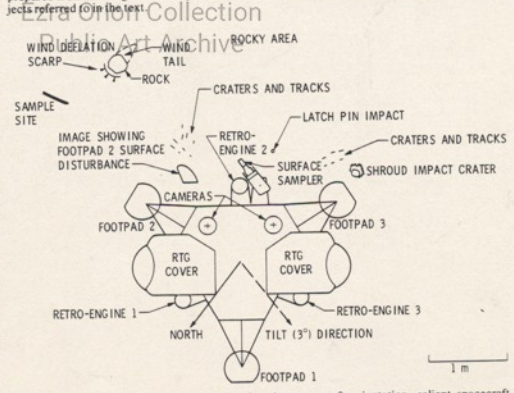

Fig. 3. Plan view of Viking 1 lander showing the spacecraft orientation, salient spacecraft parts, and location of surface disturbances and natural features relevant to the physical properties experiment. Location of the site where the surface sample was collected on sol 8 (28 July) is also shown; *RTG*, radioisotope thermoelectric generator.

shadow of the footpad on the adjacent surface indicates that the footpad has penetrated the martian material to a depth of about 3.6 cm. Unfortunately, footpad 1 cannot be viewed by the imaging system (see Fig. 3).

To date, no image of footpad 2 has been obtained, and so it is not possible to describe its attitude with respect to the surface. However, one high-resolution image in the vicinity of footpad 2 was returned: the area in the bottom left corner of this picture (see Fig. 4) is about 1.4 m from the center of footpad 2, which is 0.45 m in diameter. The surface in this picture is quite different from that in the neighborhood of footpad 3, lacking the rock fragment distribution. This surface (near footpad 2), by contrast, appears to be a relatively fine-grained soil surface, exhibiting only a few rocks (in the upper part of the picture). In the image are several additional features of interest. At the bottom left corner is a region of disturbed soil, intersected by a number of cracks or fractures running nearly parallel to the left edge of the frame. In all parts of the picture are small pits and tracks made by the impact of rock fragments or soil clods ejected by descent engine exhaust gas. From preflight tests and other data, it seems likely that such particles with dimensions of up to a few millimeters may have velocities in flight of up to several tens of meters per second. The tracks appear to belong to two groups which can tentatively be identified with ejecta from the directions of descent engines 1 and 2, respectively. The presence of the pits and tracks, assuming a particle velocity range, gives some information on the mechanical properties of the top few millimeters of surface material which in this region appears to be weaker and more porous than the soil around footpad 3.

Fig. 4. Lander camera image showing the area believed to be disturbed by the interaction of footpad 2 with the martian surface and small rimmed pits, some of which contain small fragments, produced by small fragments propelled by the engine exhaust gases (event L..L..T. 004 071159; Fr 11 A 022/004; sun elevation angle is 22.5°, sun is to the upper left). Lower width of picture, ~23 cm; upper width, ~50 cm.

Table 1. Leg stroke and footpad penetration.

Leg number	Leg stroke (cm)	Footpad penetration (cm)
1	7.0 ± 0.6	No data
2	3.2 ± 0.6	Image not yet taken
3	8.3 ± 0.6	3.6

Although the disturbed area and cracks may be natural features, they occur so close to the spacecraft that they can be more plausibly attributed to interaction of the vehicle with the surface. In particular, it seems possible to relate the disturbed area at the bottom of the frame (Fig. 4) to the penetration of footpad 2 into the martian surface soil. A disturbance as extensive as that observed (1.3 m from the center of the footpad) implies a considerable depth of penetration of footpad 2 into soil less strong than that observed around footpad 3. Alternatively, the surface material may be the same, in which case it was less displaced by the footpad impact. The question of the provenance of the disturbance and cracks in the frame in question will ultimately be resolved by imaging of footpad 2. Penetration of an object such as a footpad into a relatively dense, slightly cohesive granular material is generally accompanied by bulging and cracking of the soil to a distance from the footpad which depends on the soil properties. With additional pictures these properties can be identified more closely.

Significance of stroke gauge extensions. The Viking 1 spacecraft landed on the martian surface at a vertical velocity of 2.5 m/sec with a lateral component of less than 0.15 m/sec. After the lander came to rest, leg 1 was oriented 38.1° west of north and tilted 2.99° from the local gravity vector. The downslope direction of tilt was 36.7° west of leg 1 (9) (see Fig. 3).

The kinetic energy prevailing at touchdown was absorbed by the crushing of elements in the leg struts during leg stroking and by deforming of the surface material around the footpads. The stroke of each of the primary struts was obtained from images of the three stroke gauges. The penetration of footpad 3 was deduced from the shadow cast by the outer edge of the footpad on the martian surface. Preliminary estimates of stroke and penetration are listed in Table 1. The strokes in Table 1 indicate that the plane through the three footpad attachment points is tilted about 2° relative to the top of the lander. Since the lander is tilted about 3° relative to the local horizontal, the footpad plane (an approximation to the local surface plane) is tilted about 1° relative to the local horizontal.

A comparison of the footpad penetration and leg strokes in Table 1 with theoretical predictions imply that the surface material is a little stiffer than the lunar nominal soil model (the average density was 1.67 to 1.8 g/cm³) (*10*) and much stiffer than the most porous and weakly cohesive soil models considered during the design of the landing gear system. The theoretical landing dynamic behavior of the lander used in these preliminary comparisons was based on a vertical landing onto a horizontal surface. The prediction model made use of footpad penetration data obtained from static tests of a 3/8 model footpad penetrating various model soils, along with geometrical and load stroke properties of the landing gear.

Shroud impact. In the morning of sol 2, a shroud covering the surface sample collector head was ejected by eight springs along a trajectory inclined downward about 40° from the local horizontal. High-speed camera photographs of shroud ejection on Earth indicate an initial velocity of 3.2 m/sec. Although the final velocity at impact on Earth is 4.6 m/sec, the reduced gravity on Mars implies a smaller velocity at impact (3.6 m/sec) and a larger range from the launch site. This larger range is in fact the case because the location of the impact crater produced by the shroud (see Figs. 1 and 2) is well beyond the footpad.

Fig. 5. Enlarged image showing the latch pin (8 cm long) on the martian surface (indicated by arrow). Note the small crater and disturbed surface around the pin (event L..L..T. 005 115359, Fr 12 A 033/005; sun elevation angle is 69.6°, sun is to the left).

should be in a reduced gravity field. Possible effects due to local topography have not yet been fully analyzed.

The 480-g shroud, which is a hollow cannister with metal plate tip, produced a crater about 1 cm deep and 9 cm in diameter by the displacement of rocks and the ejection of fine debris. Unlike the case in Earth-based tests, the shroud ricocheted from the field of view in the image shown in Fig. 1.

Latch pin impact. The boom latch pin of the surface sampler, which failed to release at the scheduled time, ultimately fell to the martian surface (see Fig. 3) from an estimated height of between 1.0 and 0.9 m in the morning of sol 5 (*11*). The velocity at impact from this height at the surface of Mars is between 2.7 and 2.6 m/sec and is equivalent to a fall height near 0.36 m on Earth. The pin, a slender (8.2 cm long, 0.6 cm in diameter, and 11.3 g) rod, impacted on an end with two roller bearings and then fell over toward the spacecraft. Upon impact a small circular crater about the size of the roller bearings was produced (see Fig. 5) by the ejection of dark, very fine-grained material (probably silt size) to distances of 2.4 cm from the crater center where the rollers hit. The remainder of the pin fell toward the spacecraft, producing an elongate depression by the ejection of dark material to distances of 1.5 cm from its axis. The pin now rests in this depression (Fig. 5).

Although the exact orientation of the pin at impact is unknown, the crater, depressions, and their ejecta are consistent with those of terrestrial materials with very low cohesions, a small grain size, and reasonable densities (1.2 to 1.7 g/cm^3).

Surface temperature measurements. A temperature sensor (thermocouple) attached to the inboard side of footpad 2 was used to measure ambient temperature during the parachute phase of the landing (*12*). Its survival depended on a soft landing, which indeed was the case. Temperature readings are being recorded periodically during the day and night. Since the sensor cannot be seen directly, it is not known whether the sensor is covered with surface material. Images of the sensor will be obtained by use of a mirror on the surface sampler later in the mission to aid in the interpretation of the data.

This first report on the physical properties of the martian surface must be considered preliminary. More refined measurements are to be made, based on stroke gauge extension, footpad penetrations, stereo images of the landing site area, and other new data such as motor currents during trenching and comminution. As these data are obtained, better values of the surface properties can be reported.

RICHARD W. SHORTHILL
University of Utah Research Institute, Salt Lake City 84108
ROBERT E. HUTTON
Applied Mathematics Laboratory, TRW Systems Group, Redondo Beach, California 90278
HENRY J. MOORE, II
U.S. Geological Survey, Menlo Park, California 90278
RONALD F. SCOTT
Department of Engineering and Applied Sciences, California Institute of Technology, Pasadena 91125
CARY R. SPITZER
NASA Langley Research Center, Hampton, Virginia 23665

References and Notes

1. M. H. Carr, H. Masursky, W. A. Baum, K. R. Blasius, G. Briggs, J. A. Cutts, T. C. Duxbury, R. Greeley, J. E. Guest, B. A. Smith, L. A. Soderblom, J. B. Wellman, J. Veverka, *Science* **193**, 766 (1976).
2. T. A. Mutch, A. B. Binder, F. O. Huck, E. C. Levinthal, S. Liebes, E. C. Morris, W. R. Patterson, J. B. Pollack, C. Sagan, G. R. Taylor, *ibid.*, p. 791.
3. Surveyor Program Results, *NASA SP-184* (1969).
4. Laboratory tests were carried out at the Langley Research Center under martian atmospheric conditions with different soil models.
5. The lunar nominal soil model is an artificially prepared soil having a particle size distribution based on screen analysis provided by the results of the Apollo 11 mission. The technique employed in the fabrication of the lunar nominal model was to take volcanic rock aggregate in the size range of from 5 cm to pan size from Table Mountain, Golden, Colorado, and grind it in an allochthonous mill charged with a few steel-alloy balls. The fine fraction of the model was separated in discrete size fractions by an air classifier. The coarse-sized particles were separated by screening. The crushed rock product was then blended in individual 55-gallon (208-liter) covered steel drums to achieve the desired particle size distribution for each drum.
6. The dune sand soil model is a natural occurring dune sand of volcanic origin. The material was collected near Sunset Crater, Arizona, in the Elden Ranger District of the Coconino National Forest.
7. We prepared the lunar nominal soil originally by placing it in 7.5-cm layers in the containers. Each layer was rolled several times with a garden roller to compact it. The final bulk density obtained for the material was in the range 1.7 to 1.8 g/cm^3.
8. S. L. Hess, R. M. Henry, C. B. Leovy, J. A. Ryan, J. E. Tillman, T. E. Chamberlain, H. L. Cole, R. G. Dutton, G. C. Grune, W. E. Simon, J. L. Mitchell, *Science* **193**, 788 (1976).
9. Data were obtained by the lander performance analysis group from the inertial platform data which remained operational for 15 seconds after touchdown.
10. Viking Lander "As Built" Performance Capabilities, *NASJ-9000* (June 1976), p. XII-II.
11. The normal sequence was modified because of the failure of the boom latching pin to drop out as the boom extended. The boom was subsequently commanded to extend farther, resulting in normal operation and the ejection of the pin.
12. A. O. Nier, W. B. Hanson, A. Seiff, M. B. McElroy, N. W. Spencer, R. J. Duckett, T. C. D. Knight, W. S. Cook, *Science* **193**, 786 (1976).

13. We acknowledge the continued aid and support given to the physical properties team by L. V. Clark, D. S. Crouch, L. K. Schwab, K. Z. Bradford, and W. DeShazor of the surface sampler team. The imaging team kindly furnished the images used in this report. We thank Dr. R. B. Hargraves who gave us able assistance throughout the mission and reviewed this manuscript. Work was supported by the National Aeronautics and Space Administration.

30 July 1976

The Viking Landing Sites: Selection and Certification

Abstract. *During the past several years the Viking project developed plans to use Viking orbiter instruments and Earth-based radar to certify the suitability of the landing sites selected as the safest and most scientifically rewarding using Mariner 9 data. During June and July 1976, the Earth-based radar and orbital spacecraft observations of some of the prime and backup sites were completed. The results of these combined observations indicated that the Viking 1 prime landing area in the Chryse region of Mars is geologically varied and possibly more hazardous than expected, and was not certifiable as a site for the Viking 1 landing. Consequently, the site certification effort had to be drastically modified and lengthened to search for a site that might be safe enough to attempt to land. The selected site considered at 47.5°W,22.4°N represented a compromise between desirable characteristics observed with visual images and those inferred from Earth-based radar. It lies in the Chryse region about 900 kilometers northwest of the original site. Viking 1 landed successfully at this site on 20 July 1976.*

The initial plans for site selection included the identification of a prime and a backup landing site for each spacecraft (*1*), and an additional pair of sites to be used as a contingency, selected primarily on the basis of safety. Areas near the prime and backup sites for the Viking 1 lander were first observed by Earth-based radar in 1967 and in the period from May to July 1976—about the time of insertion of the spacecraft into orbit about Mars. The northerly sites considered for the second lander are not observable by radar at any time, and are considered therefore as somewhat more of a risk. The third pair of sites was selected where they could be readily observed by Earth-based radar, and could be used in the event that the first landing was unsuccessful. These preselected site locations

are shown in Fig. 1; the Viking 1 A sites were located at about 20°N latitude; for the Viking 2, the prime and backup B sites were at about 44°N latitude while the alternate C sites were at about 5°S latitude. The A1 site was located at the place where the largest Mars channel complex debouches onto Chryse Planitia. It was therefore considered to be the best area to observe where water and possibly near-surface ice had occurred in large quantities in the past—the optimum place to look for complex organic molecules. The B1 site was selected at the latitude of maximum water vapor concentration, the optimum place to land the biology experiment; at this longitude the two orbiters could provide relay support to either lander, and the second orbiter could observe the polar region. The C1 and C2 sites were selected primarily on the basis of their radar signatures, which indicated that they were relatively smooth. These sites also have acceptable characteristics in the Mariner 9 imagery and allow observations to be made of the polar regions.

The overall sequence of the major site certification decisions is shown in Fig. 2. Important points and mission rules were:

1) The A1 site area would be observed visually from orbit (*2*) and by the X-band Goldstone and S-band Arecibo radars (3.5 cm and 12.5 cm wavelength, respectively) from 29 May through 10 June 1976 (*3*). The A2 site could not be observed with the orbiter cameras prior to the decision to land or not land at A1, but could be studied by both Goldstone and Arecibo radars 10 June through 15 June.

2) The Viking 1 lander would land at A1 unless new information shows A1 to be unsafe.

3) Lander 2 would land at B1 unless (i) lander 1 failed, or (ii) lander 1 is delayed so that success has not been determined at the time when lander 2 must be committed, or (iii) new information shows B1 to be unsafe or of inadequate scientific interest.

4) If lander 1 either failed or was delayed, or new information caused B1 to be rejected, the lander 2 would be targeted to the best available site based on all data available.

5) The C sites at about 5°S were observed by the X-band radar at Goldstone and the S-band radar at Arecibo during the winter of 1975–1976; hence the data were available, and the sites selected in March 1976, well before the first spacecraft encountered Mars, 19 June 1976.

6) Photographs of the B1 and C1 sites would be taken before the A1 landing to obtain a broader base of Mars data to aid the interpretation of the A1 results as well as to provide additional information for choosing between the 44°N and 5°S latitudes for Viking 2.

Analysis techniques. The orbital photographs were made into uncontrolled mosaics from the rectilinear (tilts not removed) images. Then orthographic mosaics adjusted to the scale of 1 : 1,000,000 were made. Geologic and terrain maps were compiled, and hazard probabilities were entered into the computer so that statistics based on various approaches could be made. Crater counts were computed to compare subunits of areas studied. There were also comparisons of areas with each other and with Surveyor (automated spacecraft) landing sites on the moon. Contour maps and terrain statistics were computed for parts of the area by means of analytic photogrammetric techniques. The final maps were compiled after control point nets were computed. Lastly, photometric roughness maps were made—so-called digital number variance maps—that quantified brightness variations. Ellipses were then fitted to these maps with the radar interpretations being taken into account.

Results, decisions, and effects on mission plans. The prime site radar observations were completed on 10 June 1976; on 19 June 1976, Viking 1 was placed in its orbit about Mars. As a result of the

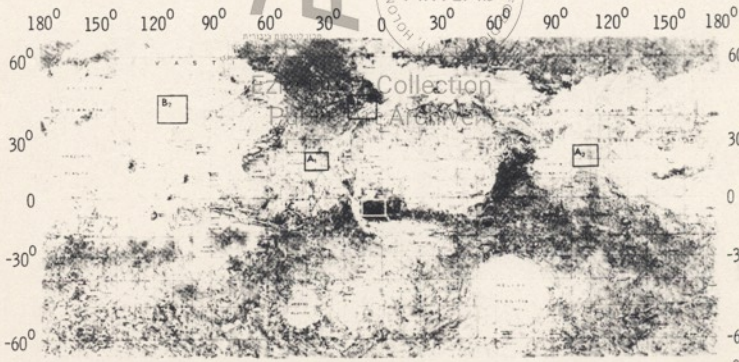

	PRIMARY	BACK-UP
VIKING 1	A-1	A-2
2	B-1	B-2
ALTERNATES	C-1	C-2

Fig. 1. Viking landing sites.

spacecraft observations taken through orbit 6 the original A1 area was rejected on 26 June primarily on the basis of the orbital imaging data, which indicated that the terrain was unexpectedly complex. Additional coverage on orbits 8 and 10 to the northwest of the original A1 area was planned, as shown in Fig. 3. Consideration was given to going to the A2 site at this time, but the three Mariner 9 high-resolution images in that area indicated the presence of knobs and small craters in that area, while the radar observations showed the area to be relatively smooth on a small scale. But there was concern that blocks, not detected by the radar, might be abundant at that location. By 1 July, the coverage from orbits 8 and 10 had been obtained and that area appeared visually satisfactory. A tentative decision was made to go to a new site "A1NW" at 23.4°N and 43.4°W, and at the same time obtain additional Arecibo radar data on 2, 3, 4, and 5 July, at 23°N. This site was selected by adjusting the 99 percent landing ellipse to avoid the hazardous features visible in the orbiter images. Radar data from Arecibo were obtained, and reviewed on 7 July. The radar observations showed the A1NW location to be an area of anomalous radar scattering, interpreted as a surface that was very rough on the scale of the lander or of very low density (or both), although the pictures looked the smoothest of any examined.

It therefore was decided to continue the search to the west in the hope of locating a site in an area of more satisfactory radar characteristics, and one that was also free of terrain hazards visible in the pictures. Additional coverage was planned on orbits 20 from 43° through 51°W, and on orbit 22 from 48.6° through 56.6°W (Fig. 3). On 11 and 12 July, the images obtained on orbits 20 and 22 were reviewed, and three possible ellipses with acceptable visual terrain were selected as follows:

A1α	22.4°N	47.5°W
A1β	22.5°N	49.0°W
A1γ	22.2°N	51.0°W

The A1α, also called A1WNW, was selected as a compromise between hazards visible in pictures, chiefly impact craters with their associated blocks and small-scale surface properties, based on radar interpretation. The landing was rescheduled for 20 July 1976. The A1α site contained two moderate sized fresh impact craters whereas A1γ contained eight larger fresh impact craters. Farther west the incised channels reappeared on the basin slope and large fresh impact craters are more abundant. The 1967 data indicated that this area is smooth. But the 1976 Arecibo coverage did not include this region.

An orbital trim maneuver, originally planned for 16 July to align the orbit over the 50°W longitude coverage area, was advanced 2 days in order to optimize conditions for a landing at 47.5° longitude. This maneuver was successfully performed on 14 July 1976. On 17 July 1976, 78 stereoscopic images of the final landing ellipse were obtained. These pictures showed slightly increased crater counts in the A1α area, due to an improved viewing geometry. They will also provide the material for the postlanding topographic and geologic maps of the area.

High-altitude observations of the A1α area on 18 July show a large diffuse cloud extending into the southwest half of the dispersion ellipse, Fig. 4, giving some concern that a dust storm might be starting in that area. A cloud was seen previously in that area on 9 July, but had cleared by 11 July. The cloud observed on 18 July was tentatively classified as a condensate probably formed by radiation cooling on the basis of appearance at several wavelengths. Its velocity was

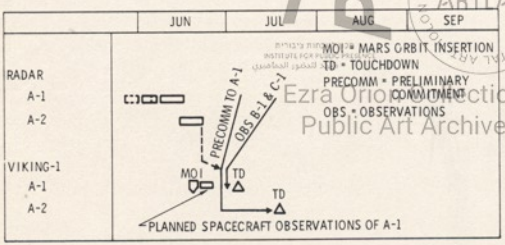

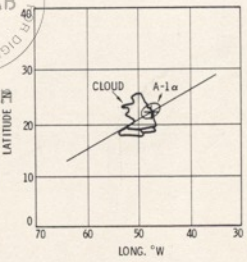

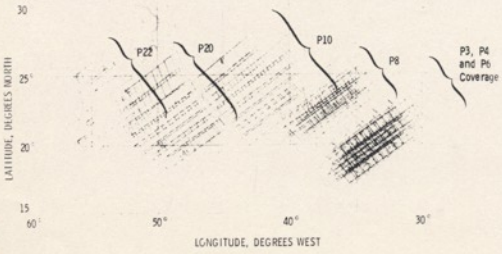

Fig. 2 (top left). Viking site certification timeline. Fig. 3 (bottom left). Viking 1 VIS observations in Chryse Planitia. Fig. 4 (above). Location of white cloud seen on 18 July high-altitude observations.

measured to be less than 3 meters per second. The low values of wind reinforced the conclusion that the cloud was a condensate. Consequently, it was believed that this feature would not interfere with either the lander entry or post-landing imaging. The successful landing occurred on 20 July 1976 at 5:12 a.m. PDT.

The lander pictures showed abundant blocks consistent with the presence of small impact craters in the vicinity. It is therefore suggested that the high radar reflectivity indicates that bedrock is near the surface and many blocks can be ejected by the impact. Such areas should be carefully considered prior to acceptance as landing sites in the future. Further discussion of both the visual and radar characteristics is presented by Carr *et al.* (*2*) and Tyler *et al.* (*3*), respectively.

H. MASURSKY
U.S. Geological Survey, Flagstaff, Arizona 86001

N. L. CRABILL
NASA Langley Research Center, Hampton, Virginia 23665

30 July 1976

References and Notes

1. H. Masursky and M. H. Strobell, *U.S. Geological Survey Interagency Report, Astro*, No. 59 (1975); *ibid.*, No. 60 (1975); H. Masursky, *Geotimes* **21** (6), 18 (1976).
2. M. H. Carr, H. Masursky, W. A. Baum, K. R. Blasius, G. A. Briggs, J. A. Cutts, R. Greeley, J. E. Guest, B. A. Smith, L. A. Soderblom, J. B. Wellman, *Science* **193**, 766 (1976).
3. G. L. Tyler, D. B. Campbell, G. S. Downs, R. K. Green, H. J. Moore, *ibid.*, p. 812.
4. The Viking Site Certification effort represented the combined efforts of nearly the entire Viking flight team. Some of those involved in the almost daily activities of the landing site staff include: M. J. Alazard, D. L. Anderson, W. A. Baum, K. Blemann, J. Boyce, G. A. Briggs, D. B. Campbell, M. H. Carr, H. Craft, J. A. Cutts, D. M. Davies, G. S. Downs, F. Drake, V. R. Eshleman, C. B. Farmer, W. Farrell, G. A. Flinn, J. Gliozzi, R. M. Goldstein, J. D. Goodlette, R. Greeley, R. R. Green, J. E. Guest, R. Hargraves, S. L. Hess, N. Hinners, W. Jakobowski, H. H. Kieffer, L. Kingsland, K. P. Klaasen, H. P. Klein, R. S. Kraemer, C. Leovy, P. T. Lyman, T. Z. Martin, H. Masursky, W. H. Michael, H. J. Moore, H. L. Morris, T. A. Mutch, J. F. Newcomb, F. T. Nicholson, W. J. O'Neil, T. Owen, F. D. Palluconi, J. D. Porter, R. J. Reichert, C. Sagan, G. Schaber, R. A. Simpson, R. W. Sjostrom, B. A. Smith, G. A. Snyder, L. Soderblom, G. A. Soffen, T. E. Thorpe, P. Toulmin, III, G. L. Tyler, E. D. Vogt, plus several hundred or so others at JPL and the U.S. Geological Survey at Flagstaff, Arizona, who also supplied brains and hands to make the system work. J. S. Martin, Jr., A. T. Young, and B. G. Lee were the recipients of the recommendations of the landing site staff and patiently endured our long march northwest across Chryse Planitia.

Radar Characteristics of Viking 1 Landing Sites

Abstract. *Radar observations of Mars at centimeter wavelengths in May, June, and July 1976 provided estimates of surface roughness and reflectivity in three potential landing areas for Viking 1. Surface roughness is characterized by the distribution of surface landing slopes or tilts on lateral scales of the order of 1 to 10 meters; measurements of surface reflectivity are indicators of bulk surface density in the uppermost few centimeters. By these measures, the Viking 1 landing site at 42.5°W, 22.4°N is rougher than the martian average, although it may be near the martian average for elevations accessible to Viking, and is estimated to be near the Mars average in reflectivity. The A1NW site at the center of Chryse Planitia, 43.5°W, 23.4°N, may be an area of anomalous radar characteristics, indicative of extreme, small-scale roughness, very low surface density, or a combination of these two characteristics. Low signal-to-noise ratio observations of the original Chryse site at 34°W, 19.5°N indicate that that area is at least twice as rough as the Mars average.*

The surface properties of Mars determined by Earth-based radar were one of several factors that were considered in selecting the Viking 1 lander site. Estimates were made of surface roughness and density based on spectral broadening and the strength of centimeter-wavelength radio echoes returned from Mars.

Radar observations have been conducted at each Mars opposition since 1963. Since 1968 a combination of geometrical constraints and system sensitivity limitations have restricted these measurements to Mars latitudes south of 15°N, that is, below the planned landing areas of both the first and second Viking missions. Recent improvements at both Arecibo Observatory (*1*) and Goldstone Tracking Station (*2*) made observations feasible at 20°N in May and June 1976 and at 23°N from Arecibo in July. At these times the planet's distance was about 2 A.U. as compared with about 0.5 A.U. at opposition. The wavelengths of observation were 3.5 cm and 12.6 cm at the Goldstone and Arecibo facilities, respectively. Observational conditions and site locations are summarized in Table 1.

The use of radar in site selection for Viking 1 was based on properties of radiowave scatter in the immediate vicinity of the sub-Earth point on Mars. Near that point, radiowave scatter is dominated by the multitude of reflections from those portions of the surface that are properly oriented to produce a mirrorlike, or near-specular, redirection of the incident energy back toward Earth. This component of the scatter is dubbed quasi-specular. For surfaces that are generally free of sharp discontinuities and are of homogeneous material and statistics, it can be shown that quasi-specular scatter is controlled by the combination of the surface slope distribution and the electromagnetic properties of the material (*3*). Under these conditions the effects of surface material and roughness are readily separated with the use of standard radar astronomy techniques (*4*). Methods used here, based on backscatter at normal incidence, should not be confused with earlier radar studies of lunar landing sites that were based on backscatter observed at oblique angles of incidence, especially the depolarized part of diffuse scatter (*5*).

Both observatories transmitted unmodulated signals. Echoes of these signals were broadened in frequency by the Doppler effect and the differing relative velocities of various scattering areas with respect to the radar. The broadening associated with quasi-specular scatter is quantitatively related to the distribution of surface slopes. A gauge of surface roughness was obtained from measurements of the one-half power bandwidth of the echo signals. The results were expressed in terms of an r.m.s. landing slope β_0. Comparative values of β_0 for lunar units are given in Table 2. The methods employed have been previously tested by comparing radar results from the moon with detailed analyses of the lunar surface at the same locations based on orbital photogrammetry (*6*).

Reflectivity corresponds to the Fresnel reflection coefficient of the mean surface material, or $\rho_0 = [(\sqrt{\epsilon} - 1)/(\sqrt{\epsilon} + 1)]^2$, where ϵ is the dielectric constant. The relationship between density of the surface and ϵ has been established from laboratory experiments and theory (*7*). The lateral scale of relevant slopes is of the order of from 1 to 10 m based on theoretical considerations and on empirical results from the moon (*8*); estimates of ρ_0 apply to the top few centimeters of the surface.

Values of β_0 depend primarily on the shape of the echo spectrum, and are generally free of systematic error. Estimates quoted below are typically accurate to about 10 percent. Estimates of ρ_0 depend on a number of multiplicative parameters which are obtained by calibration of the radar. In addition, ρ_0 is sensitive to variations in the radar, such as antenna point-

ing errors, during a period of observation. At Arecibo such pointing errors are probably the dominant error source and may occasionally be as large as a factor of about 2. At Goldstone, the error due to system calibration and pointing is estimated to be no greater than about 15 percent, but noise contributes about twice this amount. Most operational errors result in systematic underestimates of ρ_0.

The resolution varied with surface roughness, but was at most approximately the size of the Viking 1 landing ellipse, typically a circle about 300 km in diameter centered at the sub-Earth point. This resolution element moved across the surface as Mars rotated. It was also possible to infer changes in smaller areas within this larger resolution element from the detailed shapes of the echo spectra; however, no reliable quantitative information on surface properties could be obtained for these smaller areas.

Results for A1 and A1R (19.5°N, 34°W and 19.5°N, 32.5°W). Data from these sites consist of two Arecibo passes across the 30° to 35°W longitude range between 17.1° and 17.5°N latitude, and a total of six observations over this longitude range between 17.5° and 19.6°N by the Goldstone facility. The Arecibo observations did not cover the A1 sites directly, but were influenced by terrain at the extreme southwestern end of the A1 and A1R landing ellipses. It was not possible to distinguish between the A1 and A1R areas.

The Arecibo measures of r.m.s. slope show the area just south of A1 to be one of moderate to large roughness. Values of β_0 range from a minimum of $\beta_0 \simeq 5°$ to 6° to the southwest of the site, to an estimated lower bound of $\beta_0 \geq 7°$ to the southeast. The most probable value of surface reflectivity from Arecibo is $\rho_0 \simeq 0.07$, albeit this value is subject to large systematic errors. Goldstone observations on 2 days at latitudes between about 17.2° and 17.6°N yielded results consistent with those from Arecibo, $\beta_0 \simeq 6.4°$, $\rho_0 \simeq 0.08$; but the signal-to-noise ratio was low, on the order of 5 : 1. Echoes from each of four individual Goldstone observations at latitudes of 18.2°, 18.4°, 18.6°, and 19.7°N in the range of 33° to 35°W longitude were very near the detection threshold. However, echoes from other locations on Mars, especially the A2 site (see below), were readily observed at Goldstone during this same time period. Extensive system testing revealed no equipment faults. Combining all Goldstone observations at the six latitudes above yielded an apparently reliable echo detection at the A1 site and gave values of β_0 between 7° and 10°, and $\rho_0 \simeq 0.06$.

Both the Arecibo and Goldstone results indicated that the area just south of the A1 sites is approximately twice as rough as the average for Mars. The estimated reflectivity is near Mars' average. In terms of lunar results, with the same measures, this area would be characterized as similar to very rough lunar mare,

Table 1. Radar observations of Viking 1 sites.

Location	Date in 1976	One-way light time	Observational Latitude	Observational Longitude
	The A1 site from Arecibo Observatory at 12.6 cm			
19.5°N, 34°W	29 May	16.1 min	17.1°N	30° to 36°W
	31 May	16.1 min	17.5°N	30° to 36°W
	The A1 site from Goldstone Observatory at 3.5 cm			
19.5°N, 32.5°W	29 May		17.1° to 19.6°N	
	30 May		17.1° to 19.6°N	
	31 May		17.1° to 19.6°N	
	1 June		17.1° to 19.6°N	
	3 June		17.1° to 19.6°N	
	11 June		17.1° to 19.6°N	
	The A1NW site from Arecibo Observatory at 12.6 cm			
23.4°N, 43.4°W	3 July	18.2 min	23.1°N	38° to 49°W
	4 July	18.2 min	23.3°N	38° to 49°W
	The A1WNW Viking 1 landing site from Arecibo Observatory at 12.6 cm			
22.4°N, 47.5°W	3 July	18.2 min	23.1°N	38° to 49°W
	4 July	18.2 min	23.3°N	38° to 49°W
	The A2 site from Arecibo Observatory at 12.6 cm			
19.5°N, 252°W	12 June	17.0 min	19.6° to 20°N	248° to 254°W
	14 June	17.0 min	19.6° to 20°N	248° to 254°W
	The A2 site from Goldstone Observatory at 3.5 cm			
	11 June			
	13 June			
	14 June			

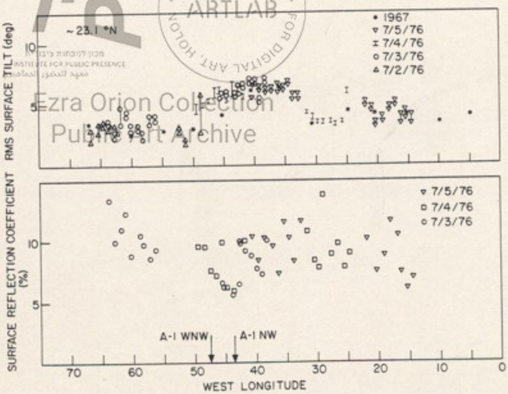

Fig. 1. Estimated values of r.m.s. landing slope and surface reflectivity at approximately 23°N latitude. Observations reported here are from 2, 3, 4, and 5 July 1976, averaged over 0.7° in longitude. Points from Carpenter (stars) are from data integrated over about 10° in longitude, at 22.5°N latitude (9). No values of reflectivity from Carpenter have been used. Data show Chryse Planitia to be generally rougher than areas to the east or west. The Viking 1 landing site at 47.5°W lies in a region of changing radar roughness. Site at 44.5°W is in a region of anomalous radar signature. Values of r.m.s. slope and reflectivity at 47.5°W correspond to average lunar mare in roughness and Mars average density, respectively.

CO_2, of about 0.003 near 135 km. The peak at mass 16 indicates a detectable concentration of O. More extensive analysis of the data should permit a quantitative statement on the abundance of atmospheric O and should also provide useful information on the concentration of CO. The relative abundances of oxygen and carbon isotopes, $^{18}O/^{16}O$ and $^{13}C/^{12}C$, appear to lie close to their terrestrial values. Peaks at masses 16 and 17 are due primarily to terrestrial H_2O released from the surface of the ion source after bombardment of the surface by ambient martian gas. The ratio $^{36}Ar/^{40}Ar$ cannot exceed the value for this parameter in the terrestrial atmosphere, and may be much lower.

The distribution of CO_2, Ar, N_2, and O_2 with altitude, as inferred from some 20 spectra taken over the height range from 140 to 190 km suggests an average temperature near 180°K, with an uncertainty of about ± 20°K. The height distribution of major gases shows a clear indication of the influence of diffusive separation and indicates that mass mixing processes in the martian atmosphere cannot play a major role for altitudes above about 140 km.

Figure 3 shows a sample of data recorded by the RPA at an altitude of about 130 km. The smooth curve through the observed points was obtained from a least squares fit to the data (*6*). The analysis indicates that O_2^+ is the major constituent of the martian ionosphere at this altitude. Carbon dioxide, CO_2^+, is less abundant by about a factor of 9, with an uncertainty of about ± 5 percent. The ions exhibit a temperature of about 160°K, and the uncertainty in temperature is also estimated to be about ± 5 percent. The temperature derived from the RPA data is consistent with the value noted above from a study of height profiles measured by the UAMS.

The direct measurement of O_2^+ as a major component of the martian ionosphere is an important new result. It lends support to earlier theoretical analyses of the martian ionosphere (*7*) which argued the importance of the reaction

$$CO_2^+ + O \rightarrow CO + O_2^+ \qquad (1)$$

as a means of converting the primary photoion CO_2^+ to the more stable form O_2^+. It suggests (*8*) a mixing ratio, O to CO_2, of about 0.03, with an uncertainty of about 50 percent, if we use the rate constant for Eq. 1 measured by Fehsenfeld *et al.* (*9*). The RPA measurement of ion composition also supports the view (*10*) that recombination fo O_2^+ can provide an important source of energetic oxygen atoms which may escape to space from upper regions of the martian atmosphere.

The measurements in the lower atmosphere indicate a surface pressure at the landing site of 7.3 mbar, with an atmospheric temperature at ground level of 241°K and a subadiabatic lapse rate for temperatures near the ground of 3.7°K km^{-1}. The atmospheric density, obtained from an analysis of the descent velocity of the payload during the parachute phase of the entry sequence, is about 0.0136 kg m^{-3} at an altitude of about 2.7 km.

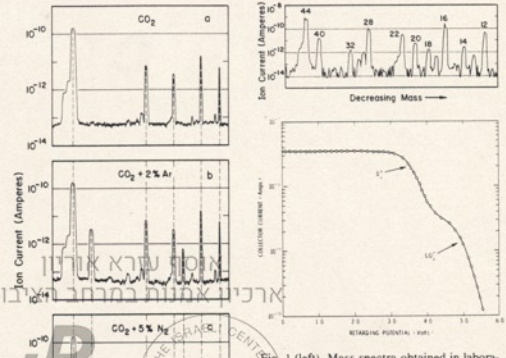

Fig. 1 (left). Mass spectra obtained in laboratory with instrument similar to that carried on Viking 1 lander. (a) Pure CO_2; (b) CO_2 containing 2 percent Ar; (c) CO_2 containing 5 percent N_2. Fig. 2 (top right). Mass spectrum obtained at an altitude of 135 km by the UAMS during the descent of Viking 1 lander to the surface of Mars on 20 July 1976. The spectrum shows the presence of CO_2, Ar, N_2, O_2, and O. A detailed analysis is required to establish the presence of CO. Also seen are peaks associated with isotopes. Fig. 3 (bottom right). Ion retarding potential curve recorded by the RPA near an altitude of 130 km during entry at a solar zenith angle of approximately 44°. The solid line theoretical curve through the data points corresponds to T_i = 158°K, $n(O_2^+)$ = 9.5 × 10^4 cm^{-3} and $n(CO_2^+)$ = 1.1 × 10^4 cm^{-3}.

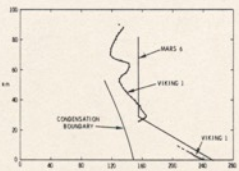

Fig. 4 (left). First analysis of the temperature profile, for the deceleration data and the direct sensing below 3.5 km. Fig. 5 (right). First analysis of the pressure profile from the acceleration data (a_x), stagnation pressure sensing (p_s), and parachute phase direct sensing (heavy dots below 3.5 km). The data are self-consistent.

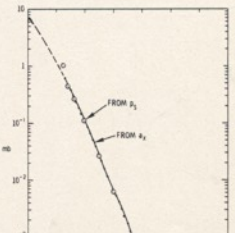

or smooth uplands, while the average surface density would be greater.

The difficulties experienced by the Goldstone facility in obtaining reliable echo detection in the immediate vicinity of the A1 and A1R sites while echoes were obtained from the area just to the south and from elsewhere indicate that at best the surface properties are no better than, or more likely are somewhat degraded with respect to, the 17.5°N latitude in terms of the desirable characteristics for landing safety.

A radar scatter simulation program was used to demonstrate the effect of surface roughness on signal detectability and to determine approximate bounds on the characteristics of the surface in the A1 area. It was shown that echoes from the A1 and A1R sites would have been observed by Goldstone each day if those sites contained an area 3° in diameter with the same radar characteristics as the A2 site.

Results for A2 (19.5°N, 252°W). Both Arecibo and Goldstone facilities obtained data from the area of the A2 ellipse. The observations yielded consistent results for r.m.s. slopes of $\beta_0 \simeq 3.5°$ to 4°. Values of ρ_0 from Arecibo varied between about 0.03 and 0.07, with an average value of 0.05; the estimate from Goldstone is $\rho_0 \simeq 0.06$. These values indicate a surface near Mars' average or slightly greater in roughness, and near lunar average, or slightly less than Mars average, in surface reflectivity.

Results for A1NW and A1WNW (23.4°N, 43.4°W and 22.4°N, 47.5°W). Observations of the A1NW and A1WNW sites were carried out by the Arecibo Observatory during the same period that the Viking 1 orbiter was conducting its photographic reconnaissance of that area. Successful observations of 40° to 50°W longitude at about 23.2°N were obtained on 2 days, with overlapping coverage in the 42° to 46°W longitude range. Additional observations were obtained about 20° to both the east and the west of the A1NW and A1WNW area, but with only partial coverage.

The Chryse Planitia basin appears to the radar to be generally rougher than the areas to either the east or the west. This result is consistent with earlier observations by Carpenter (9) at the same wavelength at 22.5°N latitude (see Fig. 1). The principal difference between the current results and those from 1967 is in signal-to-noise ratio. In 1967 it was necessary to average over 10° of martian longitude to obtain useful results. The current observations, even though at greater range, require only about 0.7° of averaging to obtain signal-to-noise ratios in excess of 10 : 1.

Table 2. Comparative values of β_0 for lunar units.

Lunar unit	β_0*
Rough uplands	9° to 10°
Smooth uplands	7°
Rough mare	5.5° to 6.5°
Average mare	4.5° to 5.5°
Smooth mare	4.5°
Average Mars	3.5°

*From 13 cm radar.

On the average, the Chryse Planitia basin is slightly smoother than the area to the south of the original A1 site, with r.m.s. slopes and reflectivities of $\beta_0 \simeq 5°$ to 6° and $\rho_0 \simeq 0.07$ to 0.08, respectively. However, the roughness data, from both the current observations and those of Carpenter, show a decline in surface roughness west of about 45°W longitude, with further decreases in roughness east and west of about 35° and 50°W, respectively. At 47°W, the formal values obtained for r.m.s. slope vary over the final landing ellipse between about $\beta_0 \simeq 4.5°$ 5.5°, with reflectivity of $\rho_0 \sim 0.07$, or greater. If correct, this value of ρ_0 implies a surface density near 2 g/cm³. At 44°W, the formal value of r.m.s. slope is $\beta_0 \simeq 6°$. There is an anomalous decrease in the apparent reflectivity in the vicinity of 44°W. Although this change was observed on two successive days (see Fig. 1), there is a question as to its reliability because of general difficulties in steering the Arecibo antenna.

The variable nature of the area around 44°W is also apparent in the shape of the echo spectra. Data from 3 and 4 July show the same effects. Spectra adjacent to those from 44°W are systematically skewed with respect to their usual, symmetrical shape. The sense of skew is opposite for sub-Earth points to the east and west. The shape changes smoothly with longitude and is consistent with a limited area of relatively weaker backscatter located near 44°W. Similar progressive changes in spectral shape have been observed in bistatic-radar experiments on the moon where the visible feature associated with the change in radar properties, usually an isolated crater, could be easily identified. Small-scale surface roughness, a very tenuous surface layer, or a combination of these could be used to explain this behavior.

The area of anomalous radar signature in Chryse Planitia coincides with the deepest, most central portions of the basin. This area is also marked by an absence of wind streaks visible in the Viking 1 images to both the east and the west. Other features of the radar data indicate that there might be local areas of relative smoothness on either side of, but principally to the east of, the anomalous area. However, no realistic quantitative results could be obtained from these features.

The radar properties of the A1WNW site appear to be similar to the average results of Chryse Planitia or to indicate a surface slightly smoother than the average of that area. But of more importance, the 47.5°W ellipse does not appear as an area of anomalous radar scatter, although it is in an area of transition. The formal results indicate that the large-scale roughness, excluding blocks, is similar to average lunar mare, while the surface reflectivity is apparently near martian average, or greater than that of the moon.

Comparison with images. Interpretation of Viking 1 orbiter images with an identification resolution near 140 m (*10*) revealed new features in the vicinity of the A1 landing site (19.5°N, 34°W). Initial impressions of the Viking images in the area placed the surface roughness in a category with rough lunar mare or smooth lunar upland. The broad-scale appearance is more akin to a lunar upland, perhaps rougher than indicated by radar track to the south, but consistent with the inferences from Goldstone data in the A1 area. The visual impressions were confirmed by photogrammetry at slope length near 500 m.

Farther to the northwest at the final landing site, the surface judged from the images appeared smoother and consistent with the radar results. That is, the surface is more akin to a lunar mare than a lunar upland. The images indicate that the aeolian processes of deflation, erosion, and deposition have occurred. Small cratering events have excavated material from an underlying dark layer about 50 m thick. These craters were subsequently modified by the wind. Bright windtail deposits were produced on the southwest sides, while their northeast flanks were stripped, exposing dark material. Of equal importance to the physical properties of the martian surface are the ubiquitous impact craters ranging in size from 200 m to several tens of kilometers. Large blocks, fragments, and crushed rock were ejected. Occasional blocks near the limit of resolution, 250 m across, are visible on the rims of craters about 20 km across. Thus, it was clear that the surface was complex with probable exposures of bare rock and the products of impact cratering, such as blocks.

fragments, crushed rock, and that the surface has been modified by the wind. Such a surface is expected to yield a larger reflection coefficient than the average lunar surface.

Images from the lander camera reveal the martian surface as relatively smooth. It is characterized by bare rock, blocks, rock fragments, and finer debris with superposed aeolian deposits and wind-deflated or eroded surfaces. These observations are consistent with the orbital images, the radar estimates of roughness, and the relatively large, compared with the moon, values of reflection coefficient obtained.

Conclusions. Radar and imaging form complementary techniques. Images provide information in the form of recognizable patterns which can be interpreted and analyzed quantitatively to provide an estimate of surface state on a lateral scale that is at one to three times the resolution of the imaging system. Inferences from Viking orbital images regarding surface structure on the scale of the lander require extrapolation of surface properties downward over 1½ to 2 orders of magnitude. Radar provides only an average measure of surface properties on the scale of the lander over an area comparable to the size of the landing ellipse. Radar observations detected an area of anomalous small-scale structure and reflectivity at the A1NW site.

The present radar observations are limited by the signal-to-noise ratio and by difficulties in absolute calibration of received power. They cannot be relied upon to detect areas of extreme roughness, such as a limited number of impact craters, which comprise only a small fraction of the resolution cell. The use of radar and images together compensates in part for the individual limitations of two techniques and provides data on all scales of surface roughness greater than about 1 m.

G. L. TYLER

Stanford University,
Stanford, California 94305

D. B. CAMPBELL

Arecibo Observatory,
Arecibo, Puerto Rico 00612

G. S. DOWNS, R. R. GREEN

Jet Propulsion Laboratory,
Pasadena, California 91103

HENRY J. MOORE

U.S. Geological Survey,
Menlo Park, California 94025

References and Notes

1. Arecibo Observatory, Arecibo, Puerto Rico, operated by Cornell University under contract with the National Science Foundation and with support from NASA.
2. Goldstone Tracking Station, the 64-m antenna near Barstow, California. This station forms part of the Deep Space Network of the Jet Propulsion Laboratory, a NASA facility.
3. D. E. Barrick, *IEEE Trans. Antennas Propag. AP-16* 4, 449 (July 1968).
4. G. L. Tyler and H. T. Howard, *J. Geophys. Res.* **78**, 4852 (1973).
5. C. Pieters, T. B. McCord, S. Zisk, J. B. Adams, *ibid.*, p. 5867.
6. H. J. Moore, G. L. Tyler, J. M. Boyce, R. W. Shorthill, T. W. Thompson, A. S. Walker, D. E. Wilhelms, S. S. C. Wu, S. H. Zisk, *U.S. Geological Survey Interagency Report: Astrogeology 75*, June 1975 (openfile report 75-284); H. J. Moore, G. L. Tyler, J. M. Boyce, R. W. Shorthill, T. W. Thompson, D. E. Wilhelms, S. S. C. Wu, S. H. Zisk, *U.S. Geological Survey Interagency Report: Astrogeology 80*, April 1976 (openfile report 76-298).
7. M. J. Campbell and J. Ulrichs, *J. Geophys. Res.* **74**, 5867 (1969).
8. G. L. Tyler, R. A. Simpson, H. J. Moore, *ibid.* **76**, 2790 (1971).
9. R. L. Carpenter, *Jet Propulsion Laboratory Space Programs Summary 37-48, III*, 157–160 (1967).
10. The theoretical resolution element, or pixel, is near 37 m. It takes an array, 3 pixels on a side, to identify a feature such as a crater.
11. We offer our deep appreciation to R. A. Simpson for his efforts in data collection, reduction, and analysis. This work was conducted at Stanford University and at the Jet Propulsion Laboratory under contract with the Viking Project. We thank the staff of the Arecibo Observatory for their cooperation and help, and V. R. Eshleman and R. M. Goldstein for guidance, and N. L. Crabill for much help.

30 July 1976

Rock Pushing and Sampling under Rocks on Mars

Prepared on behalf of the National Aeronautics and Space Administration

GEOLOGICAL SURVEY PROFESSIONAL PAPER 1081

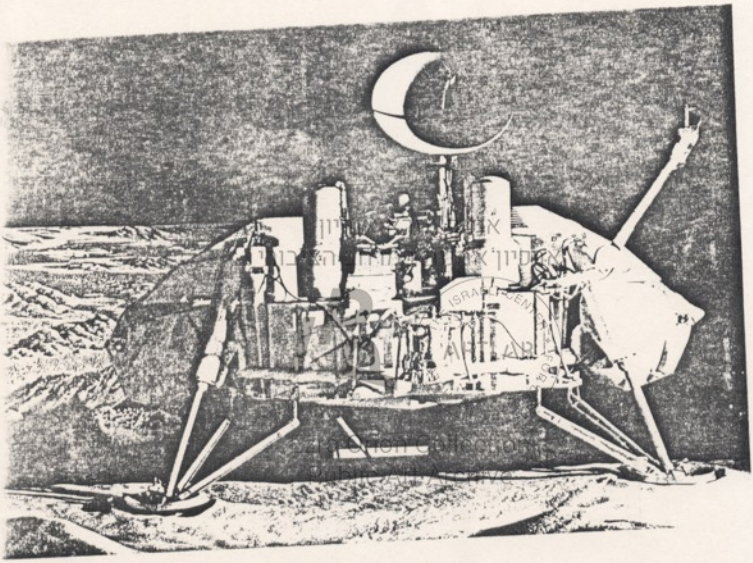

VIKING SCIENCE TEST LANDER

This full-scale model with fully operational lander camera and surface-sampler subsystems was installed adjacent to a large sand box representing the area in reach of the surface sampler. The Science Test Lander was used during the mission to develop and verify surface-sampler commands. Circular S-band radio antenna of lander is 0.76 meter across. Locations of cameras and surface-sampler subsystems are shown in figure 1.

Rock Pushing and Sampling Under Rocks on Mars

By H. J. MOORE, S. LIEBES, Jr., D. S. TROUT III, and J. V. CLARKE

GEOLOGICAL SURVEY PROFESSIONAL PAPER 1081

Prepared on behalf of the
National Aeronautics and Space Administration

U.S. DEPARTMENT OF THE INTERIOR
March 3, 1849

UNITED STATES GOVERNMENT PRINTING OFFICE, WASHINGTON : 1978

CONTENTS

ILLUSTRATIONS

TABLES

ROCK PUSHING AND SAMPLING UNDER ROCKS ON MARS

By H. J. Moore,[1] S. Liebes, Jr.,[2] D. S. Crouch,[3] and L. V. Clark[4]

ABSTRACT

Viking Lander 2 acquired samples on Mars from beneath two rocks, where living organisms and organic molecules would be protected from ultraviolet radiation. Selection of rocks to be moved was based on scientific and engineering considerations, including rock size, rock shape, burial depth, and location in a sample field. Rock locations and topography were established using the computerized interactive video-stereophotogrammetric system and plotted on vertical profiles and in plan view. Sampler commands were developed and tested on Earth using a full size lander and surface mock-up. The use of power by the sampler motor correlates with rock movements, which were by plowing, skidding, and rolling.

Provenance of the samples was determined by measurements and interpretation of pictures and positions of the sampler arm. Analytical results demonstrate that the samples were, in fact, from beneath the rocks. Results from the Gas Chromatograph-Mass Spectrometer of the Molecular Analysis experiment and the Gas Exchange instrument of the Biology experiment indicate that more adsorbed(?) water occurs in samples under rocks than in samples exposed to the sun. This is consistent with terrestrial arid environments, where more moisture occurs in near surface soil under rocks than in surrounding soil because the net heat flow is toward the soil beneath the rock and the rock cap inhibits evaporation. Inorganic analyses show that samples of soil from under the rocks have significantly less iron than soil exposed to the sun.

The scientific significance of analyses of samples taken under rocks is only partly evaluated, but some facts are clear. Detectable quantities of martian organic molecules were not found in the sample from under a rock by the Molecular Analysis experiment. The Biology experiments did not find definitive evidence for Earth-like living organisms in their sample. Significant amounts of adsorbed water may be present in the martian regolith. The response of the soil from under a rock to the aqueous nutrient in the Gas Exchange instrument indicates that adsorbed water and hydrates play an important role in the oxidation potential of the soil. The rock surfaces are strong, because they did not scratch, chip or spall when the sampler pushed them. Fresh surfaces of soil and the undersides of rocks were exposed so that they could be imaged in color. A ledge of soil adhered to one rock that tilted, showing that a crust forms near the surface of Mars. The reason for low amounts of iron in the samples from under the rocks is not known at this time.

INTRODUCTION

During the Primary Viking Mission,[5] Lander 2 acquired soil samples from beneath two rocks, where any living organisms and organic molecules would be protected from ultraviolet radiation. The acquisition of the samples required that the rocks be pushed away exposing the surface beneath them. Pushing rocks by remote control amid a dense field of other rocks (Shorthill and others, 1976; Moore and others, 1977a) some 363 million km away is a complex feat. Few people expected such a profusion of rocks on Mars, and the soil sampler was not designed for pushing rocks. Some of the rocks presented obstacles to the sampler and others were targets; consequently a detailed accurate knowledge of the topography and rock locations within reach of the sampler was mandatory for successful operations.

The purpose of this paper is to (1) describe the procedures used to push the rocks and the problems encountered, (2) show that the samples did, in fact, come from under the rocks, and (3) indicate the scientific value of acquiring samples from under the rocks.

ACKNOWLEDGMENTS

The authors are indebted to the National Aeronautics and Space Administration and countless individuals who made the Viking Mission a resounding success. The Viking Project was managed by James S. Martin and his staff at NASA Langley Research Center, Hampton, Virginia and the Viking landers were built by the Martin Marietta Corp., Littleton, Colo. Work was partly performed under NASA order L-9714 (H. Moore) and contract NAS-1-9682 (S. Liebes).

[1]U.S. Geological Survey, Menlo Park, Calif.
[2]Department of Genetics, Stanford University Medical Center, Stanford University, Stanford, Calif.
[3]Martin Marietta Corp., Littleton, Colo.
[4]NASA Langley Research Center, Hampton, Va.

[5]The Primary Mission is defined by the interval of time from the landing of Viking 1 on Mars, 20 July 1976, to 11 November 1976, the Viking spacecraft have continued to operate during the Extended Mission which ends in April 1978 (Soffen, 1976).

SURFACE SAMPLER SUBSYSTEM COMPONENTS

One of the major subsystems aboard the two Viking Landers is the Surface Sampler Subsystem (frontispiece and fig. 1). This subsystem was designed to acquire, process, and deliver surface material samples to the Biology, Molecular Analysis, and Inorganic Analysis experiments and to provide support for the Surface Physical and Magnetic Properties investigations (Soffen and Snyder, 1976). Biological analyses are conducted using three instruments (Klein and others, 1972, 1977): (1) Pyrolitic Release, (2) Labeled Release, and (3) Gas Exchange. The Gas Exchange instrument measures gases evolved from soil in the presence or absence of an aqueous nutrient, using gas chromatography. Molecular analyses are conducted using a Gas Chromatograph-Mass Spectrometer (GCMS) (Biemann and others, 1976, 1977). Inorganic analyses are conducted using an X-ray Fluorescence Spectrometer (XRFS) (Clark and others, 1976).

The Surface Sampler Subsystem consists of four major components: (1) the Acquisition Assembly, which acquires the samples and delivers them to the desired experiments; (2) the GCMS Processor, which receives samples from the Acquisition Assembly, grinds the material to a particle size less than 300 μm, and delivers metered 1-cm^3 samples to the GCMS; (3) the Biology Processor, which accepts samples from the Acquisition Assembly, sieves the material to a particle size less than 1,500 μm, and delivers metered 7-cm^3 samples to the Biology experiments; and (4) the Control Assembly, which receives digital commands from the spacecraft computer and controls the operation of and handles the data from the other three components. Samples are delivered to the XRFS through a funnel with a 1.25-cm screen. The Acquisition Assembly, with its control electronics, and the spacecraft computer were the major components involved in the rock-pushing sequences.

The Acquisition Assembly consists of a boom unit and collector head. The boom unit consists of (1) an extendable and retractable furlable boom capable of extending the tip of the collector head to a maximum of 3.45 m from the boom housing and (2) an integral gimbal capable of 288° horizontal (azimuth) movement and 74° vertical (elevation) movement. The collector head (fig. 2) consists of a stationary lower jaw for digging into the surface and a movable upper jaw for retaining the sample. The collector head can deliver a bulk sample directly to the appropriate experiment in the upright position, or it can be rotated 180° and the upper lid (in the inverted position) vibrated at 4.4 or 8.8 Hz to deliver the sample through a 2-mm sieve in the collector head lid.

The Surface Sampler Subsystem is automatically controlled by the spacecraft computer and Surface Sampler control electronics. Typical sampling sequences generally require that 40–100 discrete commands be executed; the longest sequence to date required the execution of 344 commands. Real-time command control and camera monitoring of the boom is impossible due to the one-way radio transmission time between Earth and Mars, which was about 20

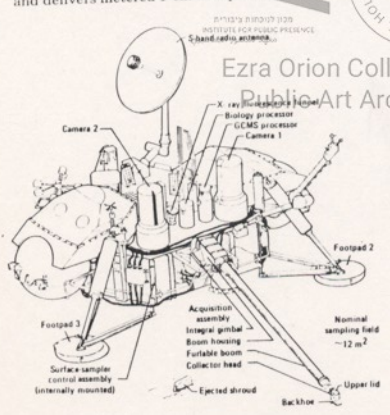

FIGURE 1.—Surface Sampler Assembly components and camera locations.

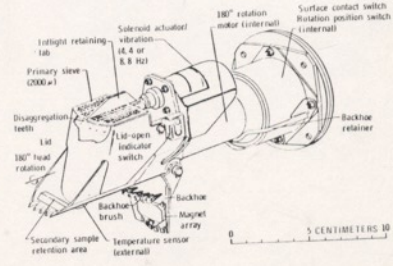

FIGURE 2.—Surface-sampler collector head.

UNITED STATES DEPARTMENT OF THE INTERIOR

CECIL D. ANDRUS, *Secretary*

GEOLOGICAL SURVEY

H. William Menard, *Director*

Library of Congress Cataloging in Publication Data

Rock pushing and sampling under rocks on Mars

(Geological Survey Professional Paper 1081)
"Prepared on behalf of the National Aeronautics and Space Administration."
Bibliography: p. 20-21
1. Life on other planets. 2. Mars (Planet)–Geology. 3. Viking Mars Program. I. Moore, Henry J. II. United States. National Aeronautics and Space Administration. III. Series: United States. Geological Survey. Professional Paper 1081.
QB54.R518 574.999'23 78-13085

For sale by the Superintendent of Documents, U.S. Government Printing Office
Washington, D.C. 20402
Stock Number 024-001-03008-6

consistent with the view that the atmosphere is composed mainly of CO_2.

Temperatures in the middle atmosphere, at altitudes Z from 25 to 90 km (Fig. 4), ranged from 120° to 165°K, with local peaks at 64 and 30 km, and would appear to join smoothly with the mass spectrometer temperatures above 140 km. At the time of entry, the CO_2 condensation boundary was about 20°K below atmospheric temperatures.

The atmospheric pressure profile to 90 km is shown in Fig. 5. The middle atmosphere data extend smoothly into the directly sensed data below 3.5 km. Ambient densities (not shown) were likewise defined over five decades, and at altitudes above 35 km were 2 to 5 times greater than the mean model to which the Viking lander was designed. At touchdown, however, density was near the pre-Viking expectation.

The pressure data indicate that the landing site is about 2.9 km below the mean martian surface, if we take an average surface pressure for the martian atmosphere equal to 6.1 mbar. The accelerometer data, however, indicate an acceleration due to gravity at the landing site of 3.7189 ± 0.0006 m sec^{-2}, which implies a planetocentric distance at touchdown of 3389.8 ± 0.03 km (*11*), while the radio science data (*12*) indicate a radius of 3389.5 ± 0.3 km. These results may be compared to the value predicted from the mean ellipsoid equation given by Standish (*13*), 3391.51 km, and would imply a terrain elevation at the landing site of -1.7 to -2.0 km, and a mean surface pressure of 6.6 to 6.7 mbar.

A. O. NIER
School of Physics and Astronomy, University of Minnesota, Minneapolis 55455

W. B. HANSON
Center for Space Sciences, University of Texas, Dallas 75080

A. SEIFF
Ames Research Center, Moffett Field, California 94035

M. B. MCELROY
Center for Earth and Planetary Physics, Harvard University, Cambridge, Massachusetts 02138

N. W. SPENCER
Goddard Space Flight Center, Greenbelt, Maryland 20771

R. J. DUCKETT
Viking Project Office, NASA Langley Research Center, Hampton, Virginia 23365

T. C. D. KNIGHT, W. S. COOK
Martin Marietta Corporation, P. O. Box 179, Denver, Colorado 80201

References and Notes

1. A. O. Nier, W. B. Hanson, M. B. McElroy, A. Seiff, N. W. Spencer, *Icarus* **16**, 74 (1972); A. Seiff, *Space Sci. Instrum.*, in press.
2. J. L. Hayden, A. O. Nier, J. B. French, N. M. Reid, R. J. Duckett, *Int. J. Mass Spectrom. Ion Phys.* **15**, 37 (1974).
3. U. G. Istomin and K. U. Grechnev, *Icarus* **28**, 155 (1976).
4. A. Dalgarno and M. B. McElroy, *Science* **170**, 167 (1970).
5. C. A. Barth, C. W. Hord, J. B. Pearce, K. K. Kelly, G. P. Anderson, A. I. Stewart, *J. Geophys. Res.* **76**, 2213 (1971).
6. W. B. Hanson, S. Sanatani, D. Zuccaro, T. W. Flowerday, *ibid.* **75**, 5483 (1970).
7. M. B. McElroy and J. C. McConnell, *ibid.* **76**, 6674 (1971); R. W. Stewart, *J. Atmos. Sci.* **28**, 1069 (1971).
8. J. C. McConnell, in *Physics and Chemistry of Upper Atmospheres*, B. M. McCormac, Ed. (Reidel, Dordrecht, 1973), p. 309.
9. F. C. Fehsenfeld, D. B. Dunkin, E. E. Ferguson, *Planet Space Sci.* **18**, 1267 (1970).
10. M. B. McElroy, *Science* **175**, 443 (1972).
11. E. J. Christensen and E. A. Euler, personal communication.
12. W. H. Michael, personal communication.
13. E. M. Standish, Jr., *Astron. Astrophys.* **26**, 463 (1973).

14. A.O.N. is indebted to J. L. Hayden for assistance in the design of the UAMS and to Ward Johnson and Stephen Richter for help in analyzing data. W.B.H. expresses his appreciation to colleagues S. Sanatani and D. Zuccaro for help with hardware and software design of the RPA. A.S. acknowledges helpful contributions by D. Kirk, P. Intrieri, R. Blanchard, R. Corridan, and S. C. Sommer. We are indebted to personnel of Bendix Systems Division, particularly D. Bianco, Steve Smith, and James Rice, for their efforts in constructing the UAMS and RPA flight instruments. Work at the University of Minnesota, the University of Texas, and Harvard University was supported by NASA under contract numbers NAS-1-9697, NAS-1-9699, and NAS-1-10492, respectively.

29 July 1976

Preliminary Meteorological Results on Mars from the Viking 1 Lander

Abstract. *The results from the meteorology instruments on the Viking 1 lander are presented for the first 4 sols of operation. The instruments are working satisfactorily. Temperatures fluctuated from a low of 188°K to an estimated maximum of 244°K. The mean pressure is 7.65 millibars with a diurnal variation of amplitude 0.1 millibar. Wind speeds averaged over several minutes have ranged from essentially calm to 9 meters per second. Wind directions have exhibited a remarkable regularity which may be associated with nocturnal downslope winds and gravitational oscillations, or to tidal effects of the diurnal pressure wave, or to both.*

The meteorology instruments and system on the Viking lander have been described (*1*), and only a brief description suffices here. Two hot film sensors orthogonally oriented in the horizontal plane are used to determine wind speed and direction by measuring the power required to maintain constant overheating with respect to an identical unheated reference sensor. A fourfold ambiguity in wind direction as sensed by this array is resolved by means of a quadrant sensor, which utilizes four thermocouples to sense temperature differences on four sides of a heated vertical rod. This is an application of the classical "wet finger" method of wind determination. This sensor also provides information and wind speed in the Reynolds-number range, in which it is now operating on Mars, and data from both the hot film and quadrant sensors are reduced together to provide best measures of wind speed and direction in the least squares sense. The reference temperature sensor is subject to radiation and conduction errors at the low pressure prevailing on Mars. Accurate temperature measurements are made by means of a set of thermocouples, which are referenced to an internal temperature measured by means of a platinum resistance thermometer. The entire array is mounted on a boom deployed 1.6 m above the surface, and 0.61 m from the nearest part of the lander body. Wind tunnel tests indicate measurement accuracies of at least ± 15 percent for wind speed in excess of 2 m/sec, ± 10° in wind direction and ± 1.5°C in temperature. Tests also indicate that effects of lander interference should not be large, but may have a small effect on flow at azimuths between about 260° and 340° (*2*). In addition, pressure is measured by means of a sensor within the lander body whose accuracy and stability are comparable with the digital resolution, about 0.07 mbar.

Table 1. Average variances for 11-minute modules during the first 5 sols. Night includes the period from 1.5 hours before sunset to 1.5 hours after sunrise; day includes the remainder of the sol.

Time	Variance		
	Temperature (°C)	Wind direction (deg)	Wind speed (m/sec)
Night	0.57	7.6	0.74
Day	2.63	24.5	2.07

All indications are that the entire system is performing nominally. Our confidence in the temperature measurements is based on the comparison between the reference and thermocouple sensors; the differences between them are those expected from radiation and conduction effects. Wind directions and

minutes during the Primary Mission. Therefore, the entire sequence to be executed must be generated and verified on Earth, transmitted to the spacecraft, and stored in the lander's computer until the specified execution time. When the sequence is executed, the computer sequentially transmits each coded digital command and waits a specific interval of time (precomputed to allow sufficient time for execution) before issuing the next command. If the command is not successfully completed, or a "no-go" signal is generated by an unsafe operation, the computer terminates power to the Surface Sampler and stops the sequence until corrective commands are transmitted from Earth.

Surface samples are acquired by moving the boom to the desired azimuth and extension distance and lowering it until the collector head contacts the surface. At that point, the collector head pivots about a ball joint, which activates a switch and terminates the downward movement. Sampling is then carried out by opening the collector head lid, extending the boom forward 15–20 cm, closing the lid, and delivering the sample to the desired experiment by another series of commands.

STEREOPHOTOGRAMMETRY

The prompt generation of accurate and suitably formatted topographic information was a prerequisite for choosing sample sites and rocks to be pushed and for planning sampler sequences. An interactive computerized video-stereophotogrammetric system (Liebes and Schwartz, 1977) was used for this purpose. The system, created to support the Viking Lander Imaging Team and to serve general project needs, was developed by one of the authors (Liebes) in collaboration with A. A. Schwartz of the Jet Propulsion Laboratory.

The primary input to the system was the digitally encoded imaging data returned by the Viking lander cameras (Huck and others, 1975; Mutch and others, 1972). Figure 3 schematically illustrates the nominal locations of the camera photogrammetric reference points, the placement and articulation of the surface sampler boom or arm, and the alignment of the Lander Aligned Coordinate System.

The stereophotogrammetry system consists of three basic elements: (1) computer hardware, (2) computer software, and (3) a stereo station. The computer hardware is that of the Interactive Image Processing Facility (Levinthal and others, 1977) at the Jet Propulsion Laboratory. A computer software applications program, called RANGER, supports the system. The stereostation is illustrated schematically in figure 4. A pair of video monitors face one another from opposite ends of a table. Images displayed on the monitors are simultaneously viewed through a centrally located scanning stereoscope. The left and right members of a stereoimage pair are routed, under the control of RANGER, to the left and right video monitors, respectively. The stereoscope enables a photogrammetrist to fuse the image pair into an apparent three-dimensional image of the martian scene.

Camera geometric calibration files developed by M. R. Wolf of the Jet Propulsion Laboratory (Patterson and others, 1977) help RANGER to accurately associate a viewing vector in the Lander Aligned Coordinate

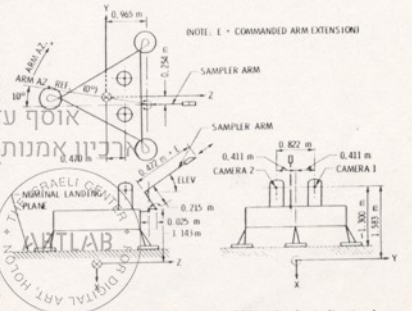

FIGURE 3.—Schematic illustration of a Viking lander indicating location of cameras, sampler arm or boom, and Lander Aligned Coordinate System.

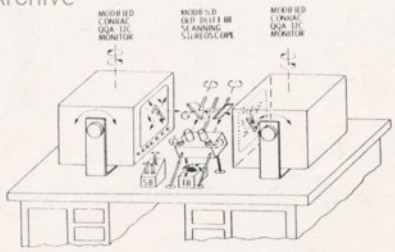

FIGURE 4.—Schematic illustration of interactive video-stereophotogrammetry station. Video monitors rest on table. Left and right camera stereoimage data are directed from computer to left and right monitors, respectively. Three-dimensional cursor is controlled by trackball device (TB). Video image routing and analog image are controlled by switchbox (SB).

System with each image point. RANGER provides the photogrammetrist with an artificial "3-space mark" consisting of an appropriately coupled pair of point cursors overlayed on the two video images. The pair of marks fuse to produce a single mark in the apparent three-dimensional image. The photogrammetrist can move the mark in a continuous manner through the martian scene. RANGER can be commanded to constrain the mark to any surface, which enables the photogrammetrist to generate arbitrary profiles of the relief such as elevation contours, vertical profiles, transverse profiles, etc.

Support for the sampler activities was invariably provided in the form of sets of profiles (called V-Profiles) representing the intersections of the martian relief with planes containing the azimuth axis of the sampler boom. The profile data were stored in computer data sets. Products consisted of photographs of the stereoimage pairs and overlaid profiles, and plots of the V-Profiles. Figure 5 illustrates a stereopair recorded after the sampler nudged Notch rock. The white lines represent 10 profiles that were generated along boom azimuth intervals of 0.5° to quantify the results of the nudge, to provide a basis for planning the subsequent attempt to displace Notch substantially, and to acquire a sample for Biology from beneath the rock. Figure 6 is a plot of the fifth profile from the left in figure 5. Sets of such V-Profiles enabled constraints such as the area accessible to the sampler (sample field) and detailed rock shapes to be established. The commands required to execute any desired sequence would be determined directly from these plots (Clark and others, 1977). The profile formatting program (implemented by R. N. Philips of the Jet Propulsion Laboratory) operated under multiparameter control that permitted variable grid intervals, measurement systems, and scales. Full-size V-Profiles were frequently plotted to aid modeling of sample areas in front of the Science Test Lander, which is discussed in the following section.

The cameras can record at resolutions of either 0.04° or 0.12°. The curves in figure 7, which illustrates theoretical uncertainty of range, apply to a pair of 0.04° images. Uncertainties will be two times as great when one image is at 0.04° and the other is 0.12° resolution, and three times as great for a pair of 0.12° resolution images. Uncertainty at any field point is here defined to be the radial dimension in plan view of the diamond-shaped region of overlap of wedges radiating out from each of the cameras, with wedge apex angles equal to the camera resolutions. Error caused by the calibration data and by thermal movement of the

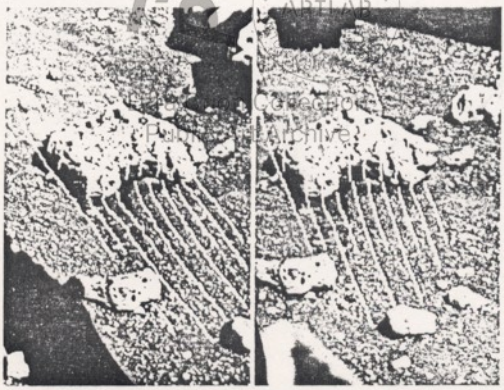

FIGURE 5.—Stereopair of pictures of Notch rock after nudge. Notch rock is about 25 cm wide and 11 cm high. Profiles (white lines) are in planes radiating from the azimuth gimbal axis spaced 0.5° apart. These reproductions have been subjected to differential enlargement and relative rotation to facilitate stereoviewing. Sampler boom visible at top with its shadow below. Vertical bar in left image is artifact of transmission.

cameras and shifts of the lander amount at most to 0.06° of image displacement, suggesting that a reasonable measure of operational ranging error is typically that shown in the figure. Within the stereoportion of the sample field, this uncertainty is typically about 2 or 3 cm.

SCIENCE TEST LANDER

An important simulation facility was available at the Jet Propulsion Laboratory during the Viking mission for developing and verifying all of the commands to be executed on Mars by the Viking surface sampler.

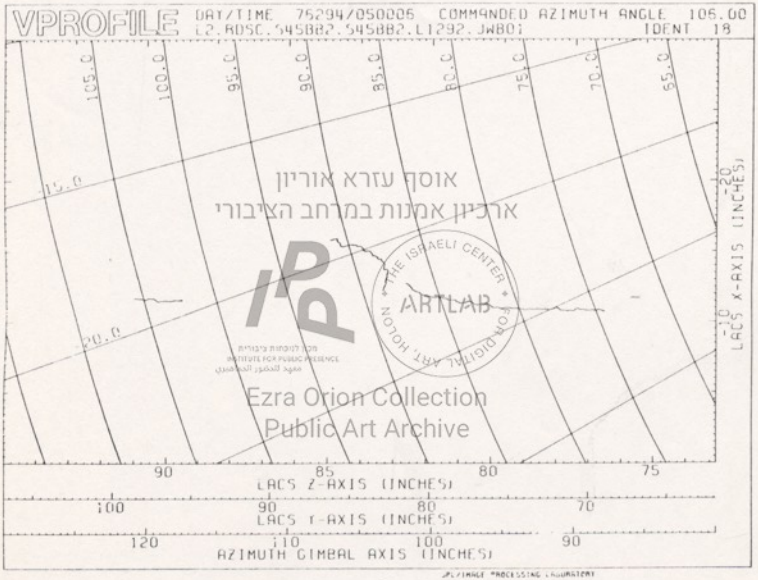

FIGURE 6.—Plot of fifth V-Profile from the left in figure 5. Gaps in profile correspond to regions not visible to both cameras. Note that the fillet at the base of the rock was not disturbed during the nudge. Sampler commands of azimuth, extension, and elevation required for subsequent rock push and sample acquisition were derived from such plots. The "range data set name" for the family of profiles appears beneath the Julian day and time in the top margin. The "IDENT" number designates the particular profile member of the set. The boom azimuth associated with the profile plane is indicated in the upper right corner. The X, Y, and Z coordinate scales appear in the plot margins. The Y and Z scales plotted on the V-Profile are azimuth-angle dependent (see fig. 3). The perpendicular distance in the Y–Z plane from the axis of the azimuth gimbal is indicated at the bottom. Each of the concentric curves denotes the position of the collector head tip at a given extension distance; that is, the curve the tip would describe as the boom is raised and lowered. These curves are here labeled with the associated extension distance (in inches). The diagonal fan of rays indicates the path of the collector head tip as the boom is extended at the indicated elevation angles.

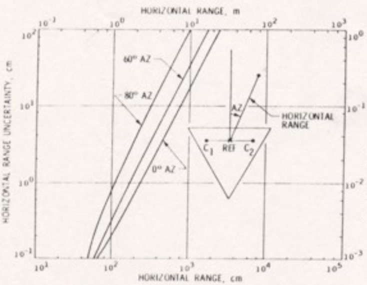

FIGURE 7.—Range uncertainty with horizontal range for paired 0.04° resolution images.

The key element of this facility, the Science Test Lander, was a full-scale Viking lander with fully operational cameras and surface sampler (frontispiece). The Science Test Lander was installed adjacent to a large sandbox which represented the area on Mars within reach of the sampler (the sample field). The subsystems were manually controlled by test equipment and, in the case of the surface sampler, by a small programmable computer. Two 10-kw tungsten-carbide lights were available for simulating martian lighting conditions during imaging tests.

Computer control of the sampler was essential to simulate and validate each sampler sequence. The sequences could thus be witnessed by scientists as well as engineers and managers responsible for assuring the safety of the sequence. The computer also provided data like that which would be returned during execution of the sequence on Mars. Surface-sampler data include commanded and achieved boom positions, discrete measurements of motor current and temperature, and switch positions. Although the surface-sampler data do not contain any timing information, it was possible to determine timing from a detailed analysis of the lander computer's memory as a continuous timed-tagged record of command and data traffic. This record permitted determination of the rates of travel of all motors, considered a measure of subsystem health. It was also a valuable diagnostic tool for understanding anomalous behavior of the sampler subsystem, and it was especially useful for evaluating the results of rock-pushing sequences.

After the landing of Viking Lander 1 on July 20, 1976, the Science Test Lander was configured to simulate as closely as possible the conditions at the site. The modeling was done by personnel of the U.S. Geological Survey using the images returned from the lander and photogrammetric analyses of the images. A sand mixture was used for the soil, and the simulated rocks were made of styrofoam. An accurate representation of the surface topography including rock locations was considered essential to developing and verifying safe and meaningful sampler sequences. Support imaging was also validated using the Science Test Lander. The real-time imaging display was particularly useful during the modeling work.

The Science Test Lander was reconfigured after the landing of Viking Lander 2 on September 3, 1976. Simulation of the second landing site took on an added importance when it was decided to search for martian organic matter and biota by acquiring samples from under rocks instead of from the exposed surface material. This necessitated an extensive program to develop rock-push sequences. The sample field was carefully surveyed for candidate rocks that met certain scientific and boom-capability criteria. Three rocks were selected for the sampler to attempt to move. Full-scale V-Profiles and contour maps of the target rocks were provided to the NASA/Manned Spacecraft Center's Lunar Receiving Laboratory, which prepared two models of each rock (one of plaster of paris and the other of epoxy resin) simulating extremes of their estimated weights on Mars. The rocks were positioned in front of the Science Test Lander using full-scale V-Profiles. These rocks were used in exhaustive tests to develop the proper techniques for rock pushing.

CRITERIA FOR ROCK SELECTION

Rocks that were eligible for pushing were limited to the sample field (fig. 8), which was defined using sampler extensions less than 279 cm (110 in.), angles of boom elevation greater than −38.1°, and boom azimuths between 90° and 250° (fig. 3). This excluded a number of promising rocks because they were either too far away, too close to the spacecraft, or on the left edge of the sample field. Five rocks (Nos. 1 through 5 in figs. 8 and 9) were considered first because they had been imaged by both cameras in high resolution early in the mission, whereas high-resolution coverage in stereo was not available in other areas. Each rock was rated from 1 to 4 in each of 11 factors, and each factor was weighted by importance.

The eleven factors were defined as follows: (1) Rollability: Was the rock deeply buried or near the surface so that it would move when pushed? (2) Obstructions: Were there objects behind the rock that might interfere with its motion? (3) Size: Was the weight of the rock small enough for it to be moved? (4)

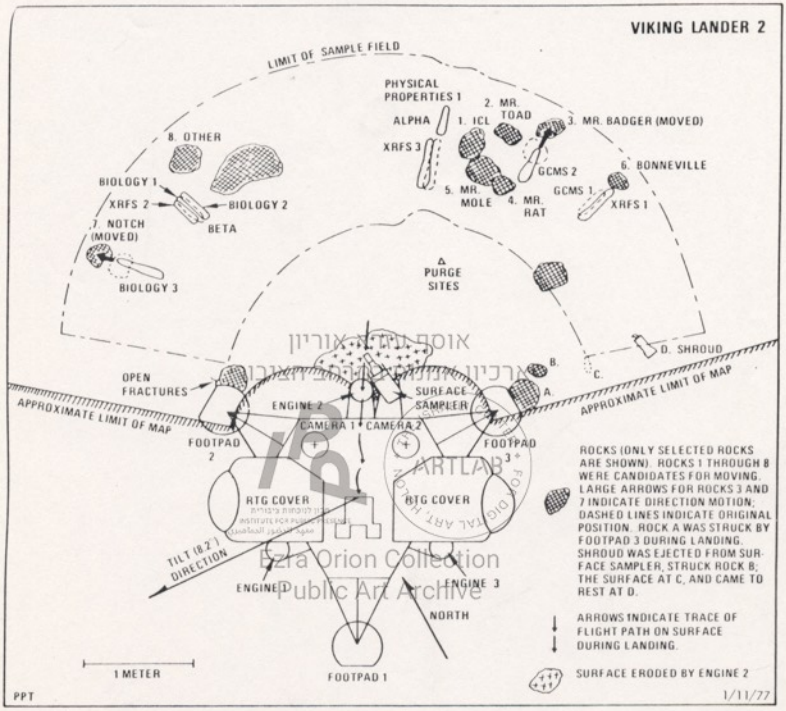

FIGURE 8.—Plan view of Viking Lander 2 and status of sample field at end of Primary Mission. Locations of selected rocks, sample acquisition trenches, and ejected shroud are shown. Original positions and positions of rocks 3 and 7 after pushing are indicated. Plane of plan view is parallel to upper surface of lander body (spacecraft Y–Z plane).

Accessibility: Were there objects in front of the rock that would interfere with the ability of the surface sampler to reach the rock or the area exposed after it moved? (5) Grippability: Was the character of the surface of the rock such that the surface sampler would not slip off? (6) Breakability: Would the rock break when moved? (7) Purchase: Was the shape and orientation of the rock on the surface favorable for moving? (8) Sampleability: Would the exposed surface be easily sampled? (9) Visibility: Would the exposed surface be visible to the cameras? (10) Surface area: Would the newly exposed area be large enough to collect samples unmixed with surface materials previously exposed to solar ultraviolet radiation? (11) Iconoclasticity: Were there any emotional reasons why the rock should be moved?

Each factor was weighted by relative importance (fig. 10), and surface area, visibility, and sampleability received the largest weightings because of their scientific importance. Large surface areas reduce the

FIGURE 9.—Camera 2 picture showing first rocks considered for pushing: (1) ICL, (2) Mr. Toad, (3) Mr. Badger, (4) Mr. Rat, and (5) Mr. Mole. Rock 6 (Bonneville) was considered for pushing later in the mission. Dimensions of rocks given in figures 10 and 12.

FACTOR	RATING WT	NAME NUMBER				
		ICL 1	Mr. TOAD 2	Mr. BADGER 3	Mr. RAT 4	Mr. MOLE 5
1. Rollability	4	3 (12)	4 (16)	3 (12)	2 (8)	1 (4)
2. Obstructions	3	3 (9)	4 (12)	4 (12)	4 (12)	4 (12)
3. Size	4	3 (12)	4 (16)	4 (16)	4 (16)	1 (4)
Mass		16.7 kg	11.5 kg	11.5 kg	9.9 +kg	25.9 +kg
4. Accessibility	3	4 (12)	2 (6)	4 (12)	4 (12)	4 (12)
5. Grippability	2	3 (6)	4 (8)	4 (8)	3 (6)	4 (8)
6. Breakability	1	3 (3)	3 (3)	3 (3)	1 (3)	2 (2)
7. Purchase	2	2 (4)	4 (8)	3 (6)	4 (8)	1 (2)
8. Sampleability	5	4 (20)	2 (10)	2 (10)	4 (20)	4 (20)
9. Visibility	5	4 (20)	2 (10)	1 (5)	4 (20)	4 (20)
10. Surface Area	5	4 (20)	1 (5)	2 (10)	2 (10)	3 (15)
cm^2 (cm)		648(18 x 36)	225(15 x 15)	360(24 x 15)	306(18 x 17)	810(30 x 27)
11. Iconoclasticity	1	4 (4)	1 (1)	1 (1)	1 (1)	1 (1)
TOTAL SCORE (140 IS PERFECT)		122	95	95	116	100

FIGURE 10.—Factors, scores, and weightings used in selection of rocks to be moved for acquiring samples under rocks. Rock 1 (ICL) received the highest scores because of large weighting of scientifically important factors: surface area, visibility, and sampleability. Iconoclasticity, a humorous factor, did not affect the outcome.

chances of mixing and contamination of the underrock sample with material that had been exposed to the sun. Good visibility allows an opportunity to assess the results of the sampling. Sampleability is the fundamental scientific requirement. The three rocks nearest the spacecraft (ICL, Mr. Mole, and Mr. Rat,[6] in figs. 8 and 9) received high scores in visibility and sampleability because the newly exposed surfaces would be favorably oriented to the cameras and the surface sampler if they moved (fig.10). Because of their location and orientation on the surface, their surface areas could be determined. ICL clearly had the largest surface area—18 cm at right angles to the surface-sampler azimuth plane and 36 cm along it, so that the chances of acquiring an unmixed sample from beneath it would be good. Rocks farther from the spacecraft generally had low scores, partly because of their location and partly because of their orientation on the surface, which reduced the observer's ability to estimate the dimension of the rock away from the spacecraft. Mr. Toad (rock 2) had the smallest estimated surface area because of its narrow base (fig. 9); considering width alone, it was too small. Visibility and sampleability were scored low because Toad was relatively far from the spacecraft, and the upper surface of the rock was barely visible, showing it was tilted away from the spacecraft. Mr. Badger (rock 3) had low scores for the same reasons. The visibility score for Badger was lowest of all because its orientation indicated the exposed surface would be difficult to view and dimensions difficult to estimate. Evidence for this unfavorable orientation was fourfold: (1) V-Profiles showed the surface adjacent to the rock was inclined and could not be viewed, (2) the upper surface of the rock was invisible, (3) the visible upper edge of the rock was convex upward and parallel to a crude layering midway in the rock, and (4) the undersurface of the rock was visible at the tip nearest the spacecraft. This orientation resulted in low scores for sampleability and a conservative estimate of its dimension in a direction away from the spacecraft.

Rock size (weight) and rollability were the chief engineering considerations. Estimates of the weight of rock that could be pushed were made assuming frictional sliding (fig. 11). For frictional sliding and boom angles constrained by the local surface and sampler capabilities, rocks as heavy as 90 and 160 Newtons (N) could be pushed. If moderate plowing occurred, the weights might be about 40 N less. Rock weights were

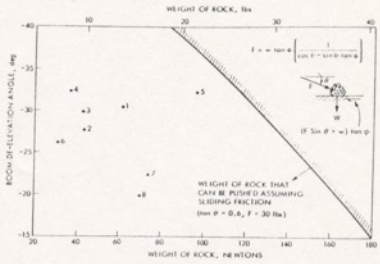

FIGURE 11.—Estimates of weights of rocks that could be pushed by the sampler assuming frictional sliding.

estimated from the dimensions, shapes, and an assumed density of 3,000 Kg/m³. Such a density is reasonable for massive mafic rock (Baird and others, 1976) but is somewhat excessive if the rocks are, in fact, vesicular. As an example, ICL's estimated weight was about 62 N assuming an ellipsoidal shape and should have moved provided that excessive plowing (because of burial) would not be required. With the exception of Mr. Mole (rock 5), the other four rocks would move if excessive plowing was not required. Mole was not only heavier than about 97 N, but it was also deeply buried (fig. 9) and would require plowing; thus it received low scores on rollability and size. Toad was clearly the most rollable because of its small base compared to its upper part. Mr. Rat (rock 4) appeared to be partly buried. In the other factors, only Toad scored low in accessibility because Mole and Rat would interfere with sample acquisition. ICL scored low in obstructions because there were two small rocks behind it. The curved and relatively smooth surfaces of Rat and ICL indicated the surface-sampler collector head might slip while pushing, but there were some pits on the surface so that the teeth of the collector head would probably grip and stay with the rock. Because many of the rocks appeared to be vesicular, it was possible that they might be fragile and break if they did not move when the sampler pushed them. Thus, partly buried rocks, such as Rat and Mole, received low scores in breakability. High scores for purchase were given to Toad and Rat because their large height-to-base ratios would provide mechanical advantage for rolling. In contrast, Mole scored low because of its small height-to-base ratio. The fact that Badger was tilted away from the lander resulted in a relatively high score for purchase.

[6] Names were assigned to rocks in order to aid memorization of the geometry of the sample field. Rocks 2 through 5 were named after characters in Kenneth Grahame's book *The Wind in the Willows* (1961), and others were simply named. The origin of the name of rock 1 (ICL) is noted later, in footnote 7.

The weighted scores tipped the balance in favor of ICL rock as the first choice. Here, the factors weighted on scientific goals were important. ICL's high score in "iconoclasticity," a factor introduced to help many tired members of the Viking Flight Team retain their sense of humor and relax, did not affect the outcome.[7]

Subsequent rock selections considered the same 11 factors as well as others (fig. 12). Bonneville (rock 6) and Notch (rock 7), two of three new candidates, were selected to be nudged (fig. 8). Bonneville had moved previously during a sample acquisition for the Inorganic Analysis experiment, and the surface that would be exposed after it moved would be shaded at the planned time of sample acquisition for Biology. The rock was in an area where the boom housing obscured the field of view of camera 1, and so there was no stereoscopic coverage. Notch won out as the push candidate because its location was well-known, its shape provided favorable grippability, its location provided good visibility, and the surface in front of it was not disturbed by previous acqusitions (as was the case for Bonneville), which reduced chances of contamination. Surface area, visibility, and sampleability were ample for Notch.

ROCK-PUSHING STRATEGY

The Acquisition Assembly was not designed for moving rocks on Mars. Therefore, when the request was made to obtain samples from under rocks after the Mars landing, appropriate sequences using the existing capabilities of the Acquisition Assembly had to be developed rapidly.

Two ways of moving rocks were considered: (1) positioning the collector head on the rock in such a manner that the backhoe could be used to drag the rock when the boom was commanded to retract and (2) positioning the collector head in front of the rock and pushing the rock forward by extending the boom. The boom can push or pull with a force of approximately 178–213 N before the motor load capability is exceeded causing decoupling of its magnetic clutch.

Tests using the Science Test Lander indicated the pushing technique was the most feasible. The major difficulty encountered was the accuracy required to push the rock at an optimum point judged from imaging to be the center of gravity. The command resolution of the boom is 0.6° in azimuth and elevation, and 0.6° cm in the extend and retract directions. Additionally, gear backlash and gravitational and thermal deflection of the boom increased the possible aiming inaccuracies. Although the gravitational deflection could be calculated, the thermal bending of the thin-walled steel boom could not be predicted with sufficient accuracy to guarantee that the collector head would not contact the surface in front of the rock and push exposed surface material into the sample site during the forward thrust.

A strategy of rock pushing was ultimately selected that provided the best way to move the rock without contaminating the sampling site. The accuracy of azimuth positioning was improved by comparing the boom-command coordinates of previously excavated trenches with the V-Profile azimuths of the centerlines of the trenches measured using the camera stereoimages. Appropriate command corrections were made as required. The azimuth backlash effect was predictable because the lander is tilted 8.2° in a westerly direction (Shorthill and others, 1976; fig. 8). Thus, the azimuth backlash consistently produced actual boom azimuths that were about 0.6° smaller than the commanded azimuths. Backlash in the extend and retract directions was negligible. The relatively large potential errors in the elevation axis (boom thermal bending, gravitational deflection, and overtraveling after motor cutoff) were eliminated by first commanding the boom to the surface until movement was terminated by actuation of the ground contact switch. This command was followed by an elevate command which was controlled by timing rather than by position achieved. Knowledge of the elevation rate of travel enabled calculation of the time required to lift the collector head tip above the surface a known amount. This technique nullified the effect of boom deflections in the upward direction. The final sequence adopted for the mission consisted of the following steps generally performed over a period of 10–15 Martian days:

1. Swing the boom to the desired azimuth (as determined from V-Profile data and corrected for calibration and lander tilt).
2. Extend the boom such that the tip would be positioned approximately 2–3 cm in front of the rock after lowering it (as determined from V-Profile data).
3. Deelevate the boom to activate the surface contact cutoff switch.
4. Elevate the boom (usually for 1–2 seconds) to position the collector head at the correct vertical position in front of the rock.
5. Extend the boom approximately 7–8 cm to verify "moveability" of the rock by subsequent imaging and boom telemetry data.

[7] ICL rock was named after an acronym for Initial Computer Load. Prior to landing, the spacecraft computers had stored commands for an automatic mission in the event that the lander could not be commanded. Had this occured, the spacecraft would have tried to collect a sample from a point just beyond ICL, but would have failed. Thus, ICL was an "iconic clast" that deserved to be pushed.

NAME / NUMBER	Mr. RAT 4	BONNEVILLE 6	NOTCH 7	OTHER 8
SIZE Width	18 cm	22 cm	25 cm	25 cm
Depth	17 cm	15-22 cm	25 cm	25 cm
Height	11 cm	5-6 cm	11 cm	13 cm
Mass	9.9 kg	6-8.4 kg	10.7-20.3 kg	9.5-19.1 kg
ADVANTAGES	Has V-Profile data stereoscopic coverage	Appears to have moved during XRFS Sol 30 dig Newly exposed area shaded at 0600	Appears to be unburied Has V-Profile data stereoscopic coverage	Has V-Profile data stereoscopic coverage
DISADVANTAGES	Near ICL rock (1) which didn't move Partly buried	Monoscopic coverage Area in front of rock "messed up" by GCMS (Sol 21) and XRFS (Sol 29, 30) trenches		Rock along SSAA gimbal axis presents possible hazard
Iconoclasticity	1	0	0	0

FIGURE 12.—Additional considerations for selection of rocks to be nudged or pushed for the second sample acquisition beneath a rock for the Biology Experiment.

6. Position the boom such that the rock and collector head could be stereoimaged and subsequent V-Profiles could be generated showing the new position of the rock.
7. Position the collector head at the new relative position (steps 1 through 4).
8. Extend the boom 20–25 cm (depending on dimensions of rock) to completely displace rock from original site. Verify rock movement by imaging and repeat steps 7 and 8 if required.
9. Perform a backhoe sequence at the original site of the rock to remove possible exposed material, followed by performance of a normal sampling sequence.

Details of the rock-push sequences used on Mars are listed in table 1.

SAMPLER MOTOR CURRENTS AND ROCK MOVEMENT

Motor currents, inferred from variations in lander bus currents, were sampled at a rate of 4 kilobits per second in the engineering data format (Format 5). This resulted in a current sample every 0.19 seconds and a current resolution of 0.039 amperes. Typical motor currents have a base current of about 0.2 amperes, normally a high current transient at motor start, a no-load condition during a gear transfer, and then a rise in current due to extension. Currents are converted to force by subtracting the base current of 0.2 amperes from the total motor current measurements, calculating the wattage from known voltages (typically 31.8 Vdc) and then using calibration data (Crouch, 1976) which gives ≈20 Newtons/watt. Thus, the resolution in force is about 25 N.

Motor currents during nudging, pushing, and sampling correlate with movements of the sampler and the rocks as viewed and measured using the pictures. This correlation is vividly illustrated by the Sol 29 acquisition for the Inorganic Analysis experiment (fig. 13). The acquisition stroke extended to the buried base of Bonneville, which was displaced upward about 0.4 cm as shown by comparison of pre- and post-sample pictures of the rock. The surface sampler extends at a rate of about 1 in. (2.54 cm) per second. The duration of high current (≈ 6.7 s, fig. 13) represents an extension near 6.7 in. (17 cm), which is in good

TABLE 1. *Sample sequences used for rock pushing and sampling under rocks*

[Engineering units are reported in inches because of use during mission and in final surface-sampler report (L. V. Clark and others, 1977). CW, clockwise; CCW, counterclockwise as viewed in fig. 8; est., estimated]

Rock	Sol[1]	Command description	Position achieved	Comments
ICL	30	Azimuth CW	186.6°	To nudge rock.
		Extend	75.4 in.	Est. distance to rock 77.4–78.0 in.
		Deelevate	(−) 33.2°	Surface contact.
		Elevate	(−)30.6°	By timing.
		Extend	78.6 in.	Sampler commanded to 83.1 in.; motor clutched; est. force 200 N. Rock did not move.
Badger	34	Azimuth CW	201.1°	To push rock, first try.
		Extend	84.4 in.	Est. distance to rock 87.4 in.
		Deelevate	(−)30.6°	Surface contact.
		Elevate	(−)30.0°	By timing.
		Extend	96.5 in.	Rock translated, tilted, and rotated; surface sampler deflected CW and went under rock.
		Retract	82.0 in.	Trench produced because rock leaned on surface sampler.
Badger	37	Azimuth CW	200.5°	To push rock, second try.
		Extend	89.1 in.	Est. distance to rock 90 in.
		Deelevate	(−)29.4°	Surface contact.
		Elevate	(−)28.1°	By timing.
		Extend	101.2 in.	Rock at extension of 97–98 in. along 200.5°; may have had larger tilt during push than afterwards.
Badger	[2]37	Azimuth CW	201.1°	To acquire sample.
		Extend	93.0 in.	Est. distance to rock 95 in.
		Deelevate	(−)28.8°	Surface contact.
		Retract	84.1 in.	Trench to clear away any surface contaminants.
		Elevate	(−)20.5°	
		Extend	87.0 in.	
		Deelevate	(−)30.6°	Surface contact.
Bonneville		Extend	93.6 in.	Sample acquisition.
	45	Azimuth CW	217.5°	To nudge rock.
		Extend	99.1 in.	Sol 29 XRFS extension of 99.4 (6 spare) mm.
		Deelevate	(−)25.6°	Prev. indicated surface sampler contact on rock.
		Elevate	(−)26.2°	Images show collector head tilted back and on rock.
		Extend	103.0 in.	Rock fell back after extension. Points on front surface moved 1 cm upward.
Notch	45	Azimuth CCW	105.8°	To nudge rock.
		Extend	84.1 in.	Est. distance to 86.2 in.
		Deelevate	(−)23.1°	Surface contact.
		Elevate	(−)22.4°	By timing.
		Extend	87.8 in.	Left edge of rock displaced about 1.5 in. (3.8 cm).
Notch	51	Azimuth CW	106.4°	To push rock.
		Extend	86.7 in.	Est. distance to rock 87.7–88 in.
		Deelevate	(−)21.8°	Surface contact.
		Elevate	(−)21.8°	By timing.
		Extend	98.0 in.	Rock translated and rotated clockwise.
Notch	51	Azimuth	107.1°	To acquire sample.
		Extend	93.6 in.	
		Deelevate	(−)20.5°	Surface contact.
		Retract	78.1 in.	Trench to clear away debris.
		Elevate	(−)15.5°	
		Extend	88.0 in.	
		Deelevate	(−)21.8°	Surface contact.
		Extend	94.6 in.	Sample acquisition.

[1] Sol is martian day from start of mission; day of touchdown is Sol 0. The duration of a martian day is about 24.65 hours.

[2] Sequence was repeated because of failure to obtain level full indication; achieved elevations were (−)29.4° and (−)30.6° for surface contacts; level full indication was obtained prior to second delivery. Elevation increase indicates shallow 1.2 in. (3 cm) depth for sample trench.

agreement with the commanded extension of 6.4 in. (16.3 cm). Thus, the increase in current at the end of the Sol 29 sample acquisition is certainly due to the interaction of the surface sampler and soil with Bonneville rock. The current increase corresponds to a force of about 50 N, a value about twice the estimated weight of the rock (22–31 N). At a deelevation angle of −29°, the horizontal component of force is about 44 N. Because the rock moved upward, a lifting force of about 22–31 N was required. The horizontal force vector along a line sloping 30° toward the surface sampler is 37.5 N, and its vertical component is 22 N, or near the estimated weight of the rock.

During the nudge of Bonneville, surface contact was made on the rock as shown by the deelevation angles (table 1) and by the pictures (fig. 13), which show the collector head resting on the rock after it extended. The high motor currents during the last part of the nudge lasted about 0.2 seconds, which represents about 0.5 cm of travel. This is consistent with about 1 cm upward motion on the face of the rock which was estimated from the pictures and suggests a pivot point on edge of the rock, which is about half as high as wide, farthest from the spacecraft. After retraction, the rock returned approximately to its prenudge position causing debris from plowed material in the rim of the previous trench to fall into that trench (fig. 13).

ICL, the first choice candidate, did not move, as demonstrated by comparing[4] prenudge and postnudge images taken by the same camera, photogrammetric measurements, and motor currents. Relatively small motor currents were measured for about 3 seconds, after which they rose to a value corresponding to a force of about 200 N above the normal extension current. The current duration compares favorably with the estimated 2–2.5-in. (5–6.4 cm) distance to the rock. Two hundred Newtons is close to the decoupling force for the sampler motor (178–213 N). The maximum horizontal component of force on ICL was 153–183 N. Because ICL was estimated to weigh 62 N, only about 67 N should be required to push it if simple sliding is assumed (see equation in fig. 11). If the sin θ term in the equation is ignored, 37 N should be required to push the rock. Thus ICL must be cemented or more deeply buried than initial interpretations indicated. It is noteworthy that there was no evidence for chipping, spalling, or scratching of ICL as a result of the attempt to push the rock. The individual teeth of the lower jaw of the collector head have an area near 1 mm^2, and so stresses of the order of 10^8 N/m^2 were exerted by the collector head. Thus, it appears that the surface of the rock is strong.

[4] Viewing of two pictures taken of the same object at different times by one camera is a sensitive way of detecting motion of the object.

speeds determined independently by the quadrant and hot film sensors are in satisfactory agreement, and the standard deviations obtained in the least-squares minimization procedure used to obtain wind speed and direction are agreeably low.

Measurements at the Chryse site (3) began about 2 hours after landing, and results of the first few sols are reported here. Data were obtained in modules spaced 1 hour and 27 minutes apart, with some gaps during periods of lander-orbiter and lander-Earth communication. The modules were 11 minutes in length, except for two somewhat longer modules each sol (4). Samples within modules were obtained at either 4-second or 8-second intervals.

Figures 1 to 4 display module-averaged data from the first four sols. The outstanding characteristic of these data is their repeatability from sol to sol. This is not completely unexpected, since this is summer in the subtropics where, in the thin, dry martian atmosphere, processes should be dominated by the very regular rates of incoming solar radiation and outgoing infrared radiation as compared to Earth. Thus, temperatures at the same time of day differ from sol to sol by only a very few Kelvins. Nevertheless, the repeatability of the wind data is striking. Despite some differences, the general nature of the wind regime is light easterly winds in the late afternoon with wind speeds decreasing to near zero as midnight is approached. Thereafter, during the night the winds blow from the southwest with regular oscillations in direction and speed.

This behavior can be plausibly understood in terms of the large-scale topography of the site. Elevation contours constructed from Mariner 9 observations (5) indicate that the lander is southwest of the center of a broad depression in the surface. This bowl is some 300 km in diameter and about 3 km deep. At the lander location, the ground slopes gently downward toward the northeast. It seems likely that the average southwest winds at night are caused by radiatively cooled air sliding downslope, a process well known on Earth. Particularly striking are the oscillations in wind direction with periods of roughly 4 hours which repeatedly occur after midnight. These are suggestive of a large-scale gravity wave oscillation, and may be associated with drainage over the entire Chryse basin.

An alternative interpretation of the diurnal oscillations in wind and pressure is that they are manifestations of a planetary scale diurnal traveling wave driven by the traveling daily heating cycle, a diurnal tide (6). A very simple model of such a planetary oscillation in which latitudinal variations of pressure are neglected suggests that the observed diurnal pressure amplitude (0.1 mbar) would be coupled with a wind speed amplitude of the order of 5 m/sec, with westerly winds coinciding with the late afternoon pressure minimum, and clockwise wind rotation. Undoubtedly both planetary scale tides and local drainage effects contribute to the repeated diurnal pattern.

Figure 5 presents evidence for diurnal variations in boundary layer characteristics. The gas temperature at 1.6 m

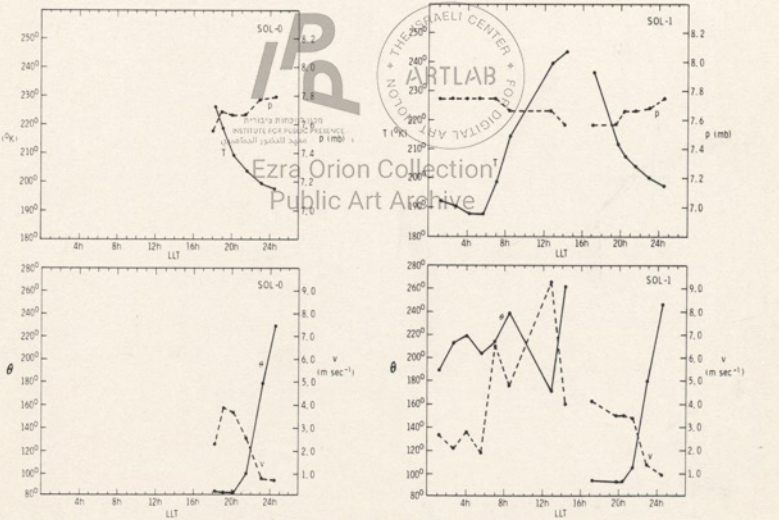

Fig. 1 (left). Module mean data for sol 0. Temperature (*T*), pressure (*P*), wind direction measured clockwise from north (*θ*), and wind speed (*V*) plotted as functions of local lander time beginning with zero at midnight (L.L.T.). Gaps in the curves are at the time of operation of the relay transmitter when the meteorology system is shut off. Pressure is plotted on an expanded scale in which the digitization increments are visible. The first module of meteorology data was initiated 1 hour and 47 minutes after touchdown of the lander on 20 July 1976. Fig. 2 (right). Module mean data for sol 1; see description of Fig. 1.

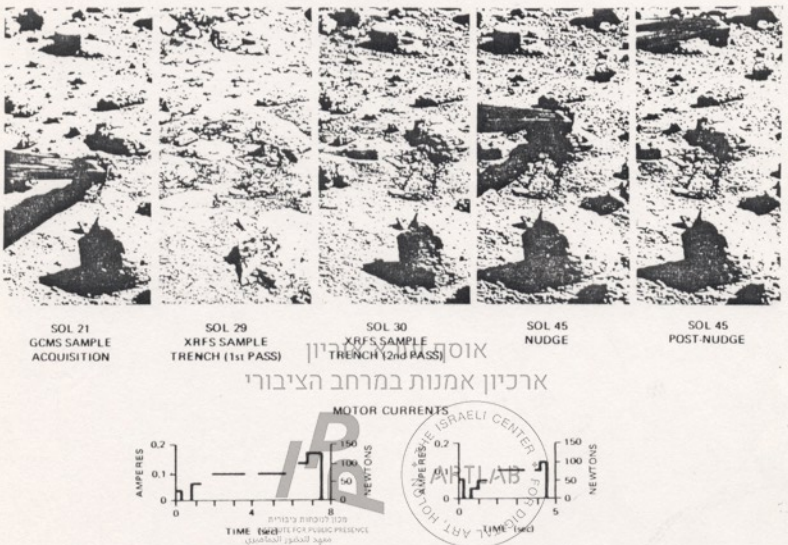

FIGURE 13.—Sequence of events at "Bonneville Salt Flats." Bonneville (rock 6) is just beyond surface sampler in the left picture (Sol 21). Left picture shows sampler acquiring sample for the Molecular Analysis (GCMS) experiment on Sol 21. Next picture shows trench formed during the first pass of acquisition for XRFS on Sol 29; comparison of pre- and post-acquisition pictures shows Bonneville was displaced 0.4 cm upward; motor currents show increase at end of acquisition stroke and correspond to upward displacement of rock. The Sol 30 picture (center) shows the second pass acquisition for XRFS; note trench has been cleaned of platy debris. Sol 45 picture (to right) shows collector head on Bonneville during nudge; note trench produced on Sol 30 is still clear of debris. Final picture at right shows sampler (upper center) and Bonneville after nudge; note debris propelled into trench by rock falling into its original position. Trenches are about 10 cm across. Motor currents for nudge (lower right) near end of stroke are larger than those for beginning of sample acquisition.

Despite the initial setback of ICL, the sampler moved on to Badger (chosen over Toad). The weight of science considerations was relegated to lesser importance, a marginal decision in view of reduced visibility and sampleability. More importantly, Badger moved in a complicated way (figs. 14 and 15). Motor currents for the Sol 34 push of Badger correlate with the results. The rock was about 3 in. (7.6 cm) from the collector head tip at surface contact, which correlates with the duration of initially low currents (3 s). This was followed by large currents for 2.5 seconds, correlating with the estimated translation of 2.6–2.8 in. (6.5–7.0 cm), which may have been accomplished by tilting, rather than sliding. Subsequent currents oscillate and correlate with the interval during which the sampler slipped down off the rock surface causing the rock to lean on it as it completed its extension (fig. 14). Most of the measured 69° counterclockwise rotation of the rock probably occurred in this last interval. Because the rock was leaning on the sampler as it retracted after the push, the collector head dug a trench along an azimuth oblique to the commanded azimuth. Badger did not move far enough on the first push, therefore a second push was executed on Sol 37. Unfortunately, motor currents were not obtained during this push. The pictures show two smooth tracks where

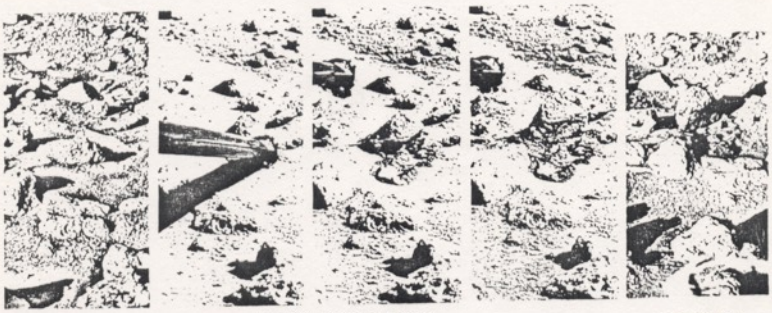

FIGURE 14.—Sequence of pictures showing history of Badger (rock 3). At left is rock prior to first push on Sol 34. Next picture (Sol 34) shows Badger leaning on sampler which is fully extended and has been driven clockwise (to right); a small unplanned trench in front of rock was produced during push. Center picture (Sol 34) shows the trench excavated as sampler retracted; azimuth of trench is oblique to azimuths through gimbal axis. Note thin "water line" ledge of soil adhering to left side of rock. Fourth picture (Sol 37) shows Badger after second push; note skid marks produced by sliding. Final picture shows second pass acquisition trench for sample under Badger; note floors of retraction trench (to clear contaminants) and acquisition trench are not visible because local surface slopes away from observer. Only end of sample trench is visible.

the rock simply slid on the surface. The Sol 37 push was followed by a sample acquisition. Motor currents for this acquisition are relatively low and oscillatory when compared with other acquisitions (compare figs. 13 and 15).

As noted above, the orientation of the surface with respect to the sampler was not expected to be favorable because it sloped away from the lander. Thus, the small motor currents measured during sampling are compatible with shallow trenching ($\approx$ 3.5 cm deep) through an irregular surface inclined away from the lander.

The nudge and push of Notch (rock 7), followed by the acquisition, was the culmination of the under-the-rock sampling activities during the Primary Mission (figs. 16 and 17). On Sol 45, Notch was nudged by pushing on a protuberance on the left edge of the rock so that it would rotate to avoid early exposure. As planned, Notch rotated about an axis on the right center side of the rock. This movement displaced the protuberance about 3.8 cm (figs. 5, 6, and 16). The motion may have been jerky, judging from the oscillating motor currents. The push before sunrise on Sol 51 was accompanied by about 47° of rotation and 9.5–10.5 in. (24–27 cm) of translation. The duration of high motor currents was about 10.5 seconds. A rapid rise in motor currents within 1 second shows that the sampler contacted the surface within 1 in. (2.5 cm) of the rock. Motor currents for the push were about 50 N larger than those during the sample acquisition. Periodically, they were 75–100 N larger. This may be compared with the estimated weight of the rock (40–76 N). Since the higher estimate assumed a rectangular rock, it is probably too large. The lower weight allows for rounded edges but may be somewhat low. For simple sliding with a friction coefficient of 0.6 and using the equation of figure 11, a rock weighing 31 N could be pushed. If the sin θ term, which allows for an increase in normal force by the sampler, is ignored, a rock weighing 40 N could be pushed. At times forces as large as 100 N were exerted and may correspond to some plowing, which is seen to be the case from the pictures.

SAMPLING RESULTS

Judgment on the provenance of the samples was relatively straightforward for Notch rock because it fulfilled the criteria of surface area, visibility, and sampleability, but this was not the case for Badger. The surface beneath Notch could be viewed directly on high-resolution pictures taken by both cameras. Direct views showed that the trenching designed to

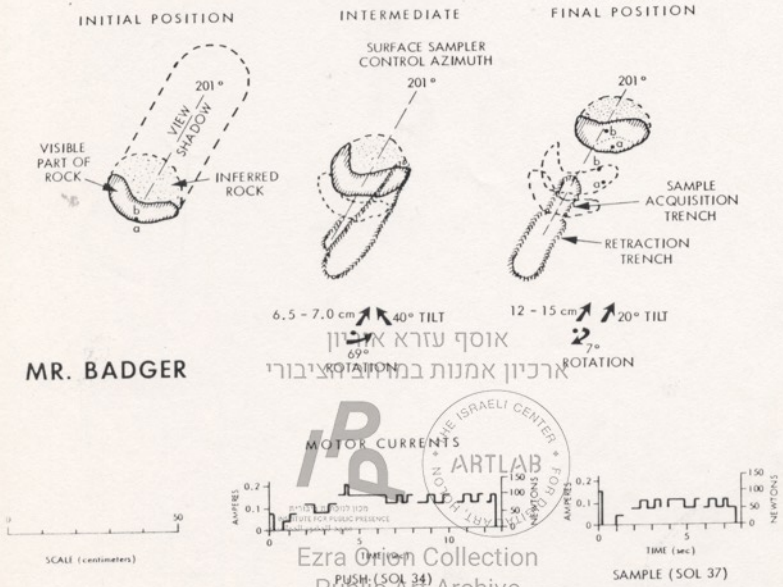

FIGURE 15.—Plan view showing movement of Badger (rock 3). Left is Badger before movement; note view shadow and area of inferred rock; 201° is azimuth through sampler gimbal axis; a and b are points on rock. Center, Badger after first push; dotted line is original position; note short trench excavated by surface sampler while extending to rock; large trench produced during retraction while Badger leaned on surface sampler; note trench is oblique to commanded azimuths; arrows below indicate motion; motor currents show approach to rock (0.6–4 s); the push (4–6.5 s); and push while Badger leaned on surface sampler (6.5–12.6 s). Last diagram shows final position of Badger; trench to clear contaminants; acquisition trench; arrows indicate motions; motor currents below are unusually low for sample acquisition.

clear away possible contamination was successful and that the acquisition occurred in the correct place. Achieved positions of the sampler were in complete accord with interpretations of the pictures. For the sample beneath Badger, judgment was at best difficult. Visibility and sampleability were not as favorable as at Notch because of the slope of the surface. The situation was more seriously affected by the post-sample acquisition pictures, one of which was a low-resolution (blue diode) picture and the other a high-resolution picture. Both were taken at low sun elevation angles, which caused extensive shadowing. The chief evidence that the sample came from beneath the rock was provided by comparing the history and locations of the rock along the azimuth axis of the sampler gimbal with achieved commands (fig. 18). Since this comparison indicated the sampler achieved the correct positions, the best estimate was that the sample did indeed come from soil originally beneath the rock. The outcome indicates that the low rating given to sampleability was appropriate. Two acquisition sequences were automatically performed because a "level full" signal was not obtained immediately after the first acquisition. Such a signal was obtained during the second acquisition sequence just before sieving of the sample into the Molecular Analysis soil delivery system.

Analytical results of the samples by the Molecular

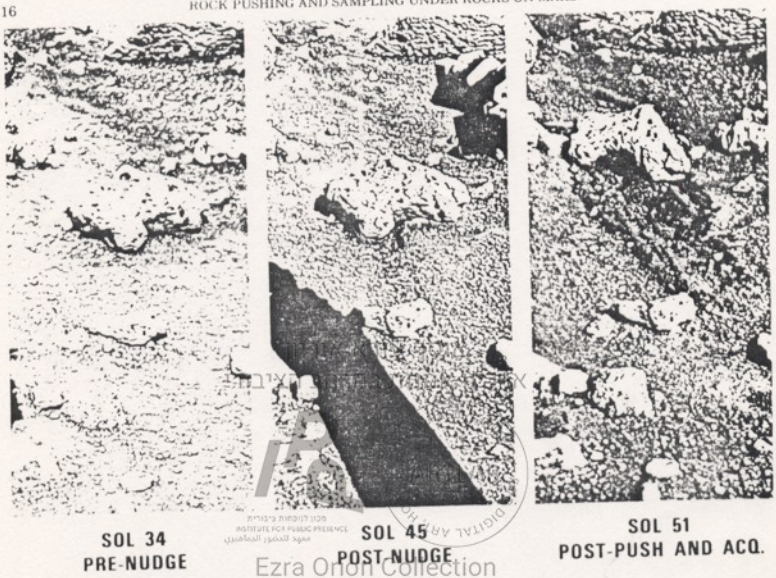

FIGURE 16.—Sequence of pictures showing Notch (rock 7, Ares Vallis, Mars). First picture shows rock before nudge on Sol 45. Next picture shows rock after nudge; note small displacement at protuberance on left side of rock. Third picture shows Notch after push and sample on Sol 51; note backhoe trench walls, plowing marks, and sampled area, which was originally under rock.

Analysis Experiment and Biology Experiment are compatible with the judgment that the samples came from beneath the rocks. The amount of water evolved during heating from 50–200°C of material from beneath Badger is much larger (0.2 percent) than that evolved from the sample exposed to the sun and heated in one step to 200°C (≈0.05 percent)(Biemann and others, 1977). Heating of both samples to 350°C and then 500°C evolved comparable amounts of water during each heating step (Biemann and others, 1977). The results of the Gas Exchange instrument of the Biology experiment are also compatible with relatively large amounts of water. Evolution (desorption) of N_2, Ar, CO_2, and O_2 from soil humidified in the presence of the nutrient in the Gas Exchange Instrument varies inversely with the mean water content of the original sample environment (Oyama and Berdahl, 1977). Reduced desorption of N_2, Ar, and CO_2 from the sample under Notch is attributed to larger amounts of adsorbed water (Oyama, 1977). Reduced O_2 evolution is attributed to the hydration of alkaline-earth and alkali-metal superoxides to produce hydrated peroxides.

By terrestrial analogy, larger amounts of water should be expected under rocks (Moore and others, 1977b). Field and laboratory studies show that soil beneath rocks in a field of soil in an arid environment has detectably more adsorbed water at depths of 2.5–5.0 cm than soil exposed to the sun and atmosphere (Jury and Bellantuoni, 1976a, b). These studies indicate the net heat flow is toward the soil beneath the rocks, and so water vapor moves under the thermal gradient toward the area beneath the rocks. The rock cap inhibits evaporation. Also, ultraviolet radiation may dehydrate exposed soils (Huguenin, 1976).

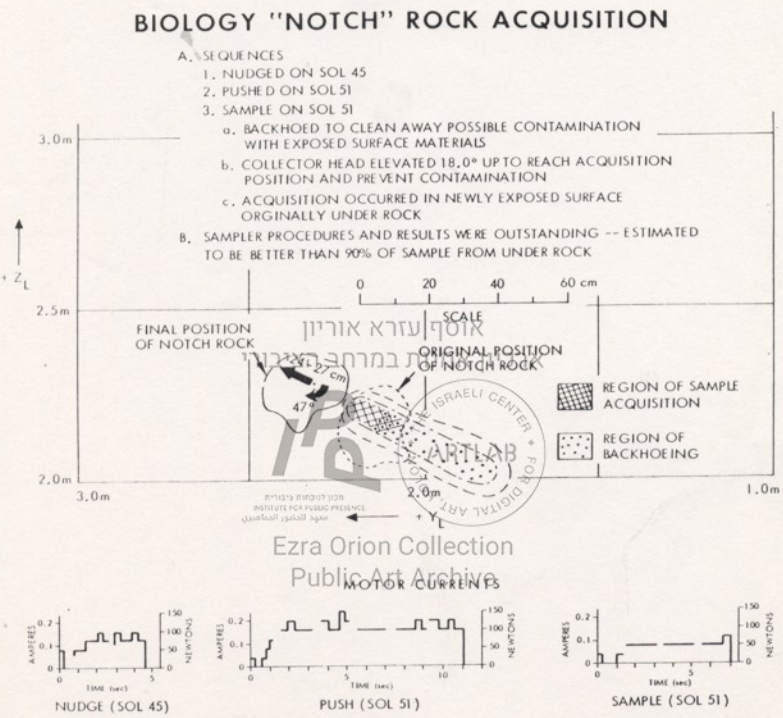

FIGURE 17.—Plan view showing movement of Notch (rock 7). Short dashed lines indicate original position of rock, solid line indicates final position of rock. Arrows show motion of rock. Motor currents are plotted at bottom. Note motor currents during push (center) are larger than those for nudge (left) and sample (right).

SCIENTIFIC VALUE

The scientific value of the samples from under the rocks was considerable (see table 2).

1. There was no evidence for large quantities of organic molecules in the sample from the sun-shielded soil beneath Badger (Biemann and others, 1977).
2. Results from the Biology experiments did not produce convincing evidence for Earth-like living organisms that thrived in the protected environment beneath Notch (Horowitz and others, 1976, 1977); the possibility for life on Mars has not been excluded, however (Levin and Straat, 1976, 1977).
3. Results of the Inorganic Analysis experiment indicate substantially less iron in the samples from under Badger and Notch than in samples exposed to the sun and atmosphere (B. C. Clark and others, 1977). The reason for the difference in iron content is not understood at this time; it may be the result

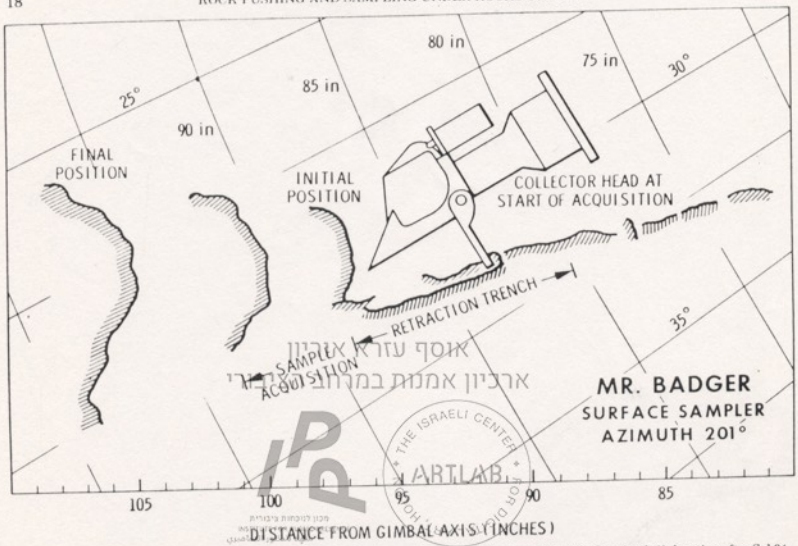

FIGURE 18.—V-Profile along sampler arm azimuth of 201°, showing surface and original location of Badger (rock 3), location after Sol 34 push, and location after Sol 37 push. Surface sampler collector head at position just before acquisition stroke; sample area and backhoe trench areas indicated by arrows. Sloping lines indicate deelevation angles; arcs are sampler extensions.

of sedimentation of magnetite-rich fine material from the atmosphere (Pollack and others, 1977) on exposed surfaces but not on covered surfaces.

4. The large amount of water (for Mars) evolved during heating of the sample from under Badger to 200°C may represent adsorbed water. If this is the case and Mars is like the Earth, adsorbed water may be present at greater depths, where it is cooler. Such a result lends strong support to models of Mars and its atmosphere requiring adsorbed water (Fanale, 1976).
5. The response of the exposed and shielded soils to the Gas Exchange instrument is providing valuable insight on the chemical environment at the surface of Mars.
6. The surface sampler did not scratch, chip, or spall the rocks, showing their surfaces are hard.
7. Color pictures were obtained of freshly exposed soil beneath Badger as well as the underside of the rock.
8. The "water line" ledge of soil adhering to the side of Badger (fig. 14) provides clear evidence of a near-surface crust.

SUMMARY AND CONCLUSIONS

The dense field of rocks on Mars was not anticipated before the Viking landings, and pushing rocks was not in the plans. Successful pushing of the rocks and sampling from the newly exposed soils beneath them required the development of imaginative procedures based on a thorough understanding of scientific requirements and the variables related to the surface sampler. Of equal importance was an accurate knowledge of the locations of the rocks within the sample field.

The endeavor to collect samples from under rocks was entirely successful. Four lines of evidence support this: (1) The pictures show that samples came from soils originally beneath the rocks; (2) the sampler positions indicate that samples came from soils originally beneath the rocks; (3) by terrestrial analogy,

TABLE 2.—*Comparison of scientific results from samples acquired from under rocks and samples directly exposed to the atmosphere and sun*

Experiment	Observed quantities or items		Under-rock samples	Exposed samples (Lander 2)	Exposed samples (Lander 1)	Comments
Biology						
Gas Exchange	predicted	Ar(nmols)	39	49	62	Predicted and observed nanomoles (nmols) of gas desorbed by humidification (Oyama and Berdahl, 1977, table 2). Differences in the Ar and N_2 found in samples are attributed to amount of adsorbed water vapor, which is largest for under-rock sample and smallest at VL-1 site; amount of O_2 evolved attributed to reaction of water vapor with superoxides and peroxides; O_2 from under-rock sample probably near 70 nmols; low O_2 evolved because there was more water under Notch (rock 7).
	found	Ar	6	4	13	
	predicted	N_2	60	76	96	
	found	N_2	13	30	83	
	predicted	O_2	2.7	3.4	4.4	
	found	O_2	70–270	190	790	
	predicted	CO_2	6,110	7,750	9,800	
	found	CO_2	6,110	7,750	9,800	
Pyrolytic Release		$^{14}CO_2$ (disintegrations per minute)				Results from this instrument are poorly understood at this time; a biological interpretation of results is unlikely (Horowitz and others, 1977).
Labeled Release		$^{14}CO_2$ (counts per minute)				Results from this instrument are consistent with a biological response and restrict possible chemical reactions that might produce the results (Levin and Straat, 1977).
Molecular Analysis	Water (percent)					No organic compounds related to the soil of Mars were detected; water analyses for Lander 1 were omitted because they are, at best, crude estimates (Biemann and others, 1977).
	heated to—	50°C	<0.01	---	---	
		200°C	0.2	0.05	---	
		350°C	0.3	0.3	---	
		500°C	0.8	1.0	---	
		500°C	0.6	0.25	---	
Inorganic Analysis	Iron (percent)		≈11.6–12.8	14.2	12.7–13.1	Data on samples from under rocks not yet available; sample from under Badger (rock 3) contains 18 percent less iron than exposed samples at VL-2 site; sample from under Notch (rock 7) contains 10 percent less iron than exposed samples at VL-2 site (B. C. Clark and others, 1977), values for under-rock sample taken as 10 and 18 percent less than 14.2 percent.

TABLE 2.—*Comparison of scientific results from samples acquired from under rocks and samples directly exposed to the atmosphere and sun—Continued*

Experiment	Observed quantities or items	Under-rock samples	Exposed samples (Lander 2)	Exposed samples (Lander 1)	Comments
Physical properties:					
Rock strength	Pictures and forces inferred from motor currents.	---	---	---	ICL (rock 1) did not scratch, chip, or spall when forces of 200 N and stresses near $10^6 N/m^2$ were exerted on it; this indicates rock is strong and does not have a weak weathered rind.
Soil structure (crust)	Pictures of disturbed rocks.	---	---	---	Ledge of soil adhering to Badger (rock 3) proves the existence of thin crust near surface.
Lander Imaging Color	Pictures of rock and soil.	---	---	---	Color data not reduced; there are no obvious differences in color between under-rock and exposed soils.

more adsorbed (?) water should be in soils under rocks than in soils exposed to the sun; (4) soils from under the rocks contain less iron than those exposed to the sun and atmosphere.

The larger amount of water evolved during heating to 200°C from soil beneath the rock than from soil exposed to the sun and atmosphere as well as the Biology experiment results on the sample from under a rock lends strong support to theories requiring storage of water and volatiles in the martian regolith. Eventually, the results may lead to a reasonable assessment of equilibrium conditions between the water vapor in the atmosphere and the water in the regolith. Although not understood at this time, the difference between the amount of iron in soils from under the rocks and soils exposed to the sun and atmosphere should be explicable.

REFERENCES CITED

Baird, A. K., Toulmin, Priestley, III, Clark, B. C., Rose, H. J., Jr., Keil, Klaus, Christian, R. P., and Gooding, J. L., 1976, Mineralogic and petrologic implications of Viking geochemical results from Mars: Interim report: Science, v. 194, p. 1288–1293.

Biemann, Klaus, Oro, John, Toulmin, Priestley, III, Orgel, L. E., Nier, A. O., Anderson, D. M., Simmonds, P. G., Flory, Donald, Diaz, A. V., Rushneck, D. R., and Biller, J. A., 1976, Search for organic and volatile inorganic compounds in two surface samples from the Chryse Planitia region of Mars: Science, v. 194, p. 72–76.

Biemann, Klaus, Oro, John, Toulmin, Priestley, III, Orgel, L. E., Nier, A. O., Anderson, D. M., Simmonds, P. G., Flory, Donald, Diaz, A. V., Rushneck, D. R., Biller, J. E., and Lafleur, A. L., 1977, The search for organic substances and inorganic volatile compounds in the surface of Mars: Jour. Geophys. Research, v. 82, p. 4641–4658.

Clark, B. C., Baird, A. K., Rose, H. J., Jr., Toulmin, Priestley, III, Christian, R. P., Kelliher, W. C., Castro, A. J., Rowe, C. D., Keil, Klaus, and Huss, G. R., 1977, The Viking X-Ray fluorescence experiment: Analytical methods and early results: Jour. Geophys. Research, v. 82, p. 4577–4594.

Clark, B. C., Baird, A. K., Rose, H. J., Jr., Toulmin, Priestley, III, Keil, Klaus, Castro, A. J., Kelliher, W. C., Rowe, C. D., and Evans, P. H., 1976, Inorganic analyses of Martian surface samples at the Viking landing sites: Science, v. 194, p. 1283–1288.

Clark, L. V., Crouch, D. S., and Grossart, R. D., 1977, Viking '75 project summary of primary mission surface sampler operations: Viking Flight Team Document VFT–019, 477 p.

Crouch, D. S., 1976, PTC surface sampler boom loading test with Format 5 and SSCA TM data: Martin Marietta Corp. Letter SST–17870–DSC dated 25 June 1976.

Fanale, F. P., 1976, Martian volatiles: Their degassing history and geochemical fate: Icarus, v. 28, p. 179–202.

Horowitz, N. H., Hobby, G. L., and Hubbard, J. S., 1976, The Viking carbon assimilation experiments: Interim report: Science, v. 194, p. 1321–1322.

——— 1977, Viking on Mars: The carbon assimilation experiment: Jour. Geophys. Research, v. 82, p. 4659–4662.

Huck, F. O., McCall, H. F., Patterson, W. R., and Taylor, G. R., 1975, The Viking Mars Lander camera: Space Sci. Instrumentation, v. 1, p. 189–241.

Huguenin, R. L., 1976, Mars: Chemical weathering as a massive volatile sink: Icarus, v. 28, p. 203–212.

Jury, W. A., and Bellantuoni, B., 1976a, Heat and water movement under surface rocks in a field of soil: I. Thermal effects: Soil Sci. Soc. America Jour., v. 40, p. 505–509.

——— 1976b, Heat and water movement under surface rocks in a field of soil: II. Moisture effects: Soil Sci. Soc. America Jour., v. 40, p. 509–513.

Klein, H. P., Lederberg, Joshua, and Rich, Alexander, 1972, Biological experiments: The Viking Mars Lander: Icarus, v. 16, p. 139–146.

Klein, H. P., Horowitz, N. H., Levin, G. V., Oyama, V. I., Lederberg, Joshua, Rich, Alexander, Hubbard, J. S., Hobby, G. L., Straat, P. A., Berdahl, B. J., Carle, G. C., Brown, F. S., and Johnson, R. E., 1976, The Viking biological investigation: Preliminary results: Science, v. 194, p. 99–105.

Levin, G. V., and Straat, P. A., 1976, Viking labeled release biology experiment: Interim results: Science, v. 194, p. 1322–1329.

———1977, Recent results from the Viking Labeled Release experiment on Mars: Jour. Geophys. Research, v. 82, p. 4663–4667.

Levinthal, E. C., Green, William, Jones, K. L., and Tucker, Robert, 1977, Processing the Viking Lander camera data: Jour. Geophys. Research, v. 82, p. 4412–4420.

Liebes, Sidney, Jr., and Schwartz, A. A., 1977, Viking '75 Mars Lander Interactive computerized Video Stereophotogrammetry system: Jour. Geophys. Research, v. 82, p. 4421–4429.

Moore, H. J., Hutton, R. E., Scott, R. F., Spitzer, C. R., and Shorthill, R. W., 1977a, Surface materials of the Viking landing sites: Jour. Geophys. Research, v. 82, p. 4497–4523.

Moore, H. J., Leibes, Sidney, Jr., Crouch, D. S., and Clark, L. V., 1977b, Rock pushing and under-rock sampling on Mars: Committee on Space Research (COSPAR) meeting, XXth, Tel Aviv, Israel, 7–18 June 1977, Proc., p. 131.

Mutch, T. A., Binder, A. B., Huck, F. O., Levinthal, E. C., Morris, E. C., Sagan, Carl, and Young, A. T., 1972, Imaging experiment: The Viking Lander: Icarus, v. 16, p. 92–110.

Oyama, V. I., 1977, The gas exchange experiment: Committee on Space Research (COSPAR) meeting, XXth, Tel Aviv, Israel, 7–18 June 1977, Proc., p. 124.

Oyama, V. I., and Berdahl, J., 1977, The Viking Gas Exchange Experiment results from Chryse and Utopia surface samples: Jour. Geophys. Research, v. 82, p. 4669–4676.

Patterson, W. R., III, Huck, F. O., Wall, S. D., and Wolf, M. R., 1977, Calibration and performance of the Viking Lander Cameras: Jour. Geophys. Research, v. 82, p. 4391–4400.

Pollack, J. B., Colburn, David, Kahn, Ralph, Hunter, June, VanCamp, Warren, Carlston, C. E., and Wolf, M. R., 1977, Properties of aerosols in the Martian atmosphere, as inferred from Viking Lander imaging data: Jour. Geophys. Research, v. 82, p. 4479–4496.

Shorthill, R. W., Moore, H. J., Hutton, R. E., Scott, R. F., and Spitzer, C. R., 1976, The environs of Viking 2 Lander: Science, v. 194, p. 1309–1318.

Soffen, G. A., 1976, Scientific results of the Viking missions: Science, v. 194, p. 1274–1276.

Soffen, G. A., and Snyder, C. W., 1976, The first Viking mission to Mars: Science, v. 193, p. 759–765.

agrees well with the ground temperature inferred by the Viking orbiter infrared temperature mapping experiment (7) in the landing site region during the predawn period, but is up to 25°C colder during the day. This is analogous to the behavior of the air and ground temperatures in terrestrial deserts, and is indicative of intense convection. Further evidence of convection appears in the behavior of wind and temperature statistics within individual modules. Both wind and temperature are much more viable during the day than during the night (Table 1), indicating relatively gusty daytime conditions.

As is clear from Figs. 1 to 4, the minimum temperatures occur just after dawn, which is at 5 : 24 L.L.T. From the three cases available, the average minimum temperature is 188°K. Unfortunately, the gap for relay link transmission includes the time of maximum temperature. The last module of data recorded before the gap is centered at 14 : 21 L.L.T. and the first module after the gap is centered at 17 : 15 L.L.T. Thus, the maximum occurs between 2.3 and 5.2 hours after noon. A least-squares harmonic analysis of the data for sols 0 to 3 places the maximum at about 15 : 30 L.L.T. with a value of 244°K.

The pressure data show a diurnal v...

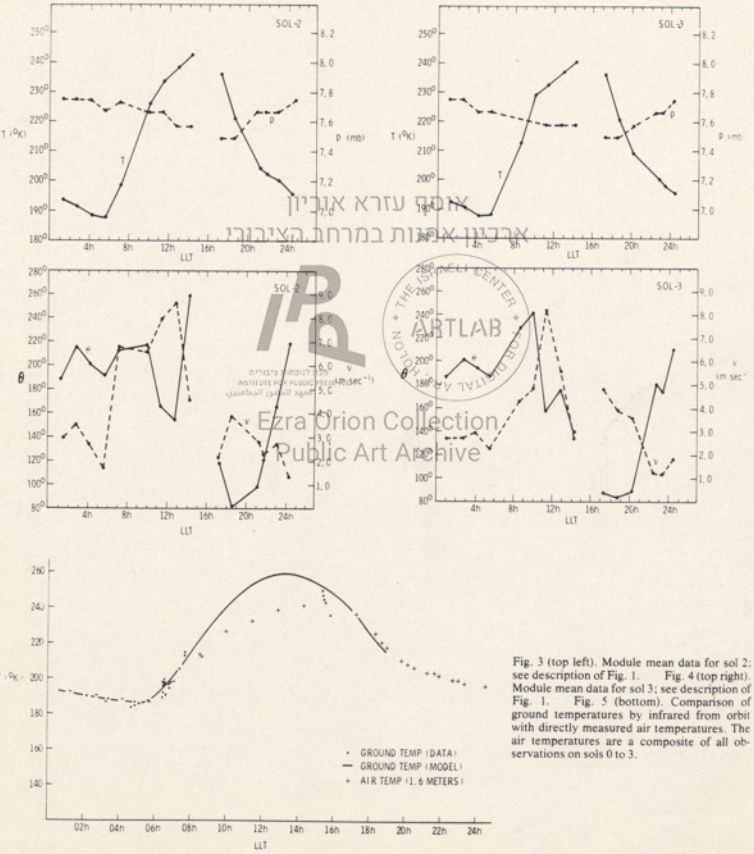

Fig. 3 (top left). Module mean data for sol 2; see description of Fig. 1. Fig. 4 (top right). Module mean data for sol 3; see description of Fig. 1. Fig. 5 (bottom). Comparison of ground temperatures by infrared from orbit with directly measured air temperatures. The air temperatures are a composite of all observations on sols 0 to 3.

tion with a difference between extremes of about 0.2 mbar. The minimum occurs about 4 hours after noon and the maximum at about 4 hours after midnight. Figures 1 to 4 exhibit this diurnal behavior even though the digitization increment of the data is a substantial fraction of the amplitude detected. The mean pressure for sols 1 to 3 is 7.65 mbar. It is worthy of note that an amplitude of 0.1 mbar is in excess of 1 percent of the mean. On Earth, that would be a diurnal amplitude greater than 10 mbar, very much larger than what is observed (about 1.5 mbar).

Finally, we note that neither the magnitude nor the direction of the measured winds is consistent with the aeolian (wind-formed) features identified in lander images (*8*). We conclude that these features were produced during another martian season, or another epoch.

S. L. HESS
Florida State University, Tallahassee
R. M. HENRY
NASA Langley Research Center, Hampton, Virginia
C. B. LEOVY
University of Washington, Seattle
J. A. RYAN
California State University, Fullerton
J. E. TILLMAN
University of Washington, Seattle
T. E. CHAMBERLAIN
TRW, Inc., Redondo Beach, California
H. L. COLE
National Center for Atmospheric Research, Boulder, Colorado
R. G. DUTTON
Martin Marietta Aerospace, Denver, Colorado
G. C. GREENE
NASA Langley Research Center
W. E. SIMON
Martin Marietta Aerospace
J. L. MITCHELL
Florida State University

References and Notes

1. T. E. Chamberlain, H. L. Cole, R. G. Dutton, G. C. Greene, J. E. Tillman, *Bull. Am. Meteorol. Soc.*, in press.
2. All directions are measured clockwise from planetary north.
3. The approximate landing point is 22.3°N, 48.0°W.
4. The term "sol" refers to the martian day of 24.660 hours and is used to avoid confusion with the terrestrial day.
5. Topographic map of Lunae Pallas Quadrangle of Mars, MC10, M5M 15/16 RCM, 1976 (U.S. Geological Survey, Reston, Va. 22092).
6. R. W. Zurek, *J. Atmos. Sci.* **33**, 321 (1976); S. Chapman and R. S. Lindzen, *Atmospheric Tides* (Gordon & Breach, New York, 1970).
7. H. H. Kieffer, S. C. Chase, Jr., E. D. Miner, F. D. Palluconi, G. Munch, G. Neugebauer, T. Z. Martin, *Science* **193**, 780 (1976).
8. T. A. Mutch, A. B. Binder, F. O. Huck, E. C. Levinthal, S. Liebes, Jr., E. C. Morris, W. R. Patterson, J. B. Pollack, C. Sagan, G. R. Taylor, *ibid.*, p. 791.
9. Supported by NASA contract NAI 9693.

27 July 1976

The Surface of Mars: The View from the Viking 1 Lander

Abstract. *The first photographs ever returned from the surface of Mars were obtained by two facsimile cameras aboard the Viking 1 lander, including black-and-white and color, 0.12° and 0.04° resolution, and monoscopic and stereoscopic images. The surface, on the western slopes of Chryse Planitia, is a boulder-strewn deeply reddish desert, with distant eminences—some of which may be the rims of impact craters—surmounted by a pink sky. Both impact and aeolian processes are evident. After dissipation of a small dust cloud stirred by the landing maneuvers, no subsequent signs of movement were detected on the landscape, and nothing has been observed that is indicative of macroscopic biology at this time and place.*

On 20 July 1976, at 1613 after local Mars midnight, the Viking 1 spacecraft touched down on the surface of Mars and immediately began transmission of photographs to Earth. Camera 2 on the Viking 1 lander obtained the first photographs ever returned from the surface of Mars—a high-resolution view of the vicinity of Viking lander footpad 3 in the near field (Fig. 1) and a low-resolution panoramic view of the middle to far field, including the sky of Mars (Fig. 2).

The Viking lander camera (*1*, *2*) is basically a multispectral radiometer with an optical-mechanical scanning mechanism that determines both the image raster and the field of view. It features an array of 12 silicon photodiodes consisting of four broadband channels with selectable focus for high-resolution imaging, one broadband channel for rapid surveys, six narrowband (about 0.1 μm) channels for multispectral imaging (color and near-infrared), and one narrowband channel for scanning the sun. The instantaneous fields of view are 0.04° for the four high-resolution channels and 0.12° for the other channels. The field of view ranges in elevation from 40° above to 60° below the horizon, and in azimuth from 0° to 342.5°. The camera scanning rates are synchronized to the lander data transmission rates of 16,000 bit/sec to the two orbiters as relay stations and 250 bit/sec directly to Earth. Image data can also be secured at preferred times and stored on a lander tape recorder for later transmission to take advantage of favorable imaging periods (for example, sun elevation angles).

High sensitivity is obtained over a wide dynamic range with only 6-bit encoding by the use of six commandable linear gains and 32 offsets. This approach was expected to require some initial trials in selecting optimum dynamic ranges after landing (*3*). However, once the atmosphere and surface brightness was approximately characterized from initial image data, it was possible to select optimum dynamic ranges for subsequent imagery and radiometry experiments.

General geological setting. The Viking 1 landing site (22.4° ± 0.15°N, 48.0° ± 0.5°W, areographic coordinates) is located about 130 km to the east of Lunae Planum, on the western slopes of the large depression, Chryse Planitia (*4*). The Chryse basin is about 5 km deep and the landing site lies about 2 km higher than the floor. Lunae Planum is separated from the more sparsely cratered Chryse Planitia by an irregular, scarplike boundary. Viking orbiter imagery shows a num-

Fig. 1. This high-resolution picture of footpad number 3 and the adjacent surface is the first image ever returned from the surface of Mars. The large rock near the center is about 10 cm across. Some of the rocks have a vesicular appearance; one in the upper right has a horizontally banded texture. Some of the texture in the smooth parts of the surface was probably produced during landing; in particular a few elongate pits near the center appear to have been produced by the impact of small pebbles thrown out by the rocket exhaust. Sediment, including small pebbles or clods, has been deposited in the concave footpad. At left are angular rocks with adjacent sediment piles. At right center is a rock which seems to have been moved about its own length to the right. It is just conceivable that the retrorocket exhaust during landing produced this offset. Refer to Fig. 3 for an orthographic sketch map of this terrain.

Fig. 2. This low-resolution panorama of the martian landscape was taken on sol 0 by camera 2. The left side, where part of the surface sampler is visible, is looking east-northeast on Mars. The other edge is northwest. The sky is brighter in the direction of the setting sun. Some of the irregularities on the skyline, particularly the one to the southeast, may be parts of the raised rims of impact craters. A shallow depression occurs in the foreground just to the right of center, and may be a shallow 3-m-diameter impact crater, possibly a secondary. At this resolution an object 6 m in size subtends one picture element at the nominal horizon. The apparent horizon sinusoid is an artifact of camera tilt (see also Fig. 5).

ber of large, scoured channels that emerge from the edge of Lunae Planum and trend eastward toward the landing site. However, no specific evidence for channeling can be seen at the landing site itself. Rather, the site can be characterized as topographically smooth at the scale of the orbiter photographs. The principal contributions to topographic relief are craters and ridges similar to those on the lunar maria. Some of the ridges west of the landing site appear to postdate the fluvial features; in other cases they are clearly cut by the channels. The regional plains unit is sparsely cratered and may be interpreted as composed largely of volcanic deposits: lunar-like ridges and uniformly flooded craters are both in evidence.

On the basis of regional relations, several models for the recent history of the site are possible: (i) the Chryse plains are predominantly volcanic, but the fluvial channels to the west have emplaced a smooth deposit in the landing area; (ii) the Chryse plains are volcanic and in part are younger than the channel deposits, particularly in the landing area; or (iii) the channel deposits are younger than the plains, but do not reach the landing site area. Among the processes inferred to have operated at the landing site are fluvial activity, flood volcanism, ridge formation, impact cratering, aeolian abrasion and transport, and chemical weathering. The last three of these processes have operated most recently. Orbiter pictures indicate that impact cratering has modified the area since the emplacement of the plains surface. The general indication from crater densities on various surfaces is that volcanism and fluvial modification of the region were not separated greatly in time (4).

Description of the surface of Mars. We first describe the initial images returned by the Viking lander cameras. The first high-resolution picture of Mars (Fig. 1) covers some 57.5° in azimuth in the near field. A circular arc concentric with the camera and of radius 1.9 m would pass through the center of the image. A map of objects in this near-field photograph is displayed in Fig. 3. The large fractured rock in the upper left of Fig. 1 is about 20 cm across. Both blocky and angular rocks are apparent, as well as finer-grained lower-albedo matrix material between the rocks reminiscent of a desert armor or pavement in which the fine-grained particles have been transported by aeolian processes, leaving behind coarser material similar to a gravel. Many of the rocks are fairly angular. Such rocks indicate (i) that the rock was recently produced or fractured; (ii) that the rock, if ancient, was long buried and shielded from erosional processes and only recently exhumed to view; or (iii) that the rock is old but that aeolian or other erosional processes in this region of Mars are feeble.

Several larger rocks exhibit irregular and pitted surfaces, and the large rock in the upper left of Fig. 1 displays intersecting linear cracks. Extending downward from this rock toward the camera is a linear vertical dark band, which may be due to a partial obscuration of the martian landscape for some tens of seconds due to clouds or dust intervening between the sun and the surface (5). Associated with several of the rocks are apparent signs of wind transport of granular material. Sand and dust were deposited during landing inside the footpad near its contact with the support strut. Small streaks and small pits near the footpad were probably caused by the landing event, the footpad kicking out material on contact with the surface.

Much detail is clearly evident in shadows; the illumination of shadows may be due both to the significant light scattering by dust in the martian atmosphere and to reflection off the surface of the spacecraft itself. The sun is to the right and shadows are cast to the left.

In the Viking 1 sol 0 panorama (Fig. 2) a view of about 300° was photographed in a single image. It consists of 2500 lines, each comprising 512 picture ele-

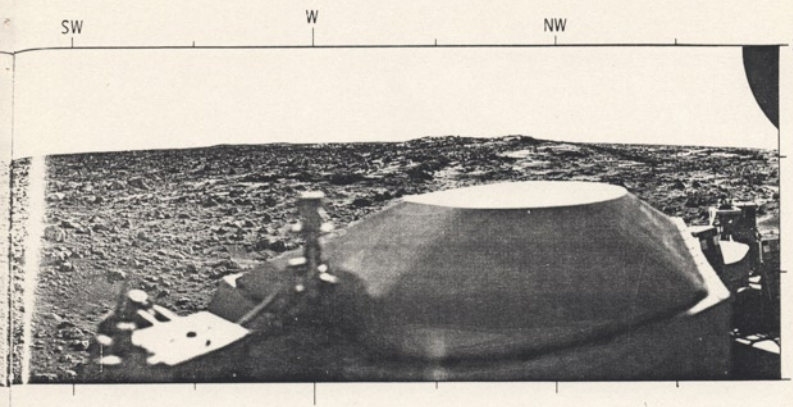

ments. Each picture element subtends 0.12° at the camera in this survey mode. The panorama is here described in sequence from left to right.

The deployed Viking meteorology boom, seen toward the east-northeast, was caged before deployment in the white cradle seen directly below. The out-of-focus spacecraft component seen in the southeast foreground of the panorama is the housing for the Viking sample arm, which is not deployed at this time. The arm and its housing are pivoted toward the spacecraft. On the ground can be seen the shadow of the meteorology boom.

The parallel lines in the sky are an artifact of the intensity digitization of the Viking lander camera and are not real features. However, the change of brightness from horizon toward zenith (and from east to southwest) is accurately reflected in this picture, obtained in late martian afternoon. At the eastern horizon to the left is a plateaulike prominence much brighter than the foreground material, perhaps because it is illuminated directly by the low sun. The plateau may be the rim of a large impact crater.

The topography of the landing site is gently rolling (as is dramatically revealed by fusing the stereo pair on the cover). In the foreground, interblock regions are darker than blocks; in the background, in contrast, blocks are darker than interblock regions. The martian nominal horizon is approximately 3 km away; however, nearby hills obscure our view of large segments of the far horizon, and distant eminences may project above the nominal horizon.

At the left of the panorama is a field of apparent small sand dunes, across which extends a band of dark boulders which continues across the panorama to the southwestern horizon. Subparallel, sinuous ridges are superimposed on the fine-grained patch in the eastern foreground.

The dark knob on the southern horizon may be composed of one or more large boulders. The dark, relatively rock-free foreground region to the southwest is a shallow, circular depression. This depression and others like it may be secondary craters. A horizontal cloud stratum can be made out about halfway between the horizon and the top of Fig. 2 in a southerly direction.

In the west foreground is the low-gain S-band antenna for receipt of commands from Earth. It is in front of the radioisotope thermoelectric generator (RTG-2), which provides the spacecraft with its electrical power. Several projections on or near the horizon may represent the remains of distant impact craters.

A continuation of the right foreground of the panorama (Fig. 4) reveals the color chart for lander camera calibration, the mirror for the Viking magnetic properties experiment, the microdot [see (*22*)], and parts of a 10 by 10 inch grid on the upper surface of the lander, as well as the high-gain S-band antenna now properly deployed for direct communication between the spacecraft and Earth. A rock can be made out just to the left of the S-band antenna support, which appears to be undercut on one side and partially buried by drifting grains on the other. In the right background are patches of smooth fine-grained material which define the beginning of a large dune field off to the right of the picture; its continuation is seen in the sol 3 panorama (Fig. 5).

The survey taken on sol 3 (Fig. 5) completes coverage of the approximately 60° of azimuth not covered on the sol 0 panorama (Fig. 2). A map of objects in this panorama is shown as Fig. 6. In the northeast is seen the upper part of the strut of footpad 2 and the deployed meteorology boom which extends through the right center of the image. Continuing from the vicinity of the spacecraft toward t horizon behind the meteorology boom is an irregular field of fine-grained material in the form of large ripples and dunes. Both dark and bright rocks extend into this part of the scene. The bright rocks form a small rocky hill just above the RTG housing in the image center and continue across the foreground. Several of these rocks, particularly those in the right foreground, are adjacent to depressions apparently scoured by the wind. Dark rocks are abundant to image right farther from the spacecraft and are partly covered by the dunes. An especially prominent dark rock in the northeast (about 8 m away) is about 3 m wide and 1 m high. Several other large dark boulders are seen toward the horizon. In general, the far horizon appears as a bright band. Horizon detail is particularly prominent

MARS ROVER SAMPLE RETURN MISSION

STATUS REPORT

JANUARY 12 - 14, 1988

VOLUME 3

ROVER TECHNOLOGY REQUIREMENTS DEFINITION

- GOAL: PRESENTATION TO RAY COLLADAY OF NASA OAST ON JANUARY 29 TO PROPOSE NEW PROGRAMS AND NEEDED AUGMENTATIONS TO EXISTING PROGRAMS FOR PATHFINDER FUNDING.

- EACH DISCIPLINE IS IDENTIFYING THE TECHNOLOGIES REQUIRED TO BUILD A VERY CAPABLE, ROBUST, INTELLIGENT, HIGHLY-AUTONOMOUS ROVER WHICH WOULD PROVIDE THE MAXIMUM SCIENCE RETURN.

- IN THE ABSENCE OF FORMAL MISSION REQUIREMENTS, SCIENCE REQUIREMENTS, AND SYSTEM FUNCTIONAL REQUIREMENTS, EACH DISCIPLINE IS OPERATING FROM A SET OF "WORKING ASSUMPTIONS" DERIVED FOR EACH FUNCTIONAL AREA.

- THESE WORKING ASSUMPTIONS WILL BE UPDATED AS A RESULT OF SWG ROVER SCENARIOS, MISSION REQUIREMENTS, AND SYSTEM TRADE STUDIES WHICH WILL BETTER QUANTIFY REQUIREMENTS (COMMUNICATIONS, DATA HANDLING/COMPUTATION, POWER, NAVIGATION, ETC.)

REPRESENTATIVE WORKING ASSUMPTIONS

- MISSION OBJECTIVE: TO COLLECT 5 KG OF SCIENTIFICALLY INTERESTING SAMPLES AND RETURN THEM TO EARTH IN GOOD CONDITION.

- PACKAGING OF ROVER IN LAUNCH VEHICLE IMPOSES SEVERE MASS AND VOLUME CONSTRAINTS

- REACHING AND RETURNING FROM INTERESTING SAMPLING SITES REQUIRES THAT ROVER POSSESS A HIGH DEGREE OF MOBILITY AND HEAT TOLERANCE.

- ROVER MUST TRAVEL 100KM IN 100 DAYS, COLLECT 1-2 SAMPLES PER DAY-SAMPLES MUST BE CAREFULLY COLLECTED, LABELED, SEALED, AND PRESERVED FOR RETURN TO EARTH.

- RTLT AND HIGH AMOUNT OF ROVER ACTIVITY AND COMPLEXITY REQUIRES SOME DEGREE OF AUTONOMY TO GET THE JOB DONE (COMPARE VIKING- 21 SAMPLES IN 2 YEARS).

SYSTEM CONTROL AND OPERATIONS

ACTIVITIES:

IDENTIFYING AND EVALUATING METHODS OF COMMANDING AND CONTROLLING THE ROVER TO OBTAIN THE GREATEST AMOUNT OF SCIENCE RETURN POSSIBLE WITHIN TIME AND COST CONSTRAINTS

TECHNOLOGY-DRIVING ASSUMPTIONS:

CURRENT COMMAND AND SEQUENCING TECHNOLOGY IS EXTREMELY SLOW-HASNOT PROGRESSED SIGNIFICANTLY PAST VIKING TECHNOLOGY WHICH REQUIRED DAYS TO CHOOSE AND ACQUIRE A SINGLE SAMPLE. ROVER WILL REQUIRE A MORE CAPABLE METHOD OF SEQUENCE GENERATION AND EXECUTION TO PERFORM MOBILITY FUNCTIONS, SAMPLE IDENTIFICATION, ANALYSIS, HANDLING, AND STORAGE FUNCTIONS, AND NAVIGATION AND RENDEZVOUS FUNCTIONS.

JUSTIFICATION:

"A DAY IN THE LIFE OF A MARS ROVER" STUDY

CARD TRAVERSE REPEATING CYCLE
(average traverse leg length 15 m)
(net average speed 5.3 m / hour)

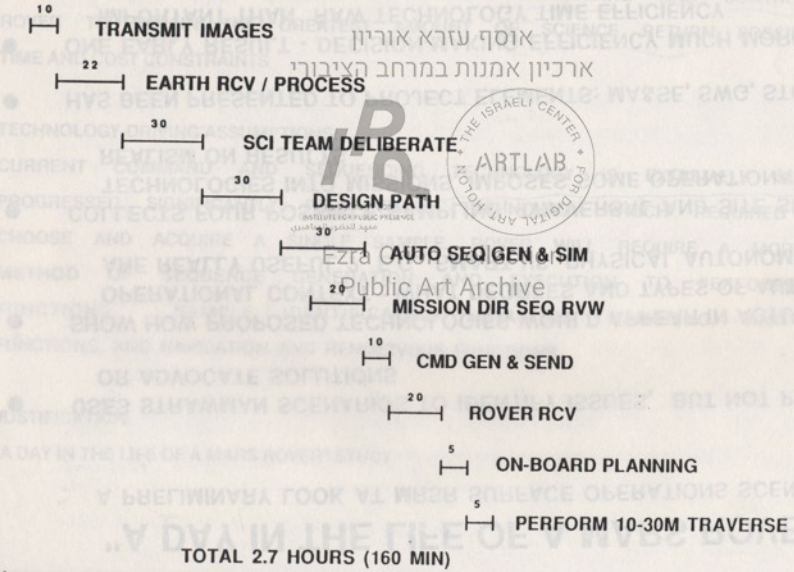

"A DAY IN THE LIFE OF A MARS ROVER"

A PRELIMINARY LOOK AT MRSR SURFACE OPERATIONS SCENARIOS

- USES STRAWMAN SCENARIOS TO IDENTIFY ISSUES, BUT NOT PROPOSE OR ADVOCATE SOLUTIONS
- SHOW HOW PROPOSED TECHNOLOGIES WOULD APPEAR IN ACTUAL OPERATIONAL CONTEXT : WHAT DEGREES AND TYPES OF AUTONOMY ARE REALLY USEFUL ? E.G., SMART VS. PHYSICAL AUTONOMY
- COLLECTS FOUR POSSIBLE SAMPLING, TRAVERSAL AND SITE SURVEY TECHNOLOGIES INTO MISSIONS, IMPOSES SOME OPERATIONAL REALISM ON RESULTS
- HAS BEEN PRESENTED TO PROJECT ELEMENTS: MA&SE, SWG, STG
- ONE EARLY RESULT - DECISION-MAKING EFFICIENCY MUCH MORE IMPORTANT THAN RAW TECHNOLOGY TIME EFFICIENCY
- WORK NEEDED: (1) AUTOMATE SCENARIO PRODUCTION PROCESS
  (2) PERFORM SIMILAR ANALYSIS WITH MORE SCIENCE, SAMPLE ANALYSIS, PRESERVATION, ETC.
  (3) CONTINUE REFINEMENT PROCESS

HYPOTHETICAL 24-HOUR TRAVERSAL PERIOD
SEMI-AUTONOMOUS HIGH COMPUTE POWER - "SPRINT" MODE

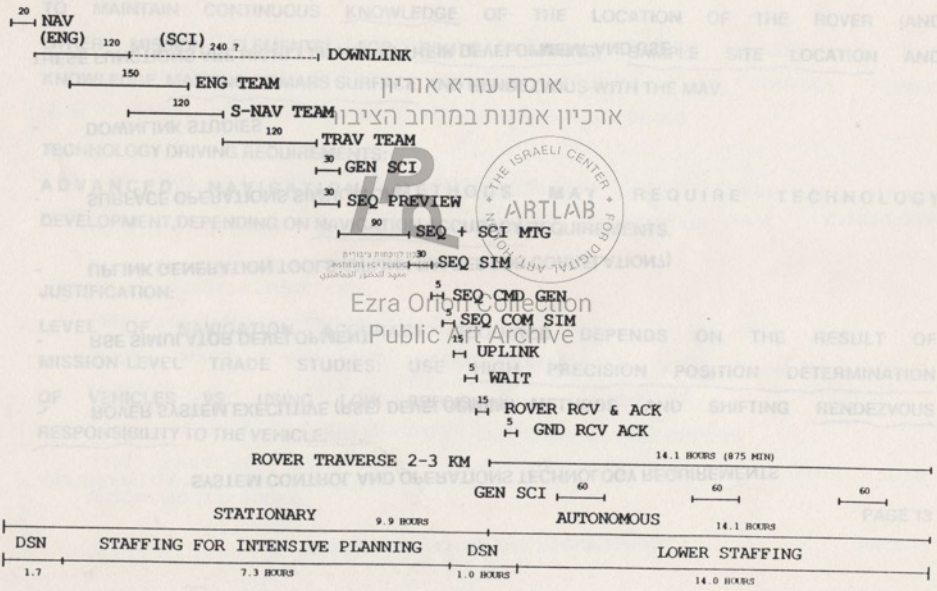

SYSTEM CONTROL AND OPERATIONS TECHNOLOGY REQUIREMENTS

- ROVER SYSTEM EXECUTIVE (RSE) DEVELOPMENT
- RSE SIMULATOR DEVELOPMENT
- UPLINK GENERATION TOOLS (UPLINK IMAGES FOR CORRELATION?)
- SURFACE OPERATIONS SIMULATOR
- DOWNLINK STUDIES

THESE FUNCTIONS ARE HIGHLY LINKED IN THEIR DEVELOPMENT AND USE

GLOBAL NAVIGATION

ACTIVITIES:

TO MAINTAIN CONTINUOUS KNOWLEDGE OF THE LOCATION OF THE ROVER (AND OTHER MISSION ELEMENTS) FOR ROUTE PLANNING, SAMPLE SITE LOCATION AND KNOWLEDGE, MAPPING OF MARS SURFACE, AND RENDEZVOUS WITH THE MAV.

TECHNOLOGY DRIVING REQUIREMENTS:

ADVANCED NAVIGATION METHODS MAY REQUIRE TECHNOLOGY DEVELOPMENT, DEPENDING ON NAVIGATION ACCURACY REQUIREMENTS.

JUSTIFICATION:

LEVEL OF NAVIGATION ACCURACY REQUIRED DEPENDS ON THE RESULT OF MISSION-LEVEL TRADE STUDIES: USE HIGH PRECISION POSITION DETERMINATION OF VEHICLES VS. USING LOW PRECISION METHODS AND SHIFTING RENDEZVOUS RESPONSIBILITY TO THE VEHICLE.

NAVIGATION TECHNOLOGY REQUIREMENTS

DEPENDING ON TRADE STUDIES:

- DIRECT DELTA-VLBI (PUTS COMPUTING POWER ON GROUND)

OR

- INVERTED DELTA-VLBI (PUTS COMPUTE POWER IN SPACE)
- OPTICAL TRACKING, MAPPING, AND IMAGE CORRELATION ARE CANDIDATES (COMPLEMENTARY WITH LOCAL NAV METHODS)

COMPUTATION/DATA HANDLING

ACTIVITIES:

ASSESS COMPUTATION AND DATA HANDLING SUBSYSTEM REQUIREMENTS FOR ROVER FUNCTIONS: NAVIGATION, MOBILITY, COMMUNICATIONS CONTROL, POWER CONTROL, SAMPLE ACQUISITION, SCIENCE DATA HANDLING AND STORAGE.

IDENTIFY AND EVALUATE COMPUTATION SYSTEM ARCHITECTURES AND TRADE STUDIES.

TECHNOLOGY DRIVING ASSUMPTIONS:

- PERFORM RELIABLE COMPUTATIONS (20-200 MIPS)
- SEVERE MASS, POWER, AND VOLUME CONSTRAINTS: MASS: 50-100KG, POWER: 50-75W, VOLUME: 1-3 CUBIC FEET.
- FAULT TOLERANCE AND FLIGHT HARDWARE REQUIREMENTS LIMIT OPTIONS
- RTLT PREVENTS REAL TIME CONTROL FROM GROUND, IMPLIES SOME AUTONOMOUS CONTROL.

MARS ROVER SAMPLE RETURN

AGENDA

JANUARY 12, 1988

167 Conference Room

1:30-5:30	MRSR Study Status Presentations	
1:30-1:45	Welcome, Agenda Review	D.Rea
1:45-4:15	Project Update	
1:45-2:00	Organization	D.Rea
2:00-3:00	Science Requirements - SWG Status	M.Carr
3:00-3:30	Planning	S.Jones
3:30-4:15	Convergence Process	R.Kahl
4:15-4:45	Sample Handling	D.Blanchard
4:45-5:30	Lander and Rover Science Instruments	D.Blanchard

JPL

Basic Computational System Architecture

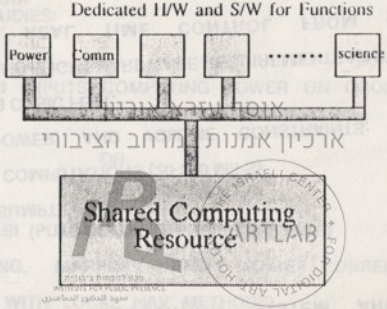

* Shared Computing Resource will be used by all subsystems to minimize the amount of H/W
* The amount of dedicated H/W and S/W will vary from a simple I/F to a processor depending on the performance of the shared computer as well as some other factors.
* The interconnection network has not been selected.

COMPUTATION TECHNOLOGY REQUIREMENTS

- ADVANCED DATA FLOW MACHINE (MAX): GEN PURPOSE PARALLEL PROCESSOR
- IMAGING PROCESSING ARCHITECTURE
- FAULT-TOLERANT DISTRIBUTED FLIGHT PROCESSOR SYSTEMS
- FLIGHT INTERCONNECTION NETWORKS

DATA HANDLING TECHNOLOGY REQUIREMENTS

- OPTICAL DATA STORAGE FLIGHT SYSTEM
- AUTONOMOUS DATA SYSTEM CONTROL
- DATA COMPRESSION: FAULT TOLERANT, HIGH RATES

COMMUNICATIONS

ACTIVITIES:

ASSESS COMMUNICATIONS REQUIREMENTS TO PERFORM ROVER AND MISSION SYSTEM FUNCTIONS: ENGINEERING TELEMETRY, LOCAL NAVIGATION AND MOBILITY, AND SCIENCE DATA.

TECHNOLOGY DRIVING ASSUMPTIONS:

- DATA RATE > 30 KBPS DOWNLINK TO 34 M DSN ANTENNA
- RECEIVE COMMANDS AT RATE >2 KBPS (LARGER IF IMAGES UPLINKED)
- PROVIDE PHASE COHERENT/NONCOHERENT COMMUNICATIONS
- CONSUME <100W DC POWER-ANTENNA PACKAGE LESS THAN 3/4 METER IN DIAMETER, SURVIVE TURNOVER
- ACTUAL COMMUNICATIONS REQUIREMENTS DEPEND ON MISSION LEVEL TRADES: WHERE WILL COMM CAPABILITY RESIDE? DEDICATED COMM ORBITER? DIRECT-TO-EARTH LINK? COMM AVAILABILITY VS MISSION PROFILE?

MARS ROVER SAMPLE RETURN

PHASED ARRAY TECHNOLOGY

COMMUNICATIONS TRADESPACE OPTIONS

X/X-DEPLOYABLE PARABOLA	X/X-PLANAR ARRAY	X/K_a-PHASED ARRAY LIMITED SCAN
FURLING/UNFURLING		
STOW AND LOCK MECHANISM		
BOOM ELECTRONICS		
AZ-EL ACTUATORS AND ENCODERS	ROTARY JOINTS	3D-TV PAN-TILT
LATCH INDICATORS	FLEX WAVEGUIDE RETRACTOR	
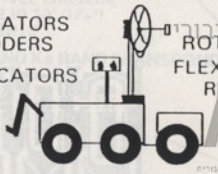		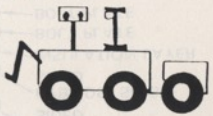
X/K_a-PARABOLA	X/K_a-BEAM WAVEGUIDE	+/– 60 deg SCAN
	OFFSET FED	FULL EBS AND ROLL BAR
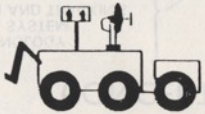	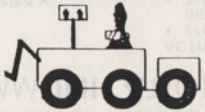	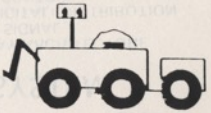

MARS ROVER SAMPLE RETURN
ACTIVE PHASED ARRAY TECHNOLOGY
CONCEPTUAL COMMUNICATIONS SYSTEM

PHASED ARRAY
CONTROL TECHNOLOGY
- VLSI DIGITAL SYSTEM
- ACQUISITION AND TRACKING CONTROL
- X-BAND MONOPULSE POINTING SENSOR

Ka BAND DISTRIBUTED
TRANSMITTER TECHNOLOGY

MMIC COMPONENTS
- POWER AMPS (0.25, 35%)
- LOW LOSS PHASE SHIFTERS
- PACKAGING
- HIGH RELIABILITY

Ka BAND EXCITER TECHNOLOGY
- X-BAND TO Ka BAND UPCONVERSION
- HIGH EFFICIENCY

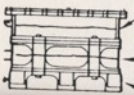

PHASED ARRAY

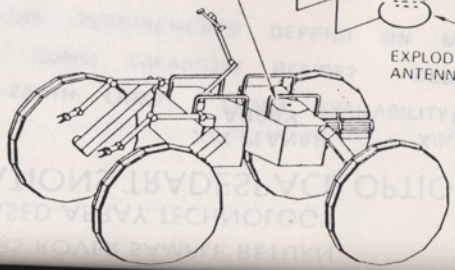

ACTIVE ARRAY ARCHITECTURE
- EFFICIENT SIGNAL (RF, DC, DIGITAL) DISTRIBUTION
- THERMAL CONTROL

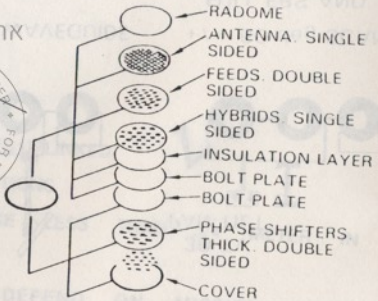

EXPLODED VIEW OF
ANTENNA ASSEMBLY

COMMUNICATIONS TECHNOLOGY REQUIREMENTS

- **INTEGRATED Ka-BAND TRANSMITTER MODULES (32 GHz)**
- **TRANSMIT/RECEIVE ARRAY**
- **X AND Ka BAND TRANSPONDER.**

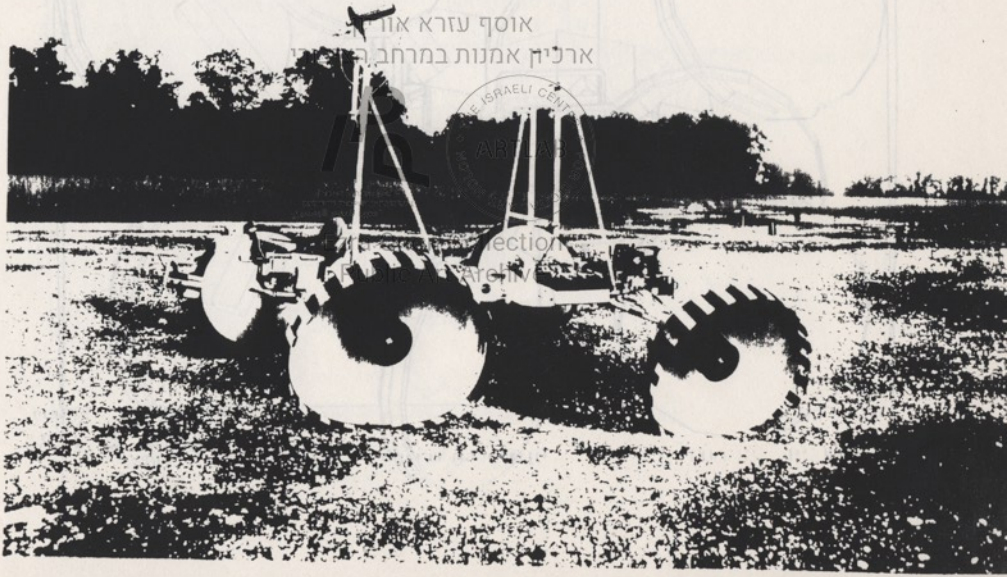

SDRC I-DEAS 2.5B: System Assembly

DATABASE: MARS ROVER STUDY
ENTITY: BODY - STEERED MARS ROVER
VIEW: 3 - ISOMETRIC
DISPLAY: 2 - HIDDEN LINE

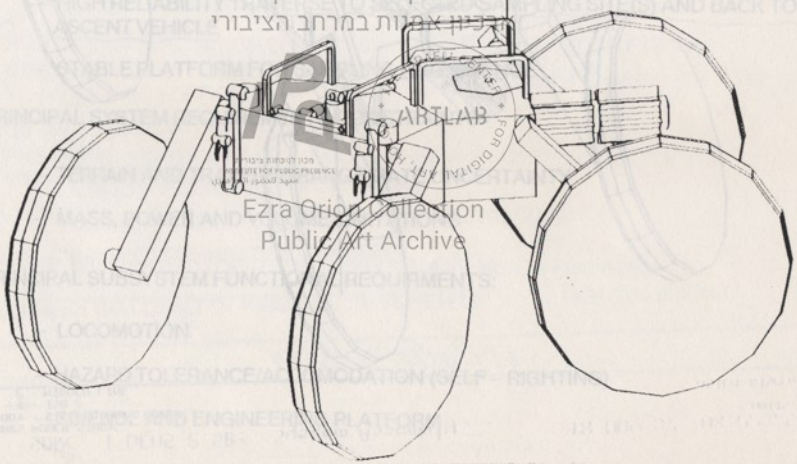

MARS ROVER SAMPLE RETURN

AGENDA

JANUARY 13-14, 1988

Wednesday, 1/13	von Karman Auditorium	
8:00-4:30	MRSR Study Status Presentations	
8:00-1:30	Aerocapture, Entry and Landing	J.Gamble
8:00- 9:30	In-house Study Presentation	
9:30-11:15	Martin Marietta Study Presentation	
11:15-12:00	Lunch	
12:00- 1:30	Lockheed Study Presentation	
1:30- 3:00	Ascent, Rendezvous and Return	D.Long
3:00- 4:30	Viking Entry and Landing Experience	Martin-Marietta
Thursday, 1/14	von Karman Auditorium	
8:00-5:00	MRSR Study Status Presentations (concluded)	
8:00-1:30	Rover	D.Pivirotto
8:00- 9:30	In-house Study Presentation	
9:30-11:15	FMC Study Presentation	
11:15-12:00	Lunch	
12:00- 1:30	Martin Marietta Study Presentation	
1:30-3:00	Orbiter	J.Randolph
3:00-4:30	Mission Design	J.Kwok
4:30-5:00	MRSR Precursor Requirements	R.Kahl

ROVER MOBILITY

TECHNOLOGY DRIVERS:

0 MISSION REQUIREMENTS

- HIGH RELIABILITY TRAVERSE TO SELECTED SAMPLING SITE(S) AND BACK TO ASCENT VEHICLE
- STABLE PLATFORM FOR SAMPLING AND SCIENCE

0 PRINCIPAL SYSTEM REQUIREMENTS/CONSTRAINTS

- TERRAIN AND TRAVERSE RANGE/RATE UNCERTAINTY
- MASS, POWER AND VOLUME LIMITATIONS

0 PRINCIPAL SUBSYSTEM FUNCTIONAL REQUIRMENTS:

- LOCOMOTION
- HAZARD TOLERANCE/ACCOMODATION (SELF – Rrighting)
- SCIENCE AND ENGINEERING PLATFORM

JPL

MARS ROVER SAMPLE RETURN MISSION

PROJECT STATUS REVIEW

ROVER SYSTEM

MOBILITY

POWER

THERMAL CONTROL

MANIPULATOR AND END EFFECTOR

JANUARY 14, 1988

BRIAN K. MUIRHEAD

ROVER MOBILITY

STATUS:

0 PERFORMED PRELIMINARY ANALYSIS OF MOBILITY SUBSYSTEM AND COMPONENT OPTIONS

- LEGS vs WHEELS
- DRIVE SYSTEM

0 DEVELOPING ROVER DYNAMICS MODELS FOR OBSTACLE TRAVERSE

0 PERFORMING TERRAIN AND SOIL MODELING AND ANALYSIS
(INCLUDES PRESIDENTS FUND PROPOSAL)

0 GRUMMAN ROVER (LUNAR) DELIVERED TO JPL FOR MOBILITY TESTBED

0 PRELIMINARY DESIGN OF "GOSSAMER DUNE BUGGY" AND OTHERS IN PROCESS

0 COMPLETED PHASE 1 OF TECHNOLOGY REQUIREMENTS PLANNING

ROVER MOBILITY

TECHNOLOGY DEVELOPMENT REQUIREMENTS: * HIGHEST PRIORITY

0 DEPLOYABLE/ADAPTIVE STRUCTURES *
- ADAPTIVE FIGURE, STIFFNESS AND DAMPING CONTROL
- WHEELS, BOOMS AND SUSPENSION

0 3D VEHICLE/GROUND ANALYTICAL MODEL *
- GENERAL FORMULATION OF SURFACE/"WHEEL" AT ALL ANGLES OF ATTACK

0 FLUID ACTUATORS *
- HIGH FORCE/DISPLACEMENT STORED ENERGY DEVICES
- DAMPING AND POSITION CONTROL

0 THERMODYNAMIC ENGINES
- AUXILIARY POWER DEVICES UTILIZING WASTE THERMAL ENERGY

0 VARIABLE SPEED/TORQUE MOTOR/TRANSMISSION SYSTEMS
- OPTIMUM POWER EFFICIENCY OVER WIDELY VARYING TERRAIN

0 FLUID DRIVES

JPL

POWER AND THERMAL CONTROL

STATUS:

0 PRELIMINARY EVALUATION OF MARS ENVIRONMENT EFFECT ON EXISTING RTG TECHNOLOGY COMPLETED: EXISTING DESIGN NOT VIABLE

0 PRELIMINARY STUDY OF AUTONOMOUS THERMAL CONTROL SYSTEM, PAY – OFF AND TECHNOLOGY IN PROCESS

0 COMPLETED PHASE 1 OF TECHNOLOGY REQUIREMENTS PLANNING

ROVER POWER

TECHNOLOGY DRIVERS:

0 MISSION FUNCTIONAL REQUIREMENT:

- PROVIDE COMPACT, LIGHTWEIGHT, VERY HIGH CAPACITY ON – BOARD POWER SYSTEM
- ENABLE MAXIMUM SCIENCE CAPABILITY/RETURN

0 PRINCIPAL SYSTEM REQUIREMENTS/CONSTRAINTS

- MARS HOSTILE ATMOSPHERE AND ROVER DYNAMIC/THERMAL ENVIRONMENT
- LIMITED LAUNCH VEHICLE MASS DELIVERY CAPABILITY

0 PRINCIPAL SUBSYSTEM REQUIREMENTS:

- DEVELOP A MARS UNIQUE ENERGY SOURCE(GPHS)/CONVERSION SYSTEM
- MAXIMIZE SPECIFIC POWER OF ELECTRICAL ENERGY SOURCE/CONVERSION AND STORAGE COMPONENTS
- MINIMIZE MASS AND VOLUME OF POWER CONDITIONING/CONTROL ELEMENTS

ROVER POWER

TECHNOLOGY DEVELOPMENT REQUIREMENTS

* HIGHEST PRIORITY

ENERGY CONVERSION

- 0 MODULAR RTG WITH ADVANCED THERMOELECTRICS (10W/kg) *
- 0 AMTEC (20W/kg, SCHEDULE RISK) *
- 0 STIRLING/BRAYTON (SCALING ISSUES AT 1kWe)

ENERGY STORAGE

- 0 Li – TiS2 BATTERY (100 Whr/kg) *
- 0 Li – Al/FeS2 BATTERY (180 Whr/kg)
- 0 BIPOLAR LEAD – ACID BATTERY (50Whr/kg)
- 0 REGENERATIVE FUEL CELL (1000 Whr/kg, SCHEDULE RISK)

POWER DISTRIBUTION

- 0 POWER INTEGRATED CIRCUITS (7W/IN ^ 3 PACKAGING DENSITY) *

ROVER THERMAL CONTROL

TECHNOLOGY DRIVERS:

0 MISSION FUNCTIONAL REQUIREMENT:

- MAINTAIN SCIENCE AND ENGINEERING SUBSYSTEMS WITHIN ALLOWABLE TEMPERATURE LIMITS FOR ALL NON – OPERATIONAL AND OPERATIONAL CONDITIONS

0 PRINCIPAL SYSTEM REQUIREMENTS/CONSTRAINTS

- PRESSURE .006 – .009 ATM
- SINK TEMPERATURE 140 – 300 K

0 PRINCIPAL SUBSYSTEM FUNCTIONAL REQUIREMENTS:

- PROVIDE HEAT REJECTION FOR ROVER ELEMENTS FOR ALL MISSION PHASES
- PROVIDE THERMAL CONDITIONING FOR SCIENCE ELEMENTS
- PROVIDE CRYOGENIC THERMAL CONTROL FOR SCIENCE AND SAMPLING

JPL

ROVER THERMAL CONTROL

TECHNOLOGY DEVELOPMENT REQUIREMENTS: * HIGHEST PRIORITY

- 0 SORPTION REFRIGERATION *
  - – UTILIZE LOW QUALITY WASTE HEAT FOR CYRO COOLING
- 0 TWO PHASE HEAT TRANSFER LOOP *
  - – HIGH PERFORMANCE, CONTROLLABLE OVER LARGE DISTANCES
- 0 THERMAL CONTROL MATERIALS *
  - – MARTIAN ENVIRONMENT COMPATIBILE MATERIALS
- 0 THERMAL ENERGY STORAGE *
  - – PHASE CHANGE ENERGY STORAGE
- 0 AUTONOMOUS THERMAL CONTROL
  - – FAST, EVALUATION AND CONTROL OF THERMAL SYSTEM STATE
- 0 REMOTE THERMAL SENSING
  - – IR CAMERA SENSING OF TEMPERATURE DISTRIBUTION
- 0 THERMAL DIODE HEAT PIPE
  - – OFF/ON UNI – DIRECTIONAL HEAT PIPE

MARS ROVER/SAMPLE RETURN MISSION

ROVER TECHNOLOGY DEVLOPMENT AREAS:

LOCAL NAVIGATION & HAZARD AVOIDANCE

SAMPLE ACQUISITION

Andrew Mishkin

JET PROPULSION LABORATORY

January 14, 1988

MARS ROVER SAMPLE RETURN MISSION
JPL ROVER TEAM STATUS

JANUARY 14, 1988

THOMAS J. PENN
ROVER SYSTEMS ENGINEER

MARS ROVER/SAMPLE RETURN MISSION

LOCAL NAVIGATION & HAZARD AVOIDANCE

ROVER FUNCTIONAL REQUIREMENT:

RELIABLE TRAVERSAL TO A VARIETY OF SAMPLING SITES IN MINIMAL TIME, UNDER CONDITIONS OF ACCEPTABLE RISK

MISSION CONSTRAINTS:

- COMMUNICATION TIME DELAYS PRECLUDE CONVENTIONAL TELEOPERATION AND REQUIRE ON-BOARD CONTINGENCY-HANDLING
- LIMITED ROVER-EARTH COMMUNICATION
- MARTIAN TERRAIN AND SURFACE PROPERTIES NOT WELL UNDERSTOOD

TECHNOLOGY OPTIONS:

- CARD (COMPUTER-AIDED REMOTE DRIVING)
- SEMI-AUTONOMOUS MOBILITY

MARS ROVER/SAMPLE RETURN MISSION

LOCAL NAVIGATION & HAZARD AVOIDANCE

TECHNOLOGY OPTION TRADEOFFS

CARD	SEMI-AUTONOMOUS ROVER
• 150-300M TRAVERSAL PER DAY	• 1-10KM TRAVERSAL PER DAY
• HUMAN INTERVENTION REQUIRED EVERY 30M	• UP TO 10KM TRAVEL W/O HUMAN INTERVENTION
• LIMITED ABILITIES IN EMERGENCIES	• ON-BOARD EMERGENCY REFLEXES
• VEHICLE NEVER TRAVELS BEYOND THE HORIZON OBSERVED BY A HUMAN BEING USING THE ROVER'S CAMERAS	• FALLBACK TO CARD USED IF NECESSARY
• LARGELY EXISTING TECHNOLOGY	• WITH CONFIDENCE PROVIDED BY ORBITAL IMAGERY, VEHICLE IS ALLOWED TO TRAVEL BEYOND ITS OBSERVED HORIZON
	• REQUIRES NEW TECHNOLOGY

MARS ROVER/SAMPLE RETURN MISSION

LOCAL NAVIGATION & HAZARD AVOIDANCE

CURRENT STATUS OF DEVELOPMENT EFFORTS

CARD

- CONCEPT DEMONSTRATED IN ARROYO SECO ADJACENT TO JPL IN ARMY-FUNDED EFFORT

- RTTV PROGRAM
  - ROBUST IMPLEMENTATION IN PROGRESS
  - TESTING WILL OCCUR AT EDWARDS AFB
  - ARMY PROGRAM (~$1M/YR)

SEMI-AUTONOMOUS ROVER

- JPL DDF EFFORT
  - CONCEPT DEMONSTRATION IN ARROYO SECO EXPECTED IN NEXT MONTH
  - 1-METER RESOLUTION ARROYO MAP COMPUTED FROM AERIAL PHOTOS
  - STEREO VISION, TERRAIN MATCHING & ROUTE PLANNING IMPLEMENTED
  - ROBUST IMPLEMENTATION WOULD REQUIRE SIGNIFICANT TECHNOLOGY DEVELOPMENT

MARS ROVER/SAMPLE RETURN MISSION

LOCAL NAVIGATION & HAZARD AVOIDANCE

TECHNOLOGY PROGRAM AREAS:

WORLD SENSING & PERCEPTION

PROVIDES UNDERSTANDING OF THE LOCAL TERRAIN ENVIRONMENT IN THE VICINITY OF THE ROVER

SURFACE PROPERTY DETERMINATION

NEEDED TO IDENTIFY UNSTABLE TERRAIN BEFORE THE ROVER TRAVERSES IT. INCLUDES DETERMINATION OF SURFACE LOAD-BEARING CAPACITU AND FRICTIONAL COEFFICIENTS

ROUTE & PATH PLANNING

ON-BOARD AUTOMATED PLANNING OF SAFE PATHS OVER THE NATURAL, UNSTRUCTURED TERRAIN OF THE MARTIAN SURFACE

EXECUTION MONITORING & REACTION

MONITORING OF VEHICLE STATUS DURING TERRAIN TRAVERSALS TO DETECT AND CORRECT MODERATE DEVIATIONS FROM PLANNED PATH; MONITORING TO DETECT AND RESPOND TO IMPENDING CATASTOPHIC EVENTS (E.G., VEHICLE ROLLOVER, SLIPPAGE ON A STEEP SLOPE) REQUIRING TIME-CRITICAL RESPONSE

VEHICLE CONTROL TECHNOLOGIES

TOOLS FOR MOBILITY CONTROL DESIGN, INTELLIGENT ACTUATORS, ACTIVE ARTICULATION TECHNOLOGY

MARS ROVER/SAMPLE RETURN MISSION

SAMPLE ACQUISITION SYSTEM

ROVER SAMPLE ACQUISITION FUNCTIONS

- SAMPLE & SAMPLE SITE SENSING
- IDENTIFICATION
- RETRIEVAL
- PREPARATION
- PACKAGING FOR ANALYSIS
- STORAGE
- REJECTION
- CONTAMINATION MANAGEMENT
- LABELLING

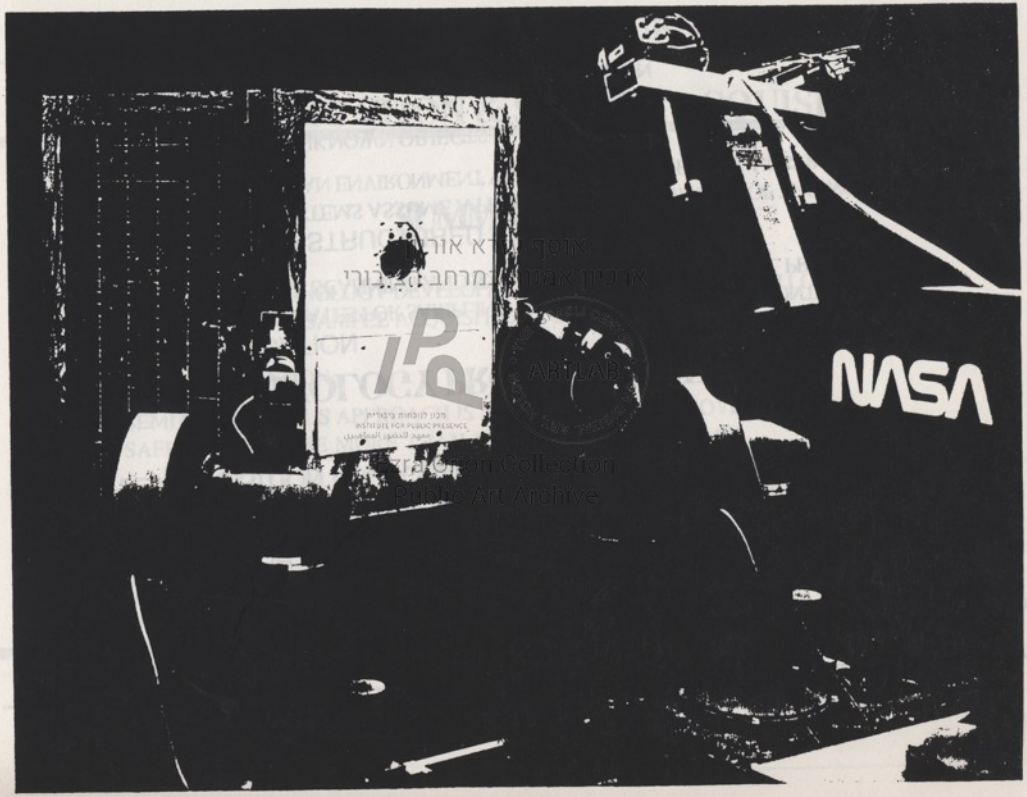
NASA

Mars Rover Sample Return

Rover Mobility & Surface Rendezvous Study

Program Review

Jet Propulsion Laboratory
Pasadena, CA

14 January 1988

Presentation Outline

Mars Terrain Design Environment — B. Clark

- Terrain Problem
- MTDE Design Tool

Mobility & Navigation Concepts — A. Spiessbach

- Methodology
- Concept Analysis & Synthesis Results
- Progress Summary & Plans

MTDE Inputs -- Terrain Components

MTDE

Topography

° **Slopes: Smooth, nominal, rough**

Surface Units

° **Physical characteristics**
- Weak (drift fines, flour-like clumps)
- Nominal (duricrust)
- Strong (adobe clods)
- Sand (cohesionless)
- Rock

° **Depth to competent surface (overburden)**

Features

° **Volcanoes, craters, scarps, channels, dunes, etc.**

Rocks

° **Shapes**
- Irregular, subrounded, round, faceted
- Smooth, pitted
- Competent, friable

° **Size**
- Boulders (blocks > 0.256 m)
- Cobbles (6.4-25.6 cm)
- Pebbles (2-64 mm)
- Sand (62.5 μm-2 mm)
- Silt (3.9-62.5 μm)
- Clay (<3.9 μm)

The MTDE Surface Can Include Multilevel Resolution

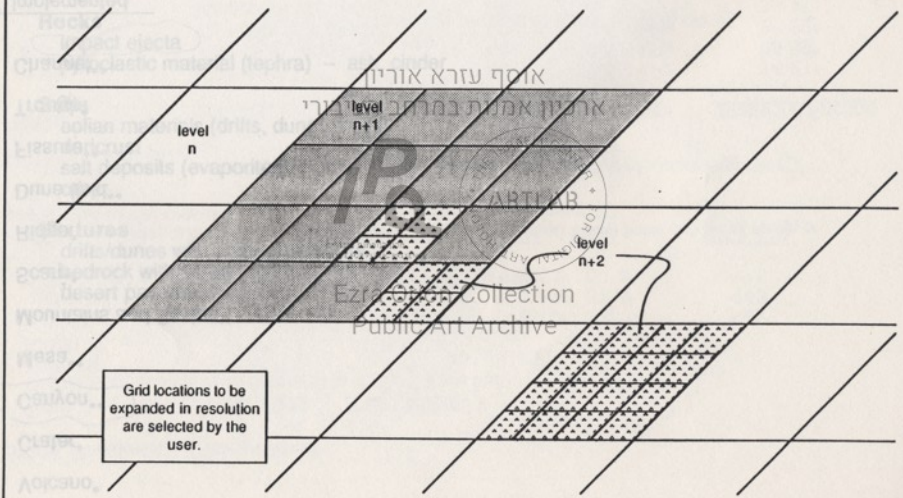

ROVER STATUS REVIEW OUTLINE

INTRODUCTION AND PREFACE — **TOM PENN**

STATUS OF ROVER TEAM FUNCTIONAL GROUPS

- **-SYSTEM CONTROL AND OPERATIONS**
- **-GLOBAL NAVIGATION**
- **-COMMUNICATIONS**
- **-COMPUTATION AND DATA HANDLING**

STATUS OF ROVER FUNCTIONAL GROUPS — **BRIAN MUIRHEAD**

- **-MOBILITY/MOBILITY CONTROL**
- **-THERMAL CONTROL**
- **-SAMPLE ACQUISITION TOOLS**
- **-POWER**

STATUS OF FUNCTIONAL GROUP — **ANDY MISHKIN**

- **-LOCAL NAVIGATION**
- **-SAMPLE ACQUISITION**
- **-JPL ROVER TESTBED**

Topographic Features

Features

Volcano*

Crater*

Canyon**

Mesa**

Mountains and Basins**

Scarp*

Ridge*

Dune field**

Fissure**

Trough*

Channel**

* Implemented
** Planned

Forces Shaping Martian Surface

MTDE

Geophysical Agents	**Tectonics, Faulting**
	Mass wasting
	Meteoroid Bombardment (impact cratering, gardening)
Wind	**Eolian deposition**
	Eolian deflation
	Physical weathering (erosion)
Volcanism	**Lava resurfacing**
	Surface expressions of intrusive s
	Geothermal perturbations (permafrost melting)
	Gases (for chemical weathering)
Water	**Fluvial transport**
	Chemical weathering
	Ice mechanics (glacial, periglacial)

The 6 Cases

MTDE

1. **Volcanic**
   cone; caldera
   lavas and pyroclastics: flood (smooth), aa, pahoehoe, ash
   wrinkle ridge
   fissure

2. **Eolian**
   sand sheet (flat); sandy slopes
   dune field (with slip faces)
   duricrust, drifts (surface units)

3. **Impact**
   craters
   ejecta blankets (rock fields)
   rocks with drifts

4. **Aqueous mediated**
   channels (troughs)
   boulder field
   ground sapping

5. **Tectonic**
   fault scarps and graben
   landslides
   scree over bedrock

6. **Preliminary Surface Model**
   random combination of slopes, soil units, rock models

Mobility & Navigation Concepts

Andy Spiessbach

MARTIN MARIETTA

Surface Characteristics

Features

Bedrock
lava -- aa, pahoehoe, flood (smooth)

Rocks
impact ejecta
pyroclastic material (tephra) -- ash, cinder

Soils
eolian materials (drifts, dunes, beds)
duricrust
salt deposits (evaporites)
other

Mixtures
drifts/dunes with embedded rocks
bedrock with scree
desert pavement

Innovation & Analysis Cycles

Concept Development

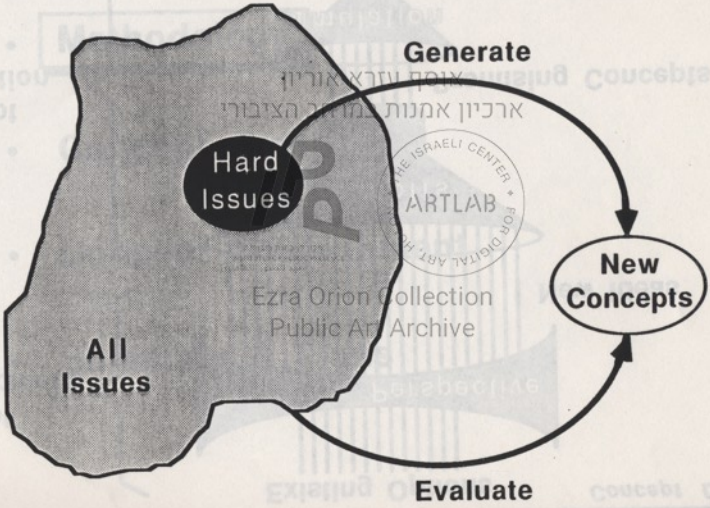

MARTIN MARIETTA

Rover Issues

Concept Evaluation

Risk

Mission

- Safety
- Reliability

Program

- Technical Risk
- Program Cost

Performance

Accessible Sites

- Traversibility
- Speed/Range
- Navigation

Sampling Capability

- Payload Mass
- Payload Configuration
- Stability

Cost

Mass

- Power
- Environmental Control
- Computation

Volume

- Redundant Systems
- Rugged Structures

MARTIN MARIETTA

Outline

- Methodology
- Concept Evaluation
- Concept Development
- Summary & Plans

Design Process

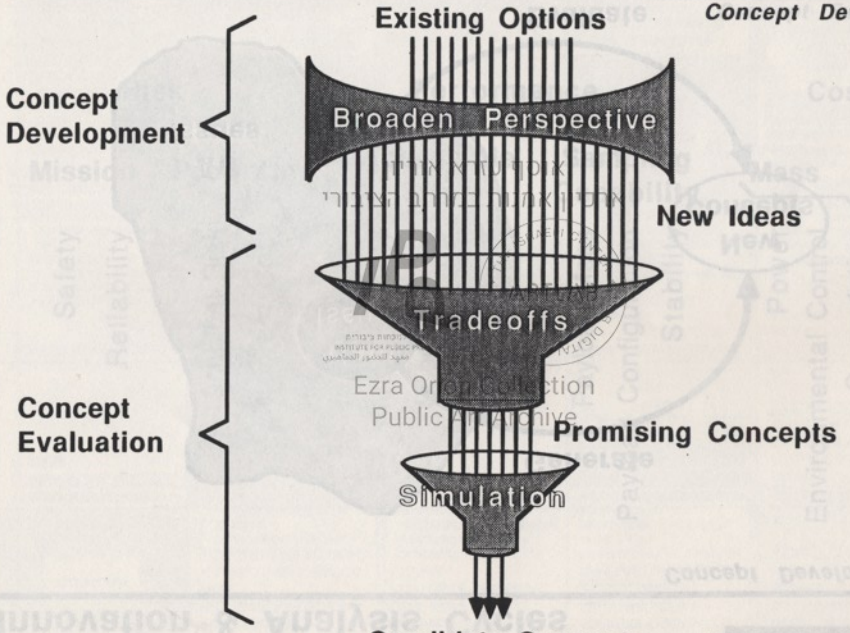

Fundamental Tradeoffs

Concept Evaluation

Issue	Option	Design Considerations
Robustness Survivability Reliability	• Rugged design ("Brawn") - Fixed performance insensitive to conditions - Reliability via simple system	• Minimum complexity, cost, technical risk • Results in largest rover design • Rigid performance capabilities - If doesn't work, can't do anything about it
	• Sophisticated design ("Brain") - Flexibility to adapt performance to conditions	• Increased complexity, cost, technical risk - Additional degrees of freedom - Active articulation - Additional sensory & processing
Level of Autonomy Control	• Teleoperated from Earth - Human makes all decisions	• Mission success (communication delay) - Operating vehicle blind for several minutes/10-100 meters risky traverse
	• Supervised Autonomy - Machine makes some decisions	• Increased complexity, cost, technical risk • Mission success (machine trustworthiness) - Decisions machine must implement unchecked could cause fatal errors • Degree of delegation unclear

MRSR ROVER TEAM OBJECTIVES

- DEFINE 3-5 CANDIDATE ROVER SYSTEM CONCEPTS (MEET REQUIREMENTS OF SWG MINIMUM, MODERATE, MAXIMUM ROVER SCENARIOS)
- DEFINE TECHNOLOGIES REQUIRED TO BUILD EACH ROVER TYPE
- DEFINE TRADE STUDIES REQUIRED TO PROCEED WITH ROVER SYSTEM DESIGN AND MISSION DESIGN
- IDENTIFY CRITICAL ROVER AND MISSION REQUIREMENTS DRIVERS
- INTEGRATE CONCEPTS FROM ROVER CONTRACTORS FMC AND MARTIN MARIETTA IN THE AREAS OF MOBILITY AND NAVIGATION/ RENDEZVOUS
- CONSIDER ALL PLAUSIBLE APPROACHES TO THE PROBLEMS: E.G. WHEELS, LEGS, TRACKS, ETC FOR MOBILITY; TELEOPERATION, CARD, SEMI-AUTONOMOUS FOR LOCAL NAVIGATION.

Mobililty Trade Space (Top Level)

Concept Evaluation

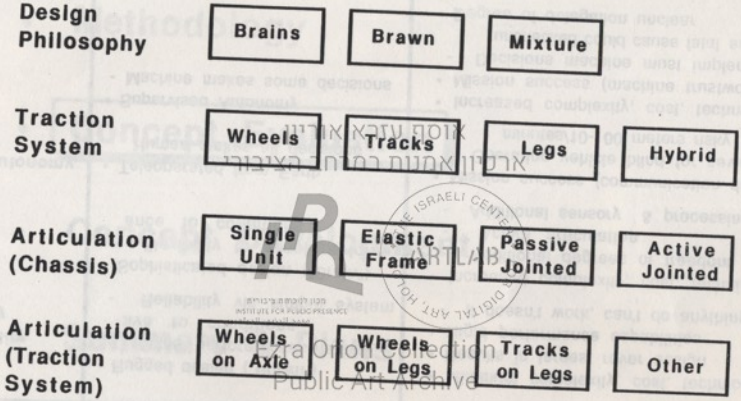

MARTIN MARIETTA

Rover Mobility Design Requirements

SOW

- safely traverse 1 km/day for 3 years
- ascend or descend 60 % hard suface grades
- ascend or descend 35 % loose sand grades
- climb vertical steps at least 1 m high
- cross crevasses at least 1 m wide
- rover and payload will experience accelerations less than 25 g's peak or 10 g's avg. over 30 msec

MARTIN MARIETTA

Rigid - 4 x 4 Minimum Envelope

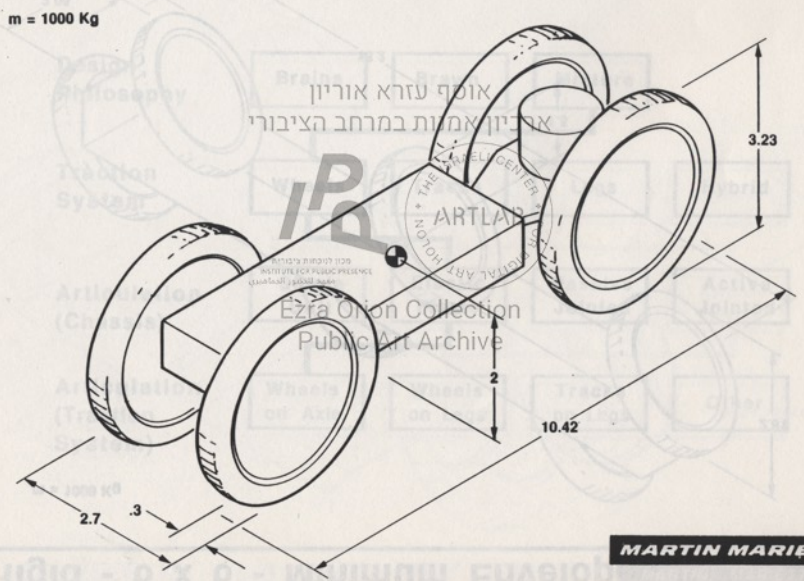

MARTIN MARIETTA

Passive Frame Articulation

Concept Evaluation

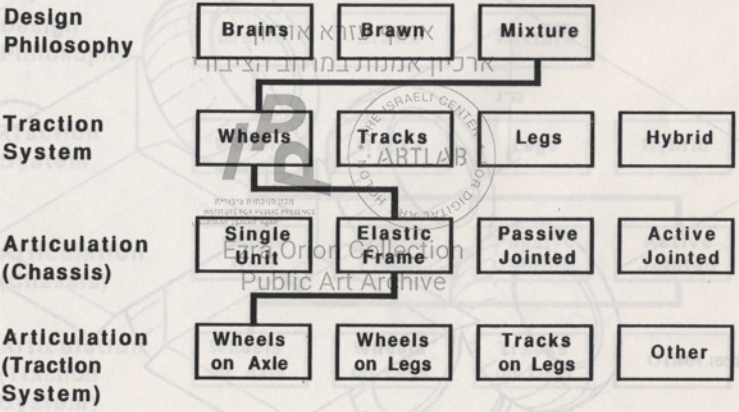

Active Frame Articulation

Concept Evaluation

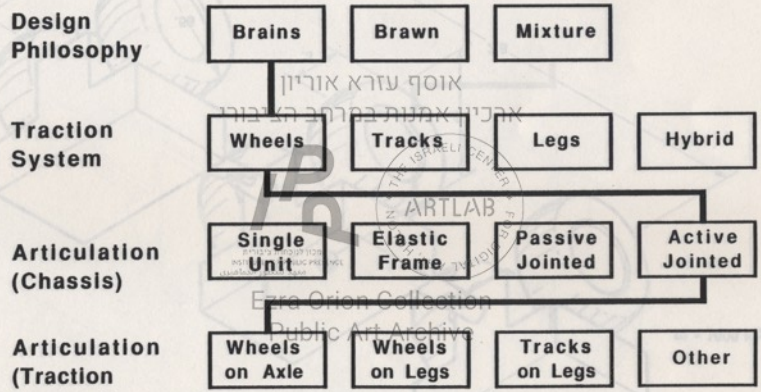

4x4 Tracked

Concept Evaluation

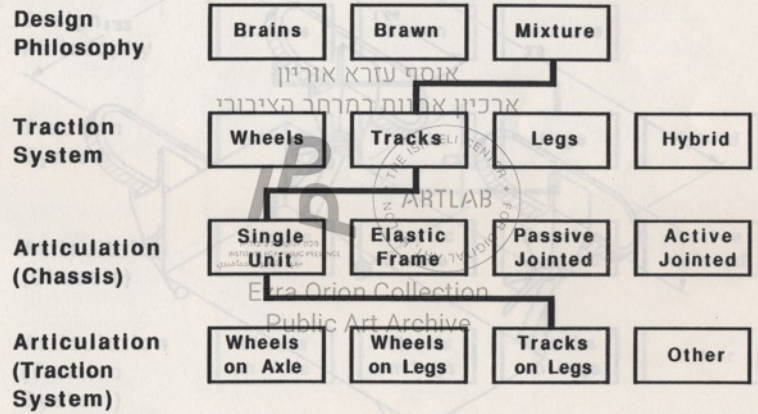

Rigid - 4 x 4 Minimum Envelope

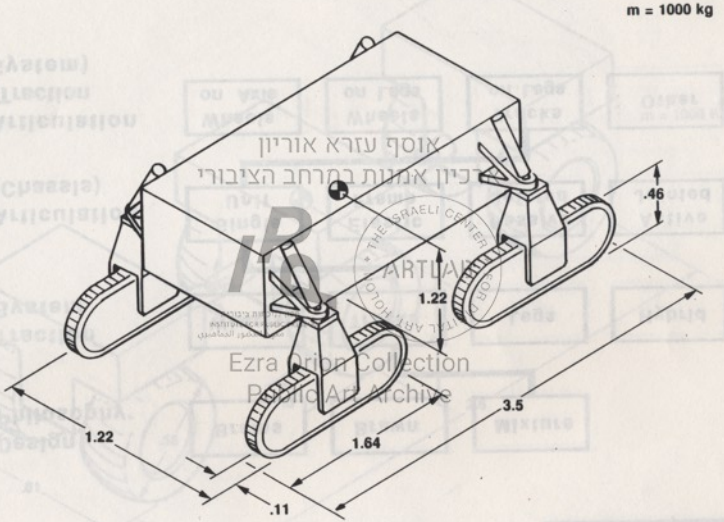

MARTIN MARIETTA

Rover Mobililty Trade Space

Design Philosophy	Brains	Brawn	Mixture	
Traction System	Wheels	Tracks	Legs	Hybrid
Chassis Articulation	Single Unit	Elastic Frame	Passive Jointed	Active Jointed
Traction System Articulation	Wheels on Axle	Wheels on Legs	Tracks on Legs	Other
Ground Contact System	Wire Mesh Tire	Cone Wheel	Inflatable Bags	Disk Footpad
Power System	Electric Motor	Other	Geared	Direct Drive
Stowage Mechanism	Fetal Pos. (Active)	Spring Load (Passive)	Additional Mechanisms	Deflate/ Inflate
Safety Features	Roll Bar	Retractable Systems	Environ. Protection	Fenders, Dust Covers
Autonomous Functions	Multiple DOF Coordination	Compliant Control	Foot/Wheel Placement	Reflex Arcs

Wheel Options

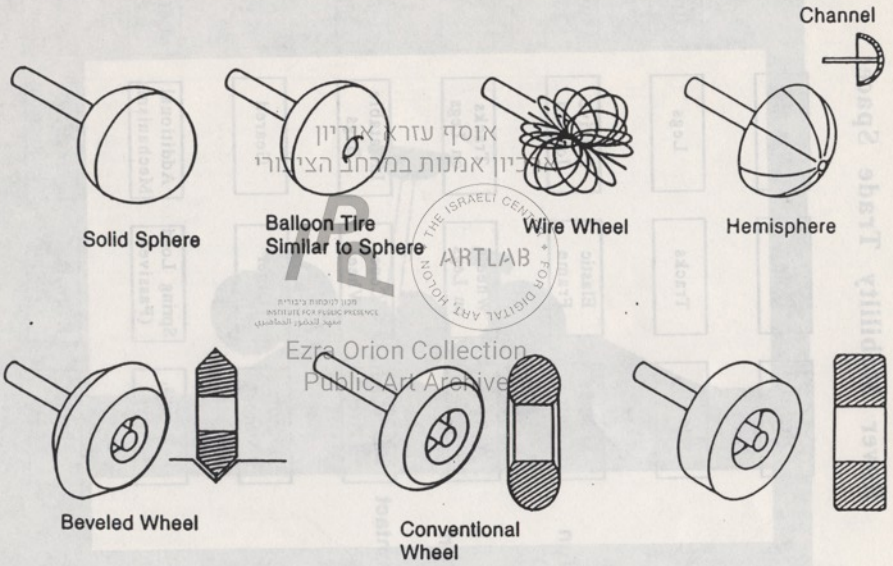

Track Options

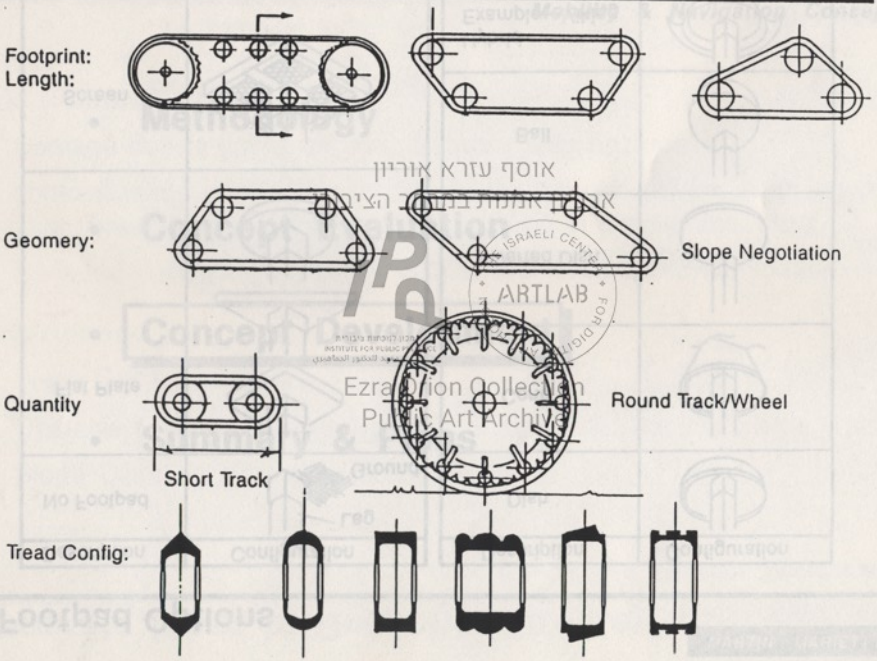

ROVER TEAM DISCIPLINES

-SYSTEMS ENGINEERING

-MOBILITY

-LOCAL NAVIGATION

-SAMPLE ACQUISITION

-THERMAL CONTROL

-POWER SYSTEMS

-COMMUNICATIONS

-COMPUTATION/DATA HANDLING

-SYSTEM CONTROL AND OPERATIONS

-GLOBAL NAVIGATION

-GUIDANCE AND CONTROL

Outline

- **Methodology**
- **Concept Evaluation**
- **Concept Development**
- **Summary & Plans**

Generate Ideas in Response to "Key" Issues

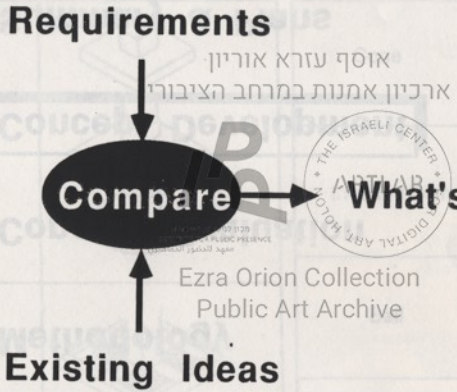

The "Hard" Mobility Issues

Concept Development

Risk (Failure)

- Damage due to tiping, slipping, bumping into hazards
- Immobilization due to tipover, hang-up, nose-in failure, wedging running gear, breaking through lava crust, sinking in porous soil, etc.,
- Reduced capability due to faults and environment contamination

Performance

- Weak Soil Crossing
- Obstacle Crossing (Crevasses, Channels, Lava, Boulder Fields, Talus)
- Slope Climbing (Energy Efficiency)

Alternative Approaches - Entrapment

Concept Development

Approach	Example	Drawbacks
Test Ground Before Committing Vehicle - Vehicle stable while force reflection, haptic touch, etc. assess danger	• 6-Legged Walker with Statically Stable Gait • Vehicle with Hazard/ Soil Strength feelers	• Reduced Speed • Added Complexity
Emergency Mechanisms	• Deployable Recovery Structures (air bags, etc) • Jack, Winch, etc.	• Mass/Volume Penalties • Mechanical Complexity • Perception Required
Breakaway Mobility Mechanisms	• Exploding bolt at leg or frame joint	• Need Redundant Mobility System to Afford Loss
Reconfigurable Mobility Mechanisms	• Umbrella mechanism to retract disk footpad to allow leg removal • Quick Disconnect Pads	• Sensors, Actuators and Algorithms • Associated Computation & Power (Mass, Volume)
Active Articulation	• Contort frame/leg to free vehicle	• Mechanical Complexity • Associated Computation & Power (Mass, Volume)

Alternative Approaches - Weak Soil

Concept Development

Approach	Example	Drawbacks
Vehicle with Large Footprint - Reduced Ground Pressure	• Large tracks (e.g. single track vehicle) • Wide/many wheels (Lunokhod) • Large walker footpads	• Extra Mass • Reduced Stowability • Steering Issues • Footpad Interference
Adaptable Vehicle - more footprint available as needed	• Extra wheels or track in contact as sink deeper • Hemispherical Wheels	• Extra Mass/Volume • Deployment Mechanisms (Failures)
Augment Basic Mobility by Mechanical Aids	• Deployable Traction Mats • Pull with Winch • Switch to Large Footpad	• Extra Mass/Volume • May Require Dextrous Arm
Change Environment	• Construct "Bridge" • Dig Down to Firm Ground	• Extra Mass/Volume • Need Dextrous Arm
Air Vehicle - fly over obstacle	• Balloon • Dirigible • Airplane	• Low Payload Mass • Landing Risks

Taxonomy Examples

Concept Development

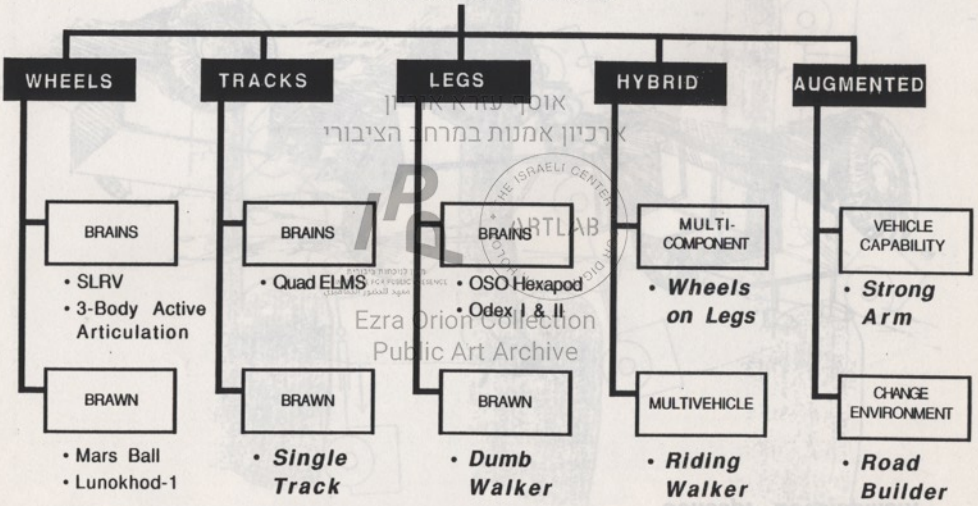

MARTIN : MARIETTA

Active Frame Articulation

Concept Development

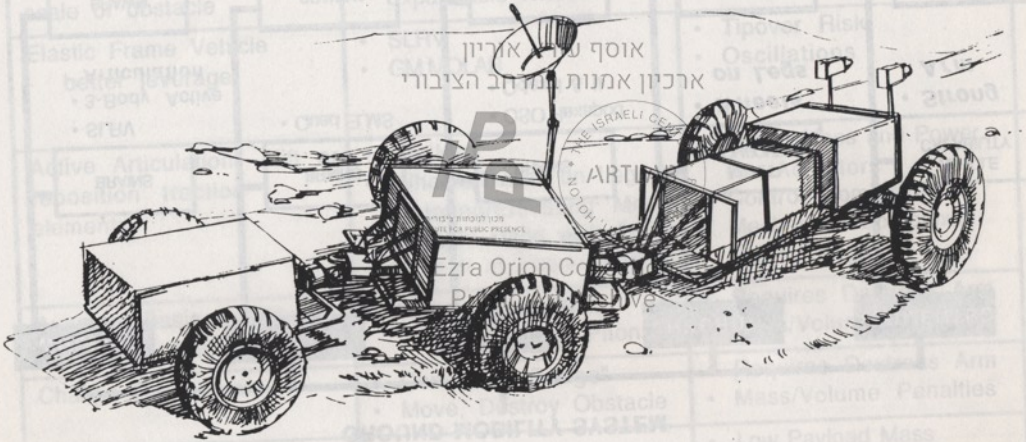

MARTIN MARIETTA

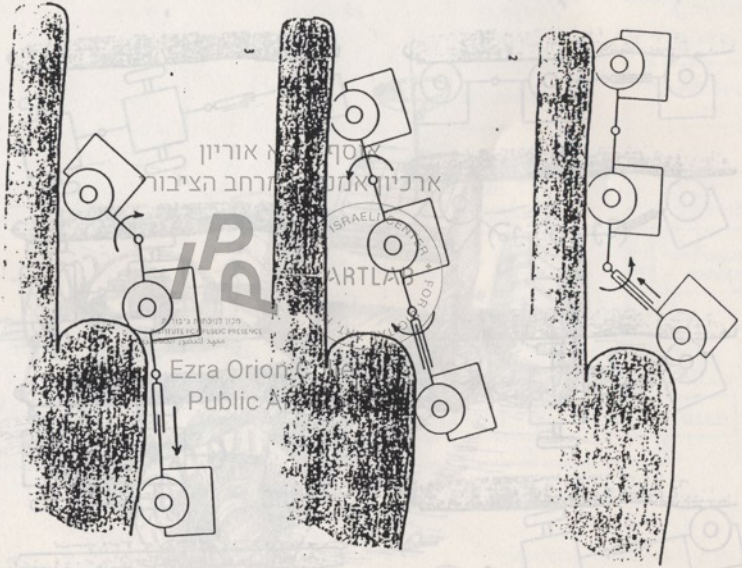

Mars Ball

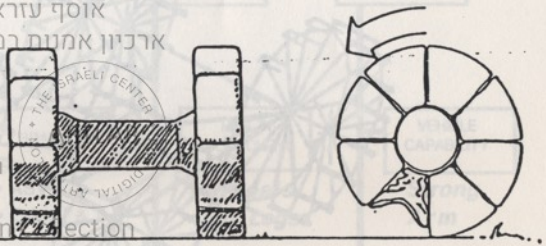

MARTIN MARIETTA

2-Body Active Articulation

Concept Development

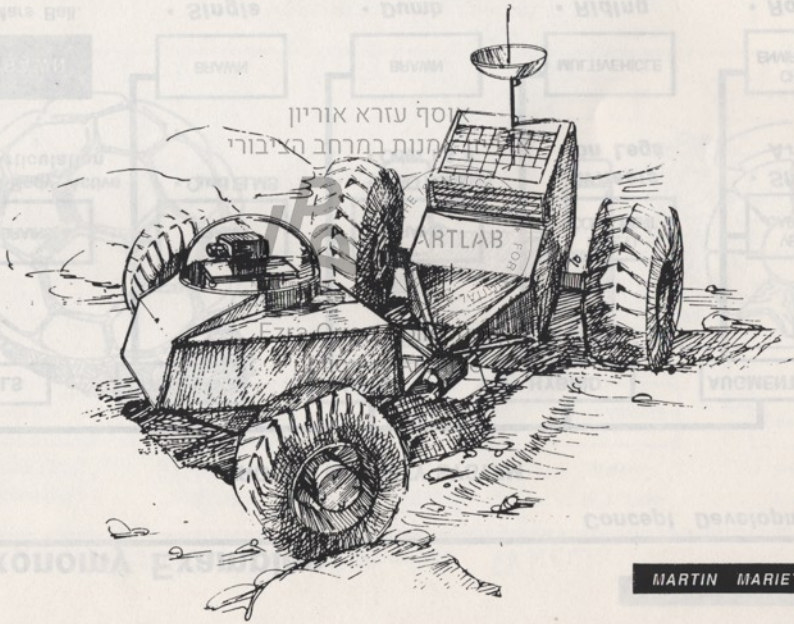

MARTIN MARIETTA

ROVER TEAM ACTIVITIES

- ROVER TEAM IS SUPPORTING ORBITER TEAM IN AREAS OF SYSTEMS ENGINEERING, GLOBAL NAVIGATION, GUIDANCE AND CONTROL, AND COMMUNICATIONS.

- ROVER TRADE SPACE DEFINITION HAS GROWN BEYOND A MANAGEABLE SET OF OPTIONS, "TAXONOMY" FORMAT HAS BEEN ADOPTED TO IDENTIFY TECHNOLOGY REQUIREMENTS. TRADE SPACE FORMAT MAY BECOME USEFUL AS SWG ROVER SCENARIOS ARE FACTORED IN TO NARROW OPTIONS.

- ROVER SYSTEMS OPTIONS DEFINITION TO BEGIN IN FEBRUARY (IN SYNCH WITH SWG DEFINITION OF THREE ROVER CAPABILITY CLASSES)

- DEFINITION OF TECHNOLOGY REQUIREMENTS FOR PATHFINDER PLANETARY ROVER FUNDING

- ROVER TEAM IS SUPPORTING CONTINUING ACTIVITIES WHICH WILL BE DESCRIBED BY THE TWO SPEAKERS TO FOLLOW.

Single Track Steering

Concept Development

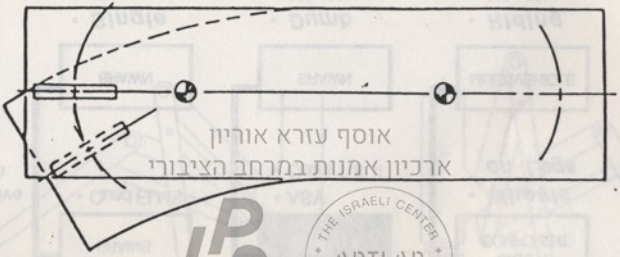

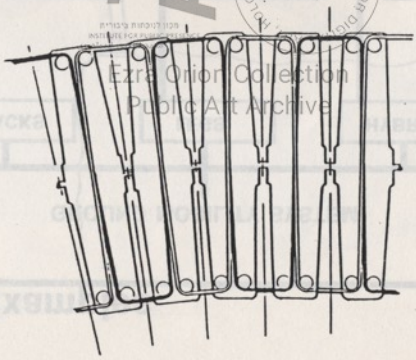

MARTIN MARIETTA

Taxonomy Examples

Concept Development

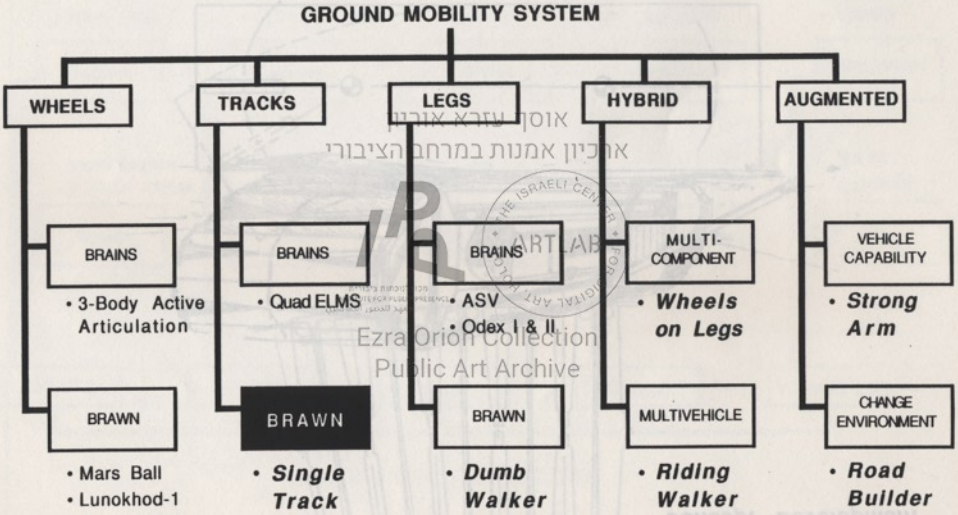

MARTIN MARIETTA

Taxonomy Examples

Concept Development

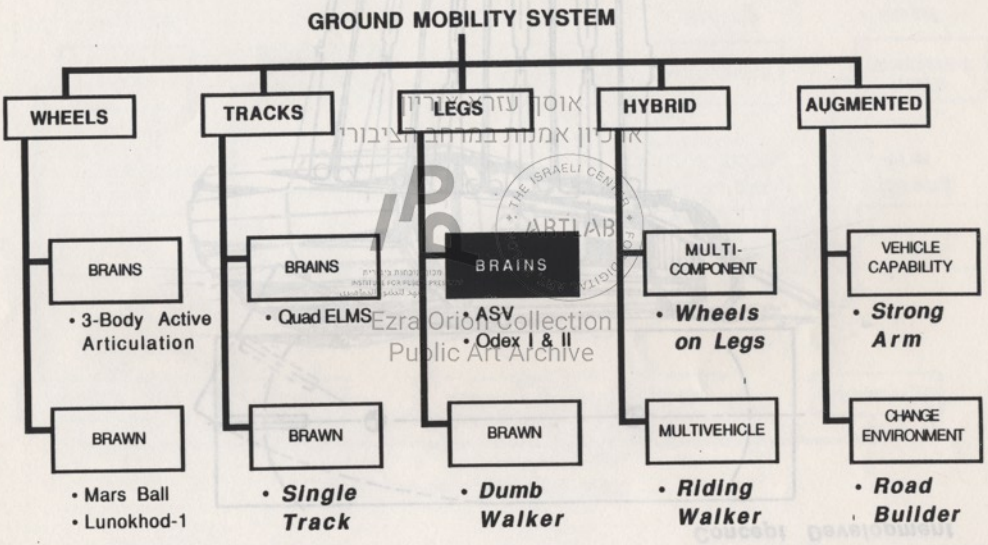

MARTIN MARIETTA

MARS ROVER CONCEPT: DEPLOYED CONFIGURATION

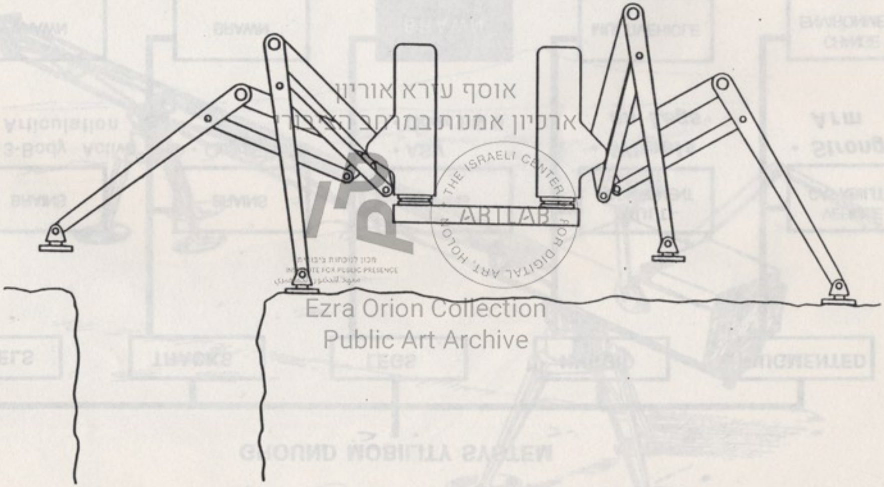

Odetics

Walking Truss

Concept Development

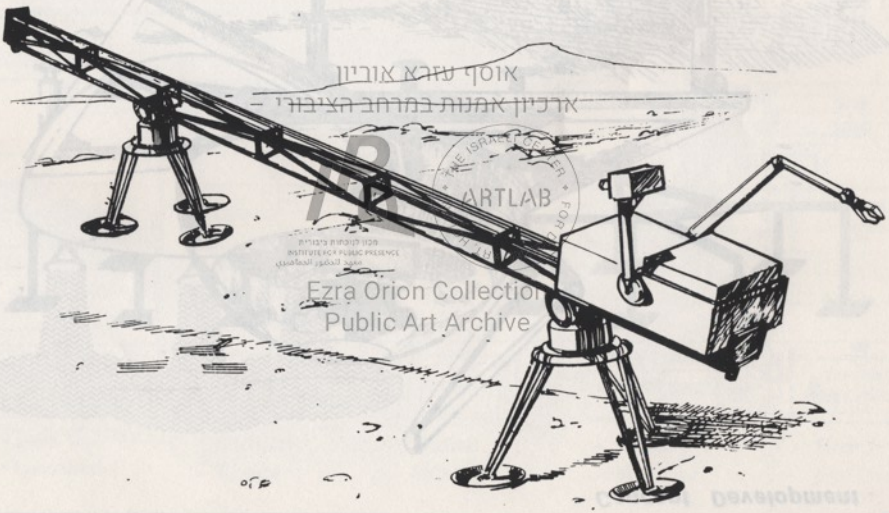

MARTIN MARIETTA

"Dumb" Walker

Concept Development

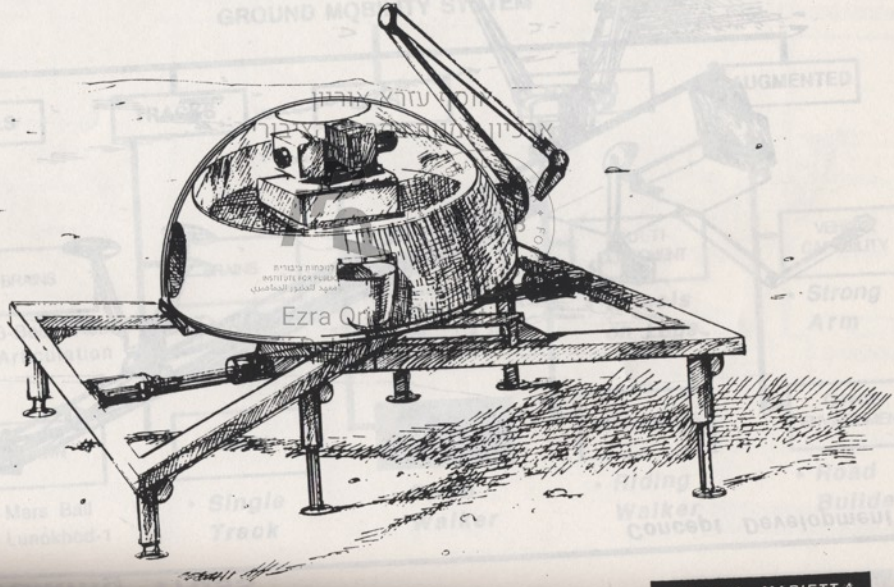

MARTIN MARIETTA

Dumb Walker Deployment

Concept Development

MARTIN MARIETTA

Marine Robot RM3

Concept Development

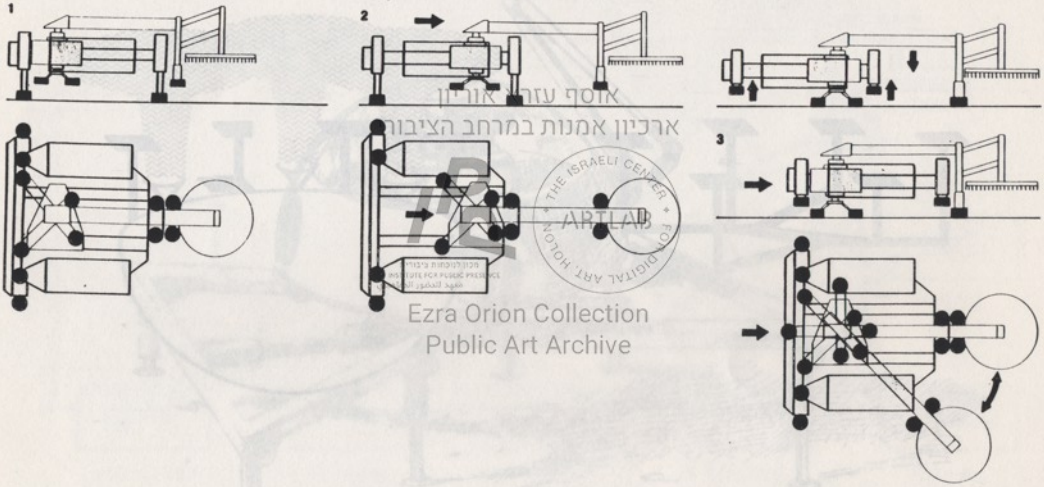

Walking Speed = 500 ft/hr
(0.15 km/hr)

Built by Normed Shipyards (France)

MARTIN MARIETTA

Taxonomy Examples

Concept Development

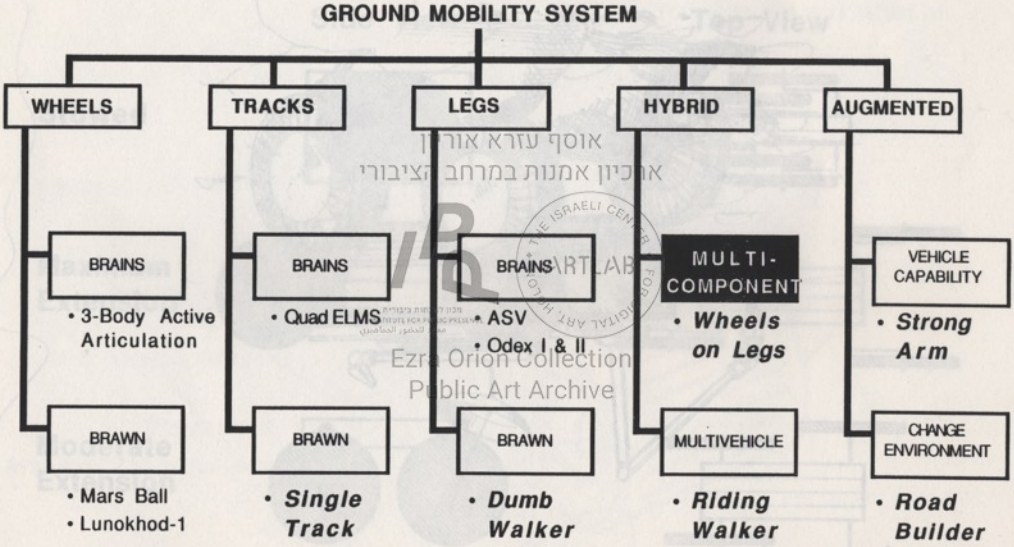

MARTIN MARIETTA

Big Wheels with Independent Elevation

Concept Development

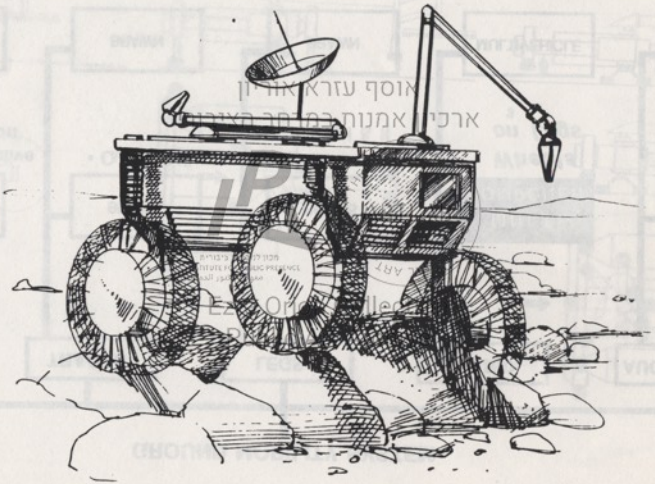

MARTIN MARIETTA

MRSR MOBILITY SUBSYSTEM TECHNOLOGY TAXONOMY

Brian K. Muirhead 12/7/87

SYSTEM REQ./CONST

MASS (kg)
- 300, 1000, 1500

POWER (watts)
- 300, 500, 1000

TERRAIN
- 1, 1.5, 2 m obstacle
- 0, 50, 100 %rough
- 0, 25, 45 deg slope

TRAVERSE (km)
- 100, 500, 1000

STOWED ENVEL.
- 2, 3, 4 m^3

RELIABILITY
- 1 fault tolerant
- 2 fault tolerant

THERMAL ENVIR.
- 100 – 300 K

LIFETIME
- 1, 2, 5 yrs

ADAPTIVE (Multi – methods to do things)
- Highly
- None

PLANETARY QUARANTINE
- No requirement
- No organics

MOBILITY FUNCTIONS

LOCOMOTION
- Peak speed (.1, 1, 10 km/hr)
- Obstacle climb/traverse
- Turn radius (0, 1, 2, 3 m)
- Stop/Park

PAYLOAD ACCOMODATION
- Sampling canister
- In situ instruments (TBD)

ENGINEERING S/S ACCOM.
- Manipulator reach (1r, 2r) (r = radius of wheels)
- RF transceiver (.5 m)
- Power source (RTG)
- Camera mount (Fixed, deploy)
- Drill (Body, arm mounted)

HAZARD ACCOMODATION
- Emergency stop
- Limited corrective action
- Extensive corrective action
- Self – righting
- Hazard Independence
- Repair

SENSING FUNCTIONS
- Traction
- Proximity
- Orientation
- Distance
- Weight distribution
- Inertial reference

TELEMETRY
- < 100 kbit/s

COMPUTATION
- Speed (.2, 1, 10 mips)
- Memory (64, 256, 1000 kbit)

AUTONOMY (local control)
- High
- Low

FAULT TOLERANCE
- Internal Redundancy
- Ruggedized
- Maintenance

MOBILITY OPTIONS

LOCOMOTION MODE
- Wheels (large, small)
- Legs
- Hybrid
- Other (balloon, plane, etc.)

CHASSIS
- Single/Double – axle
- Single/Multi – axle
- Multi/Single – axle
- Multi/Multi – axle

SUSPENSION
- Passive
- Active
- Semi – active

STEERING
- Ackerman
- Wagon
- Scuff
- Swivel
- Chassis

POSITION CONTROL
- Open loop
- Closed loop
- Closed loop, fine

SENSOR CONFIG.
- Body mounted, remote
- Fixed, deployable

HAZARD DESIGN
- Bullet proof
- Selective protection
- Spec. purpose recovery sys

SCIENCE PACKAGE
- Integrated
- Independent/Deployable

SERVICING
- Autonomous
- Telerobotic

TECHNOLOGY OPTIONS

DRIVE/TRANSMISSION SYS
- Direct drive motors
- Geared motors
- Fluid drives
- Variable speed/torque
- Thermodynamic eng.
- Hybrids

ACTUATORS
- Direct drive motors
- Geared motors
- Ball screw
- Solenoid
- Fluid actuator

ELASTIC COMPONENTS
- Springs
- Flexures
- Adaptive/intell. structures
- High damping structures

DEPLOYABLE SYSTEMS
- Wheels
- Booms

SIMULATION/MODELING
- 3D vehicle/ground model
- Real time simulation
- Many DOF

SENSORS/ENCODERS
- Inclinometer
- Gyro (Mech, optical)
- Tachometer
- Magnetic compass
- Optical, magnetic encoder
- Celestial sensor

CONTAMINATION CONTROL
- Seals, Coatings, Boots

CONTROL S/W
- Algorithms
- A/I

TECH DEVELOP. REQ / JUSTIFICATION/COMMENT

TECH. DEVELOP. REQ	JUSTIFICATION/COMMENT
Variable speed/torque motor/transmission sys.	Optimize performance for obstacle traverse and power
Fluid drives	Hydraulic primary drives w/ variable speed/torque
Thermodynamic eng.	Auxilliary mech. power unit or hybrid drive element. Enables non – electric recovery modes and alter speed/torque capability
Fluid actuator	Stored energy, low temp, high rel., dust proof, low power for active suspension or self – righting
Adaptive/intell. structures	Sense deformations and take corrective action. Figure knowledge and control of wheels, booms and suspension elements
High damping active and passive methods	In – situ changes in damping
Deployable wheels	10/1 packing factor, obstacle tolerant
3D vehicle/ground model	Full 3D formulation for any terrain at any angle of attack
Rotory/prismatic seals	Low drag, abrasion resistent, non – magnetic, low temp. rotory and sliding seals
Rules based controls	Fast, adaptive hazard

Big Wheels on Legs

Concept Development

Side View **Top View**

Stowed

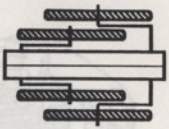

Maximum Extension

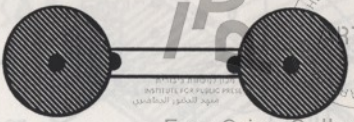

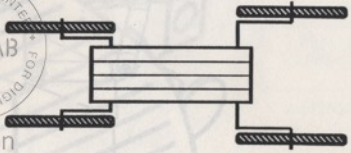

Moderate Extension

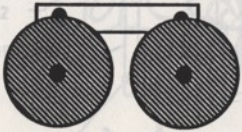

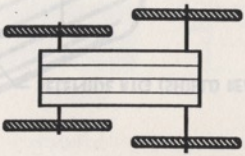

MARTIN MARIETTA

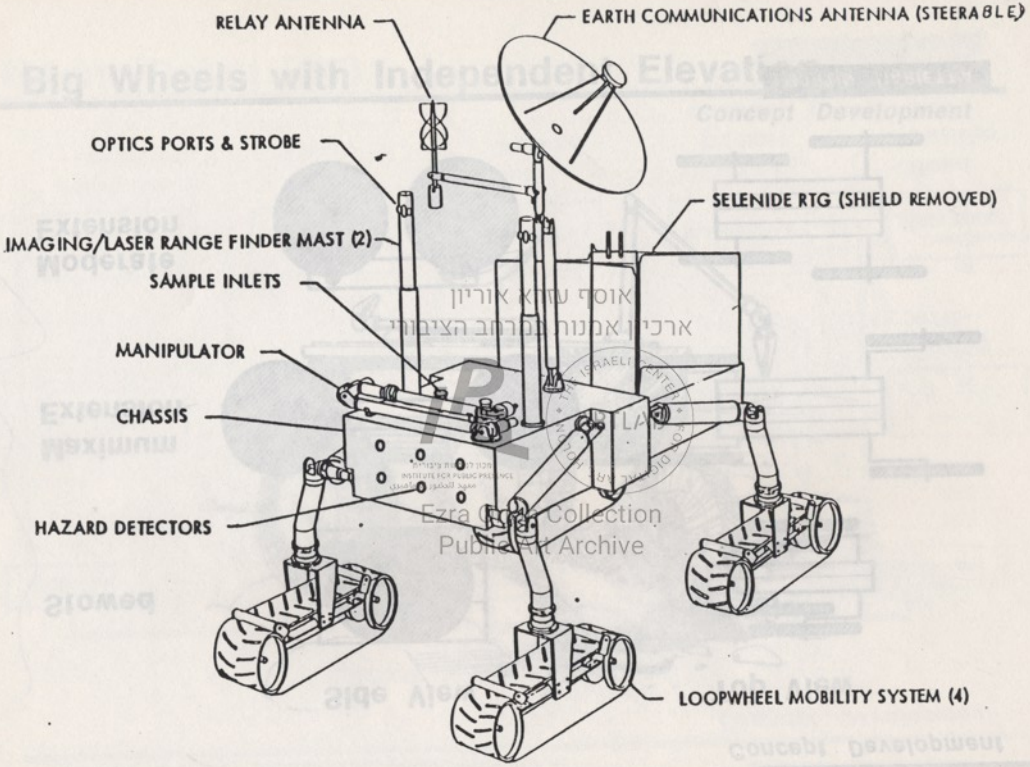

MARS ROVER
JPL 1977

Incremental Road Builder

Concept Development

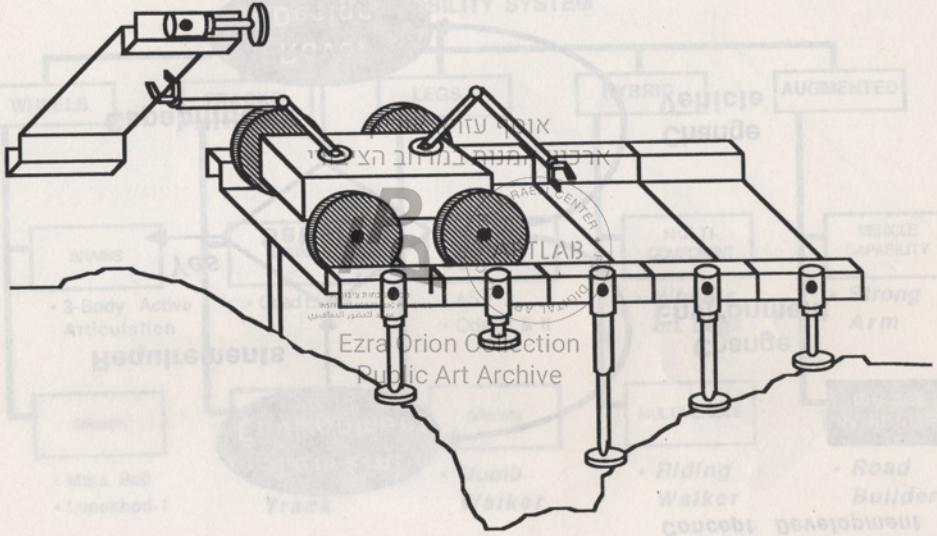

MARTIN MARIETTA

Two Approaches to Meeting Requirements

Concept Development

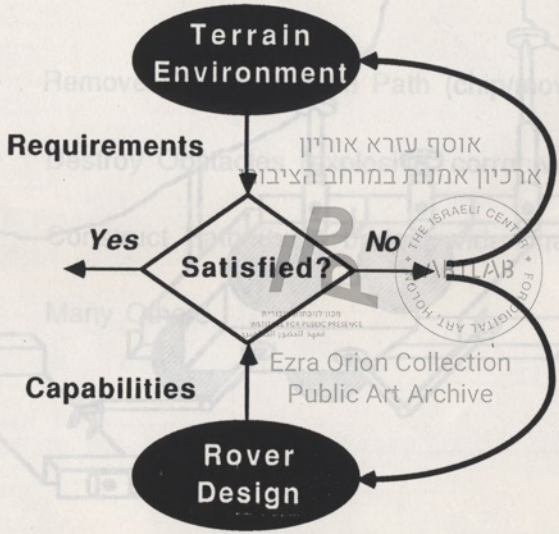

MARTIN MARIETTA

Change Circumstances - Examples

Concept Development

- Remove Obstacles from Path (chip/move rocks, fill holes)
- Destroy Obstacles (explosive, corrosive)
- Construct Path (build bridge, widen narrow corridor)
- Many Others

Surface Navigation - Minimum Configuration

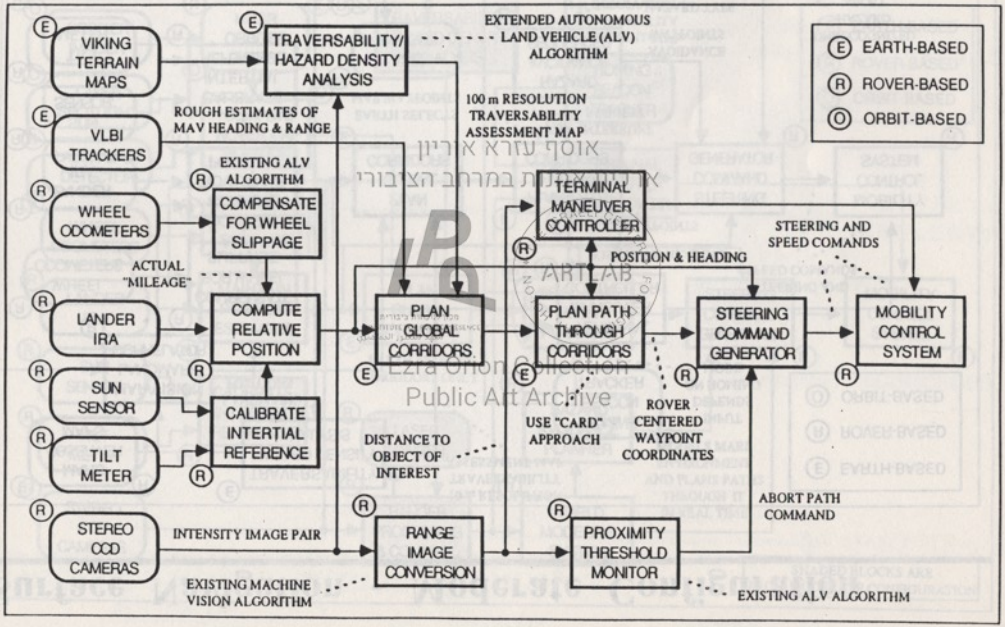

Example Rover Design Concepts

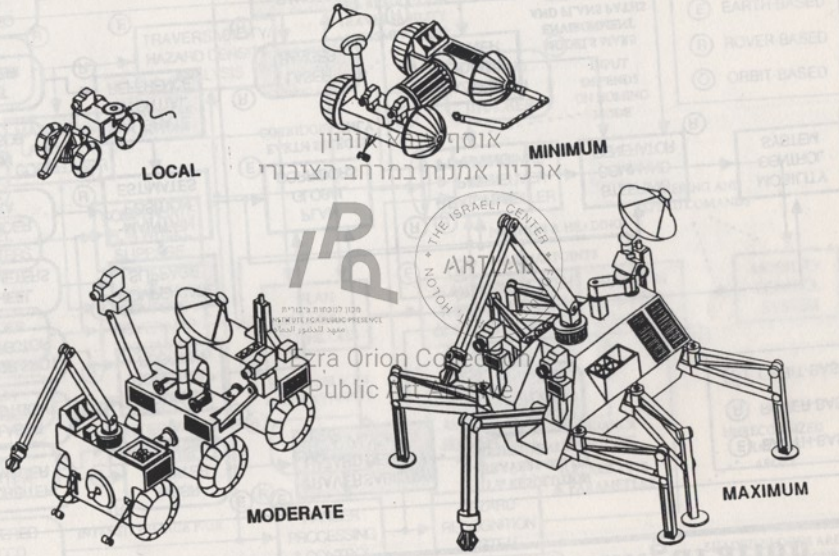

Two Approaches to Meeting Requirements

Concept Development

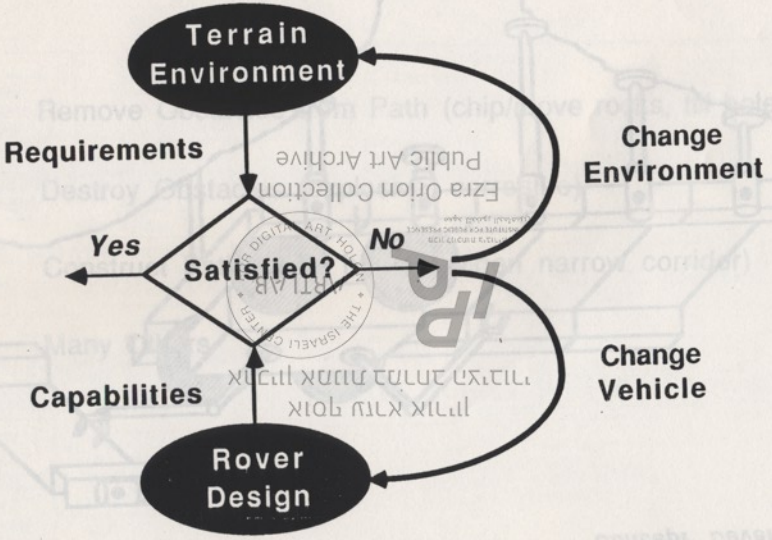

Incremental Road Builder

Concept Development

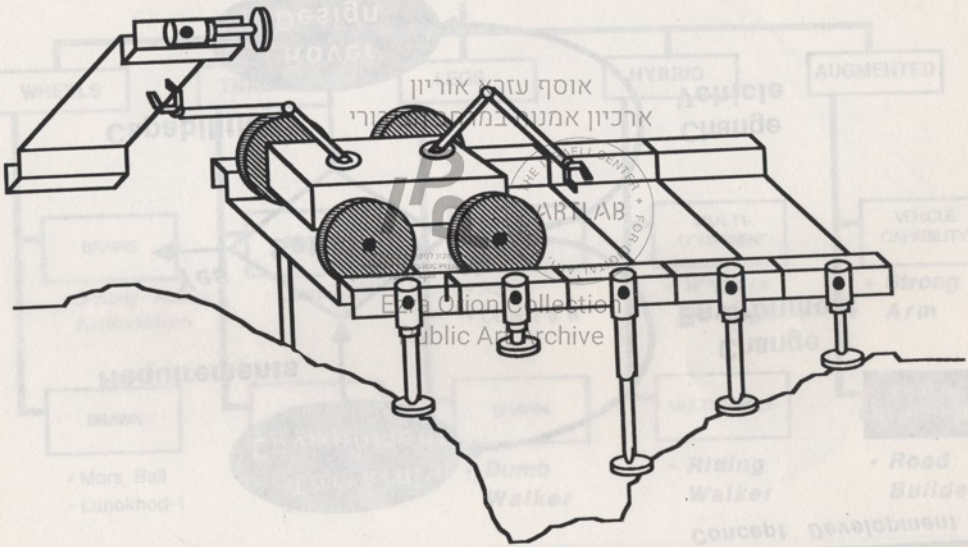

MARTIN MARIETTA

Rover Design Envelope

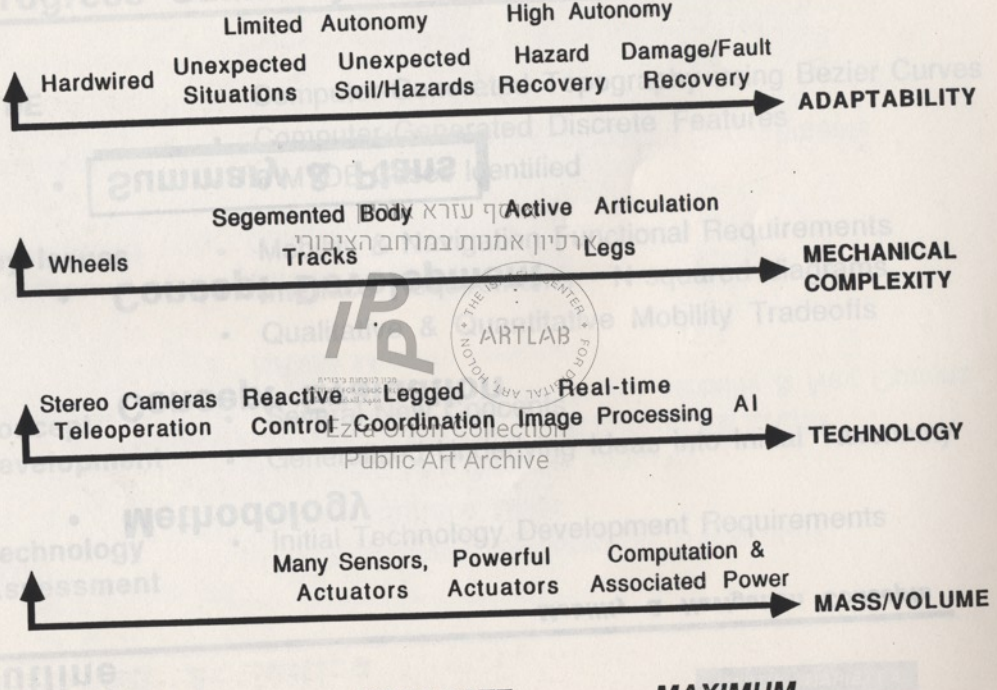

JPL

ORBITER STATUS

JAMES E. RANDOLPH

MRSR STUDY STATUS PRESENTATION

14 JANUARY 1988

Conclusions

1. **Not all Mobility Capability Has to Be "Built-in"**

2. **Terrain is not Immutable - One Can Change Environment (to a limited degree)**

3. **Lander Structures Can Be Exploited (whole or in part) for Rover**

4. **Walking Vehicles Are Not Necessarily Complex**

JPL

ORBITER ASSUMPTIONS

- **TRANFER CAPABILITIES FROM OTHER SYSTEMS TO " MOTHER" ORBITER**
- **LANDSAT CLASS OBSERVATIONAL CAPABILITY**
  LANDER SITE SERVEILLANCE, ROVER TRAVERSE SUPPORT
- **HIGH PRECISION ORBIT CONTROL**
  ENTRY VEHICLE REFERENCE
  ROVER REFERENCE
  REFERENCE FOR OBSERVATIONAL DATA
- **RELAY COMMUNICATIONS**
  ROVER
  ENTRY VEHICLE

JPL

MRSR LAUNCH CONFIGURATIONS

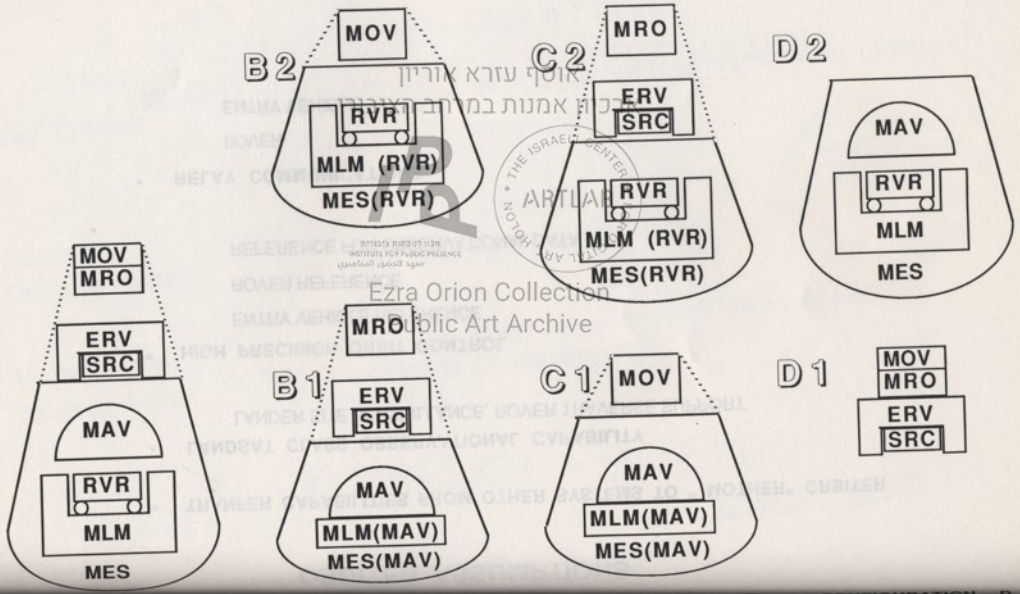

JPL

ORBITER SYSTEM OPTIONS

FUNCTIONS:

a) INTERPLANETARY AND ENCOUNTER GC & N

b) SITE SURVEILLANCE

c) SUPPORT FOR ROVER

d) RELAY COMMUNICATIONS

e) SUPPORT FOR ENTRY VEHICLE

f) RENDEZVOUS

g) SUPPORT FOR MAV

h) SUPPORT FOR ERV

OPTIONS	FUNCTIONS							
	a	b	c	d	e	f	g	h
A	X	X	X	X	X	X	X	X
B2,C1	X	X	X	X	X			
B1,C2	X			X	X	X	X	X

JER
1/14/88

JPL

ORBIT TYPES

- ELLIPTICAL, LOW PERIAPSIS, ROVER & SUN SYNCHRONOUS

  250 x 12600 km (1/3 sol), i = 116.6 degrees

  IMAGING AND RELAY COMMUNICATIONS

- CIRCULAR, RENDEZVOUS ALTITUDE

  500 km

  RENDEZVOUS AND EARTH RETURN

LANDING SITE IMAGING OBSERVATIONS AT PERIAPSIS

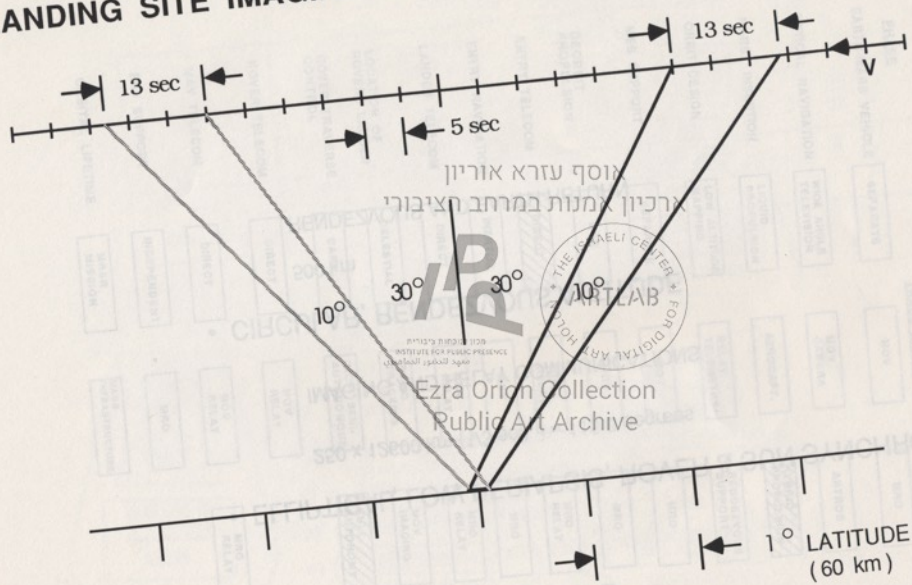

JER
1/14/88

JPL

ORBITER OBSERVATIONAL CONTROL CONCEPTS

- **10 X 10 km LANDING SITE AT 0.5 meter / pixel**

  1.5 km WIDTH X 10 km SCAN EACH DAY

  7 SCANS IN 10 DAYS

- **ORBIT POSITIONAL CONTROL**

  ~ 1 km (3 σ) DOWN RANGE

  GEODETIC ERRORS ADDITIONAL

- **IMAGE CORRELATION TRACKING CONTROL**

  ~ 0.1 km (3 σ)

  NO GEODETIC ERRORS

MRSR ORBITER IMAGING TELESCOPE

PRELIMINARY CONCEPT

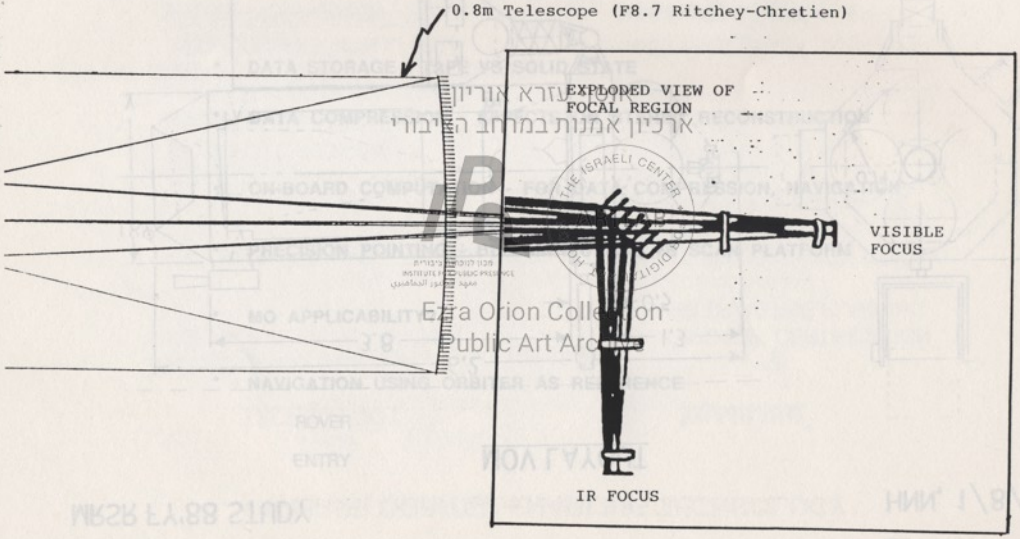

MRSR ORBITER IMAGING TELESCOPE

PRELIMINARY CONCEPT

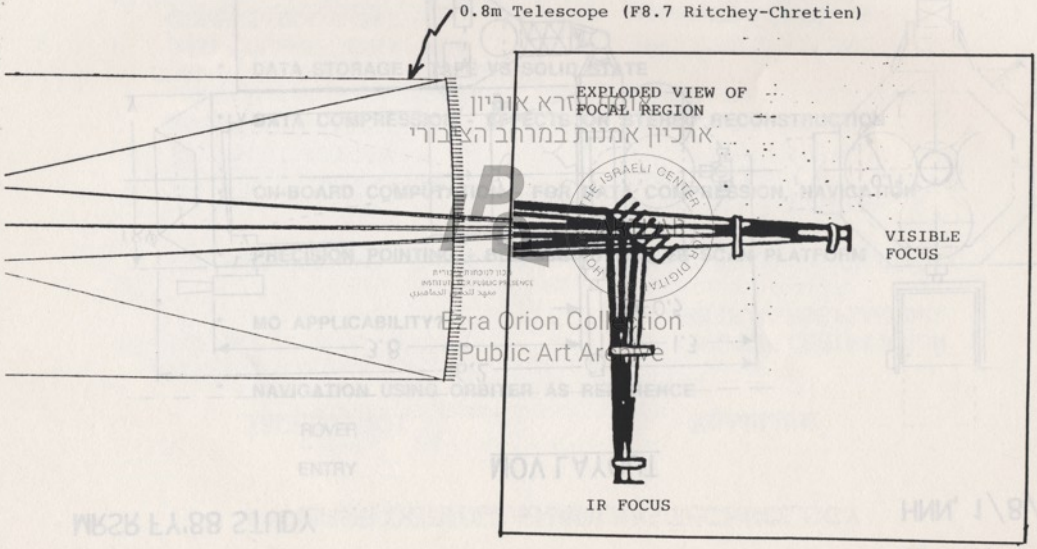

MRSR FY'88 STUDY

HNN, 1/8/88

MOV LAYOUT

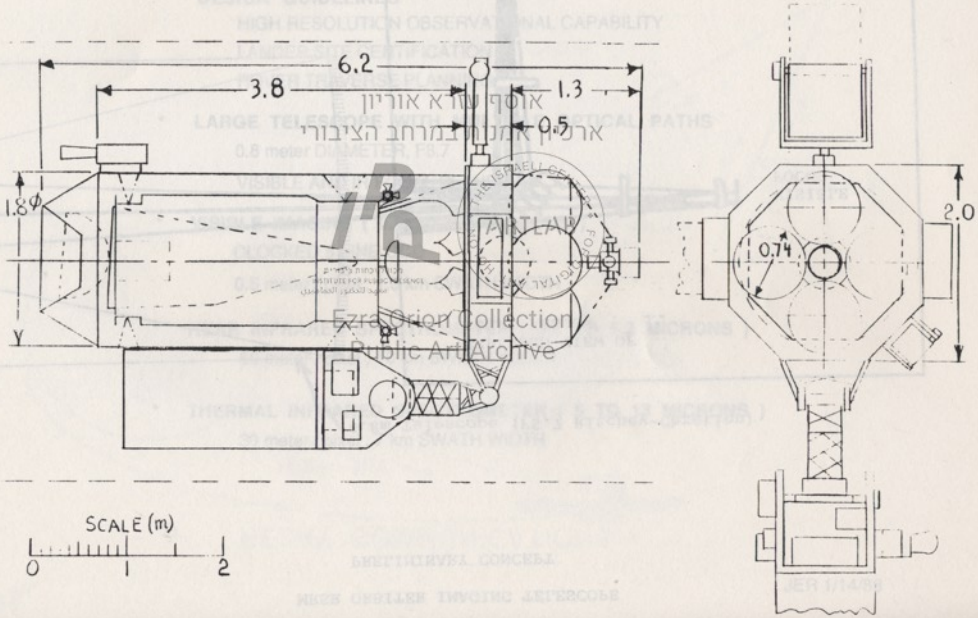

JPL

ORBITER SUPPORT FROM GENERAL ELECTRIC

- **EXTRAPOLATION FROM CORPORATE EXPERIENCE**

  MARS OBSERVER, LANDSAT, ETC.

- **DATA STORAGE - TAPE VS SOLID STATE**
- **DATA COMPRESSION - EFFECTS ON STEREO RECONSTRUCTION**
- **ON-BOARD COMPUTATION - FOR DATA COMPRESSION, NAVIGATION**
- **PRECISION POINTING - BUS MANEUVERS VS SCAN PLATFORM**
- **MO APPLICABILITY?**
- **NAVIGATION USING ORBITER AS REFERENCE**

  ROVER

  ENTRY

JER 1/14/88

MRSR ORBITER ENABLING TECHNOLOGY

TECHNOLOGY	ENABLING*
ATTITUDE CONTROL:	
SURFACE FEATURE TRACKER	LANDING SITE CERTIFICATION ROVER TRAVERSE PLANNING
PRECISION POINTING TECHNOLOGY	HI-RES IMAGING: HIGH STABILITY, HIGH RATE SLEWS
RENDEZVOUS AND DOCKING SENSOR TECHNOLOGY E.G. PROX-OPS SENSOR	RENDEZVOUS
COMPUTATION & DATA HANDLING	
DATA COMPRESSION AT HIGH COMPUTATIONAL RATES	HANDLING OF IMAGING DATA
DATA STORAGE	RELIABLE STORAGE OF 10^{10} BITS

* ENABLING SIGNIFICANT MISSION OPTIONS

JPL

MRSR MISSION DESIGN STATUS REPORT

PREPARED BY

JOHNNY H. KWOK

ALAN FRIEDLANDER

12–14 JANUARY 1988
PASADENA, CALIFORNIA

JHK
1/14/88

JPL

OUTLINE

* MISSION DESIGN TEAM ACTIVITIES
* MISSION ANALYSIS ACTIVITIES
* NAVIGATION ACTIVITIES
* MISSION REQUIREMENTS
* INFORMATION SYSTEM
* MISSION OPTIONS
* MACRO–EVENT ANALYSIS APPROACH
* MISSION PERFORMANCE MODEL AND DATABASE
* NEAR TERM SCHEDULE
* CONCERNS

JHK
1/14/88

JPL

MISSION DESIGN TEAM ACTIVITIES

* MISSION DESIGN TEAM INITIATED IN JULY 1987
* BIWEEKLY 2-HOUR MEETING FOR TECHNICAL INFORMATION EXCHANGE
* REPRESENTATIVES FROM MISSION ANALYSIS, NAVIGATION, INFORMATION SYSTEM, TDA/MOS, ORBITER, ROVER, PLANETARY OBSERVER
* MINUTES OF MEETING DISTRIBUTED TO JSC AND SAIC, AND LOGGED IN MRSR DATABASE
* FREQUENT TELECON EXCHANGE AMONG 3 CENTERS

JHK
1/14/88

JPL

MISSION ANALYSIS ACTIVITIES

* COMPLETED LANDING SITE ACCESSIBILITY STUDY REPORT – KWOK, JPL IOM 312/87.2–1321, 28 OCTOBER 1987, MRSR 05-09 (87)
* PRODUCED MARS TO EARTH HANDBOOK – SERGEYEVSKY, JPL PUBLICATION 82–43, 1 DECEMBER 1987
* COMPLETED EARTH–MARS–EARTH OPPORTUNITY STUDY – SWEETSER, JPL IOM 312/88.3–4065, 11 JANUARY 1987
* VERFIFIED CONIC APPROXIMATION WITH INTEGRATED TRAJECTORY – SWEETSER, JPL IOM 312/87.3–4037, 17 NOVEMBER 1987
* MRSR PERFORMANCE SPREADSHEET AND DATABASE UPDATED
* MACRO–EVENT ANALYSIS ONGOING
* OUTLINE OF MISSION DESCRIPTION DOCUMENT ISSUED
* DEORBIT AND ENTRY REQUIREMENTS ANALYSIS ONGOING
* AEROCAPTURE VERSUS PROPULSIVE CAPTURE RATIONALE TO BE DOCUMENTED
* IMPLEMENTATION OF COLORADO MARTIAN ATMOSPHERE MODEL INTO TRAJECTORY SOFTWARE ONGOING

JHK
1/14/88

JPL PUBLICATION 82-43

Interplanetary Mission Design Handbook, Volume I, Part 5

Mars-to-Earth Ballistic Mission Opportunities, 1992–2007

Andrey B. Sergeyevsky
Ross A. Cunniff

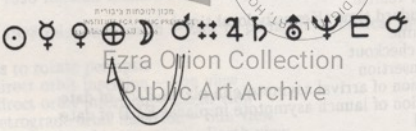

December 1, 1987

NASA
National Aeronautics and Space Administration

Jet Propulsion Laboratory
California Institute of Technology
Pasadena, California

JPL

EARTH-MARS TRANSFERS

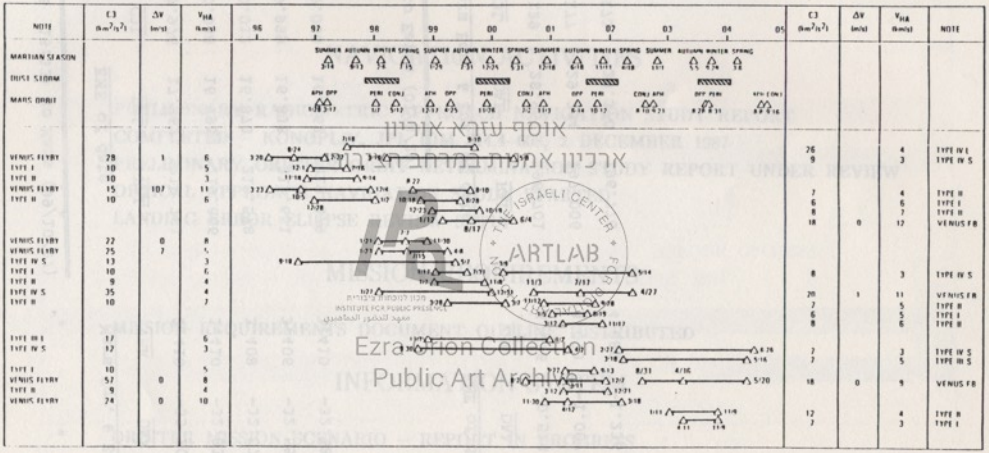

Table Comparing V-Infinities

Earth (98/12/18 18:33) to Mars (99/10/07)

	EME of date			Mars Eqr. & Eqx. of date		
Model	C3L	DAL	RAL	VHA	DAA	RAA
QTRAJ	9.976	17.562	219.761	3.410	-33.208	307.018
QSTEP	10.038	16.795	219.666	3.410	-32.833	306.594
FAST (rot.)	10.012	16.873	219.578	3.408	-32.577	306.444
FAST (red.)	9.999	16.838	219.651	3.406	-32.556	306.476
FAST (full)	10.000	16.762	219.879	3.410	-32.587	306.513

Mars (01/1/4) to Earth (01/8/29)

	Mars Eqr. & Eqx. of date			EME of date		
Model	C3L	DAL	RAL	VHA	DAA	RAA
QTRAJ	6.129	28.957	196.701	4.076	-0.518	88.861
QSTEP	6.177	29.264	197.006	4.073	-1.007	88.598
FAST (full)	6.173	29.370	196.776	4.080	-1.236	88.608

JPL

NAVIGATION ACTIVITIES

* PRELIMINARY RADIOMETRIC APPROACH NAVIGATION STUDY REPORT COMPLETED – KONOPLIV, JPL IOM 314.4-608, 2 DECEMBER 1987
* PRELIMINARY ORBITER ORBIT DETERMINATION STUDY REPORT UNDER REVIEW
* OPTICAL APPROACH NAVIGATION STUDY STARTED
* LANDING ERROR ELLIPSE REVIEW SETUP

MISSION REQUIREMENTS

* MISSION REQUIREMENTS DOCUMENT OUTLINE DISTRIBUTED

INFORMATION SYSTEM

* ORBITER MISSION SCENARIO – REPORT IN PROGRESS
* OUTLINE OF REPORT DISTRIBUTED
* PROGRESS REPORT (1/29), PRELIMINARY REPORT (4/29)

JHK
1/14/88

Figure 6: Sigma B vs. Cases

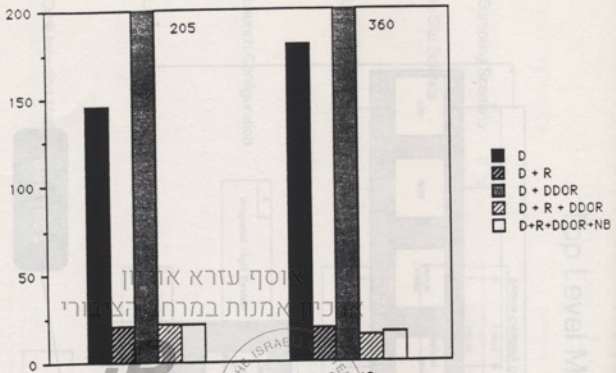

Figure 7: Sigma Flight-Path-Angle vs. Cases

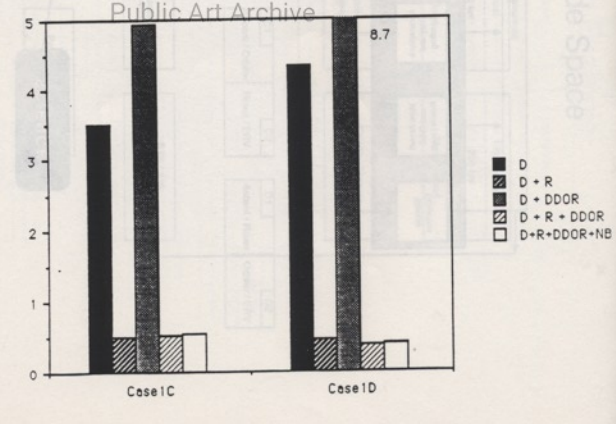

A MACRO-EVENT ANALYSIS APPROACH TO SUPPORT MRSR TARGETING DECISIONS

Prepared By

Alan Friedlander
Science Applications International Corporation

For

The MRSR Project Meeting
12-15 January 1988
JPL - Pasadena, CA

PROBLEM STATEMENT

- THE MRSR STEERING GROUP QUESTIONED WHETHER THE STUDY TEAM WAS DEVELOPING A RATIONALE FOR THE TOP-LEVEL MISSION OPTION TRADE-SPACE (i.e. LAUNCH OPPORTUNITIES, LANDING SITES, TARGETING REDUNDANCY, etc.).

- GIVEN THAT MISSION SUCCESS ACHIEVEMENT IS A HIGH PRIORITY GOAL, IT WAS STRONGLY IMPLIED THAT REDUNDANT FLIGHT SYSTEMS (i.e. two launches of identical systems) MAY BE THE BEST WAY TO REALIZE THIS GOAL.

- DESCRIBING THE TRADE SPACE IN OUR STANDARD FORMAT IS FAIRLY STRAIGHTFORWARD, BUT DOES LITTLE TO CHARACTERIZE OR QUANTIFY THE KEY ISSUE OF MISSION SUCCESS.

- AN APPROACH BASED ON EVENT TREE ANALYSIS, SIMPLIFIED TO CONSIDER ONLY MACRO-FAILURE EVENTS, IS MORE USEFUL IN DELINIATING FAILURE SEQUENCES AND POSSIBLE RESPONSE DECISIONS. FURTHERMORE, BY ADOPTING A PARAMETRIC EVALUATION VIEWPOINT, ONE CAN READILY QUANTIFY VARIOUS SUCCESS/FAILURE PROBABILITIES AND SENSITIVITY FACTORS. THIS TYPE OF ANALYSIS CAN BE PERFORMED AT AN EARLY STAGE OF THE STUDY EVEN WITHOUT DETAILED SUBSYSTEM FAILURE DATA, AND CAN HELP TO VALIDATE "A PRIORI JUDGEMENTS".

MRSR LAUNCH OPPORTUNITY / LANDING SITE TRADE SPACE

LAUNCH CONFIGURATION ..... COMBINED FLIGHT MODE, SPLIT FLIGHT MODE

NUMBER OF LAUNCHES PER OPPORTUNITY ..... ONE, TWO, FOUR

NUMBER OF LAUNCH YEAR OPPORTUNITIES ..... ONE, TWO

SITE REDUNDANCY VIA RETARGETING ..... YES, NO

LOCATION OF LANDING SITE ..... NEAR-EQUATORIAL, MID-LATITUDE, POLAR

NUMBER OF SITES PER OPPORTUNITY ..... ONE, TWO

TOTAL NUMBER OF LANDING SITES ..... ONE, TWO, THREE, FOUR

PROBLEM STATEMENT

- THE MRSR STEERING GROUP QUESTIONED WHETHER THE STUDY TEAM WAS DEVELOPING A RATIONALE FOR THE TOP-LEVEL MISSION OPTION TRADE-SPACE (i.e. LAUNCH OPPORTUNITIES, LANDING SITES, TARGETING REDUNDANCY, etc.).

- GIVEN THAT MISSION SUCCESS ACHIEVEMENT IS A HIGH PRIORITY GOAL, IT WAS STRONGLY IMPLIED THAT REDUNDANT FLIGHT SYSTEMS (i.e. two launches of identical systems) MAY BE THE BEST WAY TO REALIZE THIS GOAL.

- DESCRIBING THE TRADE SPACE IN OUR STANDARD FORMAT IS FAIRLY STRAIGHTFORWARD, BUT DOES LITTLE TO CHARACTERIZE OR QUANTIFY THE KEY ISSUE OF MISSION SUCCESS.

- AN APPROACH BASED ON EVENT TREE ANALYSIS, SIMPLIFIED TO CONSIDER ONLY MACRO-FAILURE EVENTS, IS MORE USEFUL IN DELINIATING FAILURE SEQUENCES AND POSSIBLE RESPONSE DECISIONS. FURTHERMORE, BY ADOPTING A PARAMETRIC EVALUATION VIEWPOINT, ONE CAN READILY QUANTIFY VARIOUS SUCCESS/FAILURE PROBABILITIES AND SENSITIVITY FACTORS. THIS TYPE OF ANALYSIS CAN BE PERFORMED AT AN EARLY STAGE OF THE STUDY EVEN WITHOUT DETAILED SUBSYSTEM FAILURE DATA, AND CAN HELP TO VALIDATE "A PRIORI JUDGEMENTS".

A MACRO-EVENT ANALYSIS APPROACH TO SUPPORT MRSR TARGETING DECISIONS

Prepared By

Alan Friedlander
Science Applications International Corporation

For

The MRSR Project Meeting
12-15 January 1988
JPL - Pasadena, CA

MACRO - EVENT TREE FOR MISSION OPTION 1 (CONFIGURATION A)

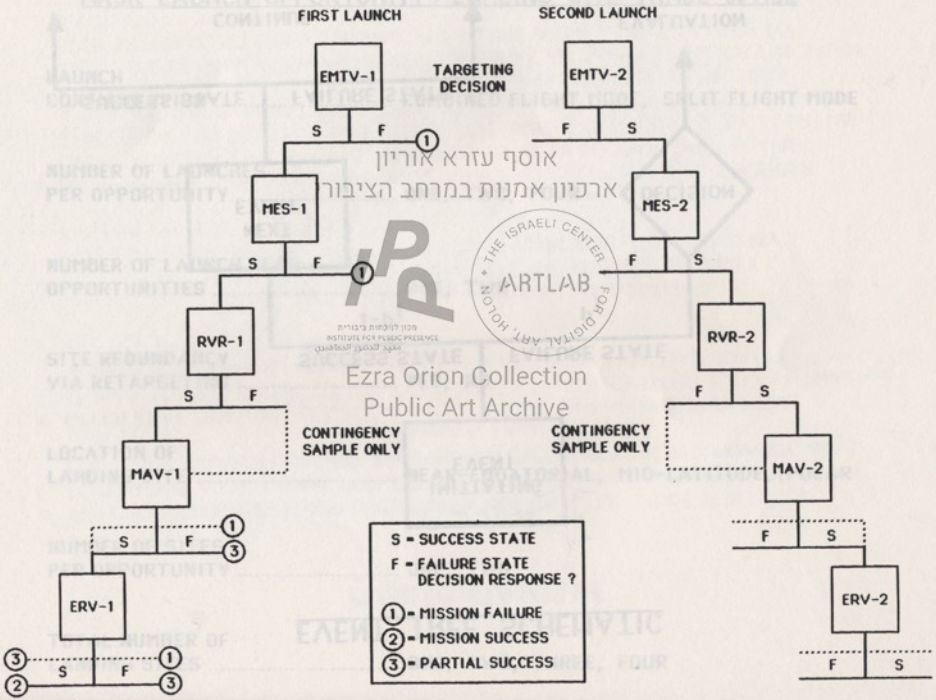

MACRO-EVENT PROBABILITIES FOR MISSION OPTION 1 - CONFIGURATION A

FAILURE PROBABILITIES

PF(EMTV) = 0.1
PF(MES) = 0.1
PF(RVR) = 0.1
PF(MAV) = 0.1
PF(ERV) = 0.1

	SINGLE MISSION (1 TARGETED SITE)		INDEPENDENT MISSIONS (2 TARGETED SITES)
TOTAL MISSION SUCCESS	0.5905		0.8323
TOTAL MISSION FAILURE	0.2054		0.0422
PARTIAL SUCCESS	0.2041		0.1255
	1.0000		1.0000
AT LEAST 1 RVR SUCCESS, NO SR	0.1385	0.0761	
AT LEAST 1 CONT. SR, NO RVR	0.0656	0.0313	
1 RVR SUCCESS, 1 CONT. SR	-	0.0182	
NO SAMPLE RETURNED	0.3439		0.1183
NO ROVER MISSION	0.2710		0.0734

SENSITIVITY TO ELEMENT FAILURE PROBABILITY
MISSION OPTION 1 – CONFIGURATION A

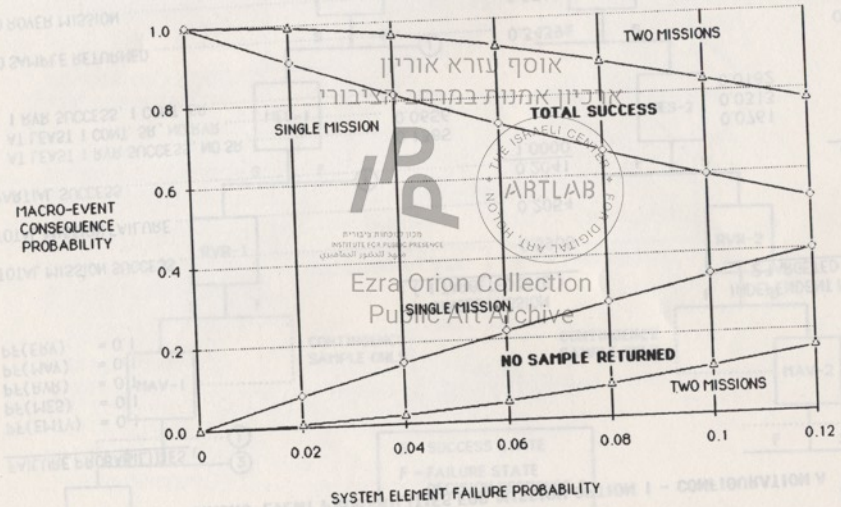

MARS ROVER SAMPLE RETURN

Mission Option 1 (Configuration A) Page 1
(Aerocapture at Mars) 21-Dec-87

Launch Opportunity 1998

Trajectory Type Conjunction, Type II

Orbit Capture Mode at Mars	A/C	Prop.
	1	0

Vinf at Earth Departure	3.161
Vinf at Mars Arrival	3.414
Vinf at Mars Departure	2.481
Vinf at Earth Return	4.064

MASS ELEMENTS:

Sample Mass	5
Sample Can. Assy	19
Rendezvous Module	126
Rover/Lndr Sci.	150
Earth Return Vehic	180
Orbiter	550
Drop Orbiter	0

PARKING ORBITS	Mars OI	Mars Dep.	Earth Circ.	Earth Ellip.
Periapse Alt. (km)	500	500	370	370
Apoapse Alt. (km)	33560.4	500	370	71356.2
Orbit Period (hr)	24.62	2.05	1.53	24.00
Deorbit Lndr from:	1	0		
Orbit Transfer	A/C	Prop		
	0	1		

RETROPROPULSION SYSTEMS	Mars Op	Term Des	Earth OI
Isp (sec)	326.00	260.00	290.00
tankage factor	0.17	0.20	0.12
engine mass	126.00	50.00	0.00

DV MANEUVERS

Outbound M/C	0.050
Periapsis raise	0.027
Deorbit maneuver	0.028
Orbit Transfer	1.144
Orbit Trims	0.150
Mars Departure	1.989
Return M/C	0.050
Earth Orbit Insert	3.918 (circ.)
	1.178 (ellip.)

Mission Option 1 (Configuration A)
SUMMARY MASS TABLE (Aerocapture at Mars) 21-Dec-87

	EARTH RETURN OPTIONS			
	Solid motor Circ.	Solid motor Ellip.	Dir.Ent.	A/C
EARTH RETURN SYSTEM				
Sample Capsule	51	51	19	19
Propellant	256	30	0	0
Inerts	31	4	131	84
	338	85	150	103
MARS DEPARTURE				
ERV	180	180	180	180
Propellant	679	414	482	433
Inerts	241	196	208	200
	1100	790	870	813
LANDED MASS				
Rendezvous Module	126	126	126	126
Ascent Propulsion	1038	1038	1038	1038
Rover/Lndr Sci.	150	150	150	150
Parachute + Inerts	133	133	133	133
Lander Structure	250	250	250	250
Term. Propulsion	276	276	276	276
	1973	1973	1973	1973
MARS ARRIVAL				
Orbiter	656	656	550	550
Drop Orbiter	0	0	0	0
Propellant	1086	780	859	802
Inerts	185	133	146	136
	1821	1462	1555	1488
M a/c 1	647	647	647	647
M a/c 2	938	686	751	704
Propellant	105	89	93	90
Inerts	144	141	142	141
	1834	1564	1633	1583
TCM MANUEVERS				
Outbound M/C Prop.	112	87	101	98
Outbound M/C Inert	19	15	17	17
BIOSHELL	185	154	162	156
LAUNCH ADAPTER	228	170	200	193
INJECTED MASS (WET)	7609	6130	6860	6427

MRSR LAUNCH VEHICLE REQUIREMENTS FOR SEVERAL MISSION OPTIONS

EARTH RETURN TO 370 KM CIRCULAR ORBIT
- PROPULSIVE CAPTURE
- AEROCAPTURE

ROVER MASS ASSUMPTIONS
- LOCAL (100 KG)
- REGIONAL (400 KG)
- EXPLORATORY (700 KG)
- ENHANCED (1100 KG)

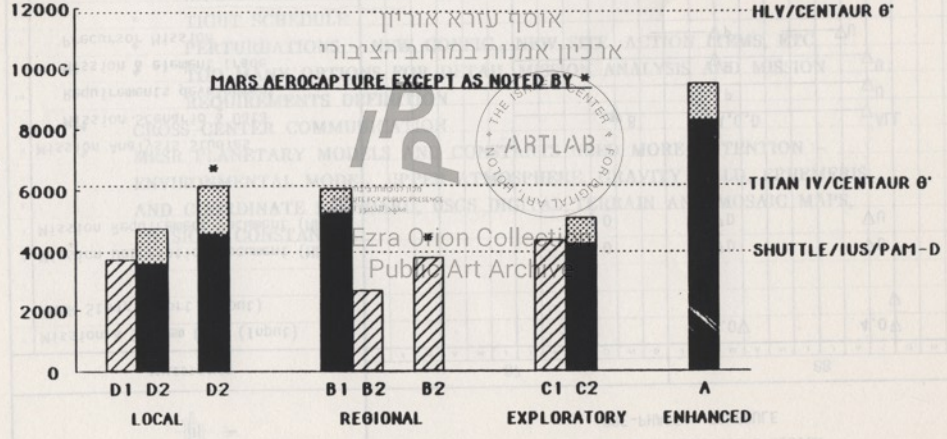

CONFIGURATION / SAMPLING CAPABILITY

JET PROPULSION LABORATORY

MRSR MISSION ANALYSIS & DESIGN
PRE-PHASE SCHEDULE

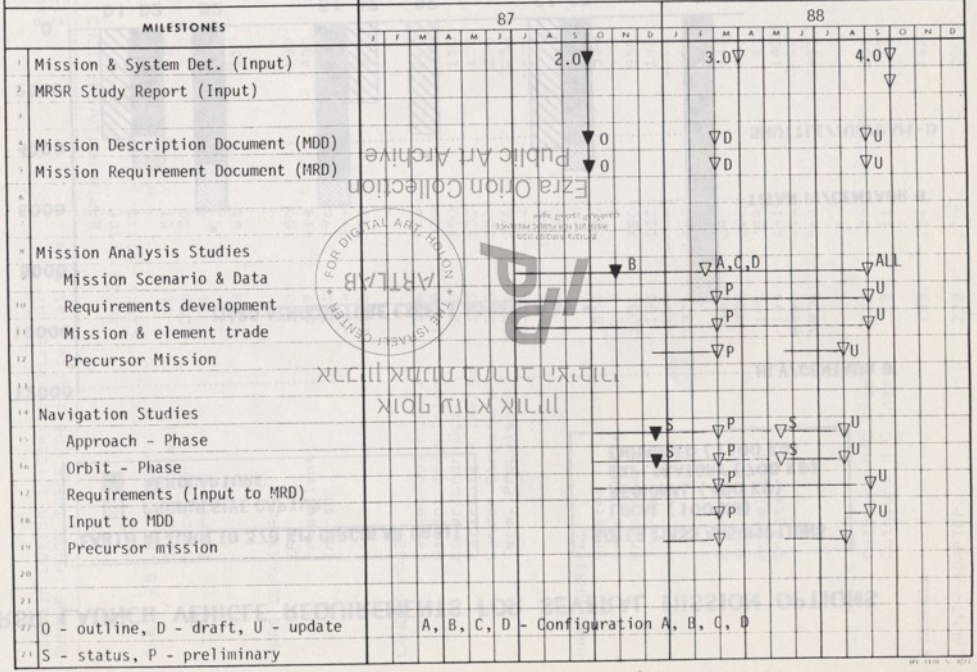

MRSR ENGINEERING PRECURSOR

REQUIREMENTS

JET PROPULSION LABORATORY

JANUARY 14, 1988

R. KAHL
JSC

AGENDA

- BACKGROUND
- ASSUMPTIONS
- MISSION REQUIREMENTS
- SPACECRAFT REQUIREMENTS
- RECOMMENDATIONS

BACKGROUND

- SIGNIFICANT SWG SUBCOMMITTEE ACTIVITY FROM MARCH TO JUNE 1987 TO IDENTIFY MRSR PRECURSOR REQUIREMENTS IN TIME FRAME TO IMPACT MARS OBSERVER PROJECT
- COMPLETED TASK AND PUBLISHED REPORT OF FINDINGS JUNE 1987
- TRANSMITTED TO MO PROJECT FOR EVALUATION
- RESULTED IN IMPLEMENTATION OF FOLLOWING:
  - ADDITIONAL HYDRAZINE PROPELLANT LOADED INTO ATTITUDE CONTROL PROPULSION SYSTEM ON BEST EFFORTS BASIS
  - PROVIDE MORE 70 METER ANTENNA TIME ON BEST EFFORTS BASIS
  - CONSIDER MODIFICATION OF MO TO ALLOW TRANSMITTAL OF SOVIET DATA FROM MARS 92 MISSION
- ITEMS SELECTED REPRESENT ONLY SMALL PART OF RECOMMENDATIONS CONTAINED IN SWG REPORT
- RESULTS WILL BE CONSIDERED IN ESTABLISHING REQUIREMENTS FOR A DEDICATED MRSR PRECURSOR MISSION

RECOMMENDATIONS

- ADOPT AS PRELIMINARY SET OF PRECURSOR REQUIREMENTS
- DISTRIBUTE FOR REVIEW AND COMMENT TO MARS TEAM AND SWG
- COMPILE AND FLESH-OUT WITH ADDITIONAL DETAILED REQUIREMENTS
- INITIATE STUDY TO EVALUATE THE POTENTIAL FOR EXISTING SPACECRAFT TO MEET REQUIREMENTS
- DEVELOP IMPLEMENTATION PLAN INCLUDING SCHEDULE AND COST OPTIONS
- DEVELOP MRSR MISSION OPTIONS INCORPORATING PRECURSOR ORBITER
  - ASSESS IMPACT TO PROJECT IMPLEMENTATION PLANNING
- PROGRESS REPORT AT MARCH REVIEW BOARD
- COMPLETE PRECURSOR STUDY AUGUST 1988

MISSION REQUIREMENTS

- CONJUNCTION CLASS MISSION, TYPE II TRAJECTORY
- LAUNCH VEHICLE TITAN/CENTAUR G'
- PROPULSIVE INSERTION INTO MARS ORBIT REQUIRED FOR SPECIFIC MISSION SCENARIO
- MISSION SCENARIO CONSISTS OF FOLLOWING COMPONENTS
  - ENGINEERING DATA FOR MRSR MISSION PLANNING
  - SUPPORT FOR MRSR MISSIONS
  - SUPPORT FOR INTERNATIONAL AND FUTURE MARS MISSIONS
- OVERALL MISSION SCENARIO OPTIMIZED ON BASIS OF TRADE-OFFS BETWEEN EFFICIENCY, TIMELY INFORMATION RETURN, COST, ETC., FOR EACH COMPONENT
  - SPACECRAFT PLACED IN ORBIT DRIVEN BY PLANETARY PROTECTION CONSIDERATIONS BETWEEN MISSION SCENARIO COMPONENTS
  - SPACECRAFT MOVED TO SUITABLE SUPPORT ORBIT FOR MRSR AND OTHER MISSIONS
  - UPON COMPLETION OF OVERALL MISSION SCENARIO SPACECRAFT PLACED IN ORBIT DRIVEN BY PLANETARY PROTECTION CONSIDERATIONS

JPL

CONCERNS

* EXPECTATION EXCEEDS RESOURCES AVAILABLE
  * INFORMATION EXPLOSION
  * TIGHT SCHEDULE
  * PERTURBATIONS – NEW CONFIG., NEW SITE, ACTION ITEMS, ETC.
  * TOO MANY OPTIONS FOR DETAIL MISSION ANALYSIS AND MISSION REQUIREMENTS DEFINITION
* CROSS-CENTER COMMUNICATION
* MRSR PLANETARY MODELS AND CONSTANTS NEED MORE ATTENTION – ENVIRONMENTAL MODEL, UPPER ATMOSPHERE, GRAVITY FIELD, EPHEMERIS AND COORDINATE STANDARD, USGS DIGITAL TERRAIN AND MOSAIC MAPS, PHYSICAL CONSTANTS

JHK
1/14/88

SPACECRAFT REQUIREMENTS

- SPACECRAFT SHALL COMPLY WITH PERFORMANCE AND ENVELOPE REQUIREMENTS FOR THE TITAN/CENTAUR LAUNCH VEHICLE
- SPACECRAFT SHALL INCORPORATE AN INSTRUMENT COMPLEMENT TO ALLOW THE DETERMINATION OF ATMOSPHERIC DENSITY, DENSITY GRADIENTS AND DISCONTINUITIES AS A FUNCTION OF ALTITUDE BETWEEN SPACECRAFT ORBIT AND SURFACE
- SPACECRAFT SHALL INCORPORATE LOW RESOLUTION (3-5 METERS) AND HIGH RESOLUTION (0.5-1 METER) IMAGING CAPABILITY
- SPACECRAFT STABILITY AND POINTING REQUIREMENTS SHALL BE SUFFICIENT TO ACCOMPLISH MISSION REQUIREMENTS
- SPACECRAFT AND INSTRUMENT LIFE SHALL BE CERTIFIED FOR 15 YEARS
- SPACECRAFT SHALL INCORPORATE APPROPRIATE COMMUNICATIONS CAPABILITY

SPACECRAFT REQUIREMENTS (CONT'D)

- A TRADE STUDY SHALL BE PERFORMED TO DETERMINE NUMBER AND TYPE OF NAVIGATION AIDS PLACED ON SURFACE CONSIDERING THE FOLLOWING
  - ACTIVE AND PASSIVE DEVICES
  - REQUIREMENTS FOR EASY IDENTIFICATION ON MAPS GENERATED
  - USEFUL LIFE
  - STANDARDIZATION FOR INTERNATIONAL USE
- SPACECRAFT SHALL PROVIDE A STANDARDIZED RELAY LINK SUITABLE FOR SUPPORT OF INTERNATIONAL MISSIONS

Single Track with Legs

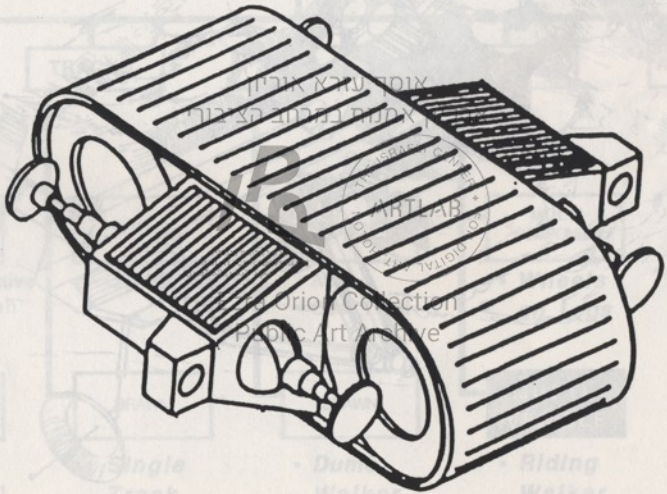

MARTIN MARIETTA

Taxonomy Examples

Concept Development

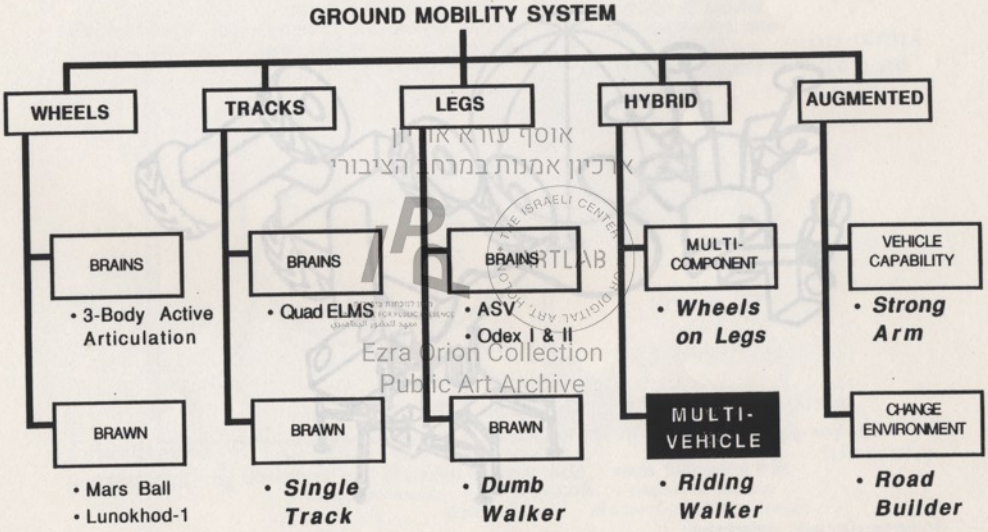

MARTIN MARIETTA

Towed Balloon

MARTIN MARIETTA

Problem Partitioning

Concept Development

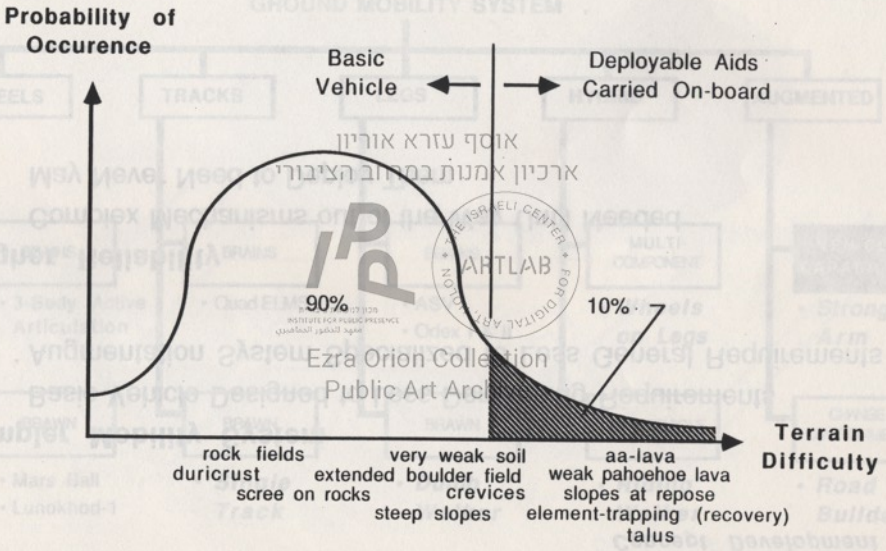

MARTIN MARIETTA

Problem Decomposition - Advantages

Concept Development

Simpler Mobility System

- Basic Vehicle Designed to Less Demanding Requirements
- Augmentation System Specialized to Less General Requirements

Higher Reliability

- Complex Mechanisms out of the Way Until Needed
- May Never Need to Deploy Them

Taxonomy Examples

Concept Development

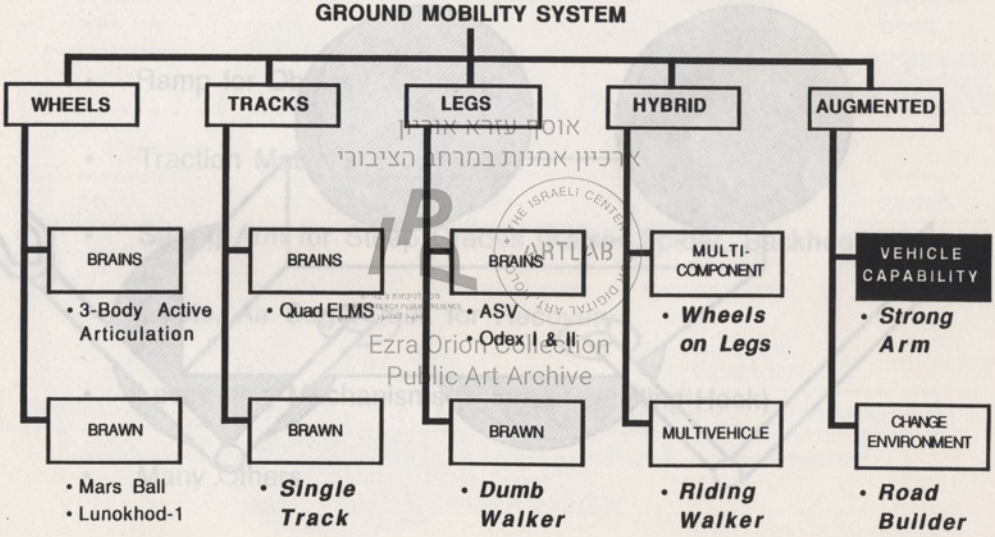

MARTIN MARIETTA

Wheeled Vehicle Augmented with Strong Arm

Concept Development

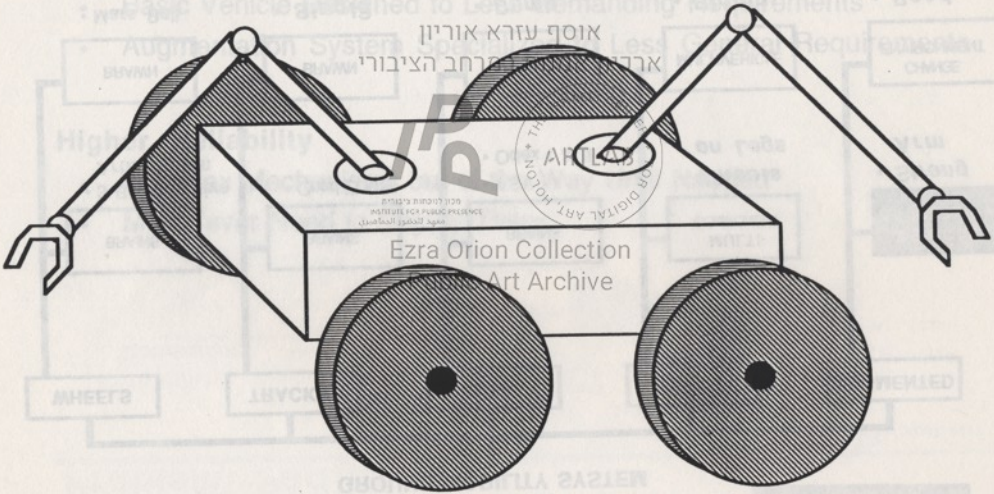

Deployable Mobility Enhancing Mechanisms

Concept Development

- Ramp for Obstacle Crossing
- Traction Mats for Weak Soil
- Strong Arm for Steep Grades (Kaiser Spider, Backhoe)
- Struts, Air Bags, Jack for Recovery
- Leveraging Mechanisms (Pitons, Grappling Hook)
- Many Others